Investigation of microglia phenotypes in an iPSC model of Huntington's Disease

A thesis submitted for the degree of
Doctor of Philosophy (PhD)
by
Nina Stöberl

December 2022

Acknowledgements

I would like to sincerely thank my supervisor Nick Allen for the opportunity to conduct my PhD at Cardiff University and for helping me with experiments, analysis, interpretation of results and writing my thesis. Thank you to my extended supervisor team consisting of Anne Rosser and Emyr Lloyd-Evans for their support and input along the way. I would like to deeply thank Lesley Jones for being my assessor and a wonderful mentor, who we sadly lost to cancer this year. I want to thank Hazel Hall-Roberts for stepping in as an additional supervisor when she joined the Cardiff DRI. Thank you so much for our monthly meetings and for your endless effort to help me finish my thesis. A big thank you goes to Tom Massey, Peter Holmans and Natalie Connor-Robson for valuable input during the writing of this thesis.

I would also like to thank the European Union's Horizon 2020 research and innovation programme under the Marie Skłodowska-Curie grant agreement No 813851 for my PhD funding. Thank you to Josep Canals Coll for organising the ASCTN training programme. I am so grateful to be part of this amazing group of 14 PhD students all across Europe. Thank you to Alzheimer's Research UK for awarding me the Pump Priming award, as well as travel funding for the ARUK conference and to the School of Biosciences for awarding me the Seedcorn Funding.

Thank you to Angela Marchbank and the School of Biosciences Genome Hub for the help with the transcriptome study. Thank you to Kate Heesom, Phil Lewis and the Proteomics Facility at the University of Bristol for the help with the proteomics study. Thank you to the Dementia Research Institute at Cardiff, which opened the lab to me and let me use all their valuable equipment. And for the welcoming atmosphere and amazing people I got to work with.

Thank you to my lab mates, which made this experience enjoyable: Elisa, Emily and Beth, who have been there from the start to support me and encourage me to continue even in the tough times, and who became great friends along the way.

Lastly, a huge thanks to my German friends, which made Cardiff more of a home, including Nicole, Sven, Stephie and Anne. And not to forget thanks to my family and friends back in Germany, which accepted that I left home for a new adventure.

Thesis summary

Huntington's disease (HD) is a neurodegenerative disorder caused by a dominantly inherited CAG repeat expansion in the huntingtin gene (*HTT*). Multiple studies indicate an involvement of neuroinflammation in HD pathology, including several PET studies demonstrating that microglial activation correlates with disease severity in HD patients. Nonetheless, an open question is whether mutant *HTT* expression leads to cell-autonomous transcriptional and functional changes in microglia, which potentially contribute to the disease pathology.

In this thesis, a patient-derived induced pluripotent stem cell (iPSC) model of HD with 109 CAG repeats (Q109), and isogenic controls with a corrected wild-type length of 22 repeats (Q22) were used. Q109 and Q22 iPSC were differentiated to microglia-like cells, as well as astrocytes and neurons. Cell types were characterised using immunocytochemistry as well as flow cytometry. Investigation of CAG repeat size was performed using PCR and capillary electrophoresis. Microglia function was investigated in monoculture using a wide range of assays as well as immunostaining of cellular compartments. Bulk RNA sequencing was performed on microglia-like cells under basal conditions and after pro-inflammatory stimulation. The secretome of microglia-like cell monocultures as well as microglia-astrocyte co-cultures was investigated via mass spectrometry.

Both, Q109 and Q22 iPSC successfully differentiated to microglia-like cells, astrocytes and neurons. Q109 microglia-like cells, astrocytes and neurons demonstrated *HTT* CAG repeat expansion in culture. Q109 microglia-like cells showed impairment in key microglia functions, including phagocytosis and endocytosis and these functional impairments were also evident on a gene expression level. Furthermore, the secretion of pro-inflammatory cytokines was increased in Q109 microglia-like cells. RNA sequencing revealed an upregulation of genes involved in translation and mismatch repair in the comparison of Q109 versus Q22 microglia-like cells. In the investigation of microglia-astrocytes co-culture supernatants, astrocytes played a more prominent role for differentially secreted proteins.

These observations demonstrate that iPSC-derived microglia-like cells can be utilized to better understand the role of microglia in HD pathology. The findings indicate a mutant *HTT* induced change in microglia transcription and cellular function which is independent of the detrimental HD brain environment.

Abbreviations

AAVS1	Adeno-associated virus integration site 1
Aβ	Amyloid-beta
AC	Astrocytes
ACM	Astrocyte conditioned media
ADF	Advanced DMEM/F-12
AD	Alzheimer's disease
ADP	Adenosine diphosphate
ALS	Amyotrophic lateral sclerosis
ANOVA	Analysis of variance
APC	Astrocyte precursor cells
α-SYN	Alpha-synuclein
ATP	Adenosine triphosphate
BSA	Bovine serum albumin
BDNF	Brain-derived neurotrophic factor
BMP4	Bone morphogenetic protein 4
CAG	Cytosine-adenine-guanosine trinucleotide
CCL	Chemokine (C-C motif) ligand
CD	Cluster of differentiation
C/EBP	CCAAT-enhancer-binding proteins
CNS	Central nervous system
CNV	Copy number variant
CNTF	Ciliary neurotrophic factor
CREB	cAMP response element-binding protein
CRISPR	Clustered regularly interspaced short palindromic repeats
CXCL1	C-X3-C motif chemokine ligand 1
DAMP	Damage-associated molecular pattern
DEG	Differentially expressed genes
DMEM	Dulbecco's modified eagle media
DNA	Deoxyribonucleic acid
EAAT	Excitatory amino acid transporter
EB	Embryoid body
ECM	Extracellular matrix
EGF	Epidermal growth factor

ESC	Embryonic stem cells
EXP	Experiment
FACS	Fluorescence-activated cell sorting
FAN1	Fanconi anemia FANC1/FANCD2-associated [endo] nuclease 1
FBS	Fetal bovine serum
FDR	False discovery rate
FITC	Fluorescein isothiocyanate
GeM-HD	Genetic modifiers of Huntington's disease consortium
GFAP	Glial fibrillary acidic protein
GFRA1	GDNF family receptor alpha 1
GLP-1R	Glucagon-like peptide-1 receptor
GM-CSF	Granulocyte macrophage colony stimulating factor
GO	Gene ontology
gRNA	Guide RNA
GWAS	Genome-wide association studies
HD	Huntington's disease
HTT	Huntingtin gene
HTT	Huntingtin protein
IBA1	Ionised calcium-binding adapter molecule 1
ICC	Immunocytochemistry
IFN-γ	Interferon γ
IGF-1	Insulin-like growth factor 1
IL	Interleukin
iPSC	Induced pluripotent stem cells
KO	Knock-out
KEGG	Kyoto encyclopaedia of genes and genomes
LIF	Leukemia inhibitory factor
LPS	Lipopolysaccharide
MAP2	Microtubule associated protein 2
mHTT	Mutant huntingtin protein
mRNA	Messenger RNA
M-CSF	Macrophage colony stimulating factor
MG	Microglia
MMP	Matrix metalloproteinase
MS	Nano-LC Mass Spectrometry
MSN	Medium spiny neurons

MTMR10	Myotubularin related protein 10
NFIA	Nuclear factor 1 A-type
NFκB	Nuclear factor kappa-light-chain-enhancer of activated B cells
NGF	Nerve growth factor
NO	Nitric oxide
NPC	Neural progenitor cells
P2RX	Purinergic receptor P2X
P2RY	Purinergic receptor P2Y
PBS	Phosphate buffered saline
PCA	Principal component analysis
PCR	Polymerase chain reaction
PGC-1α	Peroxisome proliferator-activating receptor-γ coactivator-1 α
PD	Parkinson's disease
PFA	Paraformaldehyde
qRT-PCR	Quantitative reverse-transcription PCR
RNA	Ribonucleic acid
ROS	Reactive oxygen species
RRM2B	Ribonucleotide reductase regulatory TP53 inducible subunit M2B
RT	Room temperature
SCF	Stem cell factor
SFRP4	Secreted frizzled-related protein 4
SNP	Single nucleotide polymorphism
SOX2	SRY-box transcription factor 2
TGF-β	Transforming growth factor β
TLR	Toll-like receptor
TMEM119	Transmembrane protein 119
TNF	Tumour necrosis factor
TREM2	Triggering receptor expressed on myeloid cells 2
TSPO	Translocator protein
TUBB3	Tubulin beta 3 class III
UBR5	Ubiquitin protein ligase E3 component n-recognin 5
VEGF	Vascular endothelial growth factor
VIM	Vimentin
WT	Wild type

Table of Contents

List of Figures

List of Tables

1 General Introduction

1.1 Huntington's Disease

1.1.1 Introduction to Huntington's disease

Huntington's disease (HD) is a severe neurodegenerative disorder caused by a dominantly inherited CAG trinucleotide repeat expansion in the huntingtin gene (*HTT*) on chromosome 4. HD is the most common polyglutamine-expansion neurodegenerative disease, with a prevalence of around 10.6 – 13.7 individuals per 100 000 in Western populations, and around 5 individuals per 100 000 worldwide (Paine, 2015; McColgan and Tabrizi, 2018). Most HD cases show classical autosomal dominant inheritance, and only around 3% of patients carry de novo mutations (Paine, 2015). The autosomal dominant mutation is a dynamic CAG repeat expansion in exon 1 of the *HTT* gene which leads to pathological elongation of the polyglutamine tract within the N-terminus of the huntingtin protein (HTT) (Macdonald *et al.*, 1993). Patients with more than 39 CAG repeats will develop the disease, whilst reduced penetrance is seen in patients carrying between 36 and 39 repeats (McColgan and Tabrizi, 2018).

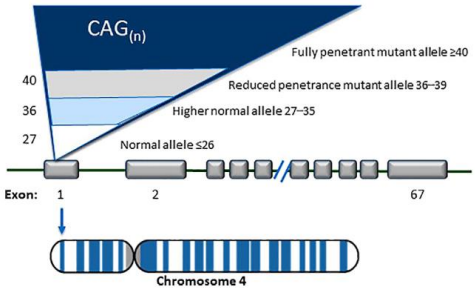

Description of gene	CAG repeat range	Risk of HD	Risk of HD in next generation
Normal	≤26	No HD	No
Higher normal	27–35	No HD	Possible
Reduced penetrance	36–39	Possible HD	Yes
Full penetrance	≥40	Definite HD	Yes

Figure 1.1: Classification of disease status in Huntington's disease. The causative mutation in Huntington's disease is an expanded cytosine-adenine-guanine (CAG) trinucleotide repeat within exon 1 of the HTT gene located on chromosome 4. Wild-type HTT possesses less than 36 CAG repeats. An expanded HTT allele with 36 or more repeats can cause HD, while gene carriers with more than 39 CAG repeats will develop HD. Figure taken from Gatto et al., 2020.

The mean age of onset of Huntington's disease is about 45 years but can rarely occur in early childhood or late life and is dependent on the *HTT* CAG repeat length and repeat expansions (Bates *et al.*, 2015). In the pre-manifest stage of disease subtle motor, cognitive and psychiatric deficits can already be identified up to 10 - 15 years before the onset of manifest disease (Ross *et al.*, 2014). The onset of manifest HD is defined as the point at which characteristic motor signs develop. Chorea, which is characterized by unwanted rapid and short-lasting movements in the extremities, face, and trunk, and loss of balance are early HD symptoms. However, family members can often notice cognitive or personality changes prior to a motor symptom onset (Novak and Tabrizi, 2011). Patients can furthermore show mild or more severe hypokinetic

movements, including slowness in executing movements (bradykinesia), balance and gait disturbance, and dystonia, which is characterized by slowly twisting and turning movements (Shannon, 2011). Memory loss usually shows a slow onset, but can ultimately progress into dementia (Nance, 2017). The most common psychiatric symptoms include depressed mood, anxiety, irritability, and apathy (van Duijn et al., 2007). Death usually occurs within 15-20 years of symptom onset and is often the consequence of heart failure or aspiration pneumonia (Gil and Rego, 2008). Current therapies provide only symptomatic relief, and despite improving quality of life, they fall short of halting or reversing the disease (Paine, 2015).

1.1.2 Brain pathology of Huntington's disease

HD is considered a multisystem degenerative disease of the human brain (Rüb *et al.*, 2016). Gross atrophy of the striatum is commonly cited as the pathological hallmark of HD, however the degeneration is not confined to this brain structure (McColgan and Tabrizi, 2018). The striatum is the primary input to the basal ganglia, which are a set of forebrain structures involved in motor control, mood, cognition, and learning (Graybiel, 1998). The striatum includes the caudate nucleus and putamen, and is primarily composed of medium spiny neurons (MSN), which are selectively vulnerable to the effects of mutant HTT (mHTT) (Plotkin and Surmeier, 2015). The remaining cells are cholinergic interneurons with local connections which modulate the output of the MSN, however they are largely unaffected in HD (Graveland, Williams and DiFiglia, 1985). Later in the disease progression, loss of cortical neurons likely results in the cognitive and personality-related changes observed in HD patients (Reiner, Dragatsis and Dietrich, 2011). Reactive microglia were shown to appear in the striatum and cortex in both early and late stages of the disease, but not in control post-mortem brains (E. Sapp *et al.*, 2001). Furthermore, an increase in activated astrocytes (Vonsattel *et al.*, 1985) and oligodendrocytes (Myers *et al.*, 1991) in the striatum was detected in post-mortem HD patient brains. Within brain cells, mHTT is misfolded and forms aggregates with toxic properties both in the nucleus and cytoplasm (Hatters, 2008; Cisbani and Cicchetti, 2012), which is in contrast to their diffuse localization in unaffected individuals. However, greater numbers of huntingtin aggregates were found to be present within the cortex than in the striatum (Gutekunst *et al.*, 1999) and also within the striatum in the spared interneurons rather than within vulnerable spiny striatal neurons (Kuemmerle *et al.*, 1999). Mutant huntingtin aggregation may therefore be a cytoprotective mechanism against polyglutamine-induced neurotoxicity.

1.1.3 The huntingtin protein

HTT is ubiquitously expressed, with high expression in the brain (Li *et al.*, 1993). It is expressed throughout the brain in neurons and glia cells (Strong *et al.*, 1993). Several early HD studies have shown that inactivation of the *HTT* gene is lethal in mice, indicating that HTT is essential for mouse embryonic development (Duyao *et al.*, 1995; Nasir *et al.*, 1995) and it was found to also be important for the formation of the nervous system (White *et al.*, 1997). HTT is a large protein of ~350 kDa with numerous functions, which interacts with effector proteins to mediate physiological processes. Approaches that identified HTT interaction partners revealed a number of cellular functions that it might be involved in, including cellular dynamics (cytoskeleton, endocytosis, trafficking, and adhesion), metabolism, protein turnover, and gene expression (transcription and RNA processing) (Harjes and Wanker, 2003). HTT may serve as a molecular scaffold, tethering multiple partners into complexes to coordinate cellular processes (Saudou and Humbert, 2016). Most HD patients express one mutant and one wild-type allele of the huntingtin gene, so that the wild-type HTT is present but at about half the normal concentration. Mice with brain-specific HTT knockout at adulthood show progressive neurodegeneration that is reminiscent of HD (Dragatsis, Levine and Zeitlin, 2000). But also heterozygous HTT knockout mice show impaired motor activity and cognitive deficits (Nasir *et al.*, 1995; O'Kusky *et al.*, 1999), indicating that the loss of normal HTT function might participate in the disease progression.

Mutant HTT forms aggregates that were initially described as being the toxic species in HD. It was suggested that these aggregates interfere with cellular functions, thereby causing cell death (Davies *et al.*, 1997). However, inclusions of mHTT were also described as being protective, as they reduce the level of the toxic protein fragments (Miller et al., 2010; Saudou et al., 1998). The toxicity of the aggregates may depend on the stage of the disease and on their nature and subcellular location (Saudou and Humbert, 2016). mHTT is cleaved by proteases, generating N-terminal fragments containing the abnormal polyglutamine stretch. These fragments can interfere with the transcriptional and autophagic machineries and cause endoplasmic reticulum stress, thereby inducing cell death (Steffan, 2010; Martin *et al.*, 2014; El-Daher *et al.*, 2015; Valor, 2015). N-terminal fragments have a high propensity to misfold and self-assemble into fibrillar aggregates (Trepte, Strempel and Wanker, 2014). Consequently, inclusion bodies are formed which consist of aggregates of mHTT fragments as well as a variety of other proteins like ubiquitin, chaperones, and components of the ubiquitin-proteasome system (Wanker *et al.*, 2019). These inclusion bodies are a pathological hallmark of HD.

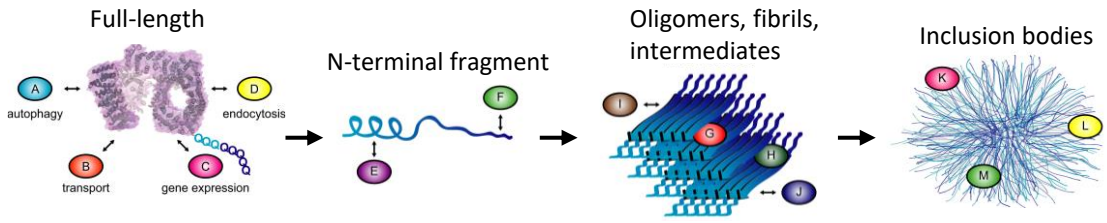

Figure 1.2: Schematic representation of different mutant huntingtin species along the aggregation cascade. Each species has different interactors (indicated through coloured ovals) and might therefore have different pathobiological roles in the disease. Figure adapted from Wanker et al., 2019.

1.1.4 Cellular pathology in Huntington's disease

A number of cellular pathologies induced by mutant *HTT* expression and the presence of mHTT toxic fragments, oligomers and aggregates have been described. Transcriptional dysregulation has long been considered a major pathogenic mechanism in HD (Kumar, Vaish and Ratan, 2014). mHTT interacts with regulators of transcription including p53 and cAMP response element-binding protein (CREB), which are involved in cell proliferation and survival (Steffan, 2010), as well as peroxisome proliferator-activating receptor-γ coactivator-1 α (PGC-1α), which is necessary for energy metabolism (Chaturvedi *et al.*, 2010). Misfolded mHTT furthermore overwhelms the chaperone machinery, diverting other misfolded clients to the proteasome and the autophagy pathways, which leads to an altered protein homeostasis (Soares *et al.*, 2019a). Altered mitochondrial function has been reported in HD and results in defects in ATP production, Ca^{2+} buffering capacity, and increased production of reactive oxygen species (ROS) (Carmo *et al.*, 2018). mHTT also interferes with normal organellar axonal transport in neurons and can reduce the transport of mitochondria to active synapses (Chilakala *et al.*, 2020). Neuronal activity as well as synaptic transmission and intrinsic neuronal excitability have been shown to be affected in HD patients and mouse models (Smith-Dijak, Sepers and Raymond, 2019). Lastly, glial dysfunction has been reported as a HD pathology. Microglia and astrocytes are critical in regulating neuronal activity and maintaining an optimal milieu for neuronal function. Activated microglia and reactive astrocytes are believed to contribute to HD pathology through transcriptional activation of pro-inflammatory genes and reactive astrocytes also display functional changes in glutamate and ion homeostasis and energy metabolism (Palpagama *et al.*, 2019).

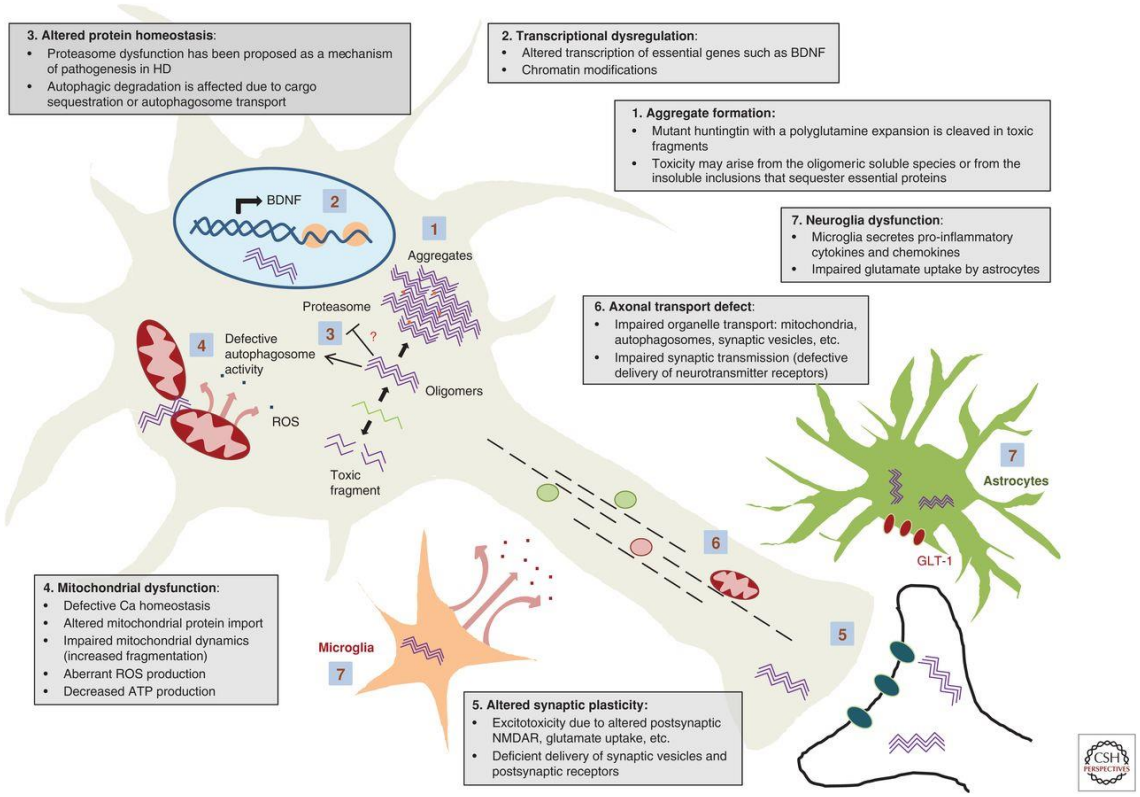

Figure 1.3: Schematic of selected mechanism of HD cellular pathology. In HD, a number of cellular pathways and mechanism are dysregulated due to mutant HTT expression. These include 1. aggregate formation, 2. transcriptional dysregulation, 3. altered protein homeostasis, 4. mitochondrial dysfunction, 5. altered synaptic plasticity, 6. axonal transport defect, 7. neuroglia dysfunction. BDNF = Brain-derived neurotrophic factor; ROS = reactive oxygen species; NMDAR = N-methyl-D-aspartate receptor. Figure taken from Jimenez-Sanchez et al., 2017.

1.1.5 Genetic modifiers of Huntington's disease

In HD patients, the number of CAG repeats in the mutant *HTT* allele inversely correlate with the age of disease onset (Andrew *et al.*, 1993; Kremer *et al.*, 1993; Macdonald *et al.*, 1993). It was found that the length of the triplet repeat is the most important factor in determining age of onset of HD and can explain 40-50% of that variance (Wexler *et al.*, 2004). Furthermore, the *HTT* CAG repeat is somatically unstable. Post-mortem brain tissue of HD patients show expansion in the *HTT* CAG repeat especially in the regions that are most susceptible to disease pathogenesis, the basal ganglia and cortex, indicating that these expansions might contribute to the selective vulnerability of certain neuronal populations (Pinto *et al.*, 2020). Dramatic mutation length increases of up to 1000 CAG repeats have been detected in human striatal cells early in the disease course when still no microscopic evidence of pathological cell loss was apparent in the striatum, indicating that somatic expansions might precede disease onset (Kennedy *et al.*, 2003). Mismatch repair (MMR) is believed to cause somatic CAG repeat expansions in HD (Iyer and Pluciennik, 2021). A number of mismatch repair proteins (including Msh2, Msh3, Mlh1, Mlh3)

were shown to be required for expansion of the *Htt* CAG repeat in mouse models of HD (Pinto *et al.*, 2013; Lai *et al.*, 2016). Next to the *HTT* CAG repeat length, genome-wide association studies (GWAS) have identified further genetic factors that modify age of onset and disease progression of HD. Over the years, a number of HD GWAS studies were performed. The Genetic Modifiers of Huntington's Disease (GeM-HD) Consortium identified a number of loci with genome-wide significant single nucleotide polymorphisms (SNP). These loci contained genes such as *MTMR10* (myotubularin related protein 10), *FAN1* (Fanconi anemia FANC1/FANCD2-associated [endo] nuclease 1), *RRM2B* (a subunit of DNA damage p53-inducible ribonucleotide reductase M2 B) and *UBR5* (an HECT domain E3 ubiquitin-protein ligase). Pathway analysis revealed that DNA repair pathways were significantly associated with age of onset (Lee *et al.*, 2015). A later GWAS replicated these findings and identified several other loci with genes that might modify the age of onset of HD, including further DNA repair genes. The authors found that an uninterrupted *HTT* CAG repeat sequence rather than the polyglutamine length dictates the timing of HD onset (Lee *et al.*, 2019). The most recent GWAS identified additional modifier effects at the *PMS1* and *PMS2* loci (Lee *et al.*, 2022).

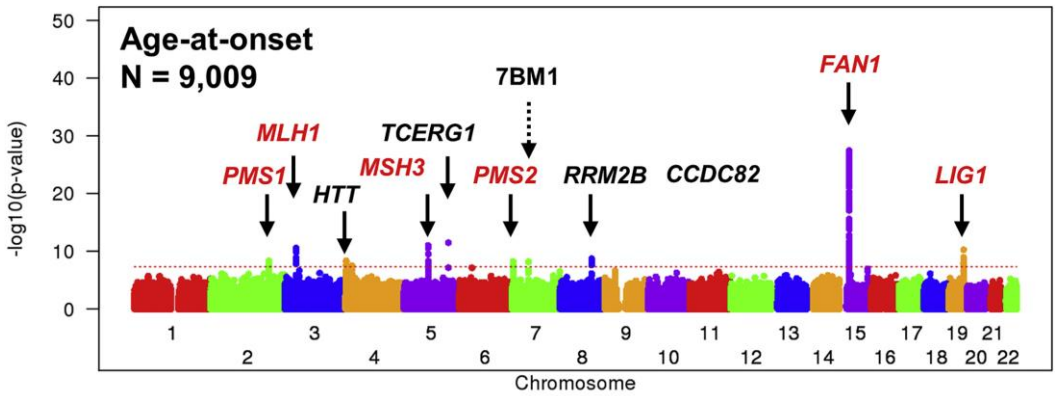

Figure 1.4: Age at Onset GWAS Signals. GWAS showing -log10(p value) for SNV association with the Z score of CAG-specific age at onset. The dotted red horizontal line shows the threshold for genome-wide significance. Solid arrows indicate loci that yield genome-wide significant signal, and candidate modifier genes are labelled with gene name. One additional locus that awaits further confirmation is noted by a dashed arrow. Red labels indicate DNA maintenance gene. Figure adapted from Lee et al., 2022.

1.2 Microglia and astrocytes

1.2.1 Microglia

Microglia are tissue-resident macrophages, and are the principal resident innate immune cells of the central nervous system (CNS), where they make up between 5% - 20% of cells in the total brain population, scattered throughout the brain (Perry, 1998). While microglia have been studied for decades, their origin remained debated. Only studies within the last 10 years indicated that they arise from progenitors in the embryonic yolk sac early during development,

which then seed the brain rudiment and appear to persist there into adulthood (Ginhoux *et al.*, 2013). Microglia morphology is characterized by a small cell body and very fine, highly ramified processes, which allow these cells to screen their local brain parenchyma for signs of pathogens or cellular damage (Leyh *et al.*, 2021a). Microglia maintain this surveying state due to receptor-ligand interactions with neurons, such as the neuronal CD200 and microglial CD200 receptor, as well as due to responses to molecules released from neurons, such as CX3CL1 that acts on microglial CX3CL1 receptors (Hanisch and Kettenmann, 2007). During development microglia shape neuronal circuits by pruning synapses, and facilitate the growth and development of surrounding neural networks by secreting neurotrophic factors such as brain-derived neurotrophic factor (BDNF), nerve growth factor (NGF) and insulin-like growth factor (IGF-1) (Nayak et al., 2015).

In response to potential danger to the CNS as well as various pro-inflammatory stimuli (such as lipopolysaccharide, LPS) microglia undergo a change in shape, gene expression and functional behaviour, passing from the surveying and ramified phenotype to an activated and more amoeboid phenotype within hours (Hanisch and Kettenmann, 2007). Microglia activation had previously been classified into two functional subtypes represented by the proinflammatory M1 state and the neuroprotective (anti-inflammatory) M2 state, however this over-simplified view has been challenged (Ransohoff, 2016; Benusa, George and Dupree, 2020). Pro-inflammatory activation is associated with the production and release of cytokines, such as tumour necrosis factor-α (TNF-α) and interleukin-1β (IL1β), as well as nitric oxide (NO) and reactive oxygen species (ROS), which enhance and stimulate the inflammatory response (Benarroch, 2005; Lull and Block, 2010). Microglia can also present antigens to cells of the adaptive immune system and attract immune cells by releasing chemokines such as CXCL10 (Hanisch and Kettenmann, 2007).

Microglia are the phagocytes of the brain and participate in remodelling of neuronal connectivity by engulfment of synapses, as well as axonal and myelin debris (Paolicelli *et al.*, 2011; Augusto-Oliveira *et al.*, 2019). The activity of microglial phagocytosis relies on specific receptors expressed on the cell surface and downstream signalling pathways that contribute to the reorganization of actin protein and the phagosome formation (Arcuri et al., 2017). Different types of receptors can initiate phagocytic function, including Toll-like receptors (TLRs) which have a high affinity to bind to foreign microbial pathogens as well as triggering receptor expressed on myeloid cells 2 (TREM2), which recognizes apoptotic cellular substances (Fu et al., 2014). Phagocytosis is regarded as beneficial for tissue homeostasis as microglia rapidly clear dying cells, preventing the increase of proinflammatory and neurotoxic molecules in the brain parenchyma (Green, Oguin and Martinez, 2016). Next to phagocytosis, other forms of endocytic uptake are important in microglia. Endocytic processes are involved in the internalization of

nutrients, antigen presentation, regulation of cell-surface receptor expression and other functions (Solé-Domènech *et al.*, 2016). After internalization of extracellular cargo molecules, these are recycled and modulated by the endosomal-lysosomal system. This system is composed of membrane-enclosed tubulo-vesicular structures: the early endosomes, recycling endosomes, late endosomes and finally the lysosomes, where the proteolytic degradation takes place (Hu *et al.*, 2015).

Immediately after cell damage in proximity to microglia, the microglia exhibit changes in Ca^{2+} transients. As in other cells, changes in the intracellular free Ca^{2+} concentration ($[Ca^{2+}]_i$) represent one of the major pathways for signal transduction in microglia (Inoue, 2002). These damage-induced Ca^{2+} transients occur on the millisecond-to-second time scale long before morphological changes are present (Seifert et al., 2011). The responsible signals are likely to be transduced by rapidly diffusible factors, such as adenosine triphosphate (ATP), which is released from injured neurons and nerve terminals (Negro *et al.*, 2016). Microglia possess functional receptors for purines and pyrimidines, including metabotropic (e.g. P2Y6, P2Y12) and ionotropic purinergic receptors (e.g. P2X7, P2X4) (Verkhratsky and Kettenmann, 1996). Honda et al. found that extracellular ATP and adenosine diphosphate (ADP) induced membrane ruffling and chemotaxis of rat primary cultured microglia (Honda *et al.*, 2001). Moreover, ATP induces the release of pro-inflammatory cytokines IL-1β, TNF-α and IL-6 from microglia (Hide *et al.*, 2000; Shigemoto-Mogami *et al.*, 2001; Chakfe *et al.*, 2002). Very strong and long stimulation by ATP may also change the function of microglia and cause cell death (Inoue, 2002).

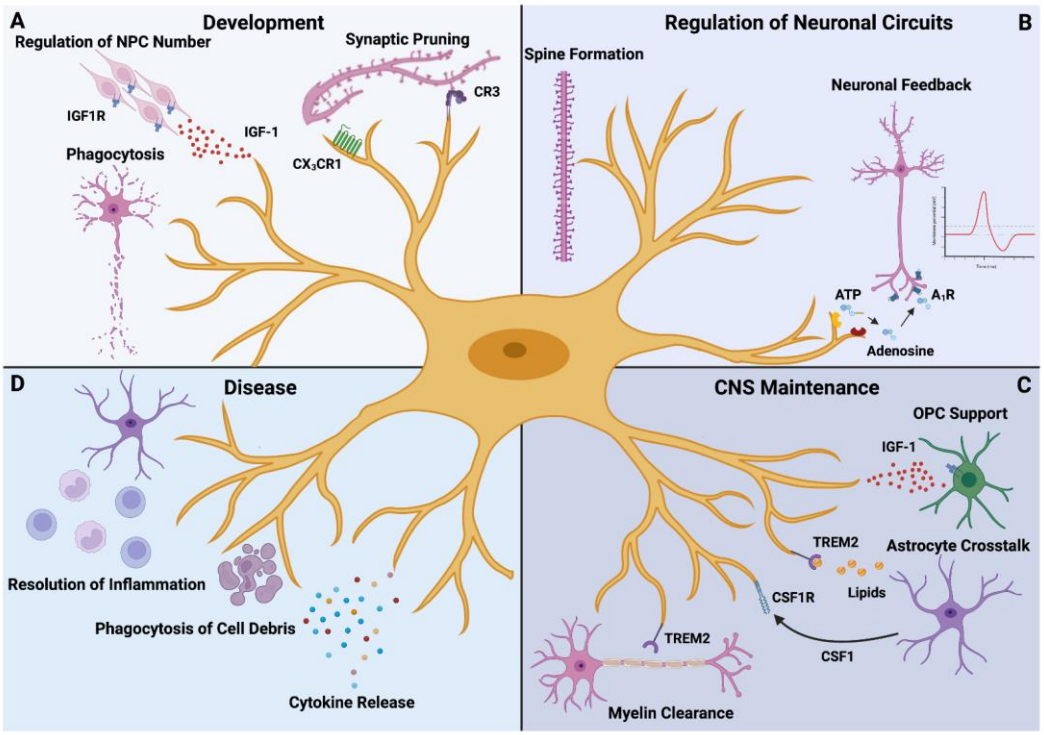

Figure 1.5: Functions of microglia in health and disease. (A) During development, microglia contribute to the regulation neuronal cell numbers by regulating NPC proliferation and removing redundant neurons through phagocytosis. They also participate in synaptic pruning. (B) Postnatally, microglia promote spine formation and can regulate neuronal activity. (C) Microglia interact with other cell types to maintain the CNS homeostasis. That includes crosstalk with oligodendrocytes and astrocytes. Microglia also clear myelin. (D) In disease, microglia secrete cytokines and phagocytose cell debris. Figure taken from Rosmus et al., 2022.

1.2.2 Astrocytes

Astrocytes are the most abundant glia cell type of the central nervous system. These star-shaped cells with many processes are essential for brain homeostasis and perform several different tasks to maintain and control healthy brain function (Sofroniew, 2009). Due to their strategic location in close contact with brain blood vessels, astrocytes participate in blood brain barrier maintenance and permeability (Colombo and Farina, 2016). Astrocytes also provide physical support to neurons, microglia and endothelial cells by forming a matrix-like structure, as well as provide these cells with factors necessary for their proper function (Chen and Swanson, 2003). Astrocytes exchange information with the synaptic neuronal elements, responding to synaptic activity and, in turn, regulating synaptic transmission. They limit the dispersion of neurotransmitters and with the release of glial transmitters such as glutamate, GABA, and ATP, astrocytes exhibit an active role in neuronal signalling (Sofroniew and Vinters, 2010). Astrocytes form broad cellular networks that can connect through gap junctions, which allow intercellular diffusion of ions, second messengers and small molecules. Astrocytic intercellular diffusion has been reported for cAMP, Ca^{2+}, glutamate, ATP and energy metabolites (Tabernero, Medina and Giaume, 2006). The uptake of glutamate from the synapse by astrocytes is particularly important as the prolonged exposure to excess glutamate can result in glutamate-mediated excitotoxicity (Bélanger and Magistretti, 2009).

Astrocytes are immune-competent cells that undergo a process called reactive astrogliosis in response to an insult to the brain (Zamanian *et al.*, 2012). Cytokines, growth factors and purines can activate astrocytes and intracellular signalling cascades that will lead to their transition into reactive states (Buffo, Rolando and Ceruti, 2010). Upregulation of the glial fibrillary acidic protein (GFAP), the main constituent of astrocyte intermediate filaments has most commonly been used as a hallmark of reactive astrocytes (Eng, Ghirnikar and Lee, 2000). In response to injury, a proportion of reactive astrocytes proliferate, increasing the number of astrocytes at the lesion site. Astrocytes become hypertrophic and upregulate GFAP, but they do not migrate towards the injury site (Bardehle *et al.*, 2013). Transcriptome analysis of reactive astrocytes showed many genes upregulated that have previously been implicated in the destruction of synapses. Reactive astrocytes are postulated to be induced through NF-κB signalling and are reported to be present in a number of neurodegenerative diseases including Alzheimer's disease

(AD), Parkinson's disease (PD), Amyotrophic lateral sclerosis (ALS), Multiple sclerosis (MS) and HD (Liddelow and Barres, 2017; Liddelow *et al.*, 2017).

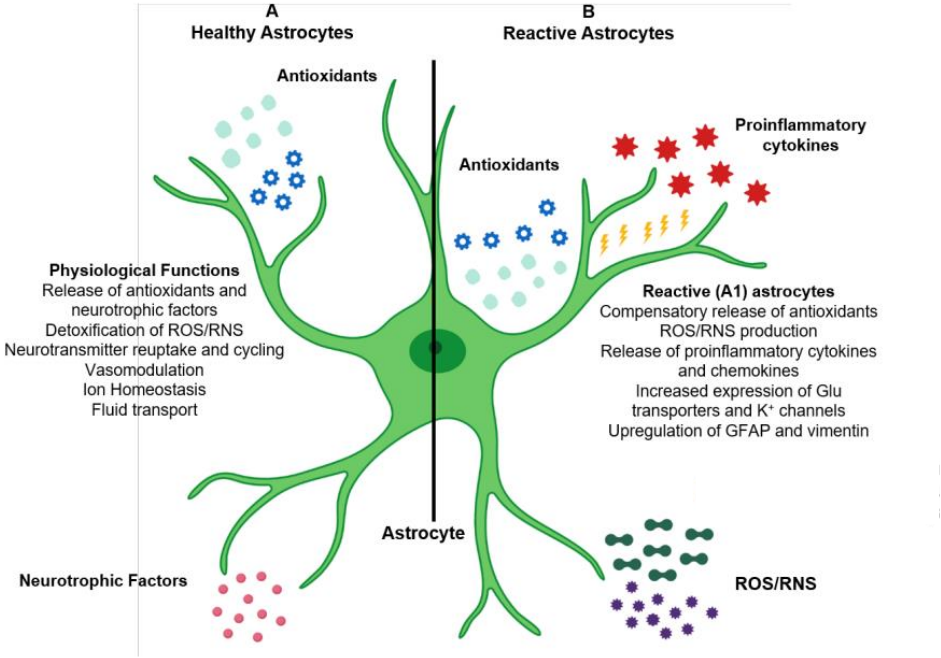

Figure 1.6: Functions of astrocytes in health and disease. (A) Astrocytes provide structural and metabolic support to neurons. They release antioxidants and neurotrophic factors and are responsible for detoxification of ROS and reactive nitrogen species (RNS). They are important for neurotransmitter reuptake and cycling, vasomodulation, ion homeostasis and fluid transport. (B) In disease, astrocytes become reactive. They secrete antioxidants, proinflammatory cytokines and chemokines as well as ROS/NOS. They upregulate GFAP and vimentin and show an increased expression of glutamate transporters and K^+ channels. Figure taken from Rizor et al., 2019.

1.2.3 Microglia-astrocyte crosstalk

Initially, the term "neuroinflammation" has been used to describe the infiltration of peripheral immune cells into the central nervous system. However, currently it is often used in relation to neurodegenerative diseases. Most neurodegenerative diseases, such as Alzheimer's disease (AD), Parkinson's disease (PD) and also HD are characterized by cellular and molecular features of inflammation in the brain (increased pro-inflammatory cytokine expression and glia activation), but immune cell infiltration from the blood stream only plays a minor role (Hensley, 2010; Samii, Nutt, & Ransom, 2004; Silvestroni et al., 2009). Nevertheless, the absence of immune cell infiltration from the periphery does not rule out a potential contribution of these cells to neuroinflammation, for example through chronic systemic pro-inflammatory cytokine production (Crotti and Glass, 2015).

In neurodegenerative diseases neuroinflammation is characterized by a reactive morphology of glial cells, including both astrocytes and microglia, as well as the presence of inflammatory mediators in the brain parenchyma (Masgrau et al., 2017; Ransohoff, 2016). Both microglia and

astrocytes become activated following detection of inflammatory stimuli and undergo morphological and transcriptional changes (Palpagama et al., 2019). Microglia-derived signals can further induce reactive astrocytes. IL1α, TNFα, and C1q, which were present after an LPS stimulation of microglia, induced reactive astrocytes (Zamanian *et al.*, 2012; Liddelow *et al.*, 2017). In contrast, TGFβ signalling from microglia to astrocytes reduced subacute neuroinflammation after stroke in mice (Cekanaviciute *et al.*, 2014; Cekanaviciute and Buckwalter, 2016). On the other hand reactive astrocytes highly express many complement components, cytokines, and chemokines that signal to microglia to regulate their immune functions (Liddelow and Barres, 2017).

1.2.4 The role of microglia in Huntington's disease

Positron emission tomography (PET) has been widely used in neuroscience research to investigate the pathophysiology of several neurological conditions including AD, PD and HD (Loane and Politis, 2011; Roussakis and Piccini, 2015; Schilling *et al.*, 2016). PET enables three-dimensional visualisation of biological compounds in tissues like the brain using specific radioligands. It has been believed that activated microglia can be visualized by a radioligand that binds to the translocator protein (TSPO), which was found to be highly expressed in activated microglia compared to homeostatic microglia in rodent models (Roussakis and Piccini, 2015). The use of TSPO PET for the study of neuroinflammation has recently been challenged, as it rather reflects density of inflammatory cells than activation state in humans (Owen et al., 2017; Nutma et al, 2022). Nonetheless, several PET studies have shown that microglia activation (or density) correlates with disease severity in HD patients (Pavese *et al.*, 2006; Politis *et al.*, 2011). This is evident in presymptomatic HD gene carriers, and can be detected up to 15 years before predicted age of onset (Tai *et al.*, 2007). These findings were confirmed by autopsy studies where activated microglia occurred in all grades of HD pathology and were found most prominent in regions that are affected in HD (striatum and cortex). Increased accumulation of activated microglia correlated with increased disease severity as well as with neuronal loss in affected regions (E. Sapp *et al.*, 2001). Singhrao et al. observed marked astrogliosis and microgliosis in post-mortem brains of HD patients, which were not found in control brains (Singhrao et al., 1999). They furthermore found that the complement components C3 and C9 were expressed by reactive microglia in HD and proposed that complement is produced locally by reactive microglia and is activated on the membranes of neurons, giving microglia an active role in inducing neuronal death (Singhrao et al., 1999).

Elevated levels of pro-inflammatory cytokines were also detected in HD patients and mouse models. Elevated levels of the pro-inflammatory cytokines IL-1β, IL-6, IL-8, and TNF-α were detected both centrally (in striatum and cerebrospinal fluid) and peripherally (in plasma) in HD

patients (Björkqvist *et al.*, 2008; Chang *et al.*, 2015; Rodrigues *et al.*, 2016). After pro-inflammatory stimulation with LPS, primary microglia from the HD R6/2 transgenic mouse model exhibited increased levels of IL-1β, IL-6, and TNF-α compared to control microglia (Björkqvist *et al.*, 2008; H. Hsiao *et al.*, 2014). In addition, higher levels of IL-1β and IL-8 were secreted by microglia in HD transgenic porcine model (Valekova *et al.*, 2016). Crotti et al. conducted genome-wide approaches and found that the expression of mutant *HTT* in primary mouse microglia promoted cell-autonomous pro-inflammatory transcriptional activation by increasing the expression and transcriptional activities of the myeloid lineage-determining factors PU.1 and CCAAT-enhancer-binding proteins (C/EBPs) (Crotti *et al.*, 2014). A recent study confirmed that microglia expressing mutant *HTT* showed significant elevations in NF-κB when stimulated with IL-6 but not when stimulated with LPS. This suggests that mHTT may alter immune responses in microglia in a stimuli dependent manner (Donley *et al.*, 2019).

In cortico-striatal brain slices and primary neuronal culture models, neuronal expression of mutant *HTT* was shown to initiate a local response of wild-type microglia, resulting in elevated cell numbers and morphological evidence of activation. Moreover, the addition of exogenous, primary wild-type microglia to mutant *HTT*-expressing neurons increased neuronal survival, and this effect was proportional to the amount of microglia added, suggesting that wild-type microglia can rescue HD neuronal phenotypes (Kraft *et al.*, 2012). However, the selective depletion of mutant *HTT* expression in myeloid lineage cells, including microglia, in the BACHD mouse model of HD lead to no significant rescue of any behavioural or neuropathological outcome measures (Petkau *et al.*, 2019). Conversely, when mutant *HTT* expression was depleted in the majority of the cells in the brain except for microglia, a significant rescue of body weight, rotarod performance and striatal volume was detected, indicating that mutant *HTT* expression in microglia only is not sufficient to cause HD phenotypes in the BACHD mouse model (Petkau *et al.*, 2019).

1.2.5 The role of astrocytes in Huntington's disease

Reactive astrocytosis is observed in HD brains and in the striatum of HD patients an increased number of GFAP positive reactive astrocytes correlated with the gradient of striatal neurodegeneration (Vonsattel *et al.*, 1985). Astrocytes of the cingulate cortex of HD patients showed enhanced staining for C3, a marker for neurotoxic astrocytes (Al-Dalahmah *et al.*, 2020). Transgenic mice expressing mutant *HTT* exclusively in astrocytes exhibit body weight loss, motor function deficits, and shorter lifespan compared with non-transgenic littermates. In these mice, reactive astrocytes were found to be accumulated in proximity to degenerated neurons and they exhibited increased proliferation and cell hypertrophy (Bradford *et al.*, 2009). Astrocyte morphology was affected in the R6/2 HD mouse model, where at 6 weeks of age, the R6/2

astrocytes showed a significant reduction in their cellular arborization relative to WT controls, which reduced further by 12 weeks of age (Benraiss *et al.*, 2016). Hsiao et al. found that in the Hdh150Q and R6/2 HD mouse models, aberrant activation of NF-κB signalling in astrocytes is associated with an enhanced inflammatory response in the brain. Primary R6/2 astrocytes were also found to be more susceptible to inflammatory stimulation by cytokines and LPS, and produced a more-damaging effect on primary R6/2 neurons than did WT astrocytes during inflammation (Hsiao et al., 2013). The expression of the glutamate transporter GLT1 was found to be lower in astrocytes from R6/2 mice compared to WT mice, and mHTT was demonstrated to suppress glutamate uptake in primary R6/2 astrocytes (Liévens *et al.*, 2001; Estrada-Sánchez and Rebec, 2012). These changes in glutamate uptake could contribute to neuronal excitotoxicity, a pathology observed in HD.

1.3 Induced pluripotent stem cells

1.3.1 Introduction to stem cells

Stem cells are unspecialized cells that can differentiate into any cell of an organism and have the ability of self-renewal. Stem cells can exist in both embryonic and adult tissue. Pluripotent stem cells (PSC) form cells of all germ layers, although they can not produce extraembryonic structures, such as the placenta (Zakrzewski, et al., 2019). Embryonic stem cells (ESC) are an example of PSC. In the late 1990s scientists were first able to isolate and culture human (h)ESC (Thomson, 1998), which provided new possibilities to model various human neurological diseases in culture, including HD (Feyeux *et al.*, 2012). However, the use of hESC is accompanied by ethical concerns regarding the use of embryonic tissue. In 2006, the discovery of induced pluripotent stem cells (iPSC) provided a more attractive and efficient way to model human diseases utilizing patient-derived stem cells without the previous ethical concerns (Takahashi and Yamanaka, 2006; Lo and Parham, 2009). The exogenous introduction of a cocktail of pluripotency-associated transcription factors such as OCT4, KLF4, SOX2 and c-MYC into terminally differentiated cells, primarily fibroblasts, was shown to be sufficient to reprogram them to a pluripotent state, indistinguishable from hESC (Takahashi & Yamanaka, 2006). iPSC have the advantages of limitless self-renewal and, in theory, they can be directed to become any somatic cell type. Moreover, they can be derived from patients in order to retain the patient's genetic background, and are accessible for gene editing (Bassett, 2017). Neurons are the most widely studied brain cells and protocols were developed to differentiate iPSC into different types of neurons, including cortical neurons (Qi et al., 2017; Shi et al., 2012) and MSN of the striatum (Lin et al., 2015; Reinhardt et al., 2013). While protocols for different neuronal cell types, as well as for astrocytes (Krencik et al., 2011; Shaltouki et al., 2013) were established early on and are now intensively studied and refined, the differentiation of microglia from iPSC was first

published only in 2016 (Muffat *et al.*, 2016). This might be attributed to the yolk sac endothelial origin of microglia, which was only discovered a few years beforehand (Ginhoux *et al.*, 2010). Since 2016, several protocols for generating microglia-like cells from iPSC have been published (Abud *et al.*, 2017; Haenseler *et al.*, 2017; Takata *et al.*, 2017), enabling the study of microglia in human culture systems. The possibility to derive different cell types of the brain creates the chance to combine cell types into various co-culture conditions, which are proven to generate a more physiological environment for the cells and can be used to study cell-cell interactions (Haenseler *et al.*, 2017; Luchena *et al.*, 2022).

1.3.2 The use of stem cells to study Huntington's disease

In order to investigate the molecular and cellular mechanisms of HD pathophysiology, many iPSC-based human HD cell models have been generated and utilized and commonly used lines are summarized in the table below:

Table 1-1: Human HD iPSC models. Adapted from (Kaye et al., 2022)

HD iPSC line	**CAG repeat length**	**Reference**
HD180i	180	Mattis et al., 2012
HD109i	109	Mattis et al., 2012
HD76	76	Vigont et al., 2021
CS77iHD-71	71	Szlachcic et al., 2015
HD70	70	Tidball et al., 2016
HD60i	60	Mattis et al., 2012
CS03iHD53	53	Lim et al., 2017
iPSHD22 iPSHD34 iPSHD11	47 42 40	Nekrasov et al., 2016
HD1 HD2	44 42	Mollica et al., 2018
CS13iHD-43	43	Lim et al., 2017

The HD109i iPSC lines used in this study were generated by the HD iPSC Consortium. They generated fourteen iPSC lines derived from fibroblasts originating from seven individuals which were healthy or affected by HD, representing cell models ranging from asymptomatic controls to HD models with varying CAG repeat numbers and disease severity (Mattis *et al.*, 2012). Most reported HD iPSC lines show that the *HTT* CAG repeat length remains stable during reprogramming, iPSC culture and differentiation (Zhang *et al.*, 2010; Camnasio *et al.*, 2012a). However, somatic expansion has been reported for the HD109i lines used in this study (Mattis *et al.*, 2012; Goold *et al.*, 2019; McAllister *et al.*, 2022). These lines are therefore an ideal tool to investigate CAG repeat expansions *in vitro*.

The HD iPSC Consortium demonstrated that neuronal stem cells (NSC) and neurons derived from HD iPSC exhibit decreased cytosolic ATP/ADP ratio, revealing that changes in energy metabolism may be an early component of HD. In addition, decreased cell adhesion, increased caspase-3 activation, and increased vulnerability to stress/toxicity were detected. Significantly, these disease-associated phenotypes correlated to CAG repeat number: more severe phenotypes were found in HD cells with longer CAG repeats (Mattis *et al.*, 2012). Moreover, studies by others using iPSC generated from HD patients have obtained novel findings into the mechanisms of HD. Proteomic analysis revealed hundreds of differential proteins expressed in HD iPSC as well as a reduction in neuronal differentiation efficiency and neurite length (Chae *et al.*, 2012). In another study (An *et al.*, 2012), restoration of the expanded CAG repeat to normal length through homologous recombination was able to restore distinct transcriptional changes in the E-cadherin and TGF-β signalling pathways to normal levels, prevent cell death, increase BDNF transcription, rescue mitochondrial dysfunction, and normalize the elevated caspase activity observed in the HD iPSC lines indicating that these alterations were directly induced by CAG expansion (Connor, 2018).

Furthermore, HD iPSC have been differentiated to astrocytes to investigate their role in HD pathology. HD iPSC derived astrocytes exhibited ultrastructural changes, namely cytoplasmic, electron clear vacuoles (Juopperi *et al.*, 2012). A similar vacuolation phenotype has previously been observed in peripheral blood lymphocytes from individuals with HD (Nagata *et al.*, 2004). Astrocytes derived from monkey iPSC expressing mutant *HTT* exhibited amongst others cytosolic mHTT aggregates and nuclear inclusions, as well as a reduced ability to uptake glutamate (Cho *et al.*, 2019). In co-culture, HD iPSC-derived astrocytes provided reduced support for the maturation of iPSC-derived neurons and when exposed to chronic glutamate stimulation, HD astrocytes were not able to protect these neurons (Garcia *et al.*, 2019). A recent paper reported that HD iPSC-derived astrocytes showed alterations in morphology, glutamate uptake and actin-mediated signalling (Reyes-Ortiz et al., 2022).

Even though protocols generating microglia from iPSC have been reported in the last few years and these cells were used for the study of neurodegenerative diseases (Haenseler and Rajendran, 2019), there have been no studies investigating the pathophysiology of microglia differentiated from HD patient-derived human iPSC. O'Regan et al. used an isogenic series of ESC which were genetically engineered to carry different CAG repeat sizes in the *HTT* gene, termed the IsoHD lines. These ESC were differentiated to a microglia phenotype, and it was shown that HD microglia produced elevated levels of cytokines in response to an immune challenge using LPS. Furthermore, the HD microglia produce elevated levels of reactive oxygen species, and their viability was affected in response to various forms of cellular stress. The

authors also used conditioned media from HD striatal neurons, which elevated apoptosis in the microglia undergoing cellular stress (O'Regan *et al.*, 2021).

1.4 Project aims

Microglia activation has been reported to take place in the pathology of HD, however, if this activation is exclusively due to mutant *HTT* expression in the microglia, a response to the detrimental HD brain environment, or a combination of both effects is currently unknown. Furthermore, despite the activated phenotype, it is not well understood if microglia show further dysregulation of their main functions in HD. Here, we investigate the hypothesis that HD microglia show cell-autonomous phenotypes using a stem cell model of HD and isogenic control iPSC. In addition, using a co-culture model of iPSC-derived astrocytes and microglia, we aimed to understand the interplay between glia cells in HD pathology.

In more detail, chapter 3 aimed to characterise HD and control iPSC-derived microglia, astrocytes and neurons. Co-culture models of microglia and astrocytes and neurons and astrocytes were established, and all three cell types were investigated for CAG repeat expansion in the *HTT* gene. Furthermore, mCherry expressing reporter cell lines were established in order to investigate microglia in co-culture with astrocytes. Chapter 4 aimed to characterise HD and control microglia-like cell morphology and function using a wide range of assays for key microglia functions as well as cellular compartments. Chapter 5 aimed to investigate gene expression changes in HD microglia-like cells using bulk RNA sequencing. Microglia were investigated in an unstimulated state and after pro-inflammatory stimulation. Chapter 6 aimed to investigate the influence of astrocytes on microglia in a co-culture model. Microglia morphology and phagocytosis were investigated in co-culture with astrocytes. In addition, microglia secreted factors and the secretome of microglia-astrocyte co-cultures were investigated using mass spectrometry.

2 Materials and Methods

2.1 Maintenance and culture of human-induced pluripotent stem cells

Human patient-derived iPSC from the HD iPSC Consortium (Mattis *et al.*, 2012) were used as a cellular HD model with 109 CAG repeats. Isogenic controls for these cells have been established using the CRISPR/Cas9 nuclease system together with a piggyBac transposon (PB) selection cassette-based homologous recombination donor which enabled a seamless correction of the expanded CAG repeat tract to a wild-type length of 22 repeats (Donaldson et al., unpublished). iPSC were maintained at 37°C in a humidified atmosphere containing 5% CO_2 and were cultured in feeder-free conditions on 6-well plates coated with Matrigel (50µg/ml) and in Essential 8 Flex medium (E8). The complete medium was changed every two days and cells were passaged at 80% confluency. For passaging, old medium was removed and cells were washed with PBS before incubation with ReLeSR for 3-5 min at room temperature. ReLeSR was removed by aspiration and fresh E8 added. The plate was gently tapped to allow detachment of colonies. Cells were centrifuged for 3 min at 1000 rpm and resuspended in E8 and replated in fresh Matrigel-coated wells.

Table 2-1: iPSC media and supplements

Consumable	**Company**	**Catalogue Number**
Essential E8 Flex medium kit	Life Technologies	A2858501
Matrigel Growth Factor Reduced Basement Membrane Matrix	Corning	354230
PBS pH 7.4 without $CaCl_2$ and $MgCl_2$	Gibco	10010-023
ReLeSR	Stem Cell Technologies	05873

2.2 CNV array

2.2.1 DNA extraction

For SNP array, DNA was extracted using the QIAamp DNA Mini Kit (Quiagen, # 51304) following manufacturer's instructions. DNA was eluted in 100 µl of nuclease-free water and kept at -20°C.

2.2.2 Illumina Global Screening Array v2.0

Copy number variation (CNV) assay was carried out by Alexandra Evans at the Medical Research Centre (MRC) at Hadyn Ellis Building, Cardiff University. 200 ng (50 ng/ul) DNA was genotyped on the Illumina Global Screening Array v2.0. The samples were analysed alongside approx. 500 additional samples using PennCNV with GRCh37 / hg19 as a reference genome. The additional samples acted as controls for the CNV calling procedure, minimising bias caused by similar samples. CNV detected in this analysis were limited to the regions identified by PennCNV as

containing large (>100kb and spanning >10 SNPs) CNV that were subsequently confirmed by visual inspection of the LRR/BAF traces.

2.3 Generation of reporter cell lines using CRISPR/Cas9 technology

2.3.1 Nucleofection

The CRISPR/Cas9 system was utilized to introduce a mCherry fluorescent reporter into the AAVS1 genomic locus of the iPSC. Prior to transfection, iPSC were incubated in E8 containing 10 µM ROCK inhibitor (RI, Y-27632) for 1 h and the ribonucleoprotein (RNP) complex was prepared. Guide RNA (gRNA) and trans-activating RNA (tracrRNA) were combined in equimolar concentration in nuclease-free duplex buffer and annealed at 95°C for 2 min. The mix was incubated with Cas9 nuclease (6.2 µg/µl diluted in Cas9 storage buffer: 10 mM Tris-HCl, pH 7.4, 300 mM NaCl, 0.1 mM EDTA, 1mM DTT) for 20 min at room temperature. Cells were washed with PBS and a single cell suspension created using Accutase cell dissociation reagent for 10 min at 37°C. Cells were counted and 200.000 cells resuspended in 20 µl P3 medium. The Amaxa P3 Primary Cell 4D-Nucleofector X Kit S was used in order to transfect the cells. RNP/Cas9 complex, the reporter vector as well as cells were added to the cuvette and gently mixed. The Amaxa 4D-Nucleofector was used according to the manufacturers protocol using program CA137. Cells were allowed to recover for about 10 min after the nucleofection and then distributed into a Matrigel-coated 12 cm dish in E8 supplemented with 10 µM RI and 1% Pen/Strep. On the following day medium was changed to E8 / 1% Pen/Strep and single cells were left growing with medium changes every other day.

Table 2-2: Consumables for generation of cell lines

Consumable	**Company**	**Catalogue Number**
Alt-R® S.p. HiFi Cas9 Nuclease V3	IDT	1081061
Nuclease-Free Duplex buffer	IDT	1072570
P3 Primary Cell 4D-Nucleofector TM X Kit S	Lonza	V4XP-3032
Penicilin/Streptomycin	Gibco	15070063
Puromycin	Gibco	A11138-03
QuickExtract DNA Extraction Solution	Cambio	QE0905T
ROCK inhibitor, Y-27632	Tocris	1254
StemPro Accutase Cell Dissociation Reagent	Life Technologies	A1110501
tracrRNA	IDT	107528

2.3.2 Selection

The transfected vector included (beside the reporter) a puromycin resistance gene, so that successfully transfected cells survived incubation with the antibiotic puromycin. As soon as single cells were grown into colonies, cells were incubated with 0.35 µM puromycin in E8 for 3 days, followed by an incubation in 0.5 µM Puromycin in E8 for a minimum of 5 days. Remaining cell colonies were picked into 96-well plates and when confluent imaged using the IncuCyte S3 live cell imaging system to detect fluorescent expression of the reporter. 96-well plates were duplicated, and DNA collected as described below, in order to conduct a PCR for the right integration of the reporter, as well as for the AAVS1 wild type allele.

2.3.3 DNA extraction

iPSC were grown to 90-100% confluency in 96-well plates and DNA extracted using QuickExtract DNA Extraction Solution (Cambio, #QE0905T). Medium was removed, 50 µl extraction solution added and the plate put on a shaker for 10 min. Cells were scratched from the bottom of the well and the solution transferred to PCR tubes. Solution was incubated at 65°C for 6 min, followed by 98°C for 2 min. The DNA was stored at -20°C until further used.

2.3.4 Polymerase chain reaction

Polymerase chain reaction (PCR) was conducted in order to identify the right integration of the reporter, as well as the AAVS1 wild type allele. Homozygous inserts of the reporter into both alleles of the AAVS1 locus showed no band for the AASV1 wild type allele and were selected for a strong expression of the reporter. Following primers were used:

Table 2-3: CRISPR screening primers

Gene	**Forward primer 5'-3'**	**Reverse primer 5'-3'**
AAVS1 Insert	CGGTTAATGTGGCTC	AGGATCCTCTCTGGC
WT AAVS1	CTGCCGTCTCTCTCCTGAGT	GTGGGCTTGTACTCGGTCAT

The PCR mix contained the following: 1x Reaction Buffer, 1 mM $MgCl_2$, 200 µM dNTPs, 0.4 µM of forward and reverse primer, 2% DMSO, 50 ng DNA sample and GoTag polymerase. The BioRad T100 Thermal Cycler was run with following conditions: 95°C for 2 min, 30 cycles of: 95°C for 30 s, 61.1°C for 30 s, 72°C for 30 s, followed by 72°C for 5 min. The PCR product was run on an 1% agarose gel at 80 V for 45 min containing SafeView nucleic acid stain. For the insert PCR the 1 kb ladder and for the WT PCR the 100 bp ladder was used.

Table 2-4: PCR consumables

Reagent	Company	Catalogue Number
1 kb DNA ladder	Promega	G5711
100 bp DNA ladder	Promega	G2101
DMSO	Sigma	276855
GoTaq Master Mix	Promega	M7122
SafeView nucleic acid stain	NBS Biologicals	NBS-SV1

2.4 Differentiation of iPSC

Table 2-5: Cell culture base media

Medium	Company	Catalogue Number
Advanced DMEM/F-12	Life Technologies	12634028
BrainPhys Neuronal Medium	Stem Cell Technologies	05790
DMEM/F-12	Life Technologies	11320033
Essential E8 Flex medium kit	Life Technologies	A2858501
Knockout DMEM/F-12	Life Technologies	12660012
Neurobasal MED SFM	Life Technologies	21103049
XVIVO-15	Lonza	BE02-060F

Table 2-6: Cell culture supplements

Medium	Company	Catalogue Number
Glutamax	Gibco	25030081
MACS NeuroBrew-21	Miltenyi Biotec	130-093-566
MACS NeuroBrew-21 (w/o Vit.A)	Miltenyi Biotec	130-097-263
N2 Supplement	Gibco	17502-048
Penicilin/Streptomycin	Gibco	15070063

Table 2-7: Coatings

Reagent	Company	Catalogue Number
Human Fibronectin protein	Merck Millipore	FC010-10MG
Matrigel Growth Factor Reduced Basement Membrane Matrix	Corning	354230
Poly-D-Lysine hyrobromide	Sigma-Aldrich	P6407

2.4.1 Directed differentiation of iPSC into microglia-like cells

iPSC were differentiated to macrophage precursor cells using a protocol adapted from Haenseler et al., 2017. iPSC were grown to approximately 70% confluency and were treated with Rock Inhibitor (RI) 1 h before starting. In order to generate embryoid bodies, iPSC were dissociated using Accutase for 10 min at 37°C, then collected in medium and pelleted for 3 min at 1000 rpm. Cells were resuspended in 1 ml EB differentiation medium and counted with the aim to achieve a final concentration of 10^4 cells/100 µl to be put into one well of a low adherence 96-well plate. Cells were distributed into the 96 well plate, centrifuged at 140 g for 3 min and gently transferred

to a tissue culture incubator at 37°C with 5% CO_2. Cells were incubated for 4 days with minimal disturbance, including a 50% medium change of the EB differentiation medium on day 2.

On D4, embryoid bodies were collected from the 96-well plate and 8 EBs transferred to one well of a 6-well plate containing 3 ml of myeloid differentiation medium. Two-thirds of the medium was changed every 5-7 days. After approximately 25 days, microglia precursor cells (MPC) were harvested once per week for the microglia differentiation.

Non-adherent MPC were collected, centrifuged for 3 min at 1000 rpm and resuspended in astrocyte-conditioned media. Cells were counted in a hemocytometer and plated at desired density into human fibronectin-coated (5µg/ml) plates. Glass coverslips and plates with glass bottom were coated with poly-D-lysine (100µg/ml) prior to the fibronectin-coating. Cells were cultured in astrocyte-conditioned media for 12-14 days with a full medium change after one week.

Table 2-8: Microglia differentiation media

Name	Days	Base medium	Supplements
EB differentiation medium	D0 - D4	Essential E8 medium	10 µM Y-27632 (RI), 50 ng/ml BMP4, 50 ng/ml $VEGF_{121}$, 50 ng/ml SCF
Myeloid differentiation medium	D4 onwards	X-VIVO15	1% Pen/Strep, 1% Glutamax, 50 nM β-mercaptoethanol, 50 ng/ml M-CSF, 50 ng/ml IL-3
Astrocyte-conditioned medium	D0 - 14 of terminal differentiation	Advanced DMEM-F12 (ADF)	50% ADF + 1% PenStrep, 1% Glutamax, 2% Neurobrew with Vit.A conditioned over astrocytes for 48 h; 50% ADF + 1% PenStrep, 1% Glutamax + 2% N2 supplement

Table 2-9: Growth factors for microglia differentiation

Growth factor	Company	Catalogue Number
BMP-4	Peprotech	120-05ET
IL-3	Peprotech	200-03
M-CSF	Peprotech	300-25
SCF	Peprotech	300-07
$VEGF_{121}$	Peprotech	100-20A

2.4.2 Directed differentiation of iPSC into cortical neurons

iPSC were differentiated to neuronal precursor cells using a protocol adapted from Shi et al 2012. One day prior to the differentiation, iPSC were dissociated into single cells using Accutase for 10 min at 37°C, collected in medium and centrifuged for 3 min at 1000 rpm. Single cells were plated into Matrigel-coated (100µg/ml) 12-well plates into a confluent layer. The next day, cells were

washed with PBS and cells were maintained in SLI for 8 days, with medium changes every day. On day 8, cells were treated with RI 1 h prior to starting, dissociated into single cells using Accutase for 10 min at 37°C and split 1:4 into a new 12-well plate coated with Matrigel (100µg/ml) using NB medium with RI. The next day, RI was taken off and medium changed every day until day 16. From day 14-16 20 µM plurisin was added to the medium if needed to kill remaining iPSC. On day 16, differentiated NPC were either frozen or expanded for terminal differentiation. Cells were incubated in NB medium + pluricin for approximately 2 days, following by incubation in NF medium for up to 7 days for proliferation.

Table 2-10: Neuronal precursor differentiation media

Name	Days	Base medium	Supplements
SLI	D1 - D8	Advanced DMEM-F12	1% PenStrep, 1% Glutamax, 1% Neurobrew (w/o) Vit.A, 10 µM SB, 200 nM LDN, 1.5 µM IWR
NB	D8 - D16	Advanced DMEM-F12	1% PenStrep, 1% Glutamax, 2% Neurobrew (w/o) Vit.A
NF	D16 +	Advanced DMEM-F12	1% PenStrep, 1% Glutamax, 2% Neurobrew with Vit.A, 20 ng/ml FGF

For terminal differentiation, NPC were plated in Matrigel- (100 µg/ml) coated plates. One hour before plating, NPC were treated with RI and cells were dissociated using Accutase in order to produce a single cell suspension. Cells were incubated in SJA + RI overnight, followed by incubation in SJA for one week with half medium changes every other day. On day 7, medium was changed to SJB and half medium changed were conducted every other day for two weeks. Experiments were conducted on day 21 of terminal differentiation.

Table 2-11: Cortical neuron differentiation media

Name	Days	Base medium	Supplements
SJA	D0 - D7	Advanced DMEM-F12	1% PenStrep, 1% Glutamax, 2% Neurobrew with Vit.A, 2 µM PD0332991, 10 µM DAPT, 10 ng/ml BDNF, 10 µM Forskolin, 3 µM CHIR99021, 200 uM Ascorbic Acid, 0.8 µM $CaCl_2$, 300 µM GABA
SJB	D7 - D21	50% Neurobasal A, 50% ACM	1% PenStrep, 1% Glutamax, 1% Neurobrew with Vit.A, 2 µM PD0332991, 200 mM Ascorbic Acid, 0.4 mM $CaCl_2$

Table 2-12: Growth factors for neuronal differentiation

Growth factor	Company	Catalogue Number
Ascorbic Acid	HelloBio	HB1238
BDNF	Miltenyi Biotec	130-93-811
$CaCl_2$	Sigma	21115
CHIR99021	HelloBio	HB1262

DAPT	HelloBio	HB3345
FGF	Peprotech	100-18B
GABA	HelloBio	HB0882
IWR-1-endo	Miltenyi	130-110-491
LDN193189	HelloBio	HB5624
PD0332991	Tocris	4786
Pluricin	Stem Cell Technology	72822
SB431542	HelloBio	HB3555
Forskolin	HelloBio	HB1348

2.4.3 Directed differentiation of NPC into astrocytes

Astrocytes were differentiated as indicated in Serio et al., 2013. iPSC were differentiated to neuronal precursors (NPC) and frozen at day 16 as indicated before. 6 Mio. NPC were thawed into a Matrigel- (50 µg/ml) coated T25 using NB medium supplemented with 20 µM plurisin. After 2 days, medium was changed to NF and cell were proliferated until confluent. Cells were then expanded for 3 passages in NEL medium using T25 flasks, splitting cells 1:5 when confluent. After expansion, cells were sorted for the astrocyte progenitor marker CD44 (Milteny, #130-113-896) using FACS. Cells were dissociated using Accutase for 10 min at 37°C and centrifuged at 1000rpm for 3 min. 10^6 cells were counted and resuspended in 98 µl NEF. 2 µl of the antibody or the isotype control were added and incubated for 10 min on ice. Cells were washed 1x with NEF and resuspended in 500 µl NEF. Cells were sorted using the FACS ARIA Fusion by using the isotype control for appropriate gating. The top positive cells were collected and replated into Matrigel (50µg/ml) coated 6-well plates for proliferation in NEF medium. Astrocyte precursor cells were proliferated until they filled a T75 and were subsequently frozen.

Table 2-13: Astrocyte precursor differentiation media

Name	**Days**	**Base medium**	**Supplements**
NB	D0 - D2	Advanced DMEM-F12	1% PenStrep, 1% Glutamax, 2% Neurobrew (w/o) Vit.A
NF	D2 - ~D9	Advanced DMEM-F12	1% PenStrep, 1% Glutamax, 2% Neurobrew with Vit.A, 20 ng/ml FGF
NEL	~D9 - ~D24	Advanced DMEM-F12	1% PenStrep, 1% Glutamax, 2% Neurobrew with Vit.A, 20 ng/ml EGT, 20 ng/ml LIF
NEF	~D24 +	Advanced DMEM-F12	1% PenStrep, 1% Glutamax, 2% Neurobrew with Vit.A, 20 ng/ml EGT, 20 ng/ml FGF

2.4.4 Preparation of astrocyte-conditioned medium

Terminally differentiated astrocytes were maintained in FBS medium with medium changes once per week. For ACM collection, ACM collection medium was conditioned on the astrocytes for 48 h. The collected media were pooled, sterile filtered and frozen down at -80°C until further

used. Each batch was tested with a CCL2 ELISA (Biotechne, #DCP00), which was used as a housekeeping reference for the amount of protein / sample. All batches were diluted down to a CCL2 concentration of 2 ng/ml (final microglia monoculture ACM concentration: 1 ng/ml).

2.4.5 Microglia - Astrocyte co-culture

Non-adherent macrophage precursors and APC were differentiated from iPSC as indicated before. APC were plated at around 70% density on Matrigel-coated (50 µg/ml) plates and were terminally differentiated for 2 weeks using CNTF medium. Non-adherent macrophage precursors were added to the terminal differentiated astrocytes in a ratio of 1:10 for differentiation to microglia for 14 days. During the first week of co-culture the medium was topped up, so that microglia could settle onto the astrocytes. After day 7, half medium changes were conducted every 3-4 days.

Table 2-14: Microglia-Astrocyte co-culture medium

Name	**Base medium**	**Supplements**
Microglia-Astrocyte co-culture medium	Advanced DMEM-F12	1% PenStrep, 1% Glutamax, 1% Neurobrew with Vit.A, 1% N2 supplement, 1µg/ml fibronectin (first week only)

2.4.6 Neuron - Astrocyte co-culture

NPC and APC were differentiated from iPSC as indicated before. APC were plated at around 70% density on Matrigel-coated (50 µg/ml) plates and were terminally differentiated for 2 weeks using CNTF medium. NPC were added to terminally differentiated astrocytes in a ratio of 5:1 for differentiation to neurons. Co-culture SJA was fed for the first seven days and from day 7 onwards co-culture SJB was used. Medium was changed every 3-4 days.

Table 2-15: Neuron-Astrocyte co-culture medium

Name	**Days**	**Base medium**	**Supplements**
Co-culture SJA (without DAPT)	D0 - D3	Advanced DMEM-F12	1% PenStrep, 1% Glutamax, 2% Neurobrew with Vit.A, 2 µM PD0332991, 10 ng/ml BDNF, 10 µM Forskolin, 200 uM Ascorbic Acid, 0.8 µM $CaCl_2$, 300 µM GABA
Co-culture SJA	D3 - D7	Advanced DMEM-F12	1% PenStrep, 1% Glutamax, 2% Neurobrew with Vit.A, 2 µM PD0332991, 10 µM DAPT, 10 ng/ml BDNF, 10 µM Forskolin, 200 uM Ascorbic Acid, 0.8 µM $CaCl_2$, 300 µM GABA
Co-culture SJB	D7 +	50% Brainphys, 50% Advanced DMEM-F12	1% PenStrep, 1% Glutamax, 1% Neurobrew with Vit.A, 2 µM PD0332991, 200 mM Ascorbic Acid, 0.4 mM $CaCl_2$

2.5 Cell characterisation by flow cytometry

Flow cytometry was performed to analyse the myeloid cell surface markers CD11b, CD14 and CD45 as well as the hematogenic surface marker CD34 using the non-adherent microglia precursor cells collected after day 25 of the differentiation protocol. Cells were collected and counted for 50.000 cells / staining. Cells were blocked using 1% FBS in PBS for 30 min at room temperature and subsequently stained with either the antibody or isotype control in 1% FBS in PBS for 30 min on ice. Cells were washed with 1% FBS in PBS for 3 times and then fixed for 10 min using 4% paraformaldehyde (PFA). Cells were washed one more time in PBS, resuspended in 100 µl PBS and transferred to round bottom tubes. Fluorescence was measured using a LSR Fortessa (BD Biosciences) and data analysed using the FlowJo software (BD Biosciences).

Table 2-16: Flow antibodies

Antibody	Clone	Isotype Control	Supplier	Catalogue Numbers
CD11b-APC	ICRF44	Mouse IgG1, κ	Biolegend	301309 / 400119
CD14-APC	61D3	Mouse IgG1, κ	Invitrogen	17-0149-42 / 17-4714-42
CD34-PeCy7	4H11	Mouse IgG1, κ	Invitrogen	25-0349-42 / 25-4714-80
CD45-FITC	HI30	Mouse IgG1, κ	Biolegend	304005 / 400307

2.6 Immunocytochemistry

Table 2-17: General immunocytochemistry items

Item	Company	Catalogue Number
Bovine Serum Albumin	Sigma	A3156
Chicken serum	Sigma	C5405
Goat serum	Sigma	G9023
Hoechst 33342	Thermo Scientific	10150888
Paraformaldehyde	Sigma	P6148
PBS pH 7.4 without $CaCl_2$ and $MgCl_2$	Gibco	10010-023

2.6.1 Fixation of cells

Cells were washed with PBS and fixed with 4% paraformaldehyde for 10 min at room temperature. Cells were washed three times with PBS and plates subsequently left tightly wrapped on 4°C until further used.

2.6.2 Immunocytochemistry

Fixed cells were incubated in blocking buffer (3% BSA, 3% serum in PBS) for 1 hour at room temperature, followed by incubation in primary antibody (diluted in blocking buffer) over night at 4˚C. Cells were washed 3 times for 5 min with PBS, followed by incubation in the secondary antibody (diluted in blocking buffer) for 1 h at room temperature. Cells were again washed 3

times for 5 min with PBS and incubated with Hoechst 33342 (1:5000 in blocking buffer) for 10 min at room temperature. Cells were washed 3 times for 5 min with PBS and when plated in black 96-well plates stored at 4˚C in the last wash until imaged. Images were taken at the Opera Phenix High Content Imaging System (PerkinElmer). When cells were plated onto coverslips, coverslips were mounted to glass slides after the last wash using mounting medium and sealed with nail polish. Slides were dried at room temperature overnight and stored at 4˚C until imaged using the Zeiss Cell Observer spinning disc confocal.

Table 2-18: Primary antibodies for ICC

Antibody	Host	Dilution	Supplier	Catalogue Number
CD11b	Rat	1:50	Abcam	AB8878
CD45	Mouse	1:100	R&D Systems	MAB1430
CD49f	Rat	1:500	Biolegend	313602
EAAT1	Rabbit	1:100	Alomone labs	AGC-021
GFAP	Mouse	1:400	Sigma	G3893
IBA1	Goat	1:100	Abcam	AB5076
MAP2	Rabbit	1:100	Abcam	AB32454
NESTIN	Mouse	1:200	Sigma	MAB5326
NFIA (PCRP-NFIA-1B8)	Mouse	1:6	DSHB	AB_2618884
SOX2	Rabbit	1:100	Millipore	AB5603
TMEM119	Rabbit	1:100	Abcam	AB185333
TUBB3	Mouse	1:400	Sigma	T8660
VIM	Goat	1:50	Abcam	AB1620

Table 2-19: Secondary antibodies for ICC

Antibody	Host	Wavelength	Dilution	Supplier	Catalogue number
goat	chicken	488	1:400	Invitrogen	A-21467
goat	chicken	594	1:400	Invitrogen	A-21468
mouse	chicken	594	1:400	Invitrogen	A-21201
mouse	goat	488	1:400	Invitrogen	A-11001
mouse	goat	594	1:400	Invitrogen	A-11005
rabbit	chicken	488	1:400	Invitrogen	A-21441
rabbit	goat	488	1:400	Invitrogen	A-11008
rat	goat	594	1:400	Invitrogen	A-11007

2.7 CAG repeat expansion assay

Genomic DNA was isolated from cells using the QuickExtract DNA Extraction Solution following manufacturer's instructions. Exon 1 of the HTT gene containing the CAG repeat was amplified using a fluorescently labelled (FAM) forward primer together with a reverse primer.

Table 2-20: Primers used for HTT CAG repeat amplification

Primer	Sequence
FAM hu HTT exon 1F	FAM-atgaaggccttcgagtccctcaagtccttc
Hu HTT 1R-4	ggcggctgaggaagctgagga

The PCR of the HTT CAG repeat was performed using LA Taq DNA polymerase with GC1 buffer, which is ideal for amplification of GC-rich regions. The PCR mix contained the following: 1x GC1 Buffer, 400 µM dNTPs, 0.5 µM of forward and reverse primer, 10 ng DNA sample and LA Taq DNA polymerase. The BioRad T100 Thermal Cycler was run with following conditions: 94°C for 1:30 min, 35 cycles of: 94°C for 30 s, 65°C for 30 s, 72°C for 1:30 min, followed by 72°C for 10 min. PCR products (0.5 µl) were mixed in non-skirted 96-well PCR plates with Hi-Di Formamide (9.1 µl) and a GeneScan-600 LIZ size standard (0.4 µl) for capillary electrophoresis. Reactions were centrifuged and denatured at 95°C for 4 min, followed by 4°C for 3 min. Samples were run on the GA3130xL Genetic Analyser (Applied Biosystems). Files were analysed using GeneMapper, Fragman (Covarrubias-Pazaran et al., 2016) and AutoGenescan (https://github.com/BranduffMcli/AutoGenescan) and quantification was performed with a 10% peak height threshold applied (Lee *et al.*, 2010).

Table 2-21: CAG repeat expansion consumables

Reagent	Company	Catalogue Number
GeneScan-600 LIZ size standard	Applied Biosystems	4408399
Hi-Di Formamide	Applied Biosystems	4311320
LA Taq PCR Mix	TaKaRa	RR002M

2.8 Functional analysis of microglia-like cells

Table 2-22: Assays and inhibitors

Consumable	Company	Catalogue Number
Bafilomycin A1	Bio-Techne	1334
Cytochalasin D	Bio-Techne	1233/1
CYTO-ID	Enzo	ENZ-5103
DQ™ Green BSA	Invitrogen	D12050
Dynasore	Bio-Techne	2897/10
Human Inflammatory Cytokine Cytometric Bead Array	BD Biosciences	551811
pHrodo™ Green Dextran	Invitrogen	P35368
pHrodo™ Red E. coli BioParticles™ Conjugate for Phagocytosis	Invitrogen	P35361
pHrodo™ Red Transferrin Conjugate	Invitrogen	P35376

pHrodo™ Red Zymosan Bioparticles™ Conjugate for Phagocytosis	Invitrogen	P35364
PP242	Bio-Techne	4257
Seahorse XF Cell Mito Stress Test Kit	Agilent	103015-100

Table 2-23: Stains

Consumable	**Company**	**Catalogue Number**
CellTracker™ Deep Red Dye	Life Technologies	C34565
LysoTracker™ Green DND-26	Invitrogen	L7526
NucBlue™ Live ReadyProbes™ Reagent (Hoechst 33342)	Invitrogen	R37605
Phalloidin-iFluor 555 Reagent	Abcam	ab176756

2.8.1 Microglia precursor cell spreading assay

Microglia precursor cell spreading was analysed by a time course, where the cells were fixed 15 min, 60 min and 120 min after plating onto fibronectin-coated black 96-well imaging plates. Cells were fixed for 10 min using 4% PFA, followed by 3 washes with PBS. Cells were permeabilized for 3 min with 0.1% Triton X-100 in PBS. After 2 washes with PBS, cells were stained with Phalloidin-iFluor 555 and Hoechst for 90 min in 1% BSA in PBS. Cells were washed 2 times with PBS and imaged at the Opera Phenix High-Content Screening System. Images were taken at 40x magnification. The Harmony software was used for image analysis and "Cell Roundness" chosen as the output measure.

2.8.2 Microglia morphology analysis

Microglia precursor cells were plated onto fibronectin-coated black 96-well imaging plates and fixed after 14 days of differentiation in ACM with and without pro-inflammatory stimulation with IFN-γ and LPS. Microglia-like cells were permeabilized for 3 min with 0.1% Triton X-100 in PBS. After 2 washes with PBS, cells were stained with Phalloidin-iFluor 555 and Hoechst for 90 min in 1% BSA in PBS. Cells were washed 2 times with PBS and imaged at the Opera Phenix High-Content Screening System. Images were taken at 40x magnification. The Harmony software was used for image analysis and "Cell Area" and "Cell Roundness" chosen as the output measure.

2.8.3 LysoTracker live staining

Microglia precursor cells were plated onto fibronectin-coated black 96-well imaging plates and differentiated to microglia-like cells for 14 with and without pro-inflammatory stimulation with IFN-γ and LPS. Microglia-like cells were stained for LysoTracker Green (200 nM) together with CellTracker Deep Red and the nuclear stain NuncBlue for 20 min at 37˚C. Cells were washed once with live cell imaging buffer. Plates were directly transferred to the Opera Phenix High Content Screening System with temperature set to 37˚C and CO_2 to 5% and cells were imaged at 40x magnification. Harmony software was used to analyse the images using the output measures "Intensity", "Number of Spots", "Total Spot Area" and "Individual Spot Area". Furthermore, a perinuclear region was defined and the percentage of "Number of Spots" within the perinuclear region compared to the whole cytosol was calculated.

2.8.4 CYTO-ID autophagy detection

The CYTO-ID kit was used for selectively staining of autophagic vesicles. Microglia precursor cells were plated into fibronectin-coated black 96-well imaging plates and differentiated to microglia for 14 days. 24 hours prior to the assay, microglia were either stimulated with IFN-γ and LPS or with 30 µM of the rapamycin analogue PP242, that was used to induce autophagy. Cells were stained according to manufactures protocol. 100 µl Microscopy Dual Detection Reagent, consisting of CYTO-ID Green Detection Reagent and Hoechst 33342 nuclear stain, together with CellTracker Far Red, were added to each well and cells were incubator at 37˚C for 30 minutes. After one wash with assay buffer, cells were imaged at the Opera Phenix High-Content Screening System with temperature set to 37˚C and CO_2 to 5% at 40x magnification. Harmony software was used to analyse the following output measures: "Intensity", "Number of Spots", "Total Spot Area" and "Individual Spot Area".

2.8.5 DQ Green BSA

The DQ Green BSA, a derivate of bovine serum albumin, was used to study proteolytic activity. The dye is strongly self-quenching and dequenching occurs with the proteolysis of the BSA conjugate. Bafilomycin A1, a potent inhibitor of cellular autophagy, was used to inhibit proteolytic activity. Microglia precursor cells were plated into fibronectin-coated black 96-well imaging plates and differentiated to microglia for 14 days. 24 hours prior to the assay, microglia were stimulated with IFN-γ and LPS. Cells were incubated with 1 µM Bafilomycin, together with CellTracker Far Red and NuncBlue for 1 hour at 37˚C. Cells were washed once and 10 µg/ml DQ Green BSA was added for 2 hours. The Opera Phenix High-Content Screening System with

temperature set to 37˚C and CO_2 to 5% was used to image the cells live at 40x magnification. Harmony software was used to analyse “Intensity”, “Number of Spots”, “Total Spot Area” and “Individual Spot Area”.

2.8.6 Phagocytosis and endocytosis assays

pH-sensitive pHrodo dyes conjugated to particles enable the study of microglial phagocytosis and endocytosis activity. The fluorescence of these dyes increases in acidic cell compartments, like the phagosome and lysosome, so that phagocytosis and endocytosis activity can be measured over time via the occurrence of fluorescent particles. Microglia precursor cells were plated into fibronectin-coated black 96-well imaging plates and differentiated to microglia for 14 days. 24 hours prior to the assay, microglia-like cells were stimulated with IFN-γ and LPS. To study phagocytosis, 50 µg/ml pHrodo Red Zymosan conjugate and 10 µg/ml pHrodo Red *E. coli* BioParticles conjugate were used. To inhibit the phagocytosis, 30 µM Cytochalasin D (CytoD) was added 1 hour prior and during the assay. To study endocytosis, 5 µg/ml pHrodo Green Dextran conjugate and 50 µg/ml pHrodo Red Transferrin conjugate were used. To inhibit endocytosis, 30 µM Dynasore was added 1 hour prior and during the assay. Microglia were stained with CellTracker Deep Red and the nuclear stain NucBlue 30 min at 37˚C prior to the assay. Medium was changed to live cell imaging solution (Invitrogen, #A14291DJ) and pHrodo particles added. Plates were directly transferred to the Opera Phenix High-Content Screening System with temperature set to 37˚C and CO_2 to 5%. Images were taken every 15 or 20 minutes for 4 hours at 40x magnification. The Harmony software was used for image analysis and “Total Spot Area” chosen as the output measure.

2.8.7 Human inflammatory cytokines assay

Microglia secreted cytokines were analysed using the flow-cytometry based BD Cytometric Bead Array (CBA) Human Inflammatory Cytokine Kit. Microglia precursor cells were plated into fibronectin-coated 96-well black imaging plates and differentiated to microglia for 14 days. Supernatant was collected 12 hours after a full medium change. Microglia-like cells were also stimulated with IFN-γ for 24 hours, and after a full medium change incubated with LPS for either 3 or 12 hours before supernatant was collected. For each sample, supernatant from 3 wells were pooled. Replicates were collected on different days and run as distinct experiments. Experiments were conducted according to manufacturer’s instructions and samples were run on the BD LSR Fortessa flow cytometer. Samples were analysed using FlowJo software and the median PE value was used. Standard curves were generated in Excel and cytokine concentrations

calculated accordingly. Concentrations were normalized to the unstimulated Q22 microglia-like cells of each experiment.

2.8.8 Seahorse XF cell mito stress test

The Seahorse XF Cell Mito Stress Test Kit was used according to manufacturer's protocol. Microglia precursor cells were plates into PDL-coated XF Cell Culture microplates and differentiated to microglia for 14 days. 24 hours prior to the experiment, microglia were stimulated with IFN-γ and LPS. The Seahorse XF96 sensor cartridge was hydrated overnight at 37°C in a non-CO_2 incubator using 200 µl Seahorse XF calibrant / well. Assay media were prepared freshly on the day of the experiment. Seahorse XF DMEM medium was supplemented with 1 mM pyruvate, 2 mM glutamine and 10 mM glucose. 175 µl assay medium was added to each well of the cell culture microplate and it was then incubated for 45 minutes at 37°C in a non-CO_2 incubator. Compounds were prepared at 10x stock concentration in assay medium: 20 µM oligomycin, 20 µM carbonilcyanide p-triflouromethoxyphenylhydrazone (FCCP) and 5 µM rotenone and antimycin A. Compounds were then added to the hydrated sensor cartridge ports. The hydrated sensor cartridge and cell culture microplate were inserted into the Seahorse XFe96 instrument, and the Cell Mito Stress Test protocol run using the Wave software.

2.8.9 Calcium imaging

Microglia precursor cells were plated into fibronectin-coated black 96-well imaging plates and differentiated for 14 days. Microglia-like cells were stained with Fluo8 (2 µM) for 1 hour at RT. Fluo8 was taken off and replaced with live cell imaging solution. Intracellular calcium changes were induced by 1 µM Ionomycin, 50 µM ATP and 50 µM ADP. Calcium imaging was conducted in the FLIPR Penta High-Throughput Cellular Screening System. Fluorescent changes were recorded every second and an output per well generated. Raw fluorescent intensity data were used to calculate the increase in intracellular calcium after stimulation compared to baseline. Fluorescent data were normalized by cell count generated using the Opera Phenix High Content Screening System directly after the calcium imaging.

Table 2-24: Calcium imaging consumables

Consumable	**Company**	**Catalogue Number**
ATP	Sigma	A9187
ADP	Sigma	A2754
Fluo-8 AM	Abcam	ab142773
Ionomycin	Merck	407950

2.8.10 Statistics for functional assays

Statistical analysis as well as graph design was carried out using GraphPad Prism 8 (GraphPad Software). The Students t-test was used for comparison of two groups at a single timepoint. When data did not pass testing for normality, Mann-Whitney test was chosen. Two-way repeated measures ANOVA with Sidak's multiple comparison test was used when cell lines and time points were factors, and repeated measures were taken. Results are reported as mean values ± SEM. Statistical significance is illustrated as follows:

Table 2-25: Statistical significance

P value	**Symbol**
$p > 0.05$	n.s.
$0.01 < p < 0.05$	*
$0.001 < p < 0.01$	**
$0.0001 < p < 0.001$	***
$p < 0.0001$	****

2.9 Bulk RNA sequencing of microglia-like cells

2.9.1 RNA preparation, library preparation and sequencing

Microglia precursor cells were seeded at 4 x 10^5 cells/well in 6-well plates and differentiated to microglia-like cells for 14 days. On day 13, microglia were stimulated with 20 ng/ml IFN-γ for 24 hours, followed by an incubation with 10 ng/ml LPS for 3 or 12 hours. The unstimulated microglia-like cells were lysed together with the 12-hour LPS timepoint samples. All cells were lysed with 300 µl RLT buffer and lysates stored at -80°C over night. RNA was isolated the next day using the RNeasy Mini Kit according to the manufacturer protocol with on-column DNase treatment. RNA samples were eluted into 30 µl RNAase-free water and handed to the Genomics Research Hub at Cardiff University School of Biosciences and all further steps of the RNA sequencing preparation were performed by Angela Marchbank and Team. RNA concentration was measured using the Qubit™ RNA High Sensitivity (HS) Assay Kit and RNA integrity numbers (RIN) defined using the 4200 TapeStation system. cDNA synthesis was performed using the Illumina TruSeq mRNA stranded protocol which generated poly-A mRNA libraries. Libraries were then again assessed for their quality with the 4200 TapeStation system and sequenced as paired-end 75 bp reads on the Illumina NextSeq500 sequencer, generating 40 million reads per sample.

Table 2-26: RNA Sequencing consumables

Consumable	**Company**	**Catalogue Number**
RNeasy Mini Kit	Qiagen	74104
RNase-Free DNase Set	Qiagen	79254

Qubit™ RNA High Sensitivity (HS) Assay Kit	ThermoFisher Scientific	Q32852
TruSeq® Stranded mRNA Library Prep	Illumina	20020594

Table 2-27: RNA concentrations and RNA integrity numbers

Sample number	Sample name	Qubit RNA HS (ng/µl)	Tape RNA HS RIN
1	2H1 no LPS	9.62	8.6
2	2H1 3h LPS	31.4	9.4
3	2H1 12h LPS	41.8	9.7
4	3H2 no LPS	38.2	9.5
5	3H2 3h LPS	44.6	9.6
6	3H2 12h LPS	51.4	9.9
7	5H9 no LPS	21.2	9.2
8	5H9 3h LPS	33.6	9.7
9	5H9 12h LPS	45.6	9.5
10	109n1 no LPS	18.4	9.5
11	109n1 3h LPS	37.6	9.7
12	109n1 12h LPS	48.2	9.8
13	109n4 no LPS	32	9.5
14	109n4 3h LPS	81	10
15	109n4 12h LPS	84	10
16	109n5 no LPS	15.4	9.5
17	109n5 3h LPS	43.6	9.7
18	109n5 12h LPS	48.6	9.8

Table 2-28: Reads per run

Sample number	Sample name	No. of clusters run 1	No. of clusters run 2	Total clusters combined
1	2H1 no LPS	20.11716	23.7232	46.53762
2	2H1 3h LPS	20.83611	22.41806	45.72285
3	2H1 12h LPS	25.68609	24.45639	46.61101
4	3H2 no LPS	21.70313	26.18921	47.67777
5	3H2 3h LPS	22.21379	23.87514	46.53554
6	3H2 12h LPS	24.97221	24.96736	47.00623
7	5H9 no LPS	23.5097	24.20045	46.44293
8	5H9 3h LPS	22.7922	24.12785	46.49596
9	5H9 12h LPS	28.08066	25.28679	46.37111
10	109n1 no LPS	23.13815	24.28007	46.32039
11	109n1 3h LPS	24.96824	23.30432	46.26055
12	109n1 12h LPS	22.50931	24.05669	46.53426
13	109n4 no LPS	25.71867	23.69806	46.51281
14	109n4 3h LPS	29.30256	25.87076	47.41018
15	109n4 12h LPS	23.44389	23.88552	46.45235
16	109n5 no LPS	23.27767	24.08559	46.70578
17	109n5 3h LPS	22.65541	23.81718	46.43671
18	109n5 12h LPS	23.33814	24.06563	46.76041

2.9.2 Processing of sample files to generate raw read counts

Processing raw data was conducted in a Unix environment provided by Cardiff University School of Biosciences. Raw RNA-Seq data (fastq files) underwent quality control using fastQC (fastqc-0.11.7-gcc-8.3.1-vapdqqz) before and after trimming with Trimmomatic (trimmomatic-0.38-gcc-8.3.1-blmw3px). Samples were aligned to the human reference transcriptome (GRCh38; Ensemble release 100) using STAR (version 2.7.3a) (Dobin *et al.*, 2013). Samtools (version 1.10) was used to sort the aligned data and duplicates were subsequently removed using picard (version 2.22.2). Raw read counts per gene were generated using the software FeatureCounts (Liao, Smyth and Shi, 2014).

2.9.3 Differential gene expression

Differential gene expression analysis was carried out in R using Deseq2, as part of the Bioconductor package SARTools (Varet *et al.*, 2016). Furthermore, Deseq2 was used to generate normalized counts.

2.9.4 Data exploration

Normalized counts were used to perform principal component analysis (PCA). Clustvist was used to generate PCA plots (Metsalu and Vilo, 2015). Clustvist was furthermore used to generate Heatmaps of selected gene sets. Volcano plots were generated with Log2 fold change (FC) on x-axis and minus Log10 of the adjusted p-value on the y-axis. The significance threshold was chosen to be $p_{adj} < 0.01$ and Log2 FC > 1.5. Volcano plots were generated using VolcaNoseR (Goedhart and Luijsterburg, 2020).

2.9.5 Gene ontology and KEGG pathway analysis

g:Profiler was used for Gene Ontology Term Enrichment, generating enriched biological processes, molecular functions as well as KEGG pathways in the datasets. Either all or the top 10 terms were plotted together with the $-Log10(p_{adj})$ of the analysis conducted.

2.10 Proteomic analysis of microglia-like cell and co-culture supernatant

2.10.1 Preparation of microglia monocultures and microglia-astrocyte co-culture for proteomics

Non-adherent microglia precursors (MPC) and astrocyte precursors (APC) were differentiated from iPSC as indicated before. APC were plated at around 80% density on matrigel-coated (50µg/ml) plates and were terminally differentiated for 2 weeks using CNTF medium. Afterwards, astrocytes were aged for 2 months, changing maintenance medium every 3-4 days. 2 days before microglia plating, Q109 and Q22 astrocytes were dissociated using Accutase and plated on Matrigel-coated 12-well plates at a density of 50.000 astrocytes / well. Q109 and Q22 MPC were either plated on fibronectin-coated 12-well plates using ACM medium or onto the astrocytes in co-culture medium, at a density of 150.000 cells / well, respectively.

Table 2-29: Media compositions

Name	Base medium	Supplements
CNTF medium	Neurobasal-A	1x PenStrep, 1x Glutamax, 1% Neurobrew with Vit.A, 10 ng/ml CNTF
Maintenance medium	Advanced DMEM-F12	1x PenStrep, 1x Glutamax, 1% Neurobrew with Vit.A
ACM	Advanced DMEM-F12	Advanced DMEM-F12 + 1x PenStrep, 1x Glutamax, 1% Neurobrew with Vit.A, conditioned over astrocytes for 48 hours, normalized by CCL2 concentration, supplemented with 1% N2
Co-culture medium	Advanced DMEM-F12	1x PenStrep, 1x Glutamax, 1% Neurobrew with Vit.A, 1% N2, 1 µg/ml fibronectin (first week only)
Collection medium	DMEM-F12	-

2.10.2 Collection of cell supernatant

Microglia-like cells and microglia-astrocyte co-cultures were differentiated for 13 days. On day 13, medium was fully replaced with collection medium in order to reduce the concentration of serum proteins in the samples. On day 14, medium was fully replaced again, adding 1 ml / well collection medium and supernatant was collected after 24 hours incubation. Supernatants were frozen and directly shipped to the University of Bristol. All further preparations of samples and mass spectrometry have been performed at the University of Bristol Proteomics Facility by Kate Heesom and team.

2.10.3 TMT labelling and high pH reversed-phase chromatography

Supernatant samples were concentrated to 70 µl using 3 kDa cut-off concentration units (Millipore Ltd.) and then digested with 1.25 µg trypsin at 37°C overnight. Samples were labelled

with Tandem Mass Tag (TMT) eleven plex reagents according to the manufacturer's protocol (Thermo Scientific) and the labelled samples pooled.

Pooled samples were evaporated to dryness, resuspended in 5% formic acid and then desalted using a SepPak cartridge according to the manufacturer's instructions (Waters). The eluate from the SepPak cartridge was again evaporated to dryness and resuspended in buffer A (20 mM ammonium hydroxide, pH 10) prior to fractionation by high pH reversed-phase chromatography using an Ultimate 3000 liquid chromatography system (Thermo Scientific). Therefore, the sample was loaded onto an XBridge BEH C18 Column (130 Å, 3.5 µm, 2.1 mm X 150 mm, Waters) in buffer A and peptides eluted with an increasing gradient of buffer B (20 mM Ammonium Hydroxide in acetonitrile, pH 10) from 0-95% over 60 minutes. The resulting fractions (4 in total) were evaporated to dryness and resuspended in 1% formic acid prior to analysis by nano-LC MSMS using an Orbitrap Fusion Tribrid mass spectrometer (Thermo Scientific).

2.10.4 Nano-LC Mass Spectrometry

High pH RP fractions were further fractionated using an Ultimate 3000 nano-LC system in line with an Orbitrap Fusion Tribrid mass spectrometer (Thermo Scientific). In brief, peptides in 1% (vol/vol) formic acid were injected onto an Acclaim PepMap C18 nano-trap column (Thermo Scientific). After washing with 0.5% (vol/vol) acetonitrile 0.1% (vol/vol) formic acid peptides were resolved on a 250 mm × 75 µm Acclaim PepMap C18 reverse phase analytical column (Thermo Scientific) over a 150 min organic gradient, using 7 gradient segments (1-6% solvent B over 1 minute, 6-1% B over 58 minutes, 15-32% B over 58 minutes, 32-40% B over 5 minutes, 40-90% B over 1 minute, held at 90% B for 6 minutes and then reduced to 1% B over 1minute) with a flow rate of 300 nl/min. Solvent A was 0.1% formic acid and Solvent B was aqueous 80% acetonitrile in 0.1% formic acid. Peptides were ionized by nano-electrospray ionization at 2.0 kV using a stainless-steel emitter with an internal diameter of 30 µm (Thermo Scientific) and a capillary temperature of 275°C.

All spectra were acquired using an Orbitrap Fusion Tribrid mass spectrometer controlled by Xcalibur 2.1 software (Thermo Scientific) and operated in data-dependent acquisition mode using an SPS-MS3 workflow. FTMS1 spectra were collected at a resolution of 120 000, with an automatic gain control (AGC) target of 200 000 and a max injection time of 50 ms. Precursors were filtered with an intensity threshold of 5000, according to charge state (to include charge states 2-7) and with monoisotopic peak determination set to peptide. Previously interrogated precursors were excluded using a dynamic window (60 s +/- 10 ppm). The MS2 precursors were

isolated with a quadrupole isolation window of 1.2 m/z. ITMS2 spectra were collected with an AGC target of 10 000, max injection time of 70 ms and CID collision energy of 35%.

For FTMS3 analysis, the Orbitrap was operated at 50 000 resolution with an AGC target of 50 000 and a max injection time of 105 ms. Precursors were fragmented by high energy collision dissociation (HCD) at a normalised collision energy of 60% to ensure maximal TMT reporter ion yield. Synchronous Precursor Selection (SPS) was enabled to include up to 10 MS2 fragment ions in the FTMS3 scan.

2.10.5 Data analysis

Analysis of raw data and statistical analysis has been performed by Phil Lewis at the University of Bristol. All downstream analysis has been performed by the PhD candidate. The raw data files were processed and quantified using Proteome Discoverer software v2.1 (Thermo Scientific) and searched against the UniProt Human database (downloaded January 2021; 169297 sequences) using the SEQUEST HT algorithm. Peptide precursor mass tolerance was set at 10 ppm, and MS/MS tolerance was set at 0.6 Da. Search criteria included oxidation of methionine (+15.995 Da), acetylation of the protein N-terminus (+42.011 Da) and Methionine loss plus acetylation of the protein N-terminus (-89.03 Da) as variable modifications and carbamidomethylation of cysteine (+57.021 Da) and the addition of the TMT mass tag (+229.163 Da) to peptide N-termini and lysine as fixed modifications. Searches were performed with full tryptic digestion and a maximum of 2 missed cleavages were allowed.

The protein abundances were normalised within each sample to total peptide amount, scaled to the protein abundances of the common pool samples for each MS run, then Log2 transformed to bring them closer to a normal distribution. Statistical significance was then determined using Welch's T-Tests between the conditions of interest. The p-values were FDR corrected using the Benjamini-Hochberg method.

2.10.6 Data exploration

Scaled abundances of all proteins were used to perform principal component analysis (PCA) as well as to generate heatmaps of selected proteins using Clustvist (Metsalu and Vilo, 2015). Volcano plots were generated with Log2 fold change on x-axis and minus Log10 of the p-value on the y-axis. The significance threshold was chosen to be 1.3 (equals 0.05) and the fold change threshold to be 1. Volcano plots were generated using the VolcaNoseR (Goedhart and Luijsterburg, 2020).

2.10.7 Gene ontology analysis

In order to understand the underlying biological processes of the investigated secreted proteins, Gene Ontology Term Enrichment was conducted. The tool g:Profiler was used to define Biological Processes and Molecular Function enriched in the up- or downregulated proteins in the conducted comparisons. Either all or the top 10 terms were plotted together with the -Log10(p_{adj}) of the analysis conducted.

2.10.8 Metascape

The Metascape web tool has been used for protein-protein interaction enrichment analysis (Zhou *et al.*, 2019). For the significantly up- or downregulated protein lists, networks that contain the subset of proteins that form physical interactions with at least one other member in the list have been created. Furthermore, if the network contained more than 3 proteins, the Molecular Complex Detection (MCODE) algorithm has been applied to identify densely connected network components (Bader and Hogue, 2003). Pathway and process enrichment analysis has been applied to each MCODE component independently, and the three best-scoring terms by p-value are retained as the functional description of the corresponding components.

3 Validation of human iPSC-derived microglia, astrocytes, and cortical neurons

3.1 Introduction

Multiple human iPSC models have been generated to investigate the molecular and cellular mechanisms of Huntington's disease pathophysiology (Camnasio *et al.*, 2012b; Chae *et al.*, 2012; Jeon *et al.*, 2012; Mattis *et al.*, 2012). iPSC lines with an expanded CAG repeat length in the *HTT* gene can be used to study mechanisms associated with HD pathology and the biological consequences of mutant *HTT* expression. The HD iPSC used in this study (Q109) were generated by the HD iPSC Consortium alongside several other iPSC lines (Mattis *et al.*, 2012). These Q109 cells, unlike most other HD iPSC, exhibit CAG repeat expansions in culture (Mattis *et al.*, 2012; Goold *et al.*, 2019; McAllister *et al.*, 2022). Somatic expansions of the *HTT* CAG repeat has been reported to be associated with an earlier age of disease onset and the CAG repeat is particularly unstable in brain regions that are vulnerable to neurodegeneration in HD (Swami *et al.*, 2009). The CAG repeat is unstable in all cell types of the brain, however, neurons seem to show greater *HTT* CAG repeat expansions than glia cells (Shelbourne *et al.*, 2007).

To date, most stem cell-based publications have focused on investigating HD phenotypes in iPSC or iPSC-derived neuronal cells. A few studies also demonstrate phenotypes in iPSC-derived astrocytes (Garcia et al., 2019; Juopperi et al., 2012; Reyes-Ortiz et al., 2022) and embryonic stem cell derived microglia (O'Regan *et al.*, 2021). Rapid advances in the stem cell field have led to the development of several reliable protocols for the differentiation of iPSC into the cell types of the brain. iPSC can be differentiated into different types of neurons, including cortical (Qi et al., 2017; Shi et al., 2012; Telezhkin et al., 2016) and striatal (Arber *et al.*, 2015; Grigor'eva *et al.*, 2020) neurons. Further protocols also enable the generation of astrocytes (Krencik et al., 2011; Shaltouki et al., 2013) and microglia (Abud *et al.*, 2017; Haenseler *et al.*, 2017; Takata *et al.*, 2017) from iPSC. In this study, patient-derived HD and isogenic control iPSC were differentiated into neurons, astrocytes, and microglia (Figure 3.1).

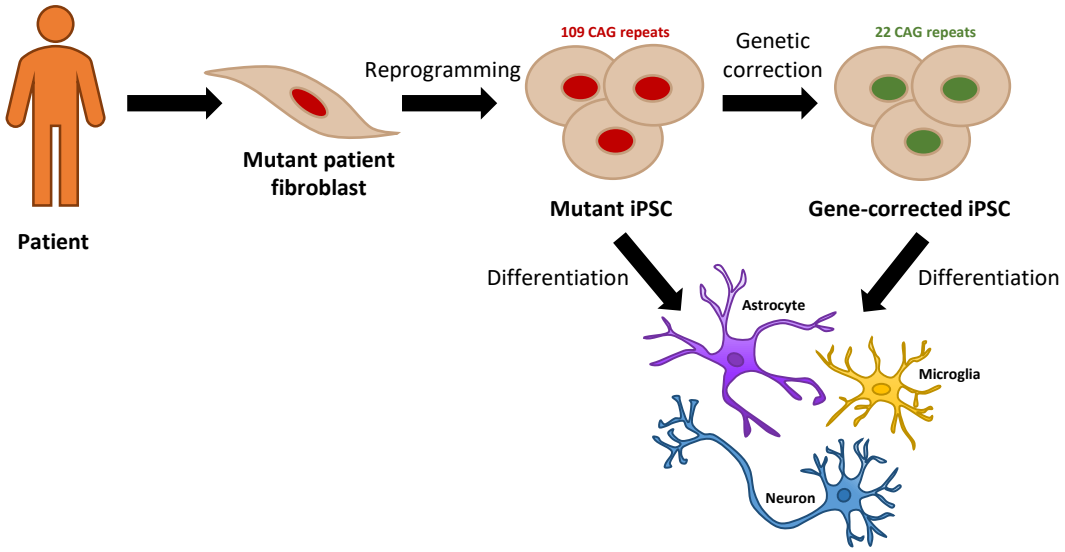

Figure 3.1: Stem cell model. The HD iPSC with 109 CAG repeats in the *HTT* gene were derived from patient fibroblasts by the HD iPSC Consortium. Isogenic controls with a wild-type length of 22 CAG repeats have been developed by genetic correction of the mutant huntingtin gene. Both iPSC lines were differentiated into microglia, astrocytes, and neurons.

Most iPSC-derived cells are analysed in monoculture, which enables the study of cell-autonomous effects. However, to understand the crosstalk between different cell types of the brain, such as paracrine signalling, damage responses, and receptor engagement, as well as to provide more physiological culture conditions, co-cultures are a preferred model system. Co-culture systems of microglia with other cell types of the brain, i.e. neurons and astrocytes, have been shown to upregulate homeostatic pathways in microglia and promote a more anti-inflammatory cytokine response (Haenseler *et al.*, 2017; Pandya *et al.*, 2017). Moreover, co-cultures of astrocytes with neurons have been shown to provide trophic support, influence neuronal maturation and bioenergetics, and regulate the extracellular environment (Du et al., 2018; Hedegaard et al., 2020; Rushton et al., 2013).

3.2 Chapter aims

This chapter first aims to validate iPSC-derived microglia-like cells, astrocytes, and neurons from both HD (Q109) and isogenic control (Q22) background. The second aim is to develop co-culture protocols for astrocytes with microglia-like cells or neurons, in order to provide more physiological culture conditions for the long-term culture of these cells. The third aim is to investigate *HTT* CAG repeat expansions in these cultures. Lastly, the fourth aim is to generate stable cell lines expressing the red fluorescence protein mCherry to discriminate cell types in co-culture.

3.3 Results

3.3.1 Information on iPSC used in this study

The Q109 iPSC line with a heterozygous mutant huntingtin gene with 109 CAG repeats was used. This Q109 line consists of three clones (109n1, 109n4, 109n5) which have been derived from patient fibroblasts by Mattis et al., 2012. To investigate direct effects of the mutant *HTT* expression, isogenic controls are a preferred model. These cells have the same genetic background as the patient-derived cells and only differ by the correction of the disease mutation. Isogenic controls for the Q109 iPSC have been established using the CRISPR/Cas9 nuclease system together with a piggyBac transposon (PB) selection cassette-based homologous recombination donor (Donaldson et al., unpublished). This system enabled a seamless correction of the expanded CAG repeat tract down to the wild-type length of the second allele (22 CAG repeats). Three clones of the isogenic controls called 2H1, 3H2, and 5H9 were used. mCherry-expressing reporter cells have been established for these cell lines to distinguish cell types in co-culture experiments (see section 3.3.7). In this thesis HD iPSC clones will be collectively referred to as 'Q109', while the isogenic controls are termed 'Q22'. If not stated otherwise, all 6 clones were used for all experiments and were referred to as "n = 3 biological replicates" in the upcoming chapters. The iPSC are again summarized in Table 3-1.

Table 3-1: iPSC used in this study

Line	iPSC clone	CAG repeat length	Parent iPSC	mCherry reporter lines
Q109	109n1	109 / 22	-	
	109n4	109 / 22	-	3 subclones generated
	109n5	109 / 22	-	
Q22	2H1	22 / 22	109n1	3 subclones generated
	3H2	22 / 22	109n1	
	5H9	22 / 22	109n1	

All iPSC clones underwent further investigation using an Illumina Global Screening Array to detect copy number variants (CNV). Four CNV were found to be present in all clones (Q109 and Q22) (Figure 3.2A). Deletions were detected at 2q22.1 (Figure 3.2B), 6q23.3 (Figure 3.2C), and 14q24.3 (Figure 3.2E), and a duplication was found at 12q14.3 (Figure 3.2D).

A

iPSC clone	2q22.1	6p23.3	12q14.2	14q24.3
109n1	Deletion	Deletion	Duplication	Deletion
109n4	Deletion	Deletion	Duplication	Deletion
109n5	Deletion	Deletion	Duplication	Deletion
2H1	Deletion	Deletion	Duplication	Deletion
3H2	Deletion	Deletion	Duplication	Deletion
5H9	Deletion	Deletion	Duplication	Deletion

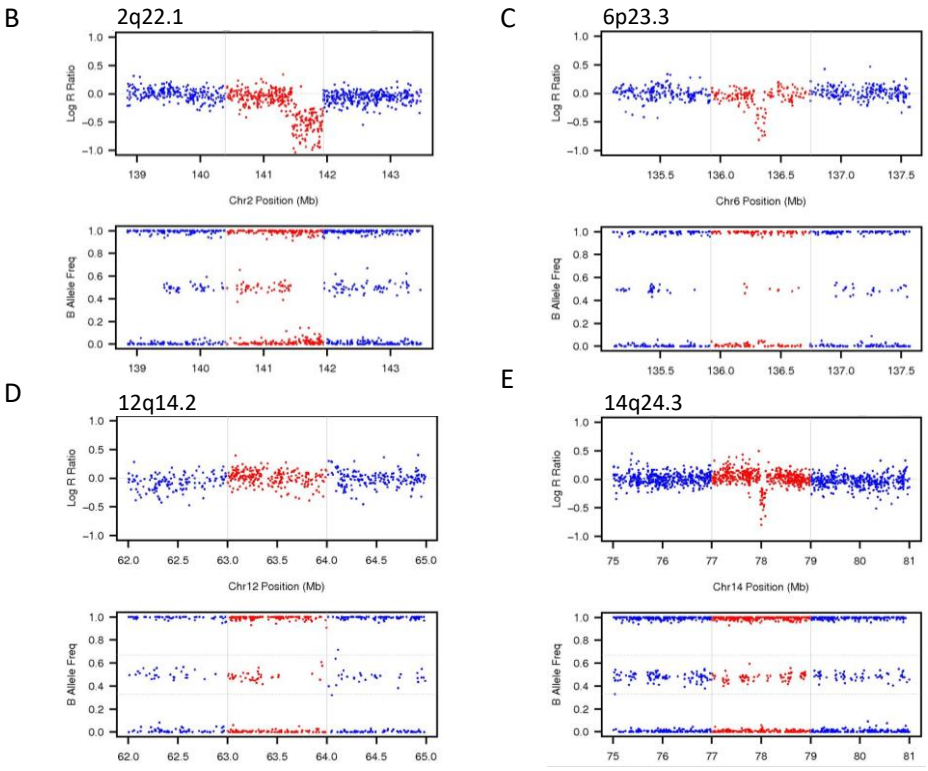

Figure 3.2: CNV Analysis of Q109 and Q22 iPSC. iPSC clones where genotyped using an Illumina Global Screening Array v2.0 and data were analysed with PennCNV with GRCh37 / hg19 as a reference genome to identify copy number variants (CNV). (A) Summary of CNV analysis which highlights that all CNV are present in all lines tested. (B) Example of the deletion at 2q22.1 is highlighted by a decrease of the Log R ratio below zero and an absence of SNPs in the B allele frequency around 0.5. (C) Example plots for the deletion at 6p23.3. (D) Example plots for the duplication at 12q14.2 characterised by an increase in the Log R ratio above zero and a split in the BAF to give 2 lines around 0.4 and 0.6. (E) Example plots for the deletion at 1q24.3.

3.3.2 Human iPSC-derived microglia cells express characteristic microglial markers

To recapitulate microglia ontogeny, iPSC were differentiated using a protocol adapted from Haenseler et al., 2017. Microglia derive from primitive, yolk sac-derived myeloid progenitors that migrate into the developing brain (Ginhoux *et al.*, 2013). The differentiation method aimed to induce the iPSC to become primitive hematopoietic stem cells through the formation of embryoid bodies. These embryoid bodies then gave rise to MYB-independent myeloid progenitors (here called microglia precursor cells, MPC) that were harvested multiple times from the culture supernatant after approximately one month. Therefore, the cultures that gave rise

to MPC were called “factories”. The MPC were differentiated to a microglia-like cell phenotype in 14 days by the addition of medium conditioned over astrocyte cultures (astrocyte conditioned medium, ACM). ACM was generates as indicated by Rushton et al., 2013 (Figure 3.3A). The use of ACM contributed with physiological amounts of factors such as macrophage colony-stimulating factor (M-CSF), granulocyte-macrophage colony-stimulating factor (GM-CSF), and transforming growth factor beta (TGF-β) to the terminal differentiation into microglia-like cells (Butovsky et al., 2014; Schilling et al., 2001).

Differentiated MPC and microglia-like cells were stained for cell type specific markers. Non-adherent MPC were plated and fixed after 15 minutes to be stained for the macrophage lineage precursor markers CD11b and the protein tyrosine phosphatase, receptor type, C (PTPRC or CD45) (Figure 3.3B). The MPC were furthermore plated in ACM for two weeks for the terminal differentiation into microglia-like cells, which increased the complexity of the cellular morphology to a ramified phenotype. Microglia-like cells were stained for the markers ionized calcium-binding adapter molecule 1 (IBA1) and the transmembrane protein 119 (TMEM119) (Figure 3.3C). Both Q109 and Q22 iPSC differentiated successfully to microglia-like cells.

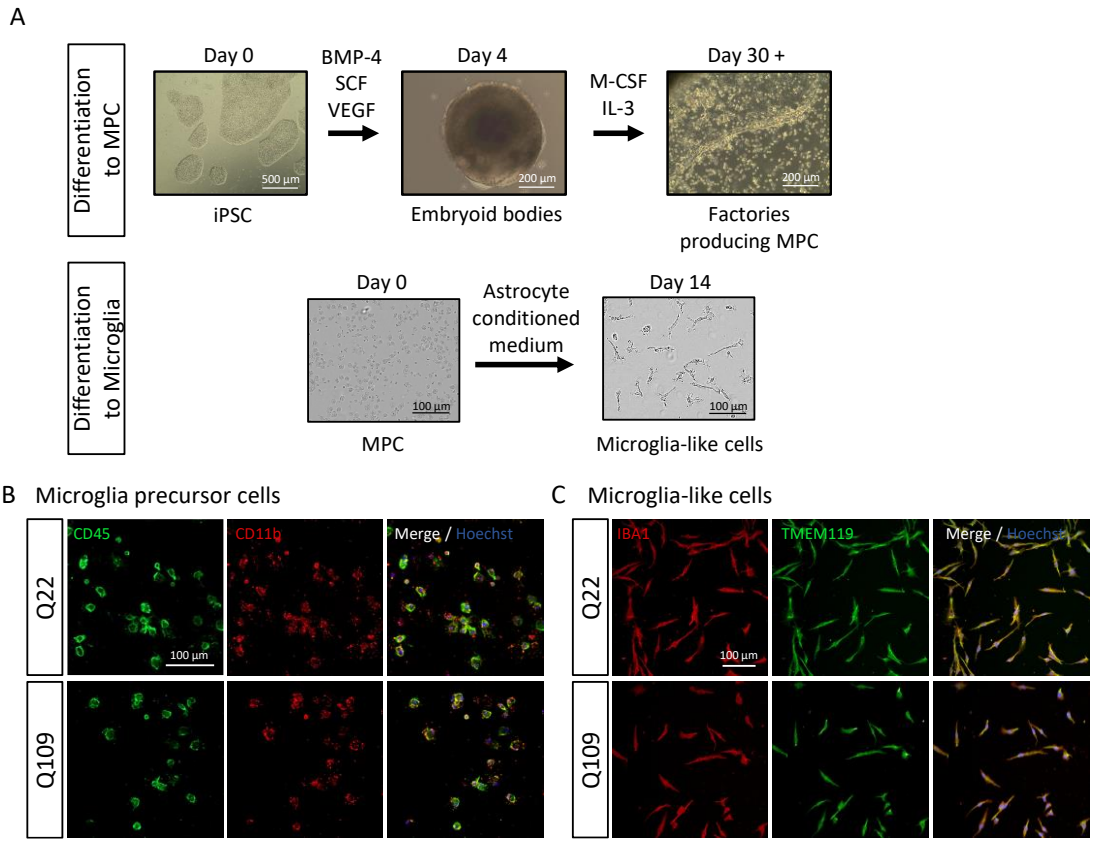

Figure 3.3: Differentiation of iPSC into microglia-like cells. (A) The addition of BMP-4, SCF and VEGF to iPSC led to the development of embryoid bodies biased to mesoderm and haematopoietic differentiation. Further addition of the factors M-CSF and IL-3 guided the production of non-adherent myeloid cells in the culture supernatant. In a second step these non-adherent microglia precursor cells (MPC) were harvested and differentiated to a microglial phenotype by the addition of astrocyte conditioned medium. Scale bars = 500 µm for iPSC, 200 µm for embryoid bodies, 200 µm for factories. (B) Confirmation of cell identity of both Q22 and Q109 MPC via CD45 an CD11b. (C) Confirmation of cell identity of both Q22 and Q109 microglia-like cells using IBA1 and TMEM119. Scale bars = 100 µm. D = day.

MPC were also quantified for the expression of myeloid markers using flow cytometry (Figure 3.4A). Q22 and Q109 MPC showed no difference in their expression of the myeloid surface markers CD11b, CD14, and CD45. Both groups exhibited approximately 80% CD11b, 96% CD14 and 95% CD45 positive cells. Furthermore, the lack of expression of the hematopoietic stem cell marker CD34 was tested to verify that the differentiation towards a myeloid phenotype was successful. Both, Q22 and Q109 MPC did not stain positive for CD34 (Figure 3.4B, right).

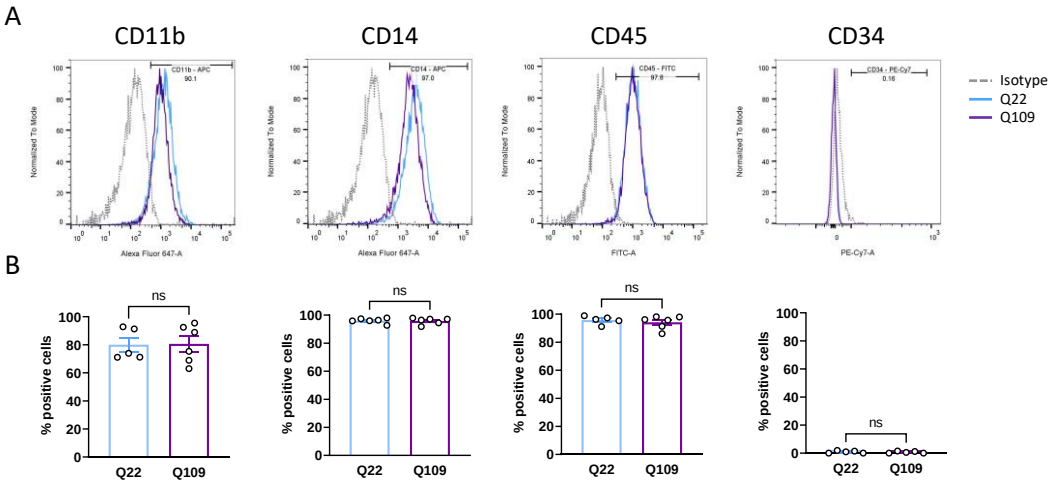

Figure 3.4: Mutant *HTT* expression did not affect the differentiation towards myeloid cells. (A) MPC were stained for myeloid surface markers CD11b, CD14, and CD45, as well as the haematopoietic surface marker CD34 and were investigated by flow cytometry. (B) Percentage positive cells for all markers were not different between Q22 and Q109 MPC. MPC stained positive for myeloid lineage markers, but not for the haematopoietic lineage marker CD34. Data are presented as mean ± SEM. n = 2-3 clones, in two independent experiments. Statistical analysis was performed using unpaired Student´s t-test. CD = cluster of differentiation. ns = not significant.

To provide a more brain-like environment for the differentiation of MPC to microglia-like cells, two different coatings that resemble parts of the extracellular matrix (ECM) of the brain were tested. Fibronectin is an ECM protein that binds to other ECM proteins as well as integrins and therefore facilitates cell adhesion. Matrigel is a commercially available undefined basement membrane matrix material secreted by Engelbreth-Holm-Swarm (EHS) mouse sarcoma cells, consisting of several ECM proteins including laminin, collagen IV, entactin, and heparin sulphate proteoglycan. Non-adherent MPC were plated on either 5 µg/ml fibronectin- or 100 µg/ml

Matrigel-coated wells to investigate cell attachment after 15 min, 60 min, and 120 min. To determine morphological properties of the cells, MPC were stained for the actin filament marker phalloidin and images were taken using the Opera Phenix High-Content Screening System (Figure 3.5A). Cell roundness was determined using the Harmony software, which defined a perfectly round cell with a roundness score of 1. MPC attached to fibronectin and started branching out within 120 min, resulting in the roundness decreasing significantly with time (Figure 3.5B, left). Matrigel-coating however did not change the MPC morphology, indicating that the cells did not attach to the matrix within the first 120 min (Figure 3.5B, right). A two-way ANOVA revealed that there was a statistically significant interaction between the effects of time and coating ($F(2, 12) = 8.615$, $p = 0.0048$). Simple main effects analysis showed that time had a statistically significant effect on the roundness ($p = 0.0033$), but coating did not ($p = 0.1193$). Due to these findings, fibronectin was used as the coating for all further experiments when microglia were investigated in monoculture.

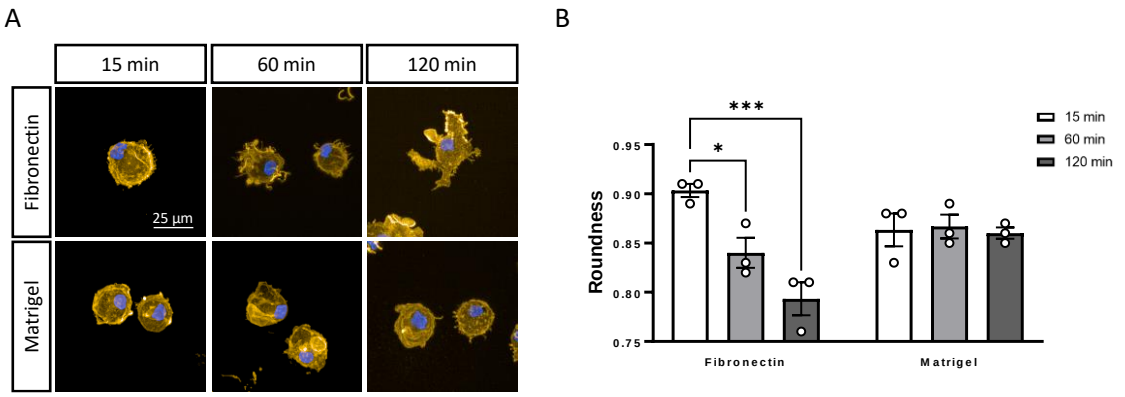

Figure 3.5: Microglia precursor cell attachment to extracellular matrix proteins. MPC were plated onto either 5 µg/ml fibronectin-coated or 100 µg/ml Matrigel-coated plates and fixed after 15, 60 and 120 min. Cells were stained for the actin filament marker phalloidin. Images were taken using the Opera Phenix High-Content Screening System and cell roundness was determined using Harmony software. (A) Representative images of MPC attaching to either fibronectin or Matrigel at the three timepoints. (B) MPC attaching to fibronectin started to branch out within 120 min and showed a significant decrease in their roundness. MPC plated on Matrigel however did not change their morphology. Scale bar = 25 µm. Data are expressed as mean ± SEM. n = 3 biological replicates in one independent experiment. Statistical analysis was performed using two-way ANOVA, followed by Tukey's honest significance test. * $p < 0.05$, *** $p < 0.001$. min = minutes.

3.3.3 Human iPSC-derived cortical neurons express characteristic neuronal markers

iPSC were differentiated into neurons according to Telezhkin et al., 2016 with minor modifications. iPSC were cultured in a medium inhibiting dual SMAD and WNT signalling to induce differentiation into neuronal progenitor cells (NPC) with forebrain fate potential. After one week, neuronal rosette formation was induced by taking away the growth factors. The generation of NPC took 16 days and terminal differentiation into cortical neurons further three

weeks (Figure 3.6A). Both Q22 and Q109 iPSC successfully differentiated to a neuronal fate illustrated by staining the NPC for the type VI intermediate filament NESTIN and the SRY-box transcription factor 2 (SOX2) (Figure 3.6B). Furthermore, fully differentiated neurons stained positive for the neuronal markers microtubule associated protein 2 (MAP2) and tubulin beta 3 class III (TUBB3) and (Figure 3.6C).

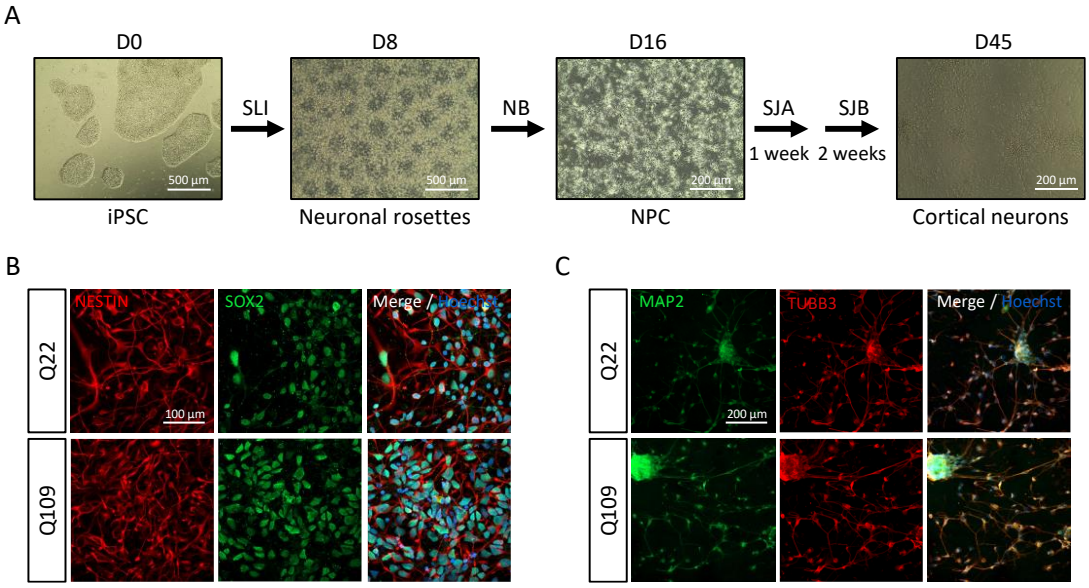

Figure 3.6: Differentiation of iPSC into cortical neurons. (A) iPSC were differentiated to neuronal precursor cells (NPC) by the inhibition of dual SMAD and WNT signalling which led to the subsequent induction of neuronal rosette formation. The NPC were terminally differentiated into neurons in 3 weeks. Scale bars = 500 µm for iPSC, 500 µm for neuronal rosettes, 200 µm for NPC, 200 µm for cortical neurons. (B) Both Q22 and Q109 NPC were stained for the type VI intermediate filament NESTIN and the SRY-box transcription factor 2 (SOX2). Scale bar = 100 µm. (C) Q22 and Q109 neurons were stained for the markers microtubule associated protein 2 (MAP2) and tubulin beta 3 class III (TUBB3). Scale bar = 200 µm. D = day.

3.3.4 Human iPSC-derived astrocytes express characteristic astrocyte markers

iPSC were differentiated into astrocytes using a protocol adapted from Serio et al., 2013. In the brain, astrogenesis happens after neurogenesis. Therefore, the differentiation of iPSC to astrocytes started with the induction of a neuronal fate and differentiation of iPSC to NPC. NPC were then differentiated into astrocyte progenitor cells (APC) using the two growth factors epidermal growth factor (EGF) and leukemia inhibitory factor (LIF). To achieve a pure population of APC without contamination of remaining NPC, cells underwent fluorescence-activated cell sorting (FACS) for the surface marker CD44. (Figure 3.7B). Positively selected cells were expanded using EGF and fibroblast growth factor (FGF). Terminal differentiation of APC to astrocytes took 14 days using ciliary neurotrophic factor (CNTF) (Figure 3.7A). Both Q22 and Q109 iPSC successfully differentiated to APC, illustrated by the positive staining for the type III intermediate filament vimentin (VIM) and the nuclear factor 1 A-type (NFIA) (Figure 3.7C). Terminally differentiated Q22 and Q109 astrocytes stained positive for the commonly used

astrocyte marker glial fibrillary acidic protein (GFAP), a type III intermediate filament, as well as CD49f, a novel marker for human astrocytes (Barbar *et al.*, 2020) (Figure 3.7D).

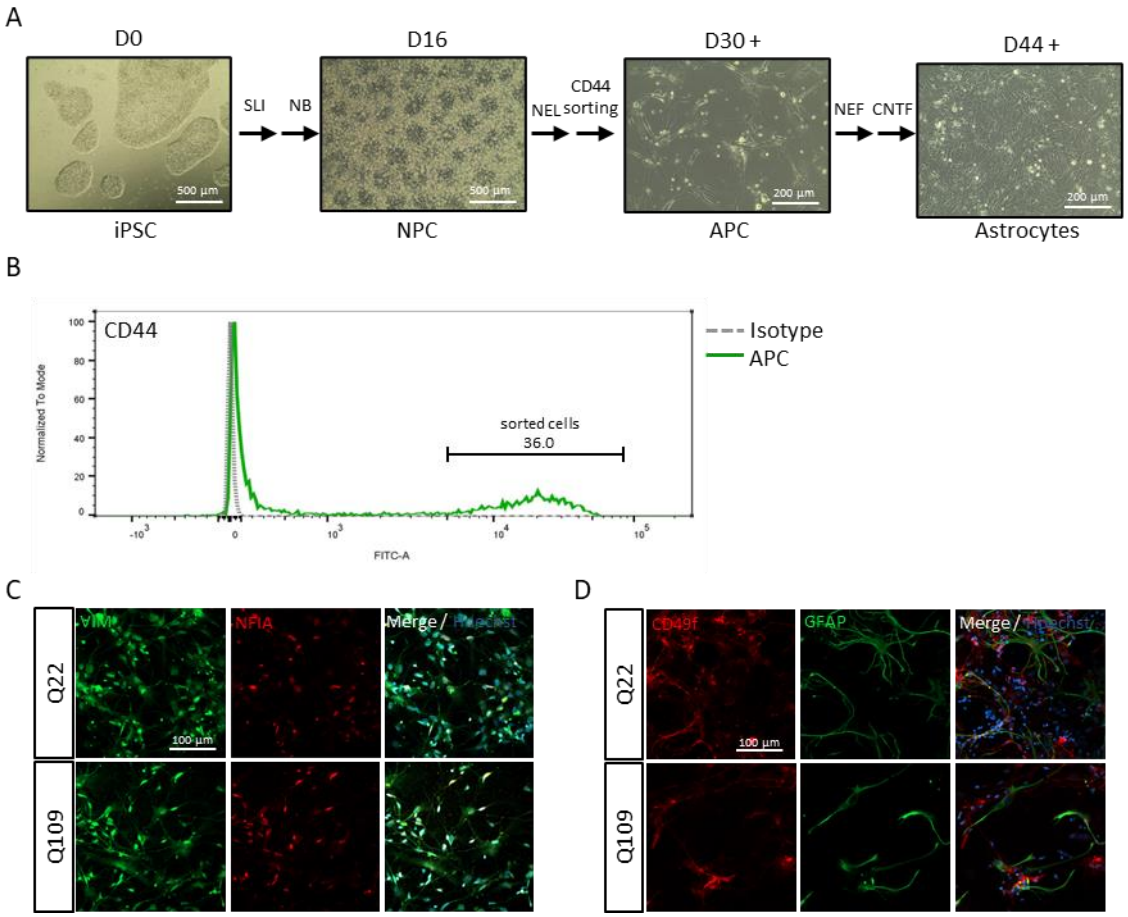

Figure 3.7: Differentiation of iPSC into astrocytes. (A) iPSC were differentiated towards a neuronal lineage. The subsequent co-application of epidermal growth factor (EGF) and leukemia inhibitory factor (LIF) (medium NEL) in prolonged culture then promoted the astroglial specification of neuronal precursor cells (NPC) towards astrocyte precursor cells (APC). Subsequent differentiation of APC in the presence of ciliary neurotrophic factor (CNTF) for 14 days led to terminally differentiated astrocytes. (B) In order to achieve a pure population of APC without contamination of remaining NPC, the APC population was sorted for the surface marker CD44. (C) Both Q22 and Q109 APC were stained for the markers vimentin (VIM) and nuclear factor 1A (NFIA). (D) Q22 and Q109 astrocytes were fixed after 14 days of differentiation in CNTF. Astrocytes were stained for the markers CD49f and glial fibrillary acidic protein (GFAP). D = day.

3.3.5 Human iPSC-derived co-cultures of astrocytes with microglia or cortical neurons

Multiple studies showed that iPSC-derived brain cells cultured in co-culture rather than monoculture upregulate pathways related to homeostatic function, provide trophic support to each other, and regulate the extracellular environment (Haenseler *et al.*, 2017; Hedegaard *et al.*, 2020). To provide a more physiological environment, co-cultures of microglia-like cells and neurons with astrocytes, respectively, were developed. Astrocytes were fully differentiated before either microglia precursor cells or neuronal precursor cells were added to the astrocyte

culture. MPC were added to astrocytes in a ratio of 1:10 and were differentiated for 14 days. The co-culture was stained for the microglia marker IBA1 and astrocyte marker EAAT1, an excitatory amino acid transporter (Figure 3.8A). NPC were added to astrocytes in a ratio of 5:1 and were differentiated for 21 days. The co-culture was stained for the neuronal marker MAP2 and the astrocyte marker GFAP (Figure 3.8B).

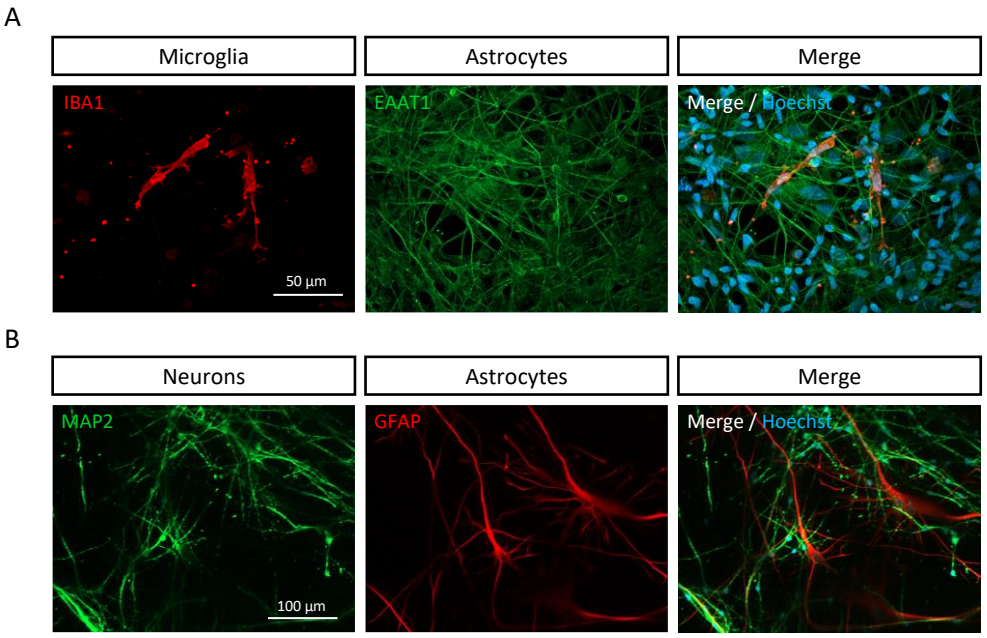

Figure 3.8: Co-cultures of astrocytes with microglia or neurons. (A) Microglia precursor cells were differentiated and added to terminally differentiated astrocytes in a ratio of 1:10 for terminal differentiation to microglia for 14 days. Representative image of IBA1 (microglia) and EAAT1 (astrocytes) co-staining. Scale bar = 50 µm. (B) Neuronal precursor cells were added to terminally differentiated astrocytes in a ratio of 5:1 for terminal differentiation to cortical neurons for 21 days. The neuron-astrocyte co-cultures was stained for the markers MAP2 (cortical neurons) and GFAP (astrocytes). Scale bar = 100 µm.

3.3.6 CAG repeat instability at the HTT locus in iPSC-derived brain cells

Repeat instability and expansion of the CAG repeat at the *HTT* locus have previously been reported for human cell lines and iPSC (Goold *et al.*, 2019; McAllister *et al.*, 2022). Here, expansion of the *HTT* CAG repeat length in differentiated Q109 cortical neurons, microglia-like cells, and astrocytes were investigated. Q109 microglia-like cells and neurons were co-cultured with Q22 astrocytes to support cell survival, and Q109 astrocytes were cultured in monoculture. Q22 astrocytes were furthermore cultured in monoculture alongside the HD cell cultures, in order to show that the WT *HTT* CAG repeat length does not expand in culture. DNA of all cultures was collected every 14 days over a period of 70 days after plating. For the cortical neuron culture, NPC were plated onto astrocytes, and therefore for the first 21 days NPC were still differentiating to mature neurons. For the microglia culture, MPC were plated onto astrocytes and MPC were differentiating to microglia-like cells for the first 14 days. APC were plated on their own and differentiated to astrocytes within the first 14 days of the observation period.

CAG repeat length at the *HTT* locus was measured via PCR and capillary gel electrophoresis. The data was analysed using a custom R script written by Branduff McAllister (https://github.com/BranduffMcli/AutoGenescan). First, Q22 astrocytes did not show CAG repeat expansion over a period of 70 days (Figure 3.9A). However, Q109 cortical neurons (Figure 3.9B), astrocytes (Figure 3.9C) and microglia-like cells (Figure 3.9D) exhibited CAG repeat expansion over 70 day period. No significant difference in the rate of *HTT* CAG repeat expansion between neurons, astrocytes and microglia-like cells was detected (Figure 3.9E).

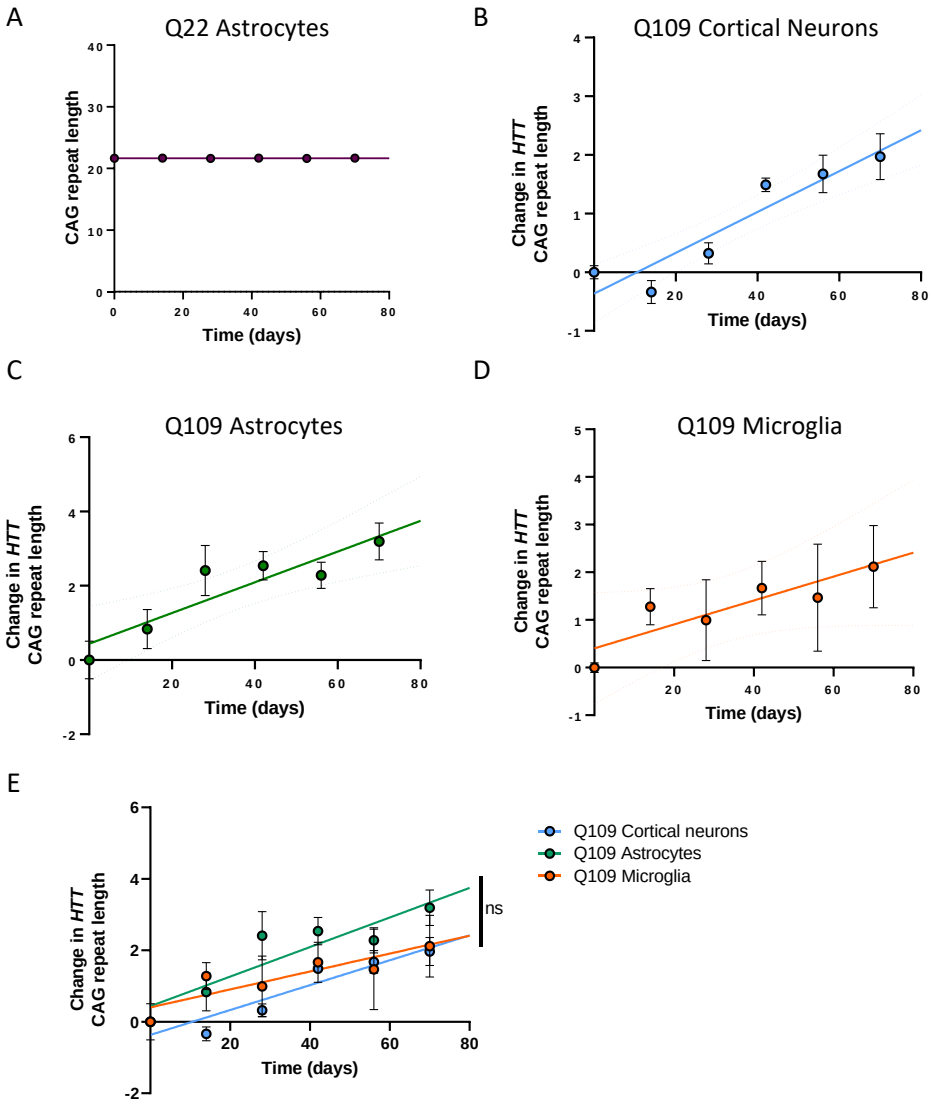

Figure 3.9: Investigating *HTT* CAG repeat instability in cortical neurons, astrocytes, and microglia. Q109 microglia-like cells and neurons were co-cultured with Q22 astrocytes. Q22 and Q109 astrocytes were cultured in monoculture. DNA was collected every 14 days for CAG repeat sizing by PCR and capillary gel electrophoresis. Data was analysed using a custom R script written by Branduff McCallister. (A) CAG repeat length of Q22 astrocytes did not change over a period of 70 days in culture. (B) Change in *HTT* CAG repeat length of Q109 cortical neurons showed expansion in culture over 70 days. Straight line shows simple linear regression and dotted lines the 95% confidence interval. (C) Change in *HTT* CAG repeat length of Q109 astrocytes. (D) Change in *HTT* CAG repeat length of Q109 microglia-like cells. (E) Comparison of cell types showed no difference in the rate of expansion between cortical neurons, astrocytes, and microglia-like cells. Data are presented as mean ± SEM. n = 3 repeats with 3 DNA collections per timepoint. Simple linear regression was performed to generate lines and for statistical analysis one-way ANOVA of the slope values, followed by Tukey's honest significance test was performed. ns = not significant.

3.3.7 Generation of mCherry reporter cell lines

Fluorescent reporter cell lines provide a useful tool for live-cell imaging and the distinction of a specific cell type in co-culture models. Therefore, the red fluorescent protein mCherry was introduced into both Q22 (clone 2H1) and Q109 (clone 109n4) iPSC at the safe harbour genomic site AAVS1 using CRISPR/Cas9. Additionally a puromycin resistance gene was introduced for efficient selection of positive cells. Positively selected clones were tested for the genomic integration of the mCherry into the AAVS1 locus (Figure 3.10A, top) as well as for the existence of the AAVS1 wild-type allele (Figure 3.10A, bottom), indicating a heterozygous insertion of the reporter into the locus. For both, Q22 and Q109, three iPSC sub-clones with homozygous insertion of mCherry into both alleles of the AAVS1 locus were selected. The reporter iPSC successfully differentiated to microglia and maintained robust mCherry expression throughout the differentiation (Figure 3.10B).

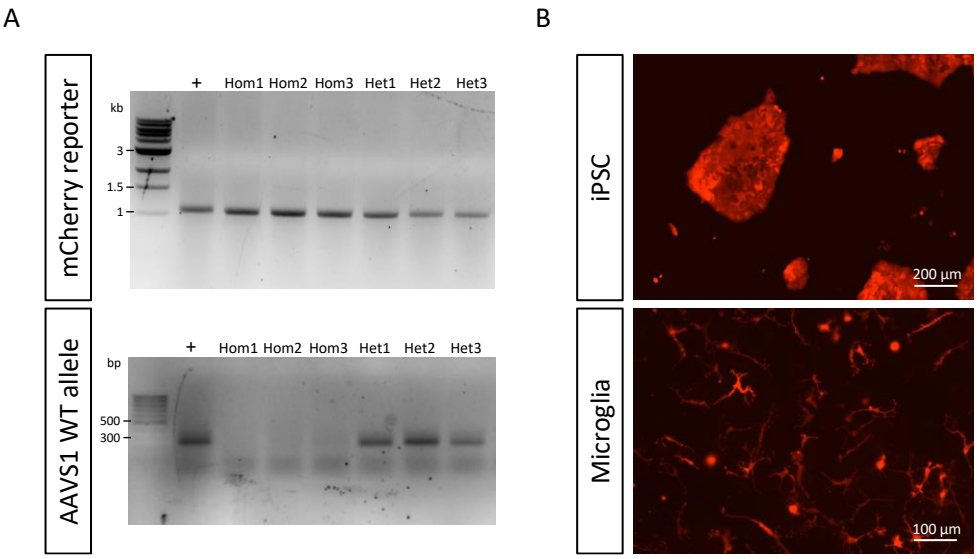

Figure 3.10: Generation of Q22 and Q109 red fluorescent reporter cell lines. Using CRISPR/Cas9 technology, the red fluorescent protein mCherry was incorporated into Q22 and Q109 iPSC. (A) Picked clones were analysed by PCR for the insertion of the reporter into the AAVS1 locus. The expected PCR product for the insertion of the mCherry reporter has a size of 1033 bp (top).The expected PCR product of the AAVS1 WT allele has a size of 254 bp (bottom). A positive control (+) was run together with the samples. Representative gels show three clones with homozygous (hom) insertion of mCherry and three clones with heterozygous (het) insertion of mCherry into the AAVS1 locus. (B) Representative images of edited iPSC and differentiated microglia-like cells. iPSC = induced pluripotent stem cells, WT = wild type, kb = kilobase, bp = base pair.

3.4 Discussion

3.4.1 Summary

In this chapter, Q22 and Q109 iPSC were introduced, underwent quality control and it was shown that these cells differentiate into microglia-like cells, neurons and astrocytes. Co-culture conditions for microglia-like cells and neurons with astrocytes were established and these were used to study the cells in long-term cultures in order to investigate *HTT* CAG repeat expansions. Furthermore, stable red fluorescent reporter cell lines for Q22 and Q109 iPSC were generated in order to study cells in co-culture conditions.

3.4.2 HD iPSC

The iPSC used in this study were derived from a patient with 109 CAG repeats at the HTT locus (Mattis *et al.*, 2012). *HTT* CAG repeat lengths of 40-45 are most common in HD patients, and CAG repeat lengths above 60 are usually seen in 'juvenile-onset HD' patients with symptom onset before the age of 21 (Bakels *et al.*, 2022). Using iPSC models with a high CAG repeat length, which does not reflect the majority of cases, has the advantage that these cells potentially exhibit more severe phenotypes and therefore might highlight changes in cellular pathology more clearly. Multiple papers have shown a dose-dependent effect of the *HTT* CAG repeat length on phenotypes in iPSC-derived brain cells, including neurons and microglia (Mattis *et al.*, 2015; O'Regan *et al.*, 2021). Therefore, the Q109 lines are a great model to investigate novel HD microglia phenotypes, and these could be then further confirmed with HD iPSC lines with lower *HTT* CAG repeat lengths. The limitation of using iPSC from a single patient in this thesis is that the patients distinct genetic background could affect experimental outcomes. Through GWAS studies it is well characterised that other than the *HTT* CAG repeat length, several genetic modifiers can affect patients age of onset and disease progression (Lee *et al.*, 2019, 2022). A repetition of experiments with HD iPSC derived from more patients, potentially with shorter *HTT* CAG repeat lengths would be of great benefit to verify the generated findings of this thesis.

3.4.3 CNV analysis

CNV analysis was performed on the Q22 and Q109 iPSC lines to detect changes to the genome. Here, three deletions and one duplication were found in all samples, indicating that these are patient specific. Previously, the Q109 lines were reported to have Chromosome 1 instability, which occurred with prolonged *in-vitro* culture (McAllister *et al.*, 2022). Therefore, in this thesis, low passage numbers of iPSC were used and the CNV of the cells was routinely checked. Abnormalities in chromosome number have been reported for iPSC, especially trisomy of Chromosome 12 and 17 (Vaz *et al.*, 2021). Chromosomal aberrations detected in early passages may occur during reprogramming, whereas for late passages it is believed that chromosomal aberrations accumulate in the process of culture adaptation *in-vitro* (Liu et al., 2020; Yoshihara et al., 2017).

3.4.4 Characterisation of iPSC-derived cells

All iPSC lines were successfully differentiated into microglia-like cells, astrocytes, and neurons. For the microglia differentiation, iPSC were differentiated to myeloid progenitors according to Haenseler et al., 2017 and van Wilgenburg et al., 2013. However, Haenseler et al. introduced the myeloid progenitors to a co-culture with neurons, supplemented with interleukin 34 (IL-34), for the differentiation to a microglia phenotype. Van Wilgenburg et al. differentiated the myeloid progenitors to macrophages using a defined concentration of macrophage colony-stimulating factor (M-CSF). In this study the myeloid progenitors were cultured in astrocyte-conditioned medium in order to introduce a brain-like environment and to differentiate the cells into microglia-like cells. Schilling et al. 2001 reported that microglia differentiation is controlled by the astrocytic factors transforming growth factor-β (TGF-β), M-CSF, and granulocyte/macrophage colony-stimulating factor (GM-CSF) and the concentrations released by astrocytes are sufficient to induce microglia ramification. Furthermore, differentiation to microglia was inhibited by neutralizing antibodies against TGF- β, M-CSF, and GM-CSF (Schilling *et al.*, 2001). Another microglia differentiation protocol used co-culture with astrocytes for the maturation of microglia for two weeks, followed by plating FACS-sorted CD39+ microglia in monoculture for experimentation (Pandya *et al.*, 2017). This protocol however is very time intensive and the effect of the FACS procedure on microglia activation is not well understood. Maguire et al. used ACM for the differentiation of iPSC to a microglia-like cell phenotype and reported these cells to stain positive for cell type specific markers (Maguire *et al.*, 2021). Astrocyte factors are not only used for microglia differentiation but are also reported to improve the differentiation of iPSC to a neuronal fate (Rushton *et al.*, 2013; Klapper *et al.*, 2019; Hedegaard *et al.*, 2020). As astrocyte-conditioned media is undefined, batch differences of ACM

may occur. Here, each batch of ACM was tested for the factor chemokine (C-C motif) ligand 2 (CCL2), which is reported to modulate cytokine production in astrocytes (Semple, Frugier and Morganti-Kossmann, 2010). As conducted by Rushton et al., 2013, we normalized the ACM to a CCL2 concentration of 1 µg/ml. Furthermore, the same batch of ACM was used for all repeats of the same experiments to reduce variability within experiments. Disadvantage of using ACM instead of a defined media is that even with normalization of batch differences through CCL2, the concentration of factors beneficial for microglia are unknown. Next to the beneficial factors, astrocytes could secrete proteins that influence microglia differentiation and function in unknown ways.

3.4.5 Complex iPSC cultures

Improved physiological relevance of iPSC cultures is a high priority in the iPSC field. The majority of current iPSC differentiation protocols produce immature or fetal-like cells (Volpato and Webber, 2020). Protocols for 3D brain organoids have been developed, in which neurons and astrocytes differentiate alongside each other and thereby mimic endogenous development (Lee *et al.*, 2017). Microglia follow a different developmental trajectory and rarely arise spontaneously in cerebral organoids. Ormel et al., 2018 reported that microglia can develop within cerebral organoids, yet other protocols introduce exogenous microglia during the organoid differentiation, to investigate microglia in these 3D structures (Abud *et al.*, 2017; Ao *et al.*, 2021; Bodnar *et al.*, 2021). Despite their advantages, organoids are costly, time-consuming and have many experimental limitations due to the 3D structure. 2D co-cultures of iPSC derived brain cell types provide a middle ground between monocultures and organoids, in which cell types can interact and influence each other's differentiation, however, investigation of cells is easier in 2D culture conditions. Cell ratios and connectivity however is less physiological than in 3D structures and different cell types can only interact in the limited 2D environment. To distinguish cell types, a red fluorescent reporter cell line has been established. These reporter iPSC successfully differentiated to microglia-like cells and maintained robust mCherry expression throughout the differentiation. Investigating specifically one cell type of interest, i.e. microglia-like cells, in co-culture is therefore possible in live cells using live-cell imaging systems with a red fluorescence channel. Generation of a second reporter cell line (e.g. using GFP as a fluorescent reporter) would further allow to distinct two cell types in live co-culture experiments.

3.4.6 HTT CAG repeat expansions

The established co-culture conditions were furthermore used for the longitudinal analysis of CAG repeat expansion in iPSC derived brain cells. Somatic *HTT* CAG repeat expansion might contribute to HD pathogenesis and accelerate degeneration in affected cells (Swami *et al.*, 2009). The somatic *HTT* CAG instability is tissue-specific and reported to be highest in the striatum and cortex (Pinto *et al.*, 2020). Most studies investigated CAG repeat expansion in whole tissue without isolating the cell types within that tissue. Shelbourne et al., 2007 compared neuron-rich (grey matter) to glial-rich (white matter) samples from human HD cases and showed that the neuron-rich tissues were more likely to have substantial CAG length gains than glia-enriched tissues. This has led to the hypothesis that *HTT* CAG repeat expansion is primarily happening in neurons of affected brain regions, which leads to their degeneration in the progression of the disease (Petersén *et al.*, 2001; Gonitel *et al.*, 2008). However, *HTT* CAG repeat expansion of specific glial cell types have previously not been investigated.

The Q109 iPSC line is one of few iPSC lines where *HTT* CAG repeat expansions have been reported and it has therefore been used to understand and study repeat expansion in iPSC and differentiated neurons (Goold *et al.*, 2019; McAllister *et al.*, 2022). However, the expansion phenotype brings a disadvantage to these iPSC, as the *HTT* CAG repeat changes with continuous culture and might lead to different experimental outcomes. These iPSC should continuously be tested for the *HTT* CAG repeat length and it is advised to leave them in culture for minimal time. Here, CAG repeat expansion at the *HTT* locus was investigated in Q109 iPSC-derived neurons, astrocytes, and microglia-like cells. All three cell types showed *HTT* CAG expansion over the experimental period of 70 days and the rate of expansion was not significantly different between cell types. However, variability was much lower between experimental repeats of the Q109 cortical neurons compared to the Q109 microglia-like cells. For all cell types, DNA was first collected 14 days after plating precursor cells for terminal differentiation and therefore cells did not reach full maturity when DNA collection was started. For future experiments, it would be interesting to see if the expansion rate is different when DNA collection only starts after full differentiation of cells. For the cortical neurons, it looked like the *HTT* CAG repeat expansion rate was low for the first 28 days and increased afterwards. For the astrocytes, it looked like the expansion rate decreased after the first 28 days. The microglia-like cells showed a more linear increase in *HTT* CAG repeat length over the 70-day period. These findings indicate that neurons and glial cells have the potential for *HTT* CAG repeat expansion and that the process itself might be independent of cell-type specific mechanisms. However, this cell-type independent *HTT* CAG repeat expansion might be specific for the Q109 iPSC line and it needs to be confirmed that expansions are also observable with shorter *HTT* CAG repeats. Furthermore, this finding might be specific for the study of iPSC-derived cell types which exhibit a rather foetal phenotype

(Volpato and Webber, 2020). Single cell based investigation of CAG repeat expansions from human post-mortem brain tissue or mouse models could be a future method of investigating cell type specific effect of somatic *HTT* CAG repeat expansions. Here, Q22 astrocytes were used for the co-culture of Q109 microglia-like cells and neurons and the *HTT* CAG repeat expansion of the Q22 astrocytes were investigated. The 22 CAG repeats remained stable over the 70-day period.

3.5 Chapter summary

- Both Q109 and Q22 isogenic control iPSC were successfully differentiated to microglia-like cells, astrocytes, and neurons and co-culture conditions successfully developed to differentiate microglia and neurons with astrocytes.
- CAG repeat expansions were found to occur in Q109 microglia-like cells, astrocytes, and neurons in *in-vitro* long-term cultures.
- mCherry reporter cell lines were successfully generated for both Q109 and Q22 iPSC

4 Functional phenotypes of mutant HTT expressing iPSC-derived microglia-like cells

4.1 Introduction

Microglia are known to play a role in the pathology of Huntington's disease (Palpagama *et al.*, 2019). Several PET studies, using the ligand translocator protein (TSPO) that is selectively expressed by activated microglia, have demonstrated that microglia activation correlates with disease severity in HD patients (Pavese *et al.*, 2006; Politis *et al.*, 2011). Activation of microglia is evident in pre-symptomatic HD gene carriers, and can be detected up to 15 years before predicted age of onset (Tai *et al.*, 2007). These imaging-based findings were confirmed by autopsy studies where activated microglia, identified by thymosin β-4, which is increased in reactive microglia, occurred in all grades of HD pathology, and were found most prominently in the striatum and cortex. Increased accumulation of activated microglia correlated with increased disease severity as well as with neuronal loss in affected regions (E Sapp *et al.*, 2001). Furthermore, marked microgliosis, defined by histocompatibility leukocyte antigens (HLA) class II staining, was observed in post-mortem brains of HD patients, which was not found in control brains (Singhrao *et al.*, 1999).

Elevated levels of the pro-inflammatory cytokines IL-1β, IL-6, IL-8, and TNF-α were detected both centrally (in striatum and cerebrospinal fluid) and peripherally (in plasma) in HD patients (Björkqvist *et al.*, 2008; Chang *et al.*, 2015; Rodrigues *et al.*, 2016). After pro-inflammatory stimulation with LPS, primary microglia from the HD R6/2 transgenic mouse model exhibited increased levels of IL-1β, IL-6, and TNF-α compared to control microglia (Björkqvist *et al.*, 2008; H. Y. Hsiao *et al.*, 2014). These findings highlight a role for microglia activation in Huntington's disease. However, whether HD microglia themselves show mHTT induced activation and further dysfunctions or if the reported activation is a response to the detrimental HD brain environment needs further investigation.

Induced pluripotent stem cells provide a valuable tool to study cell-autonomous effects in HD patient-derived cells. Several protocols for generating microglia-like cells from iPSCs have been published (Speicher *et al.*, 2019). A first paper investigated the cell-autonomous phenotypes of an engineered isogenic series of human embryonic stem cell derived microglia-like cells, where the *HTT* gene included CAG repeat lengths of 30, 45 and 81, respectively. The HD microglia were hyper-reactive to LPS stimulation in the production of pro-inflammatory cytokines such as IL-6 and TNF-α compared to the isogenic controls, and they released elevated levels of reactive oxygen species and showed increased levels of apoptosis (O'Regan *et al.*, 2021). These findings

indicate that mutant *HTT* expression induces changes in microglia, which might contribute to HD pathology.

4.2 Chapter aims

The aim of this chapter was to investigate the effect of *HTT* CAG repeat length on microglia cell-autonomous phenotypes. Thereby microglia morphology and attachment, cytokine secretion, phagocytosis and endocytosis as well as the endosomal-lysosomal pathway and autophagy, mitochondrial health and calcium signalling were investigated. All these functions were tested in unstimulated conditions and after pro-inflammatory stimulation with IFN-γ and LPS.

4.3 Results

4.3.1 Investigating cell adhesion and morphological properties of Q109 microglia-like cells

Q109 and Q22 isogenic control iPSC were differentiated to microglia precursor cells (MPC) using an established protocol (Haenseler *et al.*, 2017). Cell adhesion of floating MPC was investigated by attachment to fibronectin, a glycoprotein of the extracellular matrix, over time. MPC were fixed 15, 60 and 120 minutes after attachment and were immunoassayed using the actin filament marker phalloidin to determine differences in cellular roundness (Figure 4.1A). A two-way ANOVA revealed a significant effect of the genotype ($(F1,48) = 24.73$, $p < 0.0001$) and time ($(F2, 48) = 9.352$, $p = 0.0004$), but not the interaction on cell adhesion. The Tukey's honest significance test showed that no difference in cellular roundness was detected between Q109 and Q22 MPC directly after plating (15-minute timepoint). Q22 isogenic control MPC exhibited a significant change in their cellular roundness within 120 minutes of attachment to fibronectin, producing finely branched filopodia-like protrusions (see white arrows, Figure 4.1A). Q109 MPC however did not show an appearance of these protrusions and exhibited no significant change in morphology over the 120 minutes of attachment to fibronectin. Even though no difference in roundness was detected directly after plating (15 minutes timepoint), a significant difference in roundness between Q109 and Q22 MPC was apparent at timepoints 60 minutes and 120 minutes after plating (Figure 4.1B).

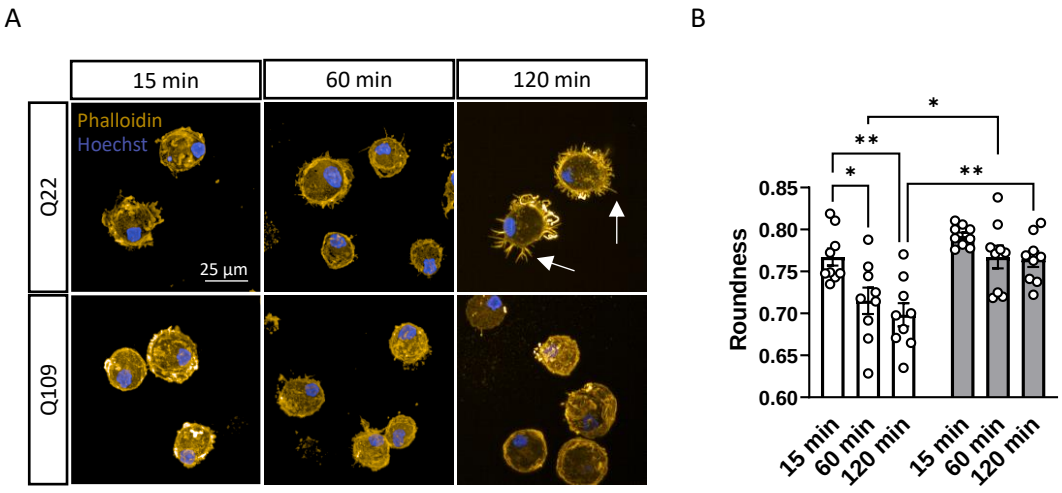

Figure 4.1: Cell adhesion to fibronectin and spreading is impaired in Q109 microglia precursor cells. Q109 and Q22 microglia precursor cells were plated onto fibronectin and fixed after 15, 60 and 120 minutes. Cells were stained for the actin filament marker phalloidin, together with the nuclear stain Hoechst. Images were taken using the Opera Phenix High-Content Screening System and cellular roundness was analysed with the Harmony software. (A) Representative images of Q22 and Q109 microglia precursor cells at three timepoints. Scale bar = 25 µm. Arrows indicate finely branched filopodia like protrusions. (B) Roundness of Q22 isogenic control cells decreased significantly over time. This decrease was not detected in the Q109 MPC. There is no difference in roundness between Q109 and Q22 MPC 15 minutes after fixing, but at 60 minutes and 120 minutes there is a significant difference. Data are expressed as mean ± SEM. n = 3 biological replicates repeated in 3 independent experiments. Statistical analysis was performed using two-way ANOVA and Tukey's honest significance test. * $p < 0.05$, ** $p < 0.01$. min = minutes.

Microglia in the healthy mature brain have a ramified morphology associated with a resting state. Loss of brain homeostasis due to disease or trauma to the brain induces profound changes to the microglia cell shape, to an ameboid, activated phenotype (Kettenmann *et al.*, 2011). iPSC-derived Q109 and Q22 MPC, plated on fibronectin, were further differentiated to a microglia-like phenotype using astrocyte-conditioned medium for 14 days. Q109 and Q22 microglia-like cells were stimulated to induce a pro-inflammatory state using IFN-γ/LPS for 24 hours. The cells were fixed and stained for phalloidin, together with the nuclear stain Hoechst (Figure 4.2A). Images were taken using the Opera Phenix High-Content Screening system and analysed with the Harmony software. Microglia-like cells were investigated for their cell area and roundness, with a roundness score between 0 and 1, and the higher the score, the rounder the cell. A two-way ANOVA revealed a significant effect of the genotype ($(F1, 32) = 4.834$, $p = 0.0352$) and stimulation ($(F1, 32) = 28.76$, $p < 0.0001$), but not the interaction on the cell area. For the roundness, the two-way ANOVA revealed a significant effect of the stimulation ($(F1, 32) = 120.6$, $p < 0.001$) but not the interaction or genotype. The Tukey's honest significance test showed that no significant difference in cell morphology was detected between Q109 and Q22 microglia-like cells. Pro-inflammatory stimulation led to an increase in cell area and decrease in roundness in both Q109 and Q22 microglia-like cells. The pro-inflammatory stimulated microglia-like cells

adapted an ameboid morphology with a loss of long ranging ramification. However, these cells showed many small finely branched filopodia like protrusions, through which the roundness score decreased compared to non-stimulated cells (Figure 4.2B).

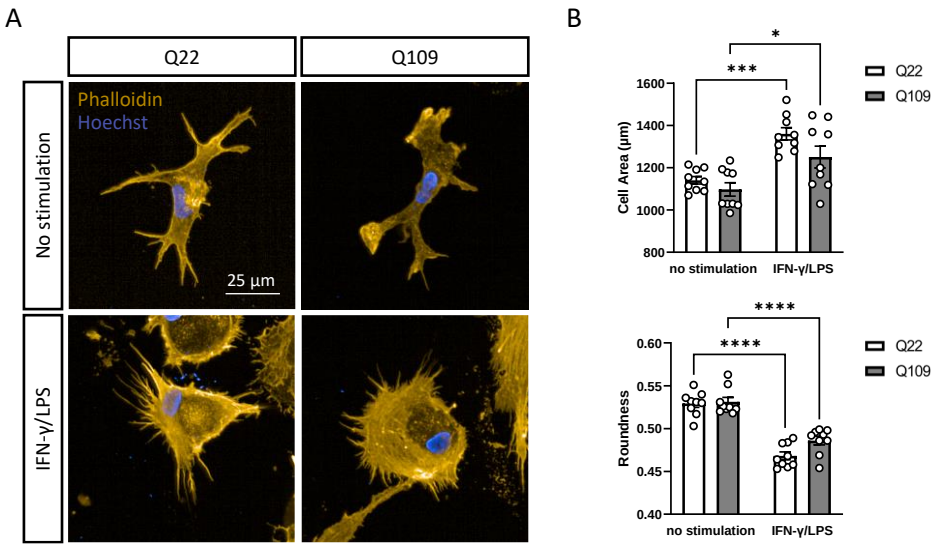

Figure 4.2: Changes in microglia-like cell morphology with pro-inflammatory stimulation. (A) Microglia-like cells were stained for phalloidin and the nuclear stain Hoechst at the Opera Phenix High-Content Screening System. Representative images of Q109 and Q22 microglia-like cells in unstimulated and pro-inflammatory stimulated condition are shown. Scale bar = 25 µm. (B) Both, Q109 and Q22 pro-inflammatory stimulated microglia-like cells exhibited significantly increased cell area and decreased roundness compared to unstimulated cells. No differences were detected between Q109 and Q22 microglia-like cells. Data are expressed as mean ± SEM. n = 3 biological replicates conducted in 3 technical replicates. Statistical analysis was performed using two-way ANOVA and Tukey's honest significance test. * $p < 0.05$, *** $p < 0.001$, **** $p < 0.0001$.

4.3.2 Q109 microglia-like cells exhibit increased secretion of pro-inflammatory cytokines

Microglia are major mediators of inflammation in the brain. They can respond to changes in their environment by producing cytokines, chemokines and by upregulating immunomodulatory surface markers (Yang *et al.*, 2010). Cytokines are used to communicate to other cells and are released for auto- and paracrine signalling (Hanisch, 2002). Q109 and Q22 microglia-like cells were assessed for the secretion of cytokines. The BD Human Inflammatory Cytokine Kit allowed for the detection of IL-8, IL-6, IL-1β, IL-10, IL-12p70 and TNF in the microglia culture supernatant via flow cytometric analysis. Microglia were differentiated for 14 days, and culture media was fully replaced before collection of supernatants after 12 hours. Q109 and Q22 microglia-like cell secretion of IL-12p70 was below detection levels of the kit. Secretion of IL-8 and IL-6 was significantly higher in Q109 microglia-like cells compared to the Q22 isogenic controls. No significant differences were detected for the cytokines IL-1β, IL-10 and TNF (Figure 4.3).

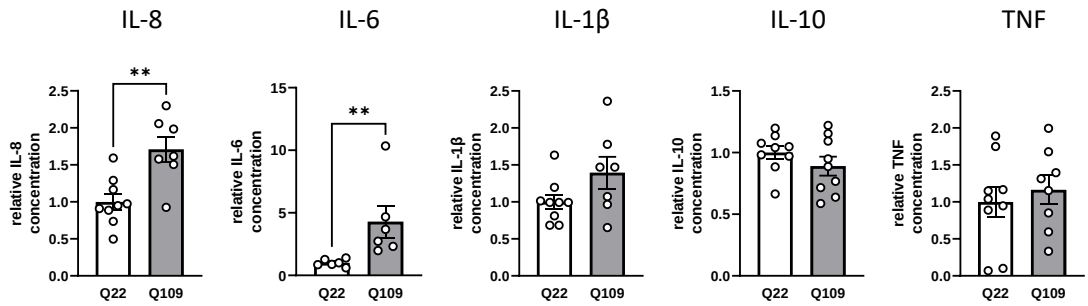

Figure 4.3: Q109 microglia-like cells exhibit increased secretion of IL-8 and IL-6 in unstimulated condition. Q109 and Q22 microglia-like cells were differentiated for 14 days. On day 14, full medium was replaced for 12 hours, and supernatants collected. The supernatants were assessed by flow cytometric analysis for the secretion of the cytokines IL-8, IL-6, IL-1β, IL-10, IL-12p70 and TNF. Q109 microglia-like cells showed an increased secretion of IL-8 and IL-6. No difference was detected for the secretion of IL-1β, IL-10 and TNF. IL-12p70 secretion was below detection levels of the used kit. Data of independent experiments were normalized to Q22 and are expressed as mean ± SEM. n = 2-3 biological replicates repeated in 3 independent experiments. Statistical analysis was performed using unpaired t-test or Mann-Whitney test (for IL-6). ** $p < 0.01$.

Cytokine secretion was additionally analysed following pro-inflammatory stimulation of microglia-like cells and compared to the unstimulated cells. Cells were stimulated with IFN-γ for 24 hours, followed by stimulation with LPS for either 3 hours or 12 hours before supernatants were collected. A two-way ANOVA revealed a significant effect of the stimulation on cytokine secretion for all tested cytokines: IL-8 ($(F2, 43) = 56.89$, $p < 0.0001$), IL-6 ($(F2, 38) = 9.393$, $p = 0.0005$), IL-1β ($(F2, 41) = 9.636$, $p = 0.0004$), IL-10 ($(F2, 46) = 6.253$, $p = 0.004$), and TNF ($(F2, 43) = 3.389$, $p = 0.043$). No significant effect was detected for the genotype or interaction. The Tukey's honest significance test showed that the increase in IL-8 secretion was significant for both Q109 and Q22 microglia stimulated for 12 hours (versus unstimulated), but also between 3 hours and 12 hours of stimulation, indicating that secretion of IL-8 is a late response to pro-inflammatory stimulation. A similar result was detected for IL-6 secretion; however the increase of IL-6 was not significant. Increase of IL-1β secretion was only significant for Q22 microglia-like cells between non-stimulated cells and stimulation for 12 hours. The increase of TNF secretion with LPS stimulation was not significant. Pro-inflammatory stimulation did not significantly affect the secretion of the anti-inflammatory cytokine IL-10 (Figure 4.4).

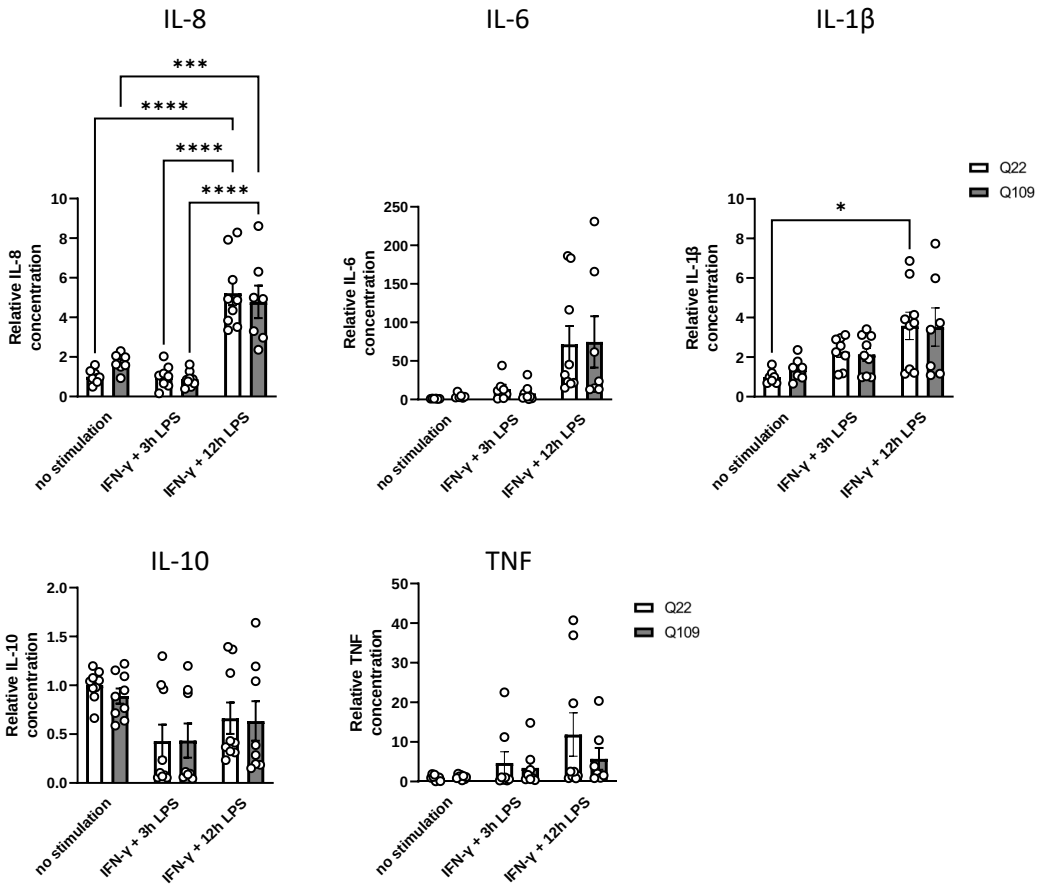

Figure 4.4: Pro-inflammatory stimulation increases cytokine secretion in both Q109 and Q22 microglia-like cells. Q109 and Q22 microglia-like cells were differentiated for 14 days. Microglia-like cells were stimulated with IFN-γ for 24 hours, followed by a full medium change and stimulation with LPS for either 3 hours or 12 hours. Supernatants were collected at these timepoints and compared to supernatant collected from unstimulated microglia-like cells. IL-8, IL-6, IL-1β and TNF were increased with stimulation. However, a significant increased cytokine secretion was only detected for IL-8 (both Q109 and Q22) and IL-1β (Q22). Data of independent experiments were normalized to unstimulated Q22 microglia-like cells and are expressed as mean ± SEM. n = 2-3 biological replicates repeated in 3 independent experiments. Statistical analysis was performed using two-way ANOVA and Tukey's honest significance test. * $p < 0.05$, *** $p < 0.001$, **** $p < 0.0001$.

4.3.3 Q109 microglia-like cells exhibit impairment in uptake of extracellular particles

Microglia contribute to brain homeostasis by rapidly clearing pathogens, apoptotic cells, and debris from the extracellular space by phagocytosis (Colonna and Butovsky, 2017). Phagocytosis is a receptor-mediated process which is triggered by receptor-ligand engagement. Q109 and Q22 microglia-like cell phagocytosis was investigated by measuring the uptake of pHrodo-labelled *E. coli* (Figure 4.5A) and Zymosan, a glucan found on the surface of yeast (Figure 4.5D). Addition of cytochalasin D (CytoD) inhibited phagocytic uptake via inhibition of actin cytoskeleton remodelling and was used as a negative control. A two-way ANOVA revealed that there was a statistically significant interaction between the effects of genotype and stimulation ($F(1, 32) = 4.254$, $p = 0.0473$) on *E. coli* phagocytosis. Simple main effects analysis showed that

stimulation had a statistically significant effect ($p < 0.0001$), but genotype did not ($p = 0.0533$). Tukey's honest significance test showed that Q109 microglia-like cells showed a significantly reduced phagocytosis of *E. coli* particles compared to the Q22 isogenic control microglia-like cells. Pro-inflammatory stimulation with IFN-γ/LPS led to a significantly decreased uptake of *E. coli* particles in both Q109 and Q22 microglia-like cells (Figure 4.5B,C). For the phagocytosis of Zymosan, two-way ANOVA revealed a significant effect of stimulation on Zymosan phagocytosis ($F(1, 24) = 150.2$, $p < 0.0001$), but not of the interaction ($p = 0.2095$) or genotype (0.8103). Tukey's honest significance test showed no difference in Zymosan phagocytosis between Q109 and Q22 microglia-like cells. Pro-inflammatory stimulation with IFN-γ/LPS had a similar effect on phagocytosis of Zymosan particles to that of *E. coli* phagocytosis and impaired the uptake significantly in both Q109 and Q22 microglia-like cells (Figure 4.5E,F).

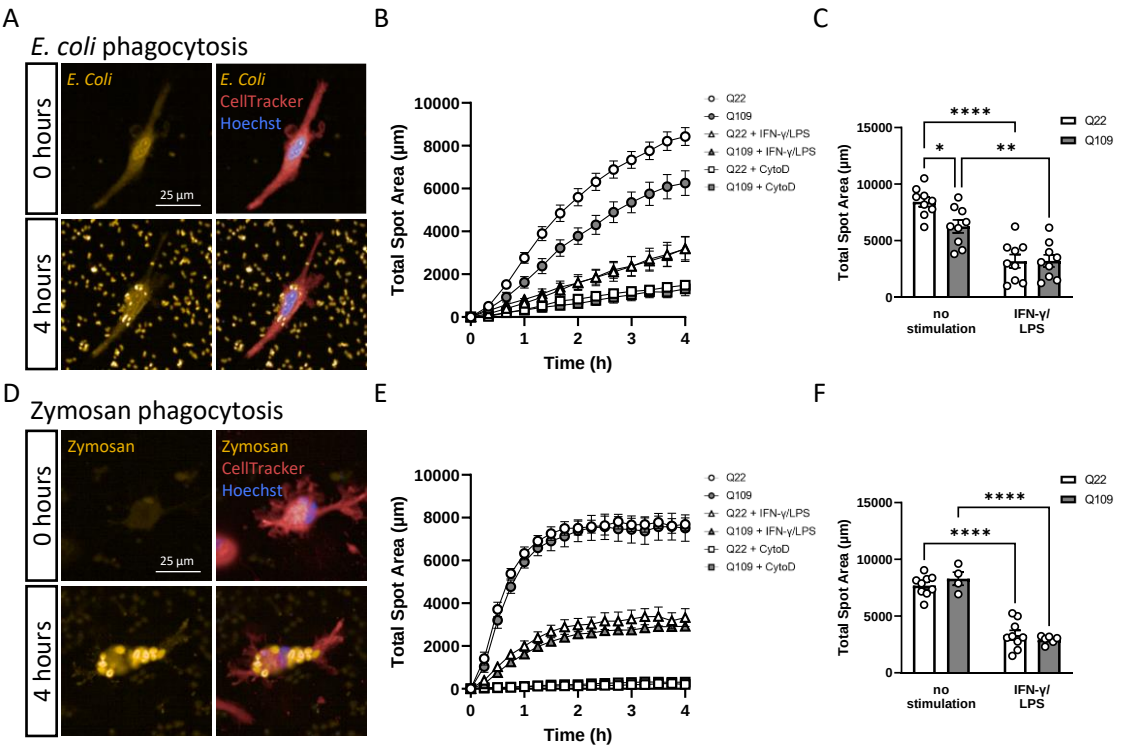

Figure 4.5: Q109 microglia-like cells show selective impairment in *E. coli* phagocytosis. (A) Phagocytosis was assessed via the uptake of pHrodo-conjugated *E. coli* particles. Representative images show the same cell at the first and last timepoint of live imaging at the Opera Phenix High-Content Screening System. (B) Q109 and Q22 microglia-like cells were imaged every 20 minutes for 4 hours with and without pro-inflammatory stimulation with IFN-γ/LPS for 24 hours. Uptake of *E. coli* particles was inhibited by the addition of 30 µM Cytochalasin D (CytoD) for 1 hour prior and during phagocytosis. (C) Total spot area of phagocytosed *E. coli* after 4 hours was significantly reduced in Q109 microglia-like cells compared to Q22 control microglia-like cells. Pro-inflammatory stimulation impaired the uptake of *E. coli* in both Q109 and Q22 microglia-like cells. (D) Representative images of Zymosan phagocytosis at first and last timepoint of live imaging. (E) Q109 and Q22 microglia-like cells were imaged every 15 minutes for 4 hours with and without pro-inflammatory stimulation with IFN-γ/LPS for 24 hours. Uptake of Zymosan particles was inhibited by the addition of 30 µM CytoD for 1 hour prior and during the phagocytosis. (F) There was no significant difference in the Zymosan phagocytosis between Q109 and Q22 microglia-like cells, but pro-inflammatory stimulation impaired the uptake of Zymosan particles in both groups. Scale bars = 25 µm. Data are expressed as mean ± SEM. n = 3 biological replicates repeated in 3 independent experiments. Statistical analysis was performed using two-way ANOVA and Tukey's honest significance test. * $p < 0.05$, ** $p < 0.01$, **** $p < 0.0001$.

While phagocytosis is used to uptake foreign particles in large vesicles that can be greater than 500 nm in diameter, microglia can also take up extracellular materials via endocytosis. Endocytosis can be split into clathrin-mediated endocytosis (CME) and macropinocytosis. CME allows the internalisation of particles between 60 - 120 nm in diameter and requires clathrin, dynamin and endophilin as key regulating proteins. CME can be measured using the glycoprotein transferrin. Macropinocytosis is endocytosis of particles around 200 nm suspended in extracellular fluid and can be measured using the complex branched glucan dextran (Kaksonen and Roux, 2018; Xiang, 2018). Q109 and Q22 microglia-like cell endocytosis was investigated by the uptake of pHrodo-labelled transferrin (Figure 4.6A) and dextran (Figure 4.6D) particles over a period of 4 hours using high-content live-cell imaging. As a negative control, addition of dynasore, a dynamine GTPase inhibitor, was used to inhibit endocytic uptake by disrupting membrane fission during endocytosis (Preta, Cronin and Sheldon, 2015). A two-way ANOVA revealed a significant effect of the genotype ($F(1, 32) = 15.08$, $p = 0.0005$) and stimulation ($F(1, 32) = 23.08$, $p < 0.0001$) on transferrin endocytosis. Tukey's honest significance test showed a significantly decreased total uptake of pHrodo-labelled transferrin in Q109 compared Q22 control microglia-like cells. Pro-inflammatory stimulation with IFN-γ/LPS led to a significantly decreased uptake of transferrin particles in both Q109 and Q22 microglia-like cells (Figure 4.6B,C). Two-way ANOVA revealed no significant effects of genotype or stimulation on dextran endocytosis. Tukey's honest significance test showed no difference in dextran endocytosis between Q109 and Q22 microglia-like cells. Pro-inflammatory stimulation with IFN-γ/LPS furthermore had no effect on dextran endocytosis (Figure 4.6E,F).

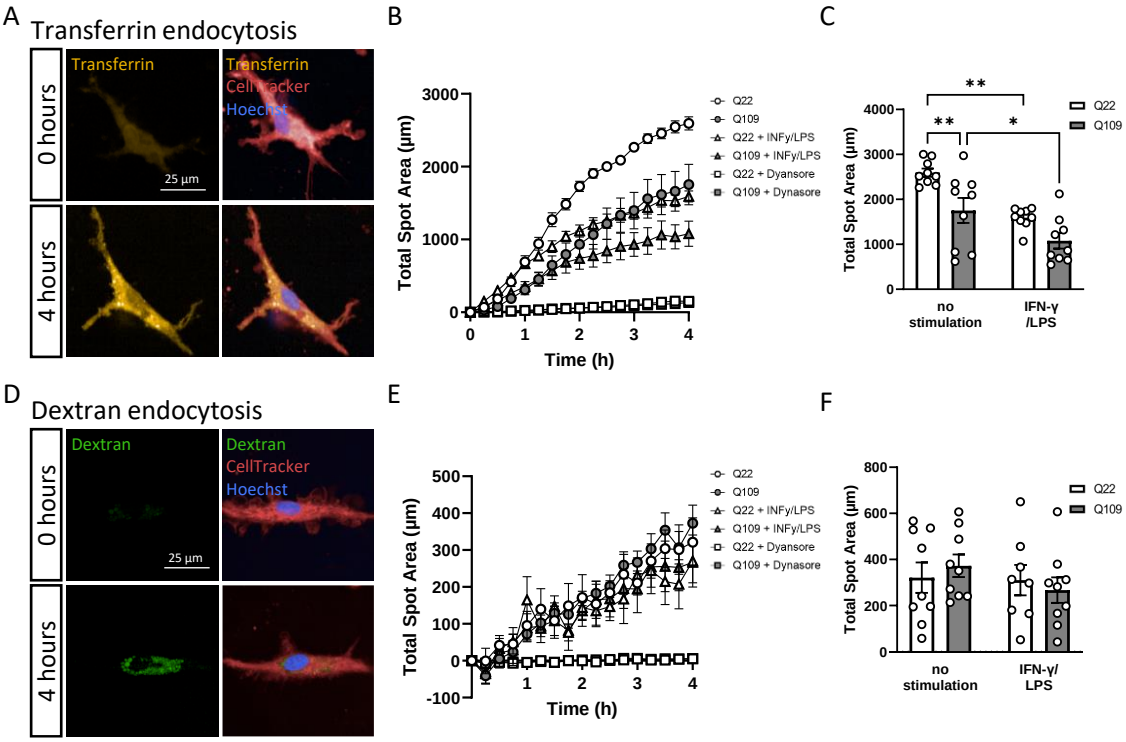

Figure 4.6: Q109 microglia-like cells show impairment in transferrin endocytosis. (A) Microglia endocytosis was assessed via the uptake of pHrodo-conjugated transferrin particles. Representative images show the same cell at the first and last timepoint of imaging at the Opera Phenix High-Content Screening System. (B) Q109 and Q22 microglia were imaged every 15 min for 4 hours with and without pre-stimulation with IFN-γ/LPS for 24 hours. Uptake of transferrin particles was inhibited by the addition of 30 µM dynasore for 1 hour prior and during the phagocytosis. (C) Total Spot Area of transferrin particles was significantly reduced in Q109 microglia-like cells compared to Q22 control microglia-like cells. Pro-inflammatory stimulation impaired the uptake of transferrin particles in both Q109 and Q22 microglia-like cells. (D) Representative images of dextran endocytosis at first and last timepoint of imaging. (E) Q109 and Q22 microglia-like cells were imaged every 15 min for 4 hours with and without pre-stimulation with IFN-γ/LPS for 24 hours. Uptake of dextran particles was inhibited by the addition of 30 µM dynasore for 1 hour prior and during the phagocytosis. (F) There was no significant difference in dextran phagocytosis between Q109 and Q22 microglia-like cells, and pro-inflammatory stimulation did not affect dextran endocytosis. Scale bars = 25 µm. Data are expressed as mean ± SEM. n = 3 biological replicates repeated in 3 independent experiments. Statistical analysis was performed using two-way ANOVA and Tukey's honest significance test. * $p < 0.05$, ** $p < 0.01$.

4.3.4 Investigation of the endosomal-lysosomal system and autophagy in Q109 microglia-like cells

Particles internalized via phagocytosis and endocytosis are sorted within the endocytic system and are transported via complex vesicular routes. This system is comprised of early and late endosomes, as well as lysosomes. Progression of endosomes into lysosomes introduces an acidic environment for proteolysis of unwanted materials (Hu *et al.*, 2015). The early endosomes function as a key sorting station in the cell where it is decided what can be reutilized and what is targeted for degradation. When early endosomes progress to late endosomes and lysosomes, the V-ATPase, a multi-subunit proton pump, is responsible for increased acidification from early

endosomes (pH 6.2) to lysosomes (pH 5) (Scott, Vacca and Gruenberg, 2014). Commonly used markers for early and late endosomes are the small GTPases RAB5 and RAB7, respectively, which organize effector proteins into specific membrane subdomains (Rink *et al.*, 2005). Q109 and Q22 microglia-like cells with and without prior pro-inflammatory stimulation were co-stained for RAB5 and RAB7 (Figure 4.7A). Intensity of the staining (intensity 594 or 488), number of endosomes (number of spots / cell) and total area covered by endosomes (total spot area) were investigated. Two-way ANOVA revealed a significant effect of the stimulation on RAB5 intensity ($F(1, 32) = 4.353$, $p = 0.0450$) and number of RAB5+ early endosomes ($F(1, 32) = 5.243$, $p = 0.0288$). It also showed a significant effect of the genotype on number of RAB5+ early endosomes ($F(1, 32) = 9.624$, $p = 9.624$) and total area covered by RAB5+ early endosomes ($F(1, 32) = 9.193$, $p = 0.0048$). Tukey's honest significance test showed that pro-inflammatory stimulated Q109 microglia-like cells exhibited significantly less RAB5+ spots than stimulated Q22 microglia-like cells. No other parameter showed a significant difference for RAB5 staining between Q109 and Q22 microglia-like cells using Tukey's honest significance test (Figure 4.7B). The same analysis was conducted for RAB7+ late endosomes. Two-way ANOVA revealed a significant effect of the stimulation on RAB7 intensity ($F(1, 32) = 7.137$, $p = 0.0118$) and number of RAB7+ late endosomes ($F(1, 32) = 4.610$, $p = 0.0395$). It also showed a significant effect of the genotype on RAB7 intensity ($F(1, 32) = 13.84$, $p = 0.0008$), number of RAB7+ late endosomes ($F(1, 32) = 25.76$, $p < 0.0001$) and total area covered by RAB7+ late endosomes ($F(1, 32) = 24.80$, $p < 0.0001$). Tukey's honest significance test showed that unstimulated Q109 microglia-like cells showed a significant reduction in RAB7 staining intensity, as well as in the number and total area of RAB7 spots. Furthermore, pro-inflammatory stimulated Q109 microglia-like cells showed a significant reduction in RAB7 spot number and total area (Figure 4.7C).

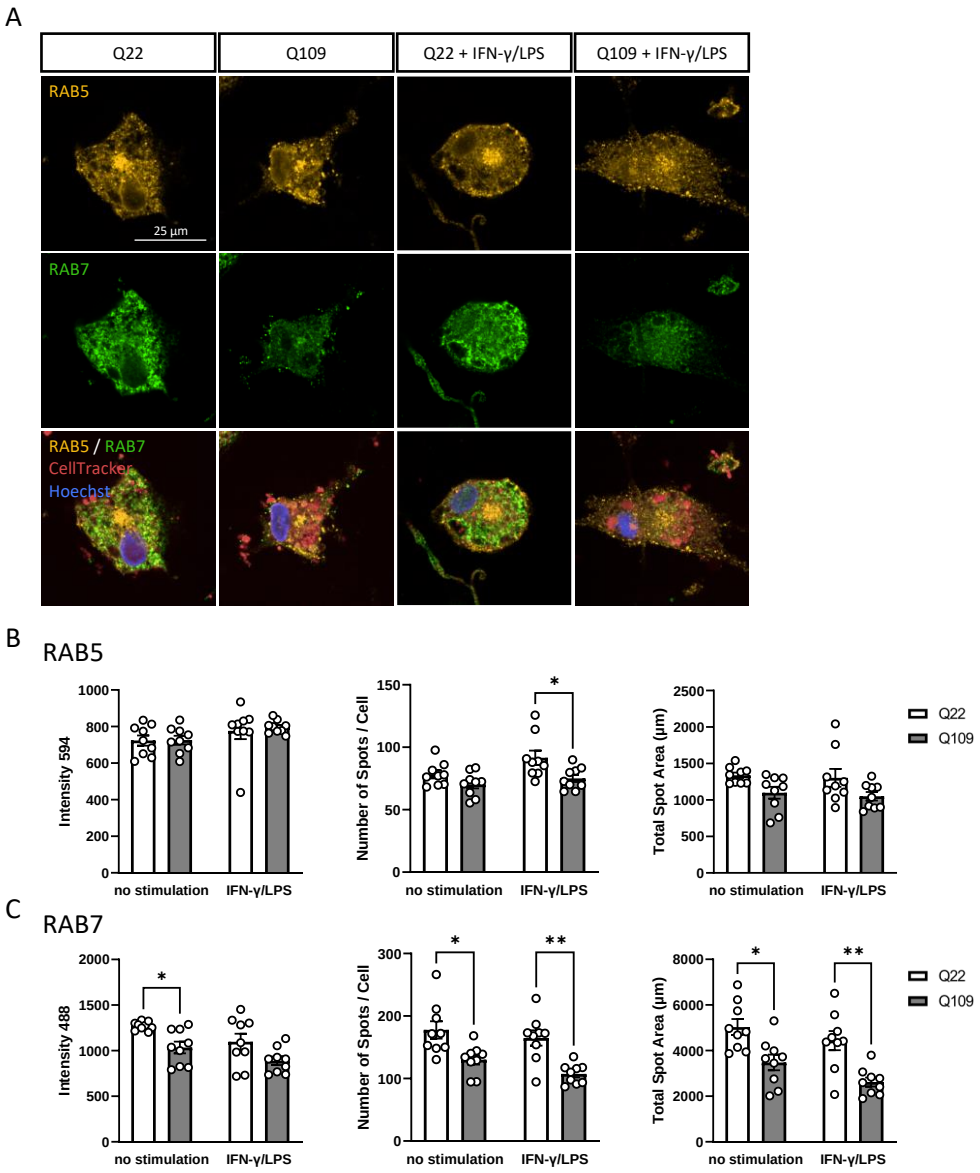

Figure 4.7: Q109 microglia-like cells exhibit reduced number of late endosomes. (A) Q109 and Q22 microglia-like cells were fixed with and without prior pro-inflammatory stimulation with IFN-γ/LPS for 24 hours. Early and late endosomes were accessed via immunostaining using the early endosome marker RAB5 and late endosome marker RAB7, together with the cytoplasmic marker CellTracker and nuclear stain Hoechst. Scale bar = 25 µm. (B) RAB5 positive early endosomes were investigated for staining intensity, number of spots / cell and total spot area. Pro-inflammatory stimulated Q109 microglia-like cells exhibited significantly less early endosomes than stimulated Q22 microglia-like cells. All other investigated measures showed no difference between Q109 and Q22 microglia-like cells. (C) RAB7 positive late endosomes were investigated for staining intensity, number of spots / cell and total spot area. Unstimulated Q109 microglia-like cells showed significantly decreased staining intensity, as well as spot number and total spot area compared to Q22 microglia-like cells. Pro-inflammatory stimulated Q109 microglia-like cells showed significantly decreased spot number and total spot area compared to pro-inflammatory stimulated Q22 microglia-like cells. Data are expressed as mean ± SEM. n = 3 biological replicates repeated in 3 independent experiments. Statistical analysis was performed using two-way ANOVA and Tukey's honest significance test. * $p < 0.05$, ** $p < 0.01$.

Lysosomes serve as organelles for storage of hydrolases, and are the final destination where proteolytic degradation takes place (Hu *et al.*, 2015). In order to investigate lysosome number, size and cellular distribution, Q109 and Q22 microglia-like cells were stained using LysoTracker Green, together with the cytoplasmic dye CellTracker Far Red and the nuclear stain Hoechst (Figure 4.8A). Microglia-like cells were imaged using high-content live-cell imaging. Prior to staining, microglia-like cells were stimulated with IFN-γ/LPS for 24 hours. Intensity of the staining (intensity 488), number of lysosomes (number of spots / cell), lysosomal size (individual spot area), and total area covered by lysosomes (total spot area) were investigated. Two-way ANOVA revealed a significant effect of the genotype on lysosomal size ($F(1, 32) = 13.43$, $p = 0.0009$). It also showed a significant effect of the stimulation on number of lysosomes ($F(1, 32) = 7.530$, $p = 0.0099$), lysosomal size ($F(1, 32) = 5.023$, $p = 0.0321$), and total area covered by lysosomes ($F(1, 32) = 12.35$, $p = 0.0013$). Tukey's honest significance test showed that without stimulation, no significant differences in the lysosomes between Q109 and Q22 microglia-like cells were detected. With stimulation, the individual lysosome size was significantly decreased in Q109 compared to Q22 microglia-like cells. The total cell area covered by lysosomes was decreased in Q22 microglia-like cells with stimulation, but not in Q109 microglia-like cells. No significant differences were detected for lysosome numbers (Figure 4.8B). Furthermore, a role for lysosomal positioning on its function has been described previously (Korolchuk *et al.*, 2011). Therefore, lysosomal positioning was investigated by defining a perinuclear region around the nucleus in an automated protocol using the Harmony software (Figure 4.8C, left). The percentage of lysosomes that were located within the perinuclear region compared to the whole cell was calculated. Two-way ANOVA revealed a significant effect of the stimulation on perinuclear lysosome numbers ($F(1, 32) = 16.33$, $p = 0.0003$). Tukey's honest significance test showed that pro-inflammatory stimulated Q22 microglia-like cells exhibited a significant increase in perinuclear lysosomes compared to unstimulated Q22 microglia-like cells. No significant difference was found between Q109 and Q22 microglia (Figure 4.8C, right).

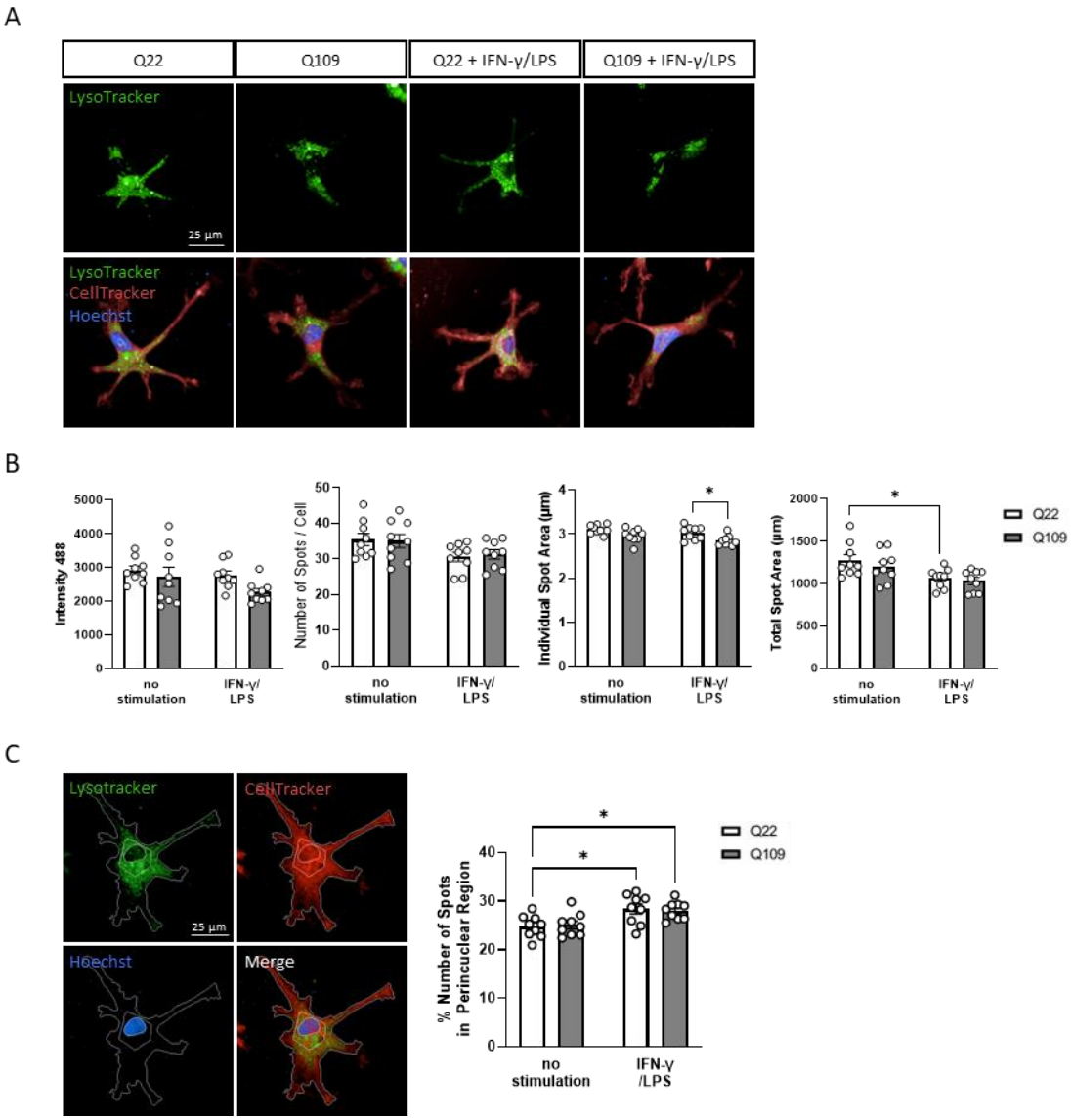

Figure 4.8: Investigation of lysosomal numbers, size, and positioning. (A) Q109 and Q22 microglia-like cell lysosomes were stained using LysoTracker Green, together with the cytoplasmic dye CellTracker and nuclear stain Hoechst. (B) Intensity 488, number of spots / cell, individual spot area, and total spot area were investigated. There was no difference in the number of lysosomes between groups, but a significant difference in the lysosomal size between pro-inflammatory stimulated Q109 and Q22 microglia-like cells was detected. Furthermore, there was a significant decrease in the total lysosomal area in stimulated Q22 control microglia-like cells compared to unstimulated Q22 microglia-like cells. (C) Lysosomal positioning was investigated by defining a perinuclear region. Percentage of number of lysosomes in the perinuclear region compared to the whole cell was investigated. Pro-inflammatory stimulation significantly increased the number of perinuclear lysosomes in Q22 microglia-like cells, but no difference was detected between the two groups. Scale bars = 25 µm. Data are expressed as mean ± SEM. n = 3 biological replicates repeated in 3 independent experiments. Statistical analysis was performed using two-way ANOVA and Tukey's honest significance test. * $p < 0.05$.

DQ BSA was used to investigate protease activity as part of the cellular degradation pathway in microglia-like cells. Upon hydrolysis of DQ BSA by proteases, a bright fluorescent product is produced. DQ BSA was combined with CellTracker Far Red and the nuclear stain Hoechst. The V-ATPase inhibitor bafilomycin A1 was used as a negative control to inhibit protease activity

(Mauvezin and Neufeld, 2015) (Figure 4.9A). Images were analysed for intensity of the fluorescent product, number of spots, individual spot area and total spot area. Two-way ANOVA revealed a significant effect of the stimulation on DQ BSA intensity ($F(2, 48) = 86.17$, $p < 0.0001$), number of DQ BSA spots ($F(2, 48) = 137.1$, $p < 0.0001$), individual spot area ($F(2, 48) = 126.4$, $p = 0.0001$), and total DQ BSA area ($F(2, 48) = 181.0$, $p < 0.0001$). No effect was detected for genotype or the interaction between genotype and stimulation. Tukey's honest significance test showed no differences between Q109 and Q22 microglia-like cells. Pro-inflammatory stimulation with IFN-γ/LPS led to a significant decrease in protease activity in both Q109 and Q22 microglia-like cells in all output measures. The addition of bafilomycin A1 almost completely inhibited the breakdown of DQ BSA (Figure 4.9B).

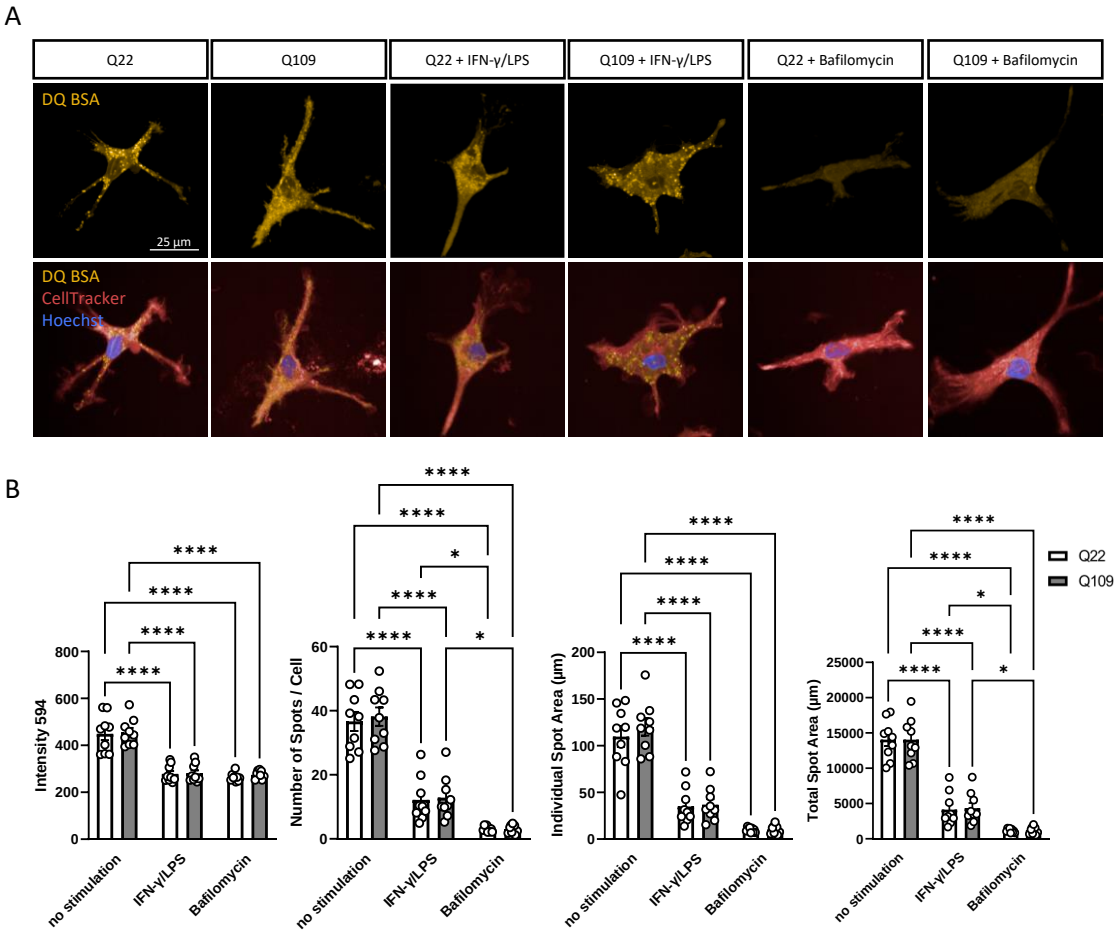

Figure 4.9: DQ BSA degradation is impaired after pro-inflammatory stimulation of both Q109 and Q22 microglia-like cells. (A) Protease activity was investigated using DQ BSA, together with the cytosolic dye CellTracker and nuclear stain Hoechst. (B) Intensity, number of spots / cell, individual spot area, and total spot area were investigated. The V-ATPase inhibitor bafilomycin A1 was used to inhibit the degradation of DQ BSA. The results indicate an impairment of proteolytic activity with pro-inflammatory stimulation of both Q109 and Q22 microglia-like cells. No difference was detected between Q109 and Q22 microglia-like cells. Bafilomycin A1 successfully inhibited proteolytic activity. Scale bar = 25 µm. Data are expressed as mean ± SEM. n = 3 biological replicates repeated in 3 independent experiments. Statistical analysis was performed using two-way ANOVA and Tukey's honest significance test. * $p < 0.05$, **** $p < 0.0001$.

Next to endosomes and lysosomes, cells carry autophagic vesicles that are important to remove misfolded or aggregated proteins, and that can clear damaged organelles (Glick, Barth and Macleod, 2010). The CYTO-ID stain was used for selectively staining autophagic vesicles. Q109 and Q22 microglia-like cells were co-stained with the cytoplasmic dye CellTracker Far Red and the nuclear stain Hoechst. 24 hours prior to the staining, microglia-like cells were stimulated with IFN-γ/LPS. As a positive control, cells were treated for 24 hours with the rapamycin analogue PP242 that inhibits mammalian target of rapamycin (mTOR) and can be used to induce autophagy (Hoang *et al.*, 2012) (Figure 4.10A). CYTO-ID intensity, number of autophagic vesicles (number of spots / cell), vesicle size (individual spot area), and total area covered by autophagic vesicles (total spot area) were investigated. Two-way ANOVA revealed a significant effect of the genotype on CYTO-ID intensity ($F(1, 45) = 11.27$, $p = 0.0016$), vesicle size ($F(1, 45) = 9.929$, $p = 0.0029$), and total area covered by autophagic vesicles ($F(1, 45) = 10.03$, $p = 0.0028$). No effect was detected for genotype or the interaction between genotype and stimulation. Tukey's honest significance test showed that without stimulation, no significant differences between Q109 and Q22 microglia-like cells were detected. With pro-inflammatory stimulation there was a significant decrease in CYTO-ID staining intensity in Q109 compared to Q22 microglia-like cells. None of the other parameters showed a significant difference in autophagic vesicles between the groups. PP242 was expected to activate autophagy, however no significant increases in any of the output measures were detected (Figure 4.10B).

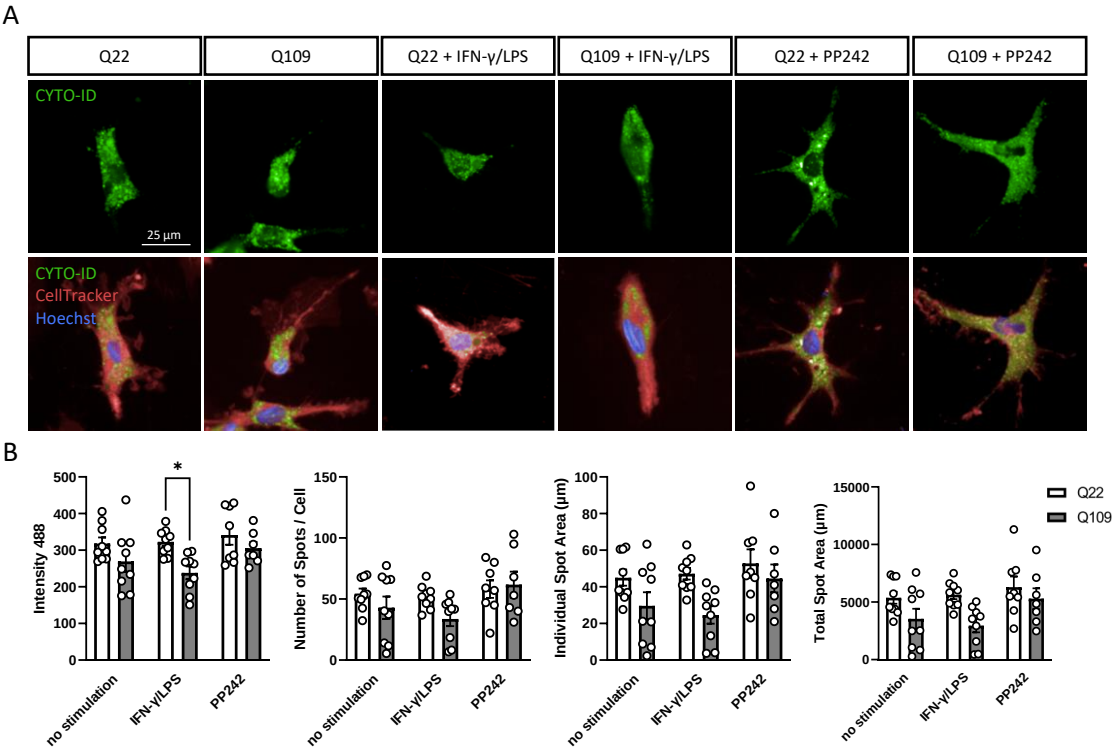

Figure 4.10: Pro-inflammatory stimulation induced a significant decrease in CYTO-ID staining intensity in Q109 microglia-like cells. (A) Autophagic vesicles were stained using the CYTO-ID dye, together with CellTracker and Hoechst. (B) Intensity 488, number of spots / cell, individual spot area, and total spot area were investigated. 30 µM of the rapamycin analogue PP242 was used to stimulate autophagy. A decrease in the intensity of the CYTO-ID dye per cell was detected in pro-inflammatory stimulated Q109 microglia-like cells compared to pro-inflammatory stimulated Q22 control microglia-like cells. No difference was detected in the vesicle number and morphology measures. Addition of PP242 did not lead to a significant increase in the autophagy measures. Scale bar = 25 µm. Data are expressed as mean ± SEM. n = 3 biological replicates repeated in 3 independent experiments. Statistical analysis was performed using two-way ANOVA and Tukey's honest significance test. * $p < 0.05$.

4.3.5 Investigation of mitochondrial respiration in Q109 microglia-like cells

Mitochondria conduct many functions in cells, including ATP production via oxidative phosphorylation, and they contribute to cellular stress responses such as autophagy and apoptosis (Nunnari and Suomalainen, 2012). The Cell Mito Stress Test is a common method to measure the key parameters of mitochondrial respiration (Gu *et al.*, 2021). Using this assay on the Agilent Seahorse XF96 machine, oxygen consumption rate (OCR) of Q109 and Q22 microglia-like cells with or without pro-inflammatory stimulation with IFN-γ/LPS was investigated. Different drugs were used to target various complexes of the electron transport chain. Basal respiration can be determined by the starting OCR. The ATP synthase (complex V) inhibitor oligomycin prevents the flow of electrons through the electron transport chain, thereby reducing the OCR. The difference of OCR before and after addition of oligomycin determines the ATP production. The uncoupling agent FCCP activates the proton conductance through the plasma membrane and thereby causing the proton gradient to collapse. This leads to a maximum rate of oxygen consumption by complex IV without ATP production. The increase in OCR between the starting OCR and the OCR after FCCP addition indicates the spare respiratory capacity, indicating the cellular response to increased energy demand under stress. Lastly, rotenone and antimycin A were added to the cells. The complex I inhibitor rotenone prevents the transfer of electrons from complex I to ubiquinone. The complex III inhibitor antimycin A prevents the electron transfer between cytochrome b and c. Adding these drugs inhibits the mitochondrial respiration and determines the non-mitochondrial oxygen consumption. The difference of the OCR before and after addition of rotenone and antimycin A determines the maximal respiration. The difference of OCR after addition of oligomycin and after the addition of rotenone & antimycin A indicates the proton leak (Figure 4.11).

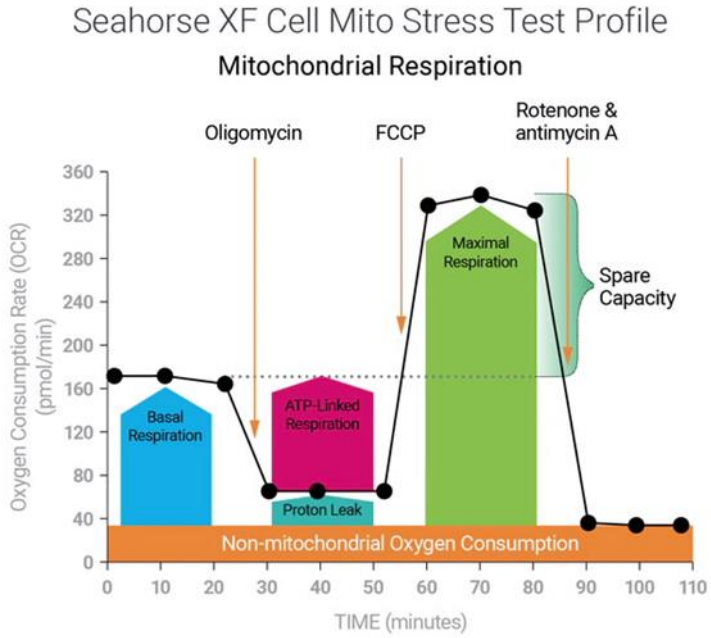

Figure 4.11: Mitochondrial Respiration Seahorse XF Cell Mito Stress Test. In order to measure mitochondrial respiration, Oxygen consumption rate (OCR) was measured with the addition of the drugs oligomycin, FCCP and antimycin A & Rotenone, which target the electron transport chain. Image taken from Agilent website (https://www.agilent.com/en/product/cell-analysis/real-time-cell-metabolic-analysis/xf-assay-kits-reagents-cell-assay-media/seahorse-xf-cell-mito-stress-test-kit-740885).

Two-way ANOVA revealed a significant effect of the genotype on basal respiration ($F(1, 20) = 8.010$, $p = 0.0103$), ATP production ($F(1, 20) = 4.822$, $p = 0.0401$), and proton leak ($F(1, 20) = 11.62$, $p = 0.0028$). It also revealed a significant effect of the stimulation on basal respiration ($F(1, 20) = 59.85$, $p < 0.0001$), ATP production ($F(1, 20) = 42.43$, $p < 0.0001$), spare respiratory capacity ($F(1, 20) = 55.28$, $p < 0.0001$), non-mitochondrial oxygen consumption ($F(1, 20) = 27.38$, $p < 0.0001$), and proton leak ($F(1, 20) = 63.15$, $p < 0.0001$). Tukey's honest significance test showed that in unstimulated conditions, no differences in mitochondrial respiration were detected between Q109 and Q22 microglia-like cells. With pro-inflammatory stimulation, Q109 microglia-like cells showed a significantly higher basal respiration than Q22 microglia-like cells. Compared to the genotype, the pro-inflammatory stimulation had a larger effect on mitochondrial respiration in both, Q109 and Q22 microglia-like cells. Basal respiration, ATP production and proton leak were significantly increased in both Q109 and Q22 pro-inflammatory stimulated microglia-like cells. Non-mitochondrial oxygen consumption was significantly increased only in Q109 pro-inflammatory stimulated compared to non-stimulated Q109 microglia-like cells. The spare respiratory capacity was decreased in both Q109 and Q22 pro-inflammatory stimulated microglia-like cells. These findings indicate that pro-inflammatory stimulated microglia-like cells have a higher energetic demand (indicated by increased basal respiration) and therefore a higher ATP production than unstimulated microglia-like cells. Due

to the higher energy demand, the pro-inflammatory stimulated microglia like-cells exhibited a significantly lower spare respiratory capacity, indicating how close the cells are to the theoretical maximal respiration. Pro-inflammatory stimulated Q109 microglia-like cells have a significantly higher basal respiration compared to Q22 microglia-like cells, suggesting an enhanced energy demand on the stimulated Q109 microglia-like cells (Figure 4.12).

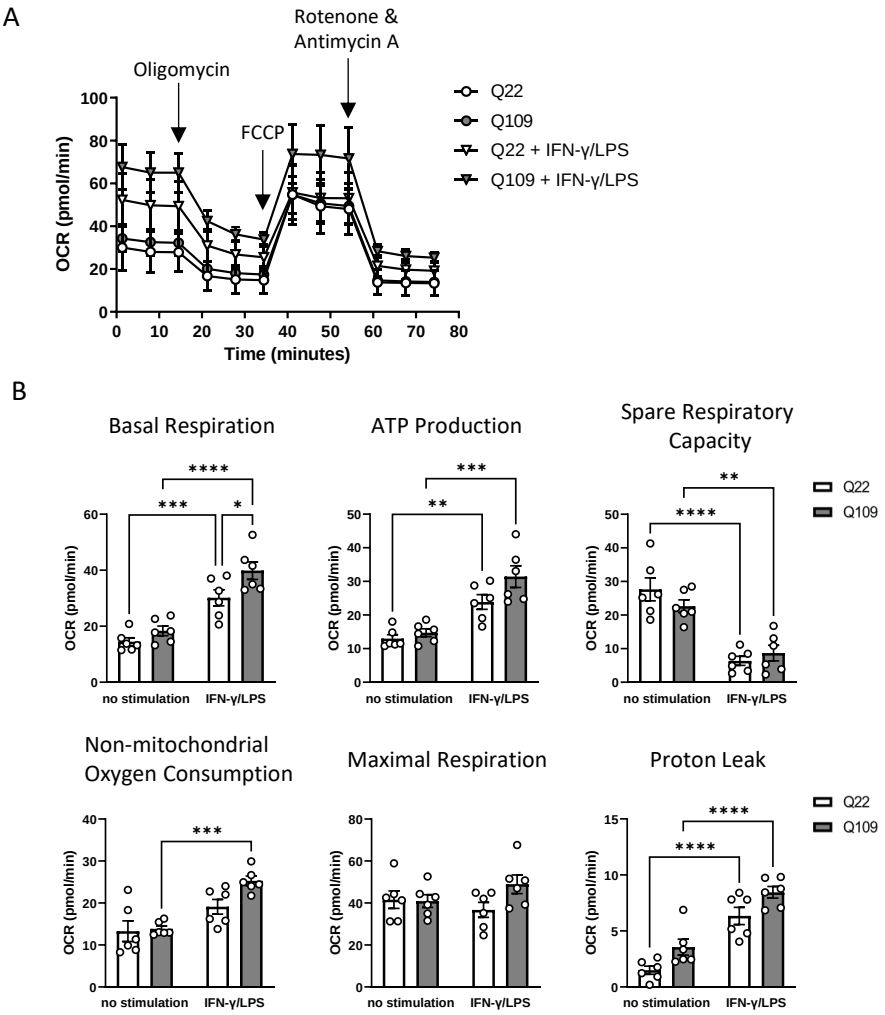

Figure 4.12: Pro-inflammatory stimulated Q109 and Q22 microglia-like cells exhibit an increased energy demand compared to non-stimulated microglia-like cells. (A) Overview of Cell Mito Stress Test showing changes in oxygen consumption rate (OCR) between Q109 and Q22 microglia-like cells in pro-inflammatory and non-stimulated conditions. (B) Investigation of mitochondrial respiration parameters. In unstimulated conditions, no differences in mitochondrial respiration were detected between Q109 and Q22 microglia-like cells. With pro-inflammatory stimulation, Q109 microglia-like cells showed a significantly higher basal respiration than Q22 microglia-like cells. Significant differences between non-stimulated and pro-inflammatory stimulated microglia-like cells, in both Q109 and Q22, were detected for Basal Respiration, ATP Production, Spare Respiratory Capacity and Proton Leak. Non-mitochondrial oxygen consumption was significantly increased in Q109 pro-inflammatory stimulated compared to non-stimulated microglia-like cells. Data are expressed as mean ± SEM. Data were normalized to cell count. n = 3 biological replicates repeated in 2 independent experiments. Statistical analysis was performed using two-way ANOVA and Tukey's honest significance test. * $p < 0.05$, ** $p < 0.01$, *** $p < 0.001$, **** $p < 0.0001$.

4.3.6 Q109 microglia-like cells show impaired calcium handling

Intracellular Ca^{2+} modulates several microglial activities, including proliferation, migration, and phagocytosis (Palomba *et al.*, 2021). Q109 and Q22 microglia-like cells were stained for the calcium indicator Fluo-8 AM and changes in intracellular calcium concentrations were measured using the FLIPR Penta High-Throughput Cellular Screening System. In order to investigate changes in intracellular calcium, the difference between baseline calcium and the maximum signal was determined. First, microglia-like cells were treated with the calcium ionophore ionomycin which facilitates the transport of extracellular Ca^{2+} across the plasma membrane and releases Ca^{2+} from its intracellular stores. Two-way ANOVA revealed a significant effect of the genotype on intracellular calcium after ionomycin stimulation ($F(1, 28) = 20.92$, $p < 0.0001$). Tukey's honest significance test showed that Q109 microglia-like cells had a significantly lower increase in intracellular calcium in response to ionomycin treatment compared to Q22 microglia-like cells (Figure 4.13A). Furthermore, intracellular calcium changes in response to the purines ATP and ADP were tested. Purine-related actions are mediated by the activation of ligand gated ionotropic P2X receptors (P2XR) and G protein-coupled metabotropic P2Y receptors (P2YR). P2XR exclusively bind ATP, while P2YR have mixed purine ligand selectivity. Two-way ANOVA revealed a significant effect of the genotype on intracellular calcium after ATP stimulation ($F(1, 32) = 36.24$, $p < 0.0001$), but not ADP stimulation ($F(1, 32) = 1.152$, $p = 0.2912$). No effect was detected for stimulation or the interaction between genotype and stimulation. Tukey's honest significance test showed that with ATP stimulation, Q109 microglia-like cells responded with a significantly lower increase of intracellular calcium than Q22 microglia-like cells (Figure 4.13B). However, with ADP stimulation, no significant difference in the increase in intracellular calcium was detected between Q109 and Q22 microglia-like cells (Figure 4.13C).

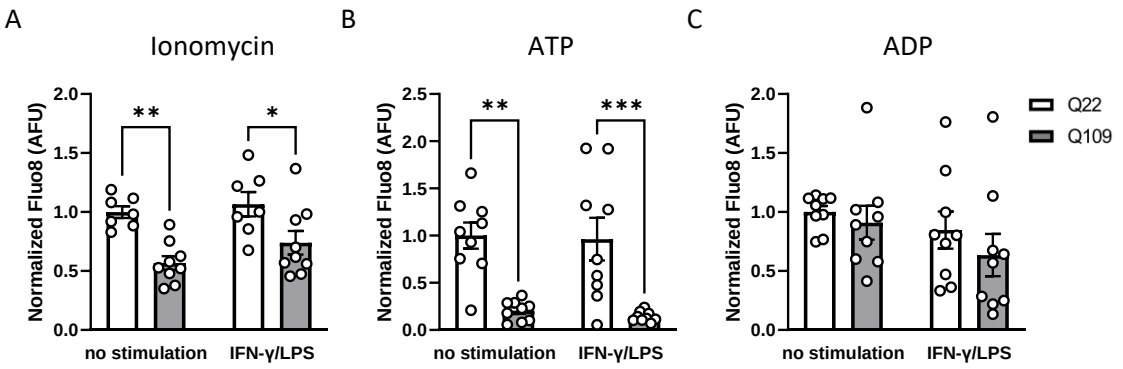

Figure 4.13: Q109 microglia-like cells show impaired calcium responses. General calcium handling using ionomycin and response to the purines ATP and ADP was measured using Fluo-8 AM and the FLIPR Penta High-Throughput Cellular Screening System. Increase in intracellular calcium as a response to 1 µM ionomycin was significantly decreased in Q109 compared to Q22 microglia-like cells. ATP and ADP increase intracellular calcium concentrations in microglia-like cells by specific ionotropic and metabotropic purinergic receptors on the microglial membrane. Q109 microglia-like cells showed significantly lower calcium responses to 50 µM ATP but not to 100 µM ADP compared to Q22 microglia-like cells. Data are expressed as mean ± SEM. Data were normalized to cell count. n = 3 biological replicates repeated in 3 independent experiments. Statistical analysis was performed using two-way ANOVA and Tukey's honest significance test. * $p < 0.05$, ** $p < 0.01$, *** $p < 0.001$.

4.4 Discussion

4.4.1 Summary

In this chapter the effects of mutant *HTT* expression on microglia morphology and function was investigated. Core functions were compared between Q109 and Q22 microglia-like cells with or without pro-inflammatory stimulation using IFN-γ/LPS. Q109 microglia showed disturbances in some of these microglia functions.

4.4.2 Pro-inflammatory stimulation

Pro-inflammatory stimulation with IFN-γ/LPS changed the microglia morphology and affected almost every function investigated in this chapter. This combined stimulation was chosen as LPS is the most commonly used experimental pro-inflammatory stimulus for microglia, however, in disease other pro-inflammatory cytokines, including IFN-γ, are present (Lively and Schlichter, 2018). Monzan et al. showed that iPSC-derived microglia-like cells stimulated with LPS and IFN-γ exhibited a common axis of transcriptomic changes with Alzheimer's disease genetic mouse models of microglia, indicating that the stimulation with LPS and IFN-γ resembles a neurodegenerative disease phenotype. The authors of this study used 10 ng/ml LPS and 10 ng/ml IFN-γ for 24 hours or 48 hours before performing single cell RNA sequencing (Monzón-Sandoval *et al.*, 2022). Here, IFN-γ was used to prime the microglia-like cells. Priming generally permits an exaggerated microglial response to a secondary inflammatory stimulus (here LPS) (Ta *et al.*, 2019). Many studies using iPSC-derived macrophages and microglia-like cells used LPS at a concentration of 100 ng/ml alone (Abud *et al.*, 2017; Badanjak *et al.*, 2021), or together with 100 ng/ml IFN-γ (Haenseler *et al.*, 2017; Hall-Roberts *et al.*, 2020; Vahsen *et al.*, 2022). Higher concentrations of LPS up to 10 µg/ml were shown to decrease viability of microglia (von Zahn *et al.*, 1997). Here, concentrations closer to the Monzón-Sandoval *et al.*, 2022 study were chosen, as the authors demonstrated robust gene transcription changes that already occur with the lower concentrations of LPS and IFN-γ.

4.4.3 Cell spreading

Cell spreading of MPC on fibronectin substrate was assayed. Some protocols for the differentiation of iPSC to microglia-like cells use the extracellular matrix protein fibronectin as a coating to support microglia attachment and maturation (Amos *et al.*, 2017; Maguire *et al.*, 2021). Fibronectin was shown to be mainly produced by astrocytes in the brain (Liesi, Kirkwood and Vaheri, 1986). Adhesion to fibronectin is mediated by integrins on the cellular surface, especially the integrins α5β1 and αvβ3 (Danen *et al.*, 2002). Chamak & Mallat highlighted that fibronectin induced the transformation of round or spindle-shaped primary rat macrophages into cells displaying a reduced cell body and extending thin and long processes. They describe this transformation of the cellular morphology to be associated with a reorganization of the vimentin network (Chamak and Mallat, 1991). Here, the attachment of MPC to the extracellular matrix protein fibronectin was tested for the first 120 minutes after plating. Q22 MPC attached to the plate and started to ramify, building small filopodia like protrusions. The Q109 MPC stayed round and did not show an occurrence of protrusions within the first 120 minutes after plating. If this effect is due to different amounts of integrins present on the microglia surface would be an interesting question for future investigations.

4.4.4 Morphology

After 14 days of differentiation on fibronectin towards a microglia-like phenotype no difference in roundness between Q109 and Q22 microglia-like cells was detected. Also, no difference in cell area was detected between Q109 and Q22 microglia-like cells. Therefore, the reported phenotype of decreased Q109 MPC attachment to fibronectin compensates with time. HD iPSC-derived cortical neurons have been reported to display an altered morphology, demonstrated by a reduced neurite length (Mehta *et al.*, 2018). This change in morphology, induced by expression of mHTT, has not been reported for astrocytes or microglia and might therefore be a phenotype distinct to neurons. When stimulated with the pro-inflammatory agents IFN-γ and LPS, the microglia-like cells showed an increase in cell soma size and a shortening of the long, branched processes towards a ramified morphology with fine protrusions. Due to the fine protrusions, the measure of cellular roundness quantified the pro-inflammatory stimulated microglia as less round than the unstimulated microglia. Yang et al. defined the ability to dynamically change their processes as one of the components of microglia plasticity. With the elongation of microglial processes, the cells scan their surrounding environments and contribute to the brain homeostasis more effectively, while the stimulation of microglia induces shortening of process length (Yang *et al.*, 2019). However, between the ramified and ameboid morphology, microglia can exhibit a variety of morphological transition states, which may reflect disease-

specific functional cell states which are still to be investigated (Leyh *et al.*, 2021b). To summarize, mutant *HTT* expression did not affect microglia-like cell morphology, however, activation with pro-inflammatory agents did for both Q109 and Q22 microglia-like cells.

4.4.5 Cytokine secretion

Pro-inflammatory cytokine secretion is an important functional microglia phenotype to assess. Microglia are the unique resident immune cells of the brain acting as primary mediators of inflammation. Therefore, most studies of microglia in Huntington's disease have focussed on cytokine release. In HD patients, elevated levels of pro-inflammatory cytokines have been detected both centrally and peripherally (Björkqvist *et al.*, 2008; Chang *et al.*, 2015; Rodrigues *et al.*, 2016). Increased levels of cytokines have also been seen in primary microglia from HD R6/2 transgenic mice after pro-inflammatory stimulation with LPS (Hsiao *et al.*, 2013). Pro-inflammatory stimulation with IFN-y and LPS has been reported to induce a hyper-responsive phenotype of HD ESC-derived microglia compared to isogenic controls (O'Regan *et al.*, 2021). However, the secretion of cytokines without prior pro-inflammatory stimulation has not been tested on HD microglia yet. Here, Q109 microglia-like cells showed an increased secretion of IL-8 and IL-6 in unstimulated conditions. This suggests that mutant *HTT* expression may activate microglia in a cell-autonomous manner and they might contribute to the neuroinflammatory pathology of HD from early on, even before degenerative processes in the HD brain further activate microglia. Pro-inflammatory gene expression in HD microglia was reported to be dependent on expression and transcriptional activities of the myeloid lineage-determining factors PU.1 and C/EBPs (Yang *et al.*, 2017). Future experiments in Q109 and Q22 microglia-like cells should include the analysis of gene expression changes in these factors. Pro-inflammatory stimulation with IFN-y and LPS increased the amount of cytokines secreted in both Q109 and Q22 microglia-like cells. An increase in IL-1β secretion was already detectable after 3 hours of LPS stimulation and increases further with a prolonged LPS stimulation of 12 hours. Increased secretion of IL-8 and IL-6 was only detectable after 12 hours of LPS stimulation. This showed that both Q109 and Q22 microglia-like cells have the capacity to increase cytokine secretion as a response to stimulation, however no significant differences between Q109 and Q22 microglia-like cells were detected after stimulation. To conclude, here it was shown for the first time that HD microglia-like cells showed basal elevation of pro-inflammatory cytokine secretion compared to isogenic control microglia-like cells.

4.4.6 Phagocytosis

In order to investigate the phagocytic function of microglia, uptake of two different cargo was tested. Even though Zymosan and *E. coli* are both taken up via the mechanism of phagocytosis, they differ in size and bind to different receptors at the microglial membrane. Zymosan is derived from a yest cell wall and is phagocytosed via binding to Toll-like receptor (TLR)2 acting in collaboration with CD14 and TLR6 (Frasnelli *et al.*, 2005; Lax *et al.*, 2020), while bacterial particles from *E. coli* are binding a complex of TLR4, MD-2, and CD14 (Sato *et al.*, 2003; Alvestegui *et al.*, 2019). Here, Q109 microglia-like cells showed an impairment in the uptake of pHrodo labelled *E. coli*, but not Zymosan compared to the Q22 control microglia-like cells. A previous investigation of HD ESC-derived microglia-like cells found no significant difference in the phagocytosis of Zymosan and *E. coli* in microglia with high *HTT* CAG repeat lengths compared to low *HTT* CAG repeat lengths. However, the data indicate a trend towards decrease in *E.coli* phagocytosis with higher CAG repeat lengths that was not significant (O'Regan *et al.*, 2021). The pro-inflammatory stimulation using IFN-y and LPS, in both Q109 and Q22 microglia-like cells, induced an impairment in phagocytosis of both *E. coli* and Zymosan particles. Previous studies have reported that LPS can increase microglial phagocytosis (Abd-El-Basset and Fedoroff, 1995; Ribes *et al.*, 2009; Sivagnanam, Zhu and Schlichter, 2010), however the activation using the combination of IFN-y and LPS might induce an activated phenotype that upregulates cytokine secretion and downregulates homeostatic functions including phagocytosis. To conclude, here it was shown for the first time that phagocytosis is impaired in HD microglia, however this phenotype is cargo specific.

4.4.7 Endocytosis

While phagocytosis is generally defined as the uptake of particles greater than 500 nm including foreign pathogens, dead or dying cells, and other particulate debris, smaller particles are ingested by endocytosis. Receptor-mediated endocytosis is the ingestion of specific substances that bind to receptors on the cell membrane in a clathrin-dependent pathway and macropinocytosis is endocytosis of small particles suspended in extracellular fluid (Xiang, 2018; Maguire *et al.*, 2022). Both ways of endocytosis were investigated in Q109 and Q22 microglia-like cells. Transferrin is an iron-binding protein that binds to the transferrin receptor and enters the cell through clathrin-mediated endocytosis (Mayle, Le and Kamei, 2012). Dextran is a polysaccharide commonly used to study macropinocytosis (Chazotte, 2009). A significant difference between Q109 and Q22 microglia was detected for the endocytosis of transferrin, but not dextran. Endocytosis defects have been reported in HEK293 and PC3 cells with polyQ aggregation (Meriin *et al.*, 2003; Yu *et al.*, 2014). It is hypothesized that protein aggregation can

inhibit clathrin-mediated endocytosis by chaperone competition. As seen in the phagocytosis assays, the pro-inflammatory stimulation led to a significant impairment in transferrin endocytosis. However, the stimulation had no effect on dextran endocytosis. To conclude, endocytosis, just like phagocytosis, seems to be affected by mutant *HTT* expression in a cargo-specific manner.

4.4.8 Endosomal-lysosomal system

After extracellular particles are taken up by microglia via the different routes of endocytosis and phagocytosis, the cargo that is designed for degradation is transferred from early endosomes to late endosome and then ultimately to lysosomes for degradation (Rink *et al.*, 2005). Multiple proteins that interact with HTT are implicated in vesicle trafficking. The HTT-associated protein 40 (HAP40) has been identified as an effector of RAB5 as HAP40 mediates the recruitment of HTT by RAB5 onto early endosomes (Pal *et al.*, 2008). The huntingtin interacting protein (HIP1) is an endocytic protein which structural integrity is crucial for maintenance of normal vesicle size (Waelter *et al.*, 2001). Proteins of the RAB family are commonly used to characterise endosomes. RAB5 is considered a marker for early endosomes and RAB7 for late endosomes (Shearer and Petersen, 2019). Here, RAB5 and RAB7 antibodies were used for immunostaining of early and late endosomes. Q109 microglia-like cells showed a reduced staining intensity, as well as reduced number of endosomes and total endosome area for the RAB7 late endosome marker. This difference was not apparent for the early endosome marker RAB5. Only after pro-inflammatory stimulation did the Q109 microglia-like cells showed a reduced number of early endosomes stained by RAB5 compared to Q22 microglia-like cells. Even though pro-inflammatory stimulation reduced endocytosis and phagocytosis, no effect of the stimulation was detected for early and late endosome markers RAB5 and RAB7.

Early studies using HD patient iPSCs investigated lysosomes using LysoTracker Red and showed that HD iPSCs and derived neurons exhibited an increased lysosomal activity, indicated by an increased LysoTracker Red intensity (Camnasio *et al.*, 2012b) as well as detected an increase in lysosomal numbers in HD iPSCs (Castiglioni *et al.*, 2012). Here, no differences in LysoTracker intensity were found between Q109 and Q22 microglia-like cells. The only difference detected was a decreased lysosomal size of pro-inflammatory stimulated Q109 microglia-like cells compared to stimulated Q22 controls. Further investigation of lysosomes could be performed by immunostaining for the lysosomal membrane proteins, such as LAMP1 and LAMP2 (Barral *et al.*, 2022). Also, the pro-inflammatory stimulation did not have an influence on LysoTracker intensity or lysosomal numbers and morphology, but a significant decrease of the total LysoTracker area of pro-inflammatory Q22 microglia-like cells compared to non-stimulated Q22

cells was detected. Furthermore, a role for lysosomal positioning on its function has been described previously and was found to take place in cells from the HD knock-in mice STHdhQ111 and primary fibroblasts from an HD patient. HD cells were shown to exhibit a perinuclear accumulation of lysosomes (Erie *et al.*, 2015). The authors hypothesize that the perinuclear accumulation of lysosomes led to altering lysosomal-dependent functions including increased basal mammalian target of rapamycin complex 1 (mTORC1) activity and premature fusion of lysosomes with autophagosomes. Here, no difference in the percentage of lysosomes in the perinuclear region between Q109 and Q22 microglia-like cells were found. However, a perinuclear accumulation of lysosomes was detected after pro-inflammatory stimulation in both Q109 and Q22 microglia, indicating that cellular stress does affect lysosomal positioning and potentially function in microglia-like cells.

Endo-lysosomal vesicles contain multiple highly potent proteolytic enzymes, which facilitate the hydrolysis of peptide bonds (López-Otín and Bond, 2008). When lysosomal proteases cathepsin D and B were overexpressed in HEK293 cells containing 145 *HTT* CAG repeats, the enzymatic activity of cathepsin D and B increased and that consequently reduced full-length and cleaved forms of the huntingtin protein, indicating a beneficial effect of sufficient protease activity in HD pathology (Liang *et al.*, 2011). DQ BSA was used to investigate lysosomal hydrolase activity. The cargo is endocytosed by microglia-like cells and gets trafficked through early endosomes to late endosomes which then fuse with acidic hydrolase containing lysosomes. These endo-lysosomes degrade DQ BSA which leads to de-quenching of the fluorescence of the dye attached to the BSA and therefore to the production of a bright fluorescent product that can be detected via imaging (Marwaha and Sharma, 2017). Even though a cargo-specific impairment of endocytosis was detected in the Q109 microglia-like cells, no difference was detected between Q109 and Q22 microglia-like cells in their ability to degrade the DQ BSA. However, pro-inflammatory stimulation decreased protease activity in both Q109 and Q22 microglia-like cells significantly. As also endocytosis was impaired by pro-inflammatory stimulation, the decreased degradation of DQ BSA might be a due to both, impairments in endocytosis as well as protease activity. Further investigation will be needed to decipher the exact mechanism behind the decreased DQ BSA degradation after pro-inflammatory stimulation. Bafilomycin A1 was used to show specificity of the staining, as it inhibits protease activity (Mauvezin and Neufeld, 2015).

Autophagy is a process that amongst other task removes misfolded or aggregated proteins and can clear damaged organelles (Glick, Barth and Macleod, 2010). In HD the expanded CAG repeat in the huntingtin gene leads to a misfolded mHTT protein that is not degraded and accumulates in the cell. These misfolded proteins aggregate and form inclusion bodies in the nucleus and cytoplasm and the extent of the inclusions correlates with the length of the *HTT* CAG repeat

(Cortes and La Spada, 2014). Both soluble and aggregated forms of mHTT are thought to be cleared preferentially through autophagy (Rubinsztein, 2006). Martinez-Vicente et al. could demonstrate in cellular and mouse models of HD that autophagic vacuoles formed at normal or even enhanced rates in HD cells and are adequately eliminated by lysosomes, but they failed to trap cytosolic cargo and thereby exhibit an inefficient engulfment of cytosolic components by autophagosomes (Martinez-Vicente *et al.*, 2010). In HD iPSC-derived medium spiny neurons (HD-MSN) a decrease in autophagy was detected using multiple assays (Oh *et al.*, 2022). The authors showed a reduced number of pre-fusion autophagosomes and post-fusion autolysosomes in HD-MSN compared to pre-HD-MSN and Ctrl-MSN. They also showed a lower CYTO-ID signal in HD-MSN. Here, the CYTO-ID stain was used for selectively labelling autophagic vesicles. The number of detected spots was not significant different between Q109 and Q22 microglia-like cells. Only a decrease in staining intensity of pro-inflammatory stimulated Q109 compared to stimulated Q22 control microglia-like cells was detected. The rapamycin analogue PP242 that inhibits mTOR was used to induce autophagy in the microglia-like cells, however no significant difference between the PP242-treated and untreated cells were detected. This might be due to the fact that already a lot of autophagic vesicles were detected in the untreated cells, so that a further increase was not detectable with the software used to analyse the images. It could also be that an ineffective concentration of the PP242 was used to stimulate autophagy in the microglia-like cells. No change in autophagic vesicles was detected with pro-inflammatory stimulation in either Q109 or Q22 microglia-like cells. It has previously been reported that autophagic flux was suppressed in LPS-stimulated microglial cells, which was indicated by a decreased expression of the autophagy marker LC3 (Ye *et al.*, 2020). Here, autophagy was only investigated by CYTO-ID, a stain that preferentially binds to pre-autophagosomes at an early stage of autophagy. As described above, autophagy is an important cellular function that is likely to be dysfunctional in HD. Therefore, Q109 and Q22 microglia-like cells should undergo further investigation of autophagy in future studies. This could include staining for the autophagic marker LC3 in order to confirm or disprove these findings.

4.4.9 Mitochondria

Mitochondria are important for oxidative phosphorylation to produce cellular ATP, and they participate in ion homeostasis, metabolic pathways, apoptosis and ROS production (Brand *et al.*, 2013). Mitochondrial function is also required to sustain the activity of ATP-dependent chaperones and proteolytic lysosomes (Soares *et al.*, 2019b). Mitochondrial dysfunction has been reported in HD, including reduction of Ca^{2+} buffering capacity, loss of membrane potential, and decreased expression of oxidative phosphorylation enzymes (Damiano *et al.*, 2010).

Mitochondrial dysfunction has been shown to take place in the pathology of HD, however the striatum is preferentially vulnerable to mitochondrial disorders and impaired oxidative phosphorylation enzyme activities are reported to be restricted to the basal ganglia in the HD brain (Browne *et al.*, 1997). The Mito Stress test has been performed on iPSC-derived medium spiny neurons, and a lower ATP production and maximal respiration has been reported for the Q109 line compared to a non-isogenic control line (HD iPSC Consortium, 2020). The only difference in the mitochondrial respiration that was found between Q109 and Q22 microglia-like cells is a significant increase in basal respiration of Q109 pro-inflammatory stimulated microglia-like cells, compared to stimulated Q22 isogenic controls. Pro-inflammatory stimulation however increased basal respiration, ATP production and the proton leak as well as decreased the spare respiratory capacity in both Q109 and Q22 microglia-like cells. In line with these findings are reports that activation of microglia by pathogens, neuronal damage or other kinds of stimulation increases their energy demand (Kalsbeek, Mulder and Yi, 2016).

4.4.10 Calcium signalling

Lastly, calcium-signalling disruption is described as one of the HD hallmark pathologies (Kolobkova *et al.*, 2017a). mHTT can affect calcium signalling in many ways, including interactions with calcium-binding proteins and mitochondrial membranes, regulation of the calcium influx from extracellular medium, and the release of calcium from intracellular stores (Kolobkova *et al.*, 2017b). It has also been shown in the HD R6/2 mice that mHTT changes the expression of calcium homeostasis genes (Luthi-Carter *et al.*, 2002). Intracellular calcium is of importance for microglia, as it modulates key activities including migration and phagocytosis (Palomba *et al.*, 2021). A decreased intracellular calcium increase in response to ionomycin stimulation was detected in Q109 microglia-like cells compared to Q22 microglia-like cells. Ionomycin was shown to enhance Ca^{2+} influx by stimulating store-regulated cation entry and not by a direct action at the plasma membrane (Morgan and Jacob, 1994). Furthermore, ATP is a purine participating in the cross-talk between neurons, astrocytes and microglia in the brain and it mediates microglia responses to brain injury as well as the migration towards the site of injury and phagocytosis of cellular debris (Davalos *et al.*, 2005; Maeda *et al.*, 2016; Illes *et al.*, 2020). Here, Q109 microglia-like cells showed decreased calcium signalling in response to ATP, but not ADP, compared to Q22 control microglia-like cells. This might be explained due to a dysfunction or decreased number of specifically P2X receptors on the microglia membrane, receptors which exclusively bind ATP (Khakh and Alan North, 2006). No effect of pro-inflammatory stimulation was detected for ionomycin, ATP and ADP. This is in contrast to a paper where LPS treatment of primary mouse microglia led to a suppression of evoked calcium signalling, indicated by reduced

calcium transients during stimulation with UTP or the complement factor 5a (Hoffmann *et al.*, 2003).

4.5 Chapter Summary

- Comparing Q109 and Q22 microglia like cells, a number of phenotypes were detected: Q109 MPC showed impaired attachment to fibronectin but Q109 and Q22 microglia-like cells showed no significant difference in their morphology. Q109 microglia-like cells exhibit increased secretion of pro-inflammatory cytokines. Q109 microglia-like cells showed decreased *E. coli* phagocytosis and transferrin endocytosis, but no difference between Q109 and Q22 microglia-like cells was detected for zymosan phagocytosis and dextran endocytosis. Q109 microglia showed a reduction in late endosomes, but no significant differences between Q109 and Q22 microglia were detected for early endosomes, lysosomes, protease activity and autophagosomes. Q109 microglia-like cell mitochondria were not impaired compared to Q22 microglia-like cells, but Q109 microglia-like cells showed a decreased response in intracellular calcium changes to stimulation with ionomycin and ATP, but not ADP.
- Pro-inflammatory stimulation using LPS and IFN-γ affected multiple of the microglia-like cell phenotypes: The stimulation induced an ameboid microglia-like cells morphology as well as increased pro-inflammatory cytokine secretion. It decreased *E. coli* and zymosan phagocytosis as well as transferrin endocytosis, but not dextran endocytosis. Stimulated microglia-like cells showed no significant change in their endosomes and autophagosomes but exhibited an increased perinuclear positioning of lysosomes and decreased protease activity. Pro-inflammatory stimulated microglia-like cells showed an increased energy demand but no effect on intracellular calcium signalling when stimulated with ionomycin, ATP and ADP.

5 Investigating transcriptional changes in Huntington's disease microglia-like cells

5.1 Introduction

Sequencing of RNA (RNA-Seq) is a common method to analyse gene expression and uncover differences between samples in an unbiased approach (Hrdlickova, Toloue and Tian, 2017). HD iPSC-derived cells have been investigated for changes in their transcriptome. Mehta et al., differentiated HD patient iPSC lines with different CAG repeat lengths into cortical neurons. They compared these patient lines with non-HD controls with CAG repeat lengths below 33 at various timepoints of the cortical neuron differentiation (Mehta et al., 2018). The authors found that when comparing HD and control cortical neurons, the top categories describing the HD gene expression changes were associated with cellular morphology, cell movement, hereditary disorder, neurological disease, and nervous system development and function (Mehta et al., 2018). The HD iPSC consortium performed bulk RNA sequencing of Q109 and non-isogenic control iPSC-derived neurons (Lim *et al.*, 2017). The authors identified differences in genes related to pathways of neuronal development and maturation. Furthermore, expression of genes involved in glutamate and GABA signalling, axonal guidance and calcium influx were found to be decreased in HD iPSC-derived neurons (Lim *et al.*, 2017). Single-nuclei RNA sequencing has recently been performed on HD iPSC-derived astrocytes. iPSC-derived astrocytes from HD patients with CAG repeat lengths of 46 and 53 were compared to control iPSC-derived astrocytes. The analysis revealed alterations in morphology, glutamate uptake, dysregulation of astrocyte identity and maturation, and dysregulated actin-mediated signalling (Reyes-Ortiz et al., 2022). Comparing results from RNA sequencing between HD iPSC-derived brain cells can uncover common and cell-type specific effects of mutant *HTT* expression. HD microglia have not yet been investigated for their transcriptional changes.

Microglia activation is a commonly reported phenotype in HD (Palpagama *et al.*, 2019) and it's cause is not well understood. Pro-inflammatory stimulation is a tool to investigate microglia activation in cell culture (Lively and Schlichter, 2018). The combination of LPS, a bacterial endotoxin, and the cytokine IFN-γ is commonly used in iPSC-derived microglia-like cells (Haenseler *et al.*, 2017; Hall-Roberts *et al.*, 2020; Vahsen *et al.*, 2022). Monzan et al., showed that the combined stimulation with LPS and IFN-γ even resembles a neurodegenerative disease transcriptional phenotype (Monzón-Sandoval *et al.*, 2022).

Genomic differences between iPSC lines arise from subchromosomal copy number variations, and single nucleotide variations. These variations commonly come from the genetic background of the iPSC donor, but can also be introduced during the generation and maintenance of iPSC lines (Liang and Zhang, 2013). Isogenic control iPSC differ from the patient iPSC only by the corrected disease mutation and thereby overlap in their CNV and SNV, representing a more reliable source for comparison of the disease phenotype (Nami *et al.*, 2021).

5.2 Chapter aims

The aim of this chapter was to perform bulk RNA sequencing on Q109 and Q22 microglia-like cells in unstimulated and pro-inflammatory activated states. Differences between Q109 and Q22 microglia-like cells were first assessed in an unstimulated state in order to investigate HD microglia cell-autonomous phenotypes. Both, Q109 and Q22 microglia-like cells received pro-inflammatory stimulation for either 3 hours or 12 hours. In order to understand the microglial response to stimulation, changes in the Q22 microglia-like cells between the unstimulated state and the two timepoints of stimulation were first investigated. Subsequently, 12-hour stimulated Q109 and Q22 microglia-like cells were compared in order to investigate differences in their response to activation. Lastly, the differentially expressed genes between Q109 and Q22 microglia-like cells were compared between the unstimulated state and after 12-hour LPS stimulation.

5.3 Results

Bulk RNA sequencing has been performed to compare the transcriptomes of Q22 and Q109 microglia-like cells. Three clones of each genotype were used in one replicate each (Q22: 2H1, 3H2, 5H9; Q109: 109n1, 109n4, 109n5). RNA was collected from microglia-like cell cultures with and without pro-inflammatory activation (Figure 5.1A). To activate the microglia-like cells they were primed using 100 ng/ml IFN-y for 24 hours, followed by stimulation with 10 ng/ml LPS for either 3 hours or 12 hours. Hierarchical clustering of all samples was performed and revealed that the Q22 clone 3H2 clustered with the Q109 samples (see Appendix Figure 9.1B). No material was left from the RNA sequencing to confirm the genotype of the sample 3H2, as it looks like the sample might have been mixed up and is a Q109. Further experiments have been conducted with microglia-like cells from the same differentiation and these also reveal that the sample 3H2 behaves likes a Q109. These functional investigations include microglia precursor attachment to fibronectin (Figure 9.1C) and calcium response to stimulation with ATP (Figure 9.1D). After long discussions, it was decided to remove the sample 3H2 from the analysis performed in this

chapter. Principle component analysis (PCA) was performed on the remaining samples and highlighted the variance in the data. Principle component (PC)1 separated Q109 from Q22 microglia-like cells. PC2 separated unstimulated from LPS stimulated samples (Figure 5.1B). Raw data including the lists of differentially expressed genes from the comparisons conducted in this chapter, as well as tables for the gene ontology analysis are added to the appendix (see Chapter 9.1).

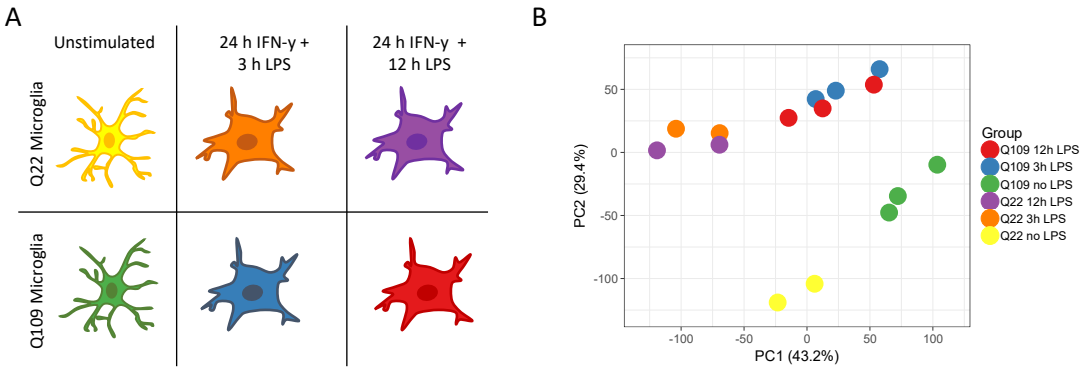

Figure 5.1: RNA sequencing experimental layout and variance in the data. (A) Schemata of the microglia-like cell conditions used in the experiment. Q22 and Q109 microglia-like cells were either investigated in an unstimulated condition or after priming with IFN-γ and stimulation with LPS for either 3 hours or 12 hours. (B) Principal component analysis of all samples separated Q109 from Q22 microglia in PC1 and unstimulated from stimulated samples in PC2.

5.3.1 Transcriptional differences between unstimulated Q109 and Q22 microglia-like cells

Unstimulated Q22 and Q109 microglia-like cells were compared (Figure 5.2A). The two groups showed distinct gene expression patterns, highlighted by separation in PC1 of the principal component analysis. PC2 showed variability between the cell lines (Figure 5.2B). The top 20 most p-value significant differentially expressed genes (DEG) were plotted in a heatmap, of which 16 were significantly downregulated in the Q109 microglia-like cells (Figure 5.2C). A volcano plot highlighted genes that were differentially expressed between Q109 and Q22 microglia-like cells with $p_{adj} < 0.01$ and Log2 fold change (FC) > 1.5 (Figure 5.2D). 1103 genes were found to be significantly upregulated, and 214 genes to be significantly downregulated in the Q109 microglia-like cells.

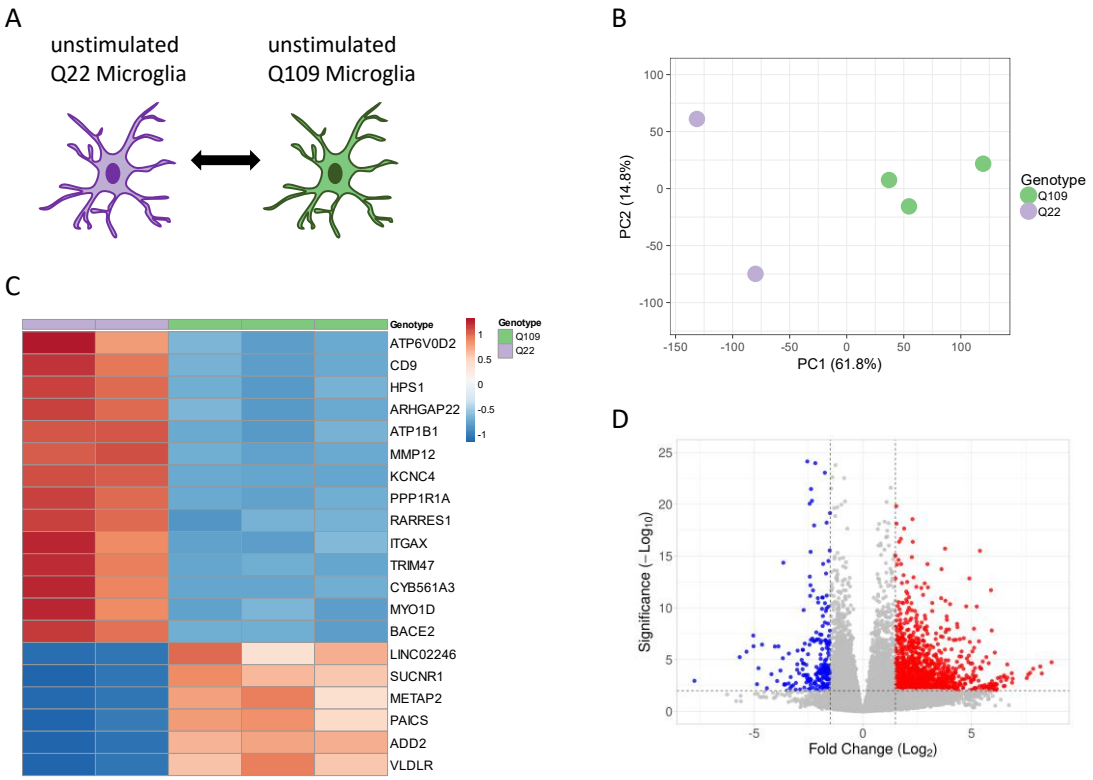

Figure 5.2: Basic characterisation of transcriptional differences between Q22 and Q109 microglia-like cells. (A) Schemata of comparison conducted. (B) PCA separated Q22 and Q109 microglia in principle component 1. PC2 showed variance between cell lines. (C) Top 20 most p-value significant genes were plotted in a clustered heatmap with a diverging colour scale. (D) The volcano plot highlighted genes that were significantly differentially expressed, indicating 1103 genes in red that were upregulated and 214 in blue that were downregulated in Q109 versus Q22 microglia-like cells.

To further investigate the DEG, these were taken forward for gene ontology analysis using g:Profiler. Enriched biological processes and KEGG pathways were generated, and the top 10 terms plotted together with the -Log10(p_{adj}). The top 10 enriched biological processes for the downregulated genes in the Q109 versus Q22 microglia-like cells, included terms relating to vesicle-mediated transport (including member of the *RAB* family, sorting nexins, members of the *SLC* family and others), immune system processes (including the genes *ADAM8/9*, cathepsins, C-X-C motif chemokine ligands, *IL10* and others), and catabolic processes (including the genes *AOAH*, *ATG5/7*, matrix metallopeptidases, *PINK1* and others) (Figure 5.3A). The top 10 biological processes enriched in the upregulated genes in the Q109 versus Q22 microglia-like cells included terms relating to cell cycle (including the genes *BMP2*, cyclin family members, cell division cycle family members and others) and organelle organisation (including the genes *ACTG1*, *BIN1*, centromere proteins, kinesin family members, ribosomal proteins and others) (Figure 5.3B). KEGG pathway analysis highlighted enriched molecular interaction, reaction and relation networks in the gene lists (Kanehisa and Goto, 2000). Significantly downregulated genes

were enriched for KEGG pathways including lysosomes (including *ATP6V0* subunits, *CD68*, cathepsins, *LAMP2* and others) endocytosis (including member of the *RAB* family, sorting nexins, members of the *SLC* family and others) and phagosome (including the genes *FCGR1A/2A*, *ITGB2/5*, *MSR1*, *STX7/12/18* and others) as well as chemokine and immune-mediated signalling (including C-C motif chemokine ligands, C-X-C motif chemokine ligands, *STAT5B* and others) (Figure 5.3C). The enriched KEGG pathways for the upregulated genes included mismatch repair (including the genes *EXO1*, *LIG1*, *MSH2/6*, *PCNA*, *POLD2* and replication factor C subunits) and the Fanconi anemia pathway (including the genes *BLM*, *BRIP1*, *EME1*, FA complementation group family members, *RAD51*, *USP1* and others) (Figure 5.3D).

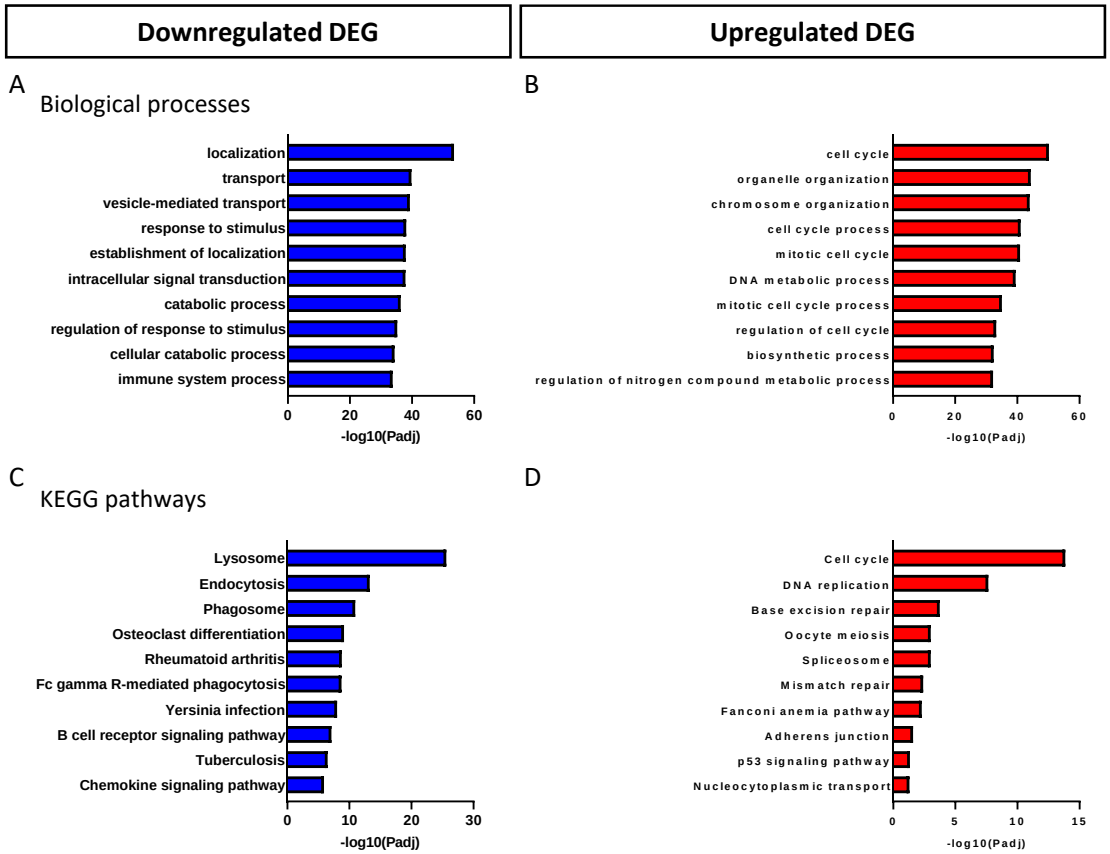

Figure 5.3: Enriched biological processes and KEGG pathways from the Q109 versus Q22 microglia-like cell comparison. All adjusted p-values < 0.01 and Log2 fold change > 1.5 genes were used for gene ontology analysis. (A) Enriched biological processes detected in the downregulated DEG. (B) Enriched biological processes in the upregulated DEG. (C) Enriched KEGG pathways detected in the downregulated DEG. (D) Enriched KEGG pathways in the upregulated DEG.

Following the findings of the gene ontology analysis, as well as previous results from the functional characterisation of Q109 microglia-like cells in chapter 4, gene sets for specific microglia functions were selected and plotted in heatmaps. The top significant GO terms from the comparison of Q109 and Q22 microglia-like cells were too big to be plotted in heatmaps. Therefore, more specific GO terms with a low number of genes were chosen, in order to check

differences between Q109 and Q22 microglia-like cells without picking genes of interest in a biased way. The GO terms "Regulation of phagocytosis, engulfment" (GO:0060099) was chosen and plotted in a heatmap. Several genes are significantly downregulated in the Q109 microglia-like cells, including the triggering receptor expressed on myeloid cells 2 (*TREM2*), a protein known to play a role in neurodegenerative diseases (Jay, von Saucken and Landreth, 2017) (Figure 5.4A). In addition, the GO term "Clathrin-dependent endocytosis" (GO:0072583) (Figure 5.4B) was chosen and plotted in a heatmap. The genes show a clear up- or downregulation in Q109 microglia-like cells, indicating clear differences in gene expression related to clathrin-dependent endocytosis.

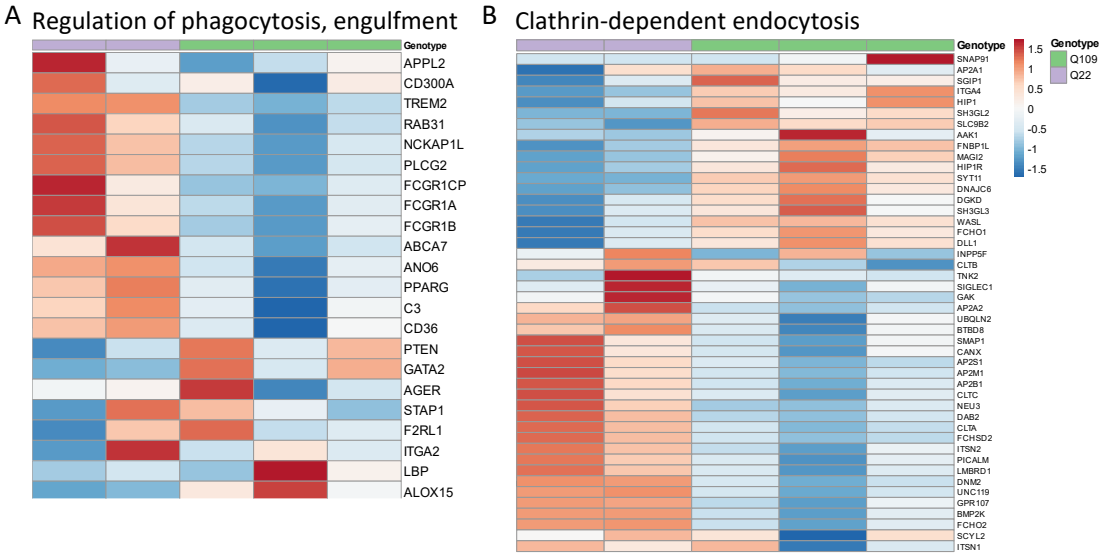

Figure 5.4: Investigation of genes implicated in phagocytosis and endocytosis. (A) Genes from the GO term "Regulation of phagocytosis, engulfment" were plotted in a heatmap, comparing the normalized gene expression between Q22 and Q109 microglia-like cells. (B) Genes from the GO term "Clathrin-dependent endocytosis" were plotted in a heatmap to compared Q109 and Q22 microglia-like cells.

Furthermore, in the genes upregulated in Q109 microglia-like cells, pathways and processes around cell cycle were detected. Mismatch repair, a significantly enriched KEGG pathway has previously been implicated in HD (Iyer and Pluciennik, 2021). MMR has been suggested to play a role in the CAG repeat expansion in HD and a number of MMR genes are known to have an effect on age of onset of the diseases, which has been implicated through their identification in GWAS studies (Lee *et al.*, 2019, 2022). A list of MMR genes has been taken from Iyer and Pluciennik, 2021 and was plotted in a heatmap to compare the normalized counts of Q109 and Q22 microglia-like cells. A clear distinction between Q109 and Q22 microglia-like cells was detected. Only for the genes *MLH1* and *MLH3* a great difference in gene expression between Q22 control microglia-like cells was detected (Figure 5.5A). Furthermore, the KEGG pathway "DNA replication" was found to be the second most significant in the KEGG analysis of genes

upregulated in Q109 microglia-like cells. All genes of this pathway were plotted in a heatmap and highlighted that most genes of the pathway were upregulated in Q109 microglia-like cells (Figure 5.5B).

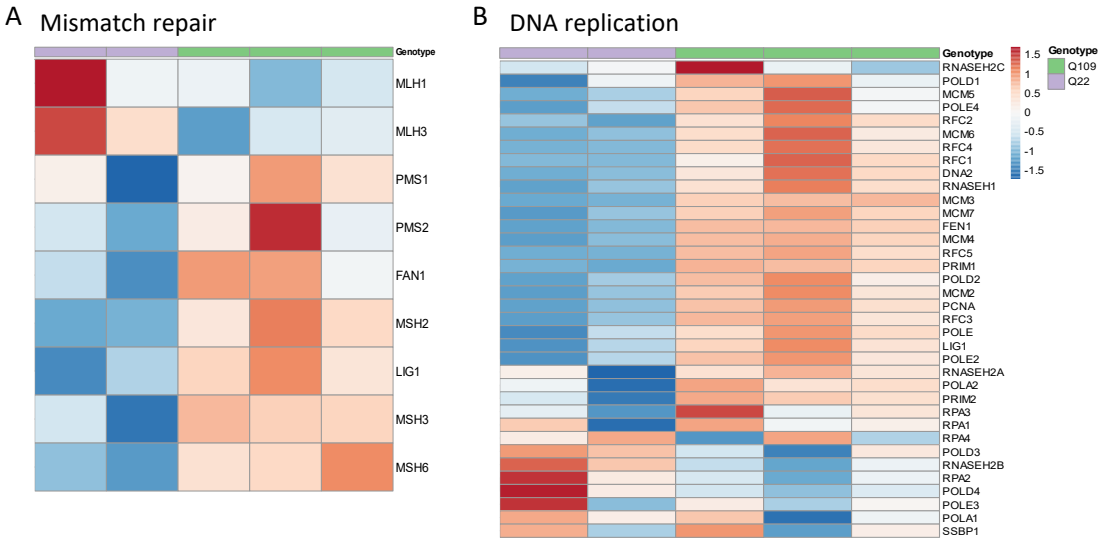

Figure 5.5: Investigation of genes implicated in mismatch repair and DNA replication. (A) Mismatch repair genes known to be involved in HD were plotted in a heatmap comparing Q22 and Q109 microglia-like cells. (B) Genes from the KEGG pathway DNA replication were plotted in a heatmap to compare Q22 and Q109 microglia-like cells.

5.3.2 The effect of pro-inflammatory stimulation on Q22 microglia-like cells

Microglia activation is a phenotype commonly described in HD and has been detected in patients using PET imaging (Pavese et al., 2006; Politis et al., 2011), as well as in post-mortem studies (Singhrao *et al.*, 1999; E. Sapp *et al.*, 2001) and mouse models (Savage et al., 2020; Creus-Muncunill et al., 2022). A combination of pro-inflammatory stimuli, commonly used in iPSC-derived microglia-like cells, was used to mimic HD-associated microglia activation. Microglia-like cells were primed with IFN-γ for 24 hours, followed by incubation with LPS for either 3 or 12 hours to detect direct and long-term effects of the stimulation. In order to investigate general effects of pro-inflammatory stimulation on iPSC-derived microglia-like cells first, the effect on the Q22 control microglia-like cells was explored (Figure 5.6A). A PCA compared unstimulated microglia-like cells with 3 hours or 12 hours of pro-inflammatory stimulation. PC1 separated the unstimulated microglia-like cells from the ones stimulated with LPS. PC2 separated the two Q22 clones (Figure 5.6B). Comparisons between the groups were conducted and volcano plots generated to show the amount of differentially expressed genes. Comparing 12-hour LPS stimulated versus 3-hour LPS stimulated microglia-like cells, 83 genes were found to be significantly downregulated, and 67 genes significantly upregulated in 12-hour LPS stimulated Q22 microglia-like cells (Figure 5.6C). Comparing 3-hour LPS stimulated with unstimulated Q22

microglia-like cells, 859 genes were significantly upregulated, and 892 genes downregulated in 3-hour LPS stimulated Q22-microglia-like cells (Figure 5.6D). Lastly, comparison of 12-hour LPS stimulated versus unstimulated Q22 microglia-like cells showed a similar volcano plot than the 3-hour LPS versus unstimulated comparison, with 888 genes significantly upregulated and 918 genes significantly downregulated in 12-hour LPS stimulated Q22 microglia-like cells (Figure 5.6E).

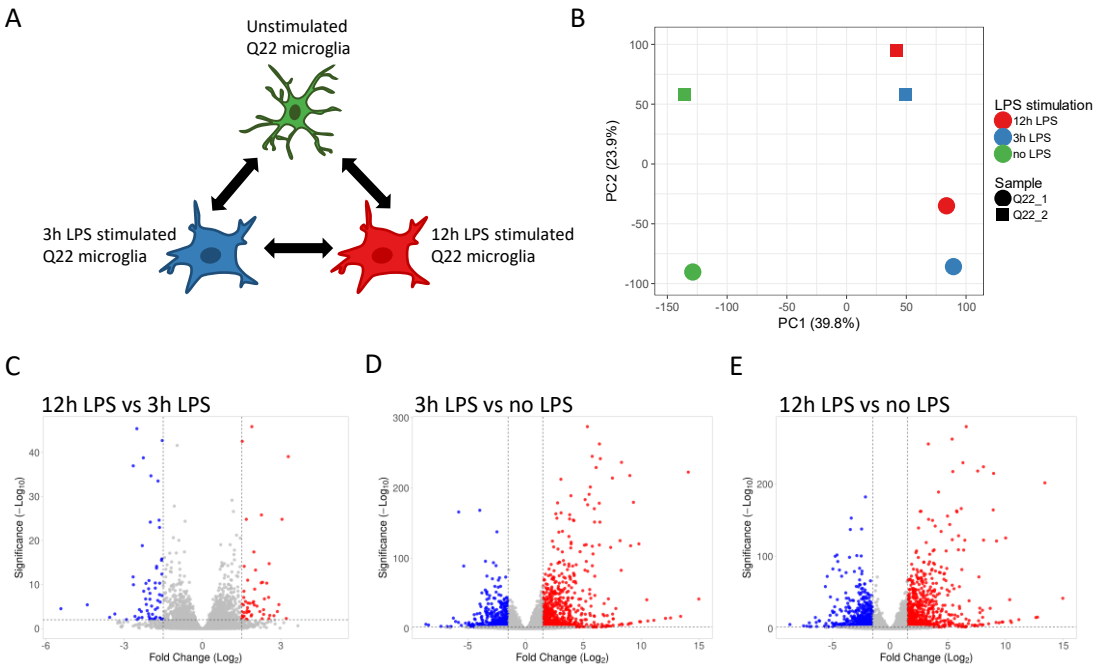

Figure 5.6: Comparison of the effect of different lengths of LPS stimulation on Q22 microglia-like cells. (A) Schemata of comparison conducted. (B) PCA clustered unstimulated Q22 samples from the LPS stimulated Q22 samples in PC1. PC2 showed the variance between the two samples. (C) Volcano plot comparing 12h versus 3h LPS stimulated Q22 microglia-like cells. 83 genes were significantly downregulated, and 67 genes were significantly upregulated using Log2 FC > 1.5 and $p_{adj} < 0.01$. (D) Volcano plot comparing 3h versus no LPS stimulated Q22 microglia-like cells. 892 genes were significantly downregulated, and 859 genes were significantly upregulated. (E) Volcano plot comparing 12h versus no LPS stimulated Q22 microglia-like cells. 918 genes were significantly downregulated, and 888 genes were significantly upregulated.

In order to investigate differences between stimulation times further, Venn diagrams were generated for the differentially expressed genes. Genes that were differentially expressed only in the 3-hour verses no LPS stimulation comparison or the 12-hour verses no LPS stimulation comparison, as well as the overlapping genes underwent GO enrichment analysis and the top enriched biological processes are shown in tables. In the appendix (see section 9.1), the list of DEG in the different comparisons as well as the full list of significant enriched biological processes are available. Here, only a brief overview of differences between stimulation times in Q22 microglia-like cells are presented.

All p-value significantly downregulated genes were added to a Venn diagram, showing overlap of genes between comparisons (Figure 5.7A). Gene ontology analysis was conducted on the gene lists and all or the top 5 enriched biological processes were plotted in a table. The majority of downregulated genes overlapped between either 3-hour LPS or 12-hour LPS versus no LPS stimulation (42%) and were enriched for multicellular organismal processes, localization, and transmembrane and metal ion transport (Figure 5.7B). Genes that were downregulated significantly in the comparison of 3-hour LPS versus no LPS (25%) showed enrichment for the biological processes involved in the regulation of biological processes as well as well as leukocyte migration involved in inflammatory response (Figure 5.7C). Downregulated genes that only significantly changed in the comparison of 12-hour LPS versus no LPS stimulation (26%) were enriched for metabolic processes and regulation of localization (Figure 5.7D).

Next, all significantly upregulated genes were added to a Venn diagram, to show the overlap of genes between comparisons (Figure 5.7E) and gene ontology analysis was conducted. Again, the majority of genes were upregulated in both the comparisons of 3-hour LPS and 12-hour LPS versus no LPS (49%). These were enriched for the biological functions of immune responses (Figure 5.7F). The genes only significantly upregulated in the comparison 3-hour LPS vs no LPS (17%) were enriched for the biological functions of multicellular organismal process, intracellular signal transduction, response to stimulus and regulation of biological processes (Figure 5.7G). Genes that are significantly upregulated only in the comparison 12-hour LPS vs no LPS stimulation (18%) exhibited top 5 biological processes related to response to (external) stimulus (Figure 5.7H). This indicates that both timepoints of LPS stimulation induced an increased gene expression of genes important for immune responses, thereby highlighting that the effectiveness of the pro-inflammatory treatment.

A

Downregulated DEG

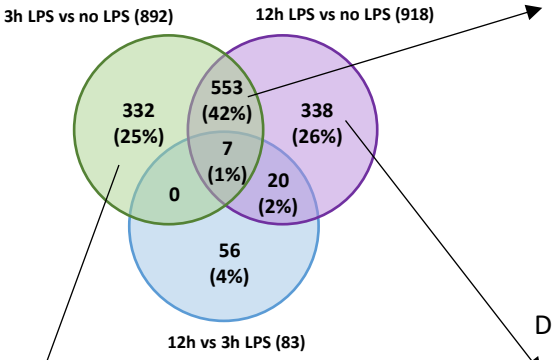

B

Biological Process	Term ID	-log10(p_{adj})
regulation of multicellular organismal process	GO:0051239	7.46
localization	GO:0051179	5.94
multicellular organismal process	GO:0032501	5.88
transmembrane transport	GO:0055085	5.79
metal ion transport	GO:0030001	5.58

C

Biological Process	Term ID	-log10 (p_{adj})
regulation of cellular process	GO:0050794	3.31
biological regulation	GO:0065007	2.83
regulation of biological process	GO:0050789	2.37
leukocyte migration involved in inflammatory response	GO:0002523	1.3

D

Biological Process	Term ID	-log10 (p_{adj})
oxoacid metabolic process	GO:0043436	3.83
small molecule metabolic process	GO:0044281	3.78
organic acid metabolic process	GO:0006082	3.62
carboxylic acid metabolic process	GO:0019752	2.98
regulation of localization	GO:0032879	2.27

E

Upregulated DEG

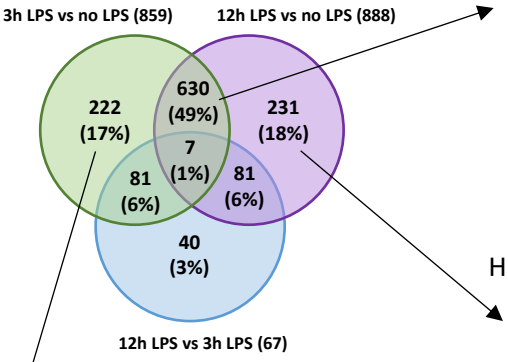

F

Biological Process	Term ID	-log10(p_{adj})
immune system process	GO:0002376	69.03
immune response	GO:0006955	63.62
defense response	GO:0006952	55.28
response to cytokine	GO:0034097	54.80
response to other organism	GO:0051707	51.72

G

Biological Process	Term ID	-log10(p_{adj})
positive regulation of multicellular organismal process	GO:0051240	5.89
intracellular signal transduction	GO:0035556	4.90
response to stimulus	GO:0050896	4.42
positive regulation of biological process	GO:0048518	4.32
regulation of multicellular organismal process	GO:0051239	4.22

H

Biological Process	Term ID	-log10(p_{adj})
response to stimulus	GO:0050896	4.63
response to external stimulus	GO:0009605	4.13
antigen processing and presentation of exogenous peptide antigen	GO:0002478	3.10
response to other organism	GO:0051707	2.77
response to external biotic stimulus	GO:0043207	2.76

Figure 5.7: Venn diagrams comparing different LPS stimulation times. (A) Venn diagram displaying overlap between downregulated gene lists. The majority of genes that were downregulated in the comparisons of 3h LPS vs no LPS and 12h LPS vs no LPS were overlapping between the two comparisons. (B) Gene ontology analysis highlighted enriched biological functions of the genes that overlapped between the comparisons of 3h LPS vs no LPS and 12h LPS vs no LPS. The top 5 terms were plotted in a table with term ID and the -Log10(p_{adj}). (C) Gene ontology analysis highlighted all enriched biological functions of the genes only significantly different in the comparison of 3h LPS vs no LPS stimulation. (D) Top 5 enriched biological processes of the genes significantly different only in the comparison of 12h vs no LPS. (E) Venn diagram displaying overlap between upregulated gene lists. (F) Top 5 enriched biological processes of the genes overlapping between the comparisons 3H LPS vs no LPS and 12h LPS vs no LPS. (G) Top 5 enriched biological processes of the genes significantly different only in the comparison of 3h vs no LPS. (H) Top 5 enriched biological processes of the genes significantly different only in the comparison of 3h vs no LPS.

5.3.3 The effect of pro-inflammatory stimulation on Q109 and Q22 microglia-like cells

In order to investigate whether Q109 and Q22 microglia-like cells differ in their responses to a prolonged pro-inflammatory stimulation, the transcriptome data of 12-hour stimulated Q22 and Q109 microglia-like cells were compared (Figure 5.8A). A PCA analysis was conducted and *HTT* CAG repeat length separated the microglia-like cells in PC1. PC2 showed the variance between cell lines (Figure 5.8B). The top 20 most p-value significant DEG were plotted in a heatmap, of which 15 were significantly downregulated in the Q109 microglia-like cells (Figure 5.8C). A volcano plot highlighted genes that were differentially expressed between 12-hour LPS stimulated Q109 and Q22 microglia-like cells with $p_{adj} < 0.01$ and Log2 fold change (FC) > 1.5 (Figure 5.8D). 493 genes were found to be significantly upregulated, and 118 genes to be significantly downregulated in the 12-hour stimulated Q109 microglia-like cells.

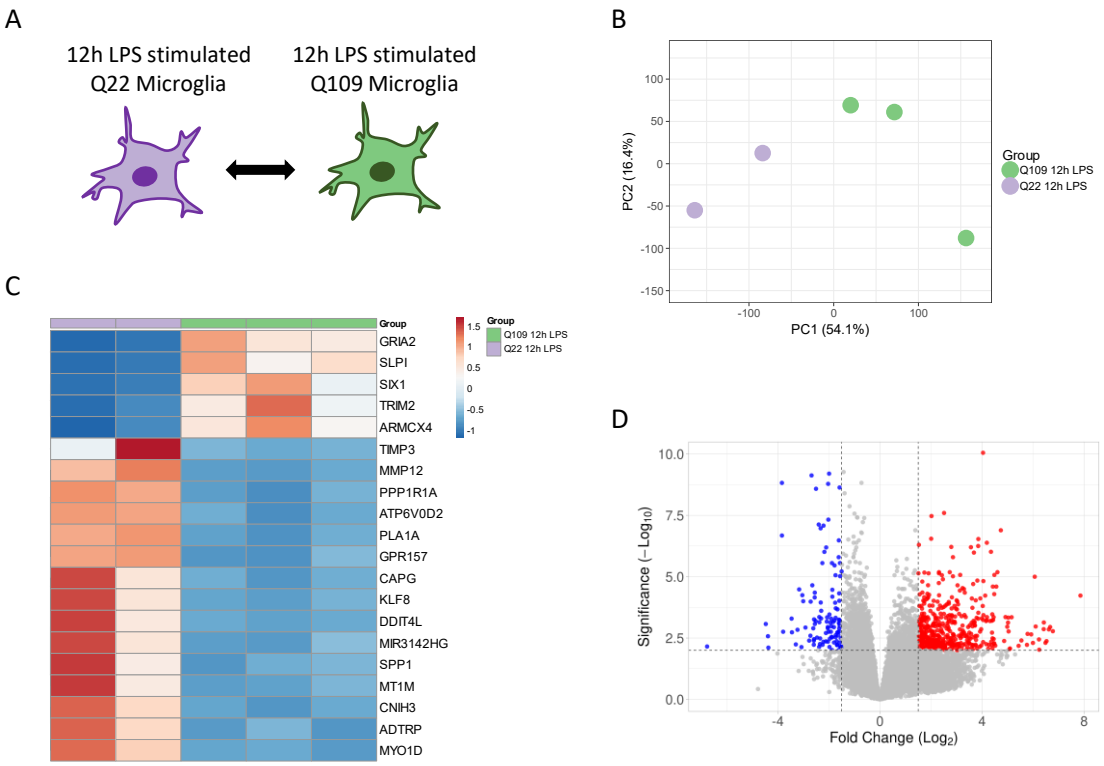

Figure 5.8: Basic characterisation of transcriptional differences between 12-hour LPS stimulated Q22 and Q109 microglia-like cells. (A) Schemata of comparison conducted. (B) PCA separated stimulated Q22 and Q109 microglia in principle component PC1. PC2 shows the variance between cell lines. (C) Top 20 most p-value significant genes were plotted in a clustered heatmap. (D) The volcano plot highlighted genes that were significantly differentially expressed, indicating 493 genes in red that were upregulated and 118 in blue that were downregulated in 12-hour LPS stimulated Q109 versus 12-hour LPS stimulated Q22 microglia-like cells.

The p-value significant genes between 12-hour stimulated Q109 versus Q22 microglia-like cells were further taken forward for gene ontology analysis using g:Profiler. Enriched biological processes were generated, and the top 10 terms plotted with the -Log10(p_{adj}). The top 10 enriched biological processes for the genes downregulated in the Q109 versus Q22 microglia-like cells included the cellular response the metal ions cadmium and copper and cellular zinc ion homeostasis (including the genes *AQP1*, *MMP9* and members of the metallothionein family) and movement of cell or subcellular component (including the genes *ACTA2*, *ADAM8*, C-C motif chemokine ligands, *L1CAM* and others) (Figure 5.9A). The top 10 enriched biological processes for the genes upregulated in the Q109 versus Q22 microglia-like cells can be summarized by developmental processes (including the genes *BMP2*, *CNTF*, *NCAM1/2*, *NRG1* and others) (Figure 5.9B).

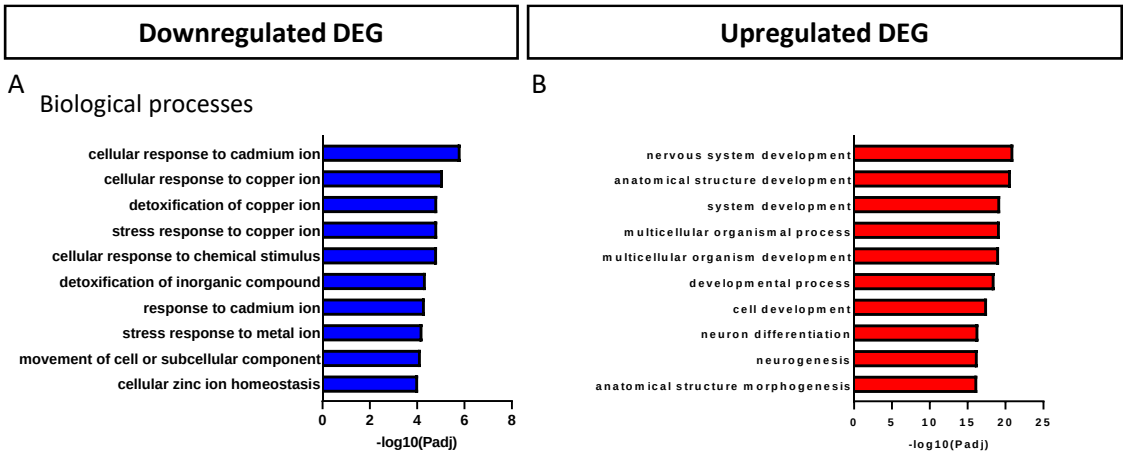

Figure 5.9: Enriched biological processes of 12-hour LPS stimulated Q109 versus Q22 microglia-like cell comparison. All genes with adjusted p-value < 0.01 and Log2 fold change > 1.5 were used for gene ontology analysis. (A) Enriched biological processes detected in the downregulated genes. (B) Enriched biological processes in the upregulated genes.

Lastly, DEG of the comparison of unstimulated Q109 versus Q22 microglia-like cells were compared to the 12-hour LPS stimulated Q109 versus Q22 microglia-like cells. Venn diagrams were generated for the differentially expressed genes. Genes that were differentially expressed only in the unstimulated Q109 vs Q22 comparison or 12-hour LPS Q109 vs Q22 comparison, as well as the overlapping genes underwent GO enrichment analysis, and all or the top 5 enriched biological processes are shown in tables. In the appendix (see section 9.1), the list of DEG in the different comparisons as well as the full list of significant enriched biological processes are available. Here, only a brief overview of differences between the unstimulated and 12-hour LPS stimulated comparisons are presented.

First, a Venn diagram was generated for the significantly downregulated genes of both comparisons. Fewer genes were detected to be significantly downregulated than upregulated in the comparison of Q109 versus Q22 microglia-like cells, in both, unstimulated and 12-hour LPS stimulated conditions. 23% of significantly downregulated genes were overlapping between the two comparisons. These genes underwent GO analysis and were enriched for the biological processes around cellular response to copper and cadmium ions (Figure 5.10B). 57% of significantly downregulated genes were only downregulated in the unstimulated Q109 versus unstimulated Q22 microglia-like cells. GO analysis revealed that these genes were enriched for the biological functions of immune response (Figure 5.10C). Lastly, 20% of the significantly downregulated genes were only downregulated in 12-hour LPS stimulated Q109 microglia-like cells compared to stimulated Q22 microglia-like cells. These were enriched for biological processes of apoptotic processes, and response to decreased oxygen levels (Figure 5.10D).

Also, the significantly upregulated genes were plotted in a Venn diagram (Figure 5.10E). 25% of significantly upregulated genes were overlapping between the two comparisons. These genes underwent GO analysis and were enriched for the biological processes around nervous system development (Figure 5.10F). The majority (61%) of the upregulated genes was only significant in the unstimulated Q109 versus Q22 microglia-like cell comparison. These genes were enriched for the biological processes of cell cycle and chromosome organisation (Figure 5.10G). The genes only significantly upregulated in the 12-hour LPS stimulated Q109 versus Q22 microglia-like cells (13%) were enriched for biological processes involved in anatomical structure development and cell projection organisation (Figure 5.10H).

A

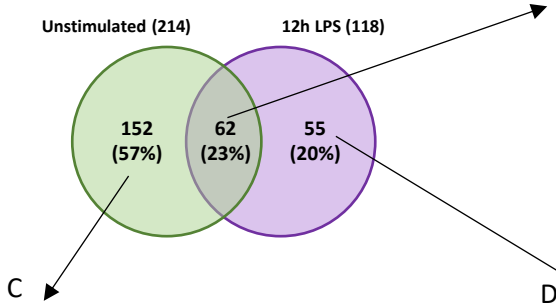

B

Biological Process	Term ID	-log10(p_{adj})
stress response to copper ion	GO:1990169	6.55
detoxification of copper ion	GO:0010273	6.55
cellular response to cadmium ion	GO:0071276	6.23
cellular zinc ion homeostasis	GO:0006882	6.08
detoxification of inorganic compound	GO:0061687	6.06

C

Biological Process	Term ID	-log10(p_{adj})
inflammatory response	GO:0006954	9.01
defense response	GO:0006952	8.90
immune response	GO:0006955	7.7
response to stimulus	GO:0050896	7.54
defense response to other organism	GO:0098542	6.11

D

Biological Process	Term ID	-log10(p_{adj})
epithelial cell apoptotic process	GO:1904019	2.31
response to hypoxia	GO:0001666	1.87
response to decreased oxygen levels	GO:0036293	1.76

E

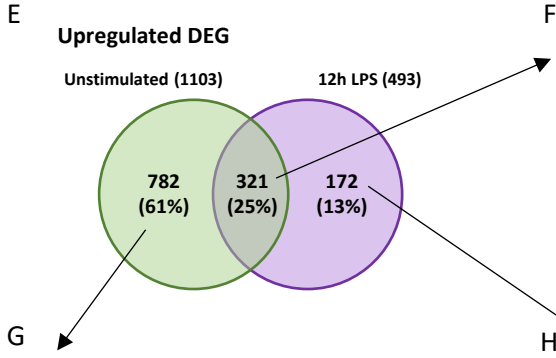

F

Biological Process	Term ID	-log10(p_{adj})
nervous system development	GO:0007399	11.53
anatomical structure development	GO:0048856	9.63
cell development	GO:0048468	9.61
generation of neurons	GO:0048699	9.45
multicellular organism development	GO:0007275	9.15

G

Biological Process	Term ID	-log10(p_{adj})
regulation of cellular process	GO:0050794	20.54
chromosome organization	GO:0051276	18.21
mitotic cell cycle process	GO:1903047	16.50
mitotic cell cycle	GO:0000278	16.45
cell cycle	GO:0007049	16.35

H

Biological Process	Term ID	-log10(p_{adj})
anatomical structure morphogenesis	GO:0009653	4.79
anatomical structure development	GO:0048856	3.17
plasma membrane bounded cell projection organization	GO:0120036	2.96
cell projection organization	GO:0030030	2.74
developmental process	GO:0032502	2.47

Figure 5.10: Comparing Q109 versus Q22 microglia-like cells in unstimulated and stimulated conditions. The DEG of the comparison of unstimulated Q109 versus Q22 microglia-like cells were compared to the DEG of the comparison of 12-hour stimulated Q109 versus Q22 microglia-like cells using. (A) Venn diagram showing overlap of significantly downregulated genes. (B) Top 5 biological processes enriched in the genes overlapping between comparisons. (C) Top 5 biological processes enriched in the genes only significant in the unstimulated comparison. (D) Top 5 biological processes enriched in the genes only significant in the 12-hour LPS comparison. (E) Venn diagram showing overlap of significantly upregulated genes. (F) Top 5 biological processes enriched in the genes overlapping between comparisons. (G) Top 5 biological processes enriched in the genes only significant in the unstimulated comparison. (H) Top 5 biological processes enriched in the genes only significant in the 12-hour LPS comparison.

5.4 Discussion

5.4.1 Removal of sample 3H2 from the analysis

As indicated at the beginning of the chapter, it has been decided to remove a sample from the RNA sequencing analysis. This was been done without confirmation of the genotype of the sample and a mix up of cells is therefore a speculation and not proved. It might be possible to identify the *HTT* CAG repeat length of the sample from the RNA sequencing raw data, however the PhD candidate does not have the expertise to conduct such an analysis. Further functional investigation of cells from the same differentiation has been added to the Appendix (Figure 9.1) to show that the sample 3H2 also performed oddly in other experiments. These experiments were repeated with other microglia differentiations, however there was no funding available to repeat the bulk RNA sequencing.

5.4.2 Summary

In this chapter Q109 and Q22 microglia-like cells underwent bulk RNA sequencing. Differences due to the mutant *HTT* expression were investigated. Furthermore, microglia-like cells underwent pro-inflammatory stimulation. The effect of the stimulation on Q22 control microglia-like cells was investigated first, followed by the comparison between Q109 and Q22 pro-inflammatory microglia-like cells.

A previous RNA sequencing study investigating human prefrontal cortex from HD and neuropathological normal controls revealed an extensive increase in inflammatory and developmental gene expression in the HD brains (Labadorf *et al.*, 2016). Gene transcription changes have not been investigated in HD microglia yet. Miller et al. performed bulk RNA sequencing of primary monocytes from thirty manifest HD patients and thirty-three control subjects. Pathway analysis revealed widespread enrichment of proinflammatory functional gene sets and upstream regulator analysis together with Western blotting suggested that the NFκB pathway plays a key role in mediating these transcriptional changes (Miller *et al.*, 2016). RNA sequencing of human peripheral blood cells of HD patients and healthy controls also showed a

dysregulation of immune-related functions and an inflammatory response was detected (Andrade-Navarro *et al.*, 2020). All these studies highlight that inflammation is happening in the pathology of HD and further investigation of immune cells are needed. A striking problem in the investigation of microglia is that single-nuclei RNA sequencing has been shown to be particularly difficult in detecting microglia signatures (Thrupp *et al.*, 2020). These findings are in line with a recent study that performed single-nuclei sequencing of the striatum of the HttQ175/+ mouse model of HD. Microglia and Chat+ interneurons had to be excluded from the analysis because of insufficient cell numbers (Malaiya *et al.*, 2021). Therefore, performing bulk RNA sequencing on HD iPSC-derived microglia-like cells might be a first step towards understanding transcriptional changes in HD microglia.

5.4.3 Transcriptional differences between Q109 and Q22 microglia-like cells

The transcriptomes of Q109 and Q22 microglia-like cells were compared. Using principal component analysis, the two groups clustered apart in PC1. A high number of DEG was detected, which were mostly upregulated. Interestingly, this phenotype of transcriptional dysregulation was also detected in bulk RNA sequencing of the prefrontal cortex of 20 HD patients compared to 49 neuropathologically normal controls, where 19% of the detected genes were differentially expressed and predominantly upregulated (Labadorf *et al.*, 2016). Transcriptional dysregulation is suggested to be a central feature of HD pathology. Research showed that wild type HTT can bind to transcriptional regulators, some of which regulate histone acetylation/deacetylation to control amongst others the expression of neuronal survival signals (Schulte and Littleton, 2011). It was found that the toxic N-terminal fragments of mHTT can modulate transcriptional processes not only by modifying chromatin, but also through a direct interaction with genomic DNA (Kumar, Vaish and Ratan, 2014). The protein region encoded by exon 1 of the mutant *HTT* gene can bind DNA directly in the absence of other proteins and can alter DNA conformation. It has been shown that the polyQ expansion encoded in exon 1 can increase HTT-DNA interactions, with binding to recognition elements of transcription factors. All this evidence together shows that the mHTT protein is known to induce transcriptional changes.

In the HD patient prefrontal cortex samples, an enrichment for genes implicated in development was found (Labadorf *et al.*, 2016). Recently, the field of microglia research moved from a dualistic classification of good or bad microglia towards the acknowledgement of multiple microglia states (Paolicelli *et al.*, 2022). A microglia signature that is important for development has been defined for CD11c+ microglia (Butovsky *et al.*, 2006). The gene signature for developmental CD11c+ microglia include factors involved in astrocyte and neuronal differentiation, tissue remodelling, and myelinogenesis accompanied by downregulation of

immune function-related genes. Two of the genes that define the CD11c+ developmental signature were detected among the top 20 most p-value significantly differently expressed genes between Q109 and Q22, and they were downregulated in Q109 microglia-like cells. First, ITGAX is encoding the protein CD11c itself. It has been previously shown that reduction of CD11c+ microglia correlated with clinical progression in chronic experimental autoimmune demyelination using the EAE mouse model (Mayrhofer *et al.*, 2021). Second, ATP6V0D2 is a macrophage-specific V-ATPase subunit and was shown to be implicated in inflammasome activation and bacterial infection by facilitating autophagosome-lysosome fusion (Xia *et al.*, 2019).

All DEG between Q109 and Q22 microglia-like cells underwent gene ontology and KEGG pathway analysis. Genes downregulated in Q109 microglia-like cells were enriched for terms of the endosomal-lysosomal pathway, including vesicle mediated transport, lysosomes, endocytosis, and phagocytosis. These cellular compartments and microglia functions have been intensively studied in Chapter 4 of this PhD thesis and an impairment in Q109 microglia-like cell endocytosis, as well as reduced numbers of late endosomes were detected. Furthermore, impaired phagocytosis was detected in the functional analysis of Q109 microglia-like cells. These findings were followed up and specific gene sets were plotted in heatmaps. Genes within the GO term "Regulation of phagocytosis, engulfment" were mostly downregulated in Q109 microglia-like cells. Among these genes was triggering receptor expressed on myeloid cells 2 (*TREM2*). *TREM2* expression is restricted to microglia in the brain and has been implicated in basic microglia function including, phagocytosis, apoptosis, and inflammatory responses (Ulland and Colonna, 2018; Akhter *et al.*, 2021). Furthermore, *TREM2* surface expression rapidly declines on activation of myeloid cells with Toll-like receptor ligands or with inflammatory cytokines (Turnbull *et al.*, 2006). Here, *TREM2* expression was detected to be lower in Q109 compared to Q22 microglia like cells.

The differentially upregulated genes in Q109 microglia-like cells were enriched for pathways around cell cycle, DNA replication and mismatch repair. Accumulation of N-terminal mHTT fragments in the nuclei of HD brain cells has been suggested to contribute to HD pathology. Liu and colleagues found that in the R6/2-J2 mouse model of HD, medium spiny neurons that exhibited perinuclear inclusions expressed cell-cycle markers that are typically not seen in the striatum of WT mice. These MSN with nuclear inclusions were preferentially lost in the disease progression (Liu *et al.*, 2015). It has also been reported that mHTT affects cortical progenitor cell division and development of the mouse neocortex (Mollina 2014). Goodnight and colleagues used transgenic monkey pluripotent stem cells to investigate HD astrocytes. They reported cell cycle pathway genes to be highly impacted during differentiation. However, they showed these

pathways to be depleted in HD NPC, but upregulated in HD astrocytes compared to control cells, indicating that the effect of mHTT on the cell cycle might be complex and cell type dependent (Goodnight *et al.*, 2019).

Amongst the differentially upregulated genes in Q109 microglia-like cells that are part of the pathways of cell cycle and DNA replication are *BIN1* and *CDK5*. The BIN1 locus contains the second-most significant genetic risk factor for late-onset Alzheimer's disease and BIN1 was shown to regulate the activation of proinflammatory and disease-associated responses in microglia (Sudwarts *et al.*, 2022). The proline-directed Ser/Thr kinase cyclin 5 (*CDK5*) has previously been implicated in mutant *HTT* induced learning and memory deficits. Genetic reduction of *Cdk5* in mutant *Htt* knock-in mice was shown to attenuate corticostriatal learning deficits as well as hippocampal-dependent memory decline (Alvarez-Periel *et al.*, 2018). The KEGG pathway analysis of the genes upregulated in Q109 microglia-like cells showed enrichment for the mismatch repair pathway. MMR is known to be involved in the generation of CAG repeat expansions in HD (Iyer and Pluciennik, 2021). A list of MMR genes has been taken from that paper and was plotted in a heatmap to compare the normalized count of Q109 and Q22 microglia-like cells. Most MMR genes are upregulated in Q109 versus Q22 microglia-like cells, except MLH1 and MLH3. However, for these two genes the two Q22 cell lines show major differences. In order to confidently report changes in gene expression of the MMR genes, a follow up study using qPCR would be needed.

5.4.4 The effect of pro-inflammatory stimulation on Q22 microglia-like cells

In order to understand the effect of pro-inflammatory stimulation on iPSC-derived microglia-like cells, Q22 control microglia-like cells were compared when stimulated with LPS for either 3 hours or 12 hours (after priming with IFN-γ for 24 hours) to unstimulated Q22 microglia-like cells. Stimulated and unstimulated Q22 microglia-like cells clearly clustered apart using a PCA. A number of DEG were detected between stimulated and unstimulated Q22 microglia-like cells, which were mainly upregulated in the stimulated cells. Compared to that a small number of genes were differentially expressed between 3-hour and 12-hour LPS stimulated Q22 microglia-like cells. Previous research has shown that the effect of LPS stimulation is time-dependent. In primary glial cultures isolated from the rat brain, exposure to LPS caused an increase in the cytokine TNF-α from 2 to 6 hours after stimulation, but no increase in the TNF-α concentration was detected 24 hours after LPS stimulation (Shemi, Azab and Kaplanski, 2000). In THP-1 human monocytic cells LPS exposure led to an increase in cytokine IL-8 levels, which was only detectable after 24 and 48 hours of LPS stimulation, but not after 6 or 2 hours. Here, the authors detected an increase in IL-6 and TNF-α 6 - 48 hours after LPS stimulation (Liu *et al.*, 2018). This shows that

the effect of LPS is time-sensitive, however these studies investigated the secretion of proteins and not gene expression changes after stimulation.

Gene ontology analysis has been conducted on the significantly upregulated and downregulated genes that were either specific for the comparison of 3-hour LPS treatment versus no stimulation, 12-hour LPS treatment versus no stimulation and for the genes overlapping between comparisons. Almost half of the DEG were overlapping between the comparisons of LPS timepoints to the unstimulated Q22 microglia-like cells, indicating that gene transcription was already altered after 3 hours of LPS stimulation. The genes upregulated with LPS stimulation were enriched for biological pathways of "response to stimulus", "immune response", and "response to cytokine", indicating that the pro-inflammatory stimulation had worked. The investigation conducted gave a first insight in changes of iPSC-derived microglia-like cells with pro-inflammatory stimulation. The generated gene sets will be available online and can be used for a deeper understanding of genes and pathways that are affected in future studies.

On another note, here, microglia-like cells were primed with IFN-γ for 24 hours before LPS treatment. Pulido-Salgado et al. compared LPS treatment with treatment of IFN-γ + LPS for 6 hours each on primary murine microglia. The authors found differential responses to LPS and LPS + IFN-γ in many genes. In response to LPS, the microglia were more proliferative, pro-inflammatory and phagocytic. However, in response to LPS + IFN-γ inhibited genes were involved in pain, cell division and, unexpectedly, production of some inflammatory mediators (Pulido-Salgado *et al.*, 2018).

5.4.5 The effect of pro-inflammatory stimulation on Q109 and Q22 microglia-like cells

Lastly, 12-hour LPS stimulated Q109 and Q22 microglia-like cells were compared in order to investigate differences in their transcriptome after pro-inflammatory activation. Single cell RNA sequencing of iPSC-derived microglia suggested that pro-inflammatory stimulation with LPS + IFN-γ shows significant overlap, although directional inconsistency, to genes that change their expression levels in neurodegeneration, indicating that pro-inflammatory stimulated iPSC microglia-like cells could resemble activation states that occur in disease (Monzón-Sandoval *et al.*, 2022).

12-hour LPS stimulated Q109 and Q22 microglia-like cells clustered apart using PCA. Just like in unstimulated conditions, the majority of DEG were upregulated in Q109 microglia-like cells. When the significantly downregulated genes were further investigated using gene ontology analysis, the detected biological processes were enriched for terms around the cellular response to cadmium and copper ions as well as cellular zinc ion homeostasis. Copper has been

demonstrated to bind to N-terminal fragments of huntingtin, which supports an involvement of abnormal copper metabolism in HD (Xiao *et al.*, 2013). Overexpression of several genes involved in copper metabolism has been shown to reduce polyQ-mediated toxicity in a yeast model of HD (Hands *et al.*, 2010). Furthermore, inhibition of members of the matrix metalloproteinase (MMP) family have been identified to reduced Htt fragment accumulation in a high-throughput western blot-based screen using HEK 293T cells transfected with a Htt138Q construct (Miller *et al.*, 2010). Also, changes in microglial ion homeostasis have been reported to be of importance for microglial activation, including proliferation, migration, cytokine release and reactive oxygen species production. This activation is mediated by ion channels and ion transporters in microglial cells (Li *et al.*, 2021).

The significantly upregulated genes in stimulated Q109 versus Q22 microglia-like cells were enriched for biological pathways around developmental processes and nervous system development. The genes upregulated in Q109 microglia-like cells included the neural cell adhesion molecule (*NCAM*). Immunostaining of the human striatum showed that NCAM staining was minimal in the healthy control striatum, but in the HD striatum many dot- and thread-like structures are found, indicating a re-expression of the growth-related protein in HD (Nihei and Kowall, 1992). Furthermore, RNA sequencing of the human prefrontal cortex in HD and neuropathologically normal controls revealed differentially expressed genes enriched for developmental genes (Labadorf *et al.*, 2015). This might indicate that dysregulation of developmental genes is a non-cell-type specific transcriptional change induced by mutant *HTT* expression.

5.4.6 Follow-up experiments

This chapter provided an exploration of the RNA sequencing data generated for unstimulated and pro-inflammatory stimulated Q109 and Q22 microglia-like cells. The data can be used for further investigation of specific questions and for the study of genes and pathways of interest. Future studies could conduct protein-protein interaction studies and upstream regulator analysis. The most significant differentially expressed genes of the comparisons should be confirmed via qPCR, in order to gain confidence in the findings. Furthermore, if any upstream regulators or pathways of interest were found, these can be further validated using qPCR as well. Findings from the transcriptome analysis should also be followed up with functional investigation of HD microglia-like cells in order to test if the transcriptional dysregulation leads to microglia dysfunction.

5.5 Chapter summary

- Mutant *HTT* expression induced gene expression changes in unstimulated microglia-like cells related to endocytosis, phagocytosis and lysosomes, as well as cell cycle and DNA replication.
- Stimulation with LPS induced a pro-inflammatory phenotype in both, Q22 and Q109 microglia.
- Differences between Q109 and Q22 microglia-like cells after pro-inflammatory stimulation related to cellular response to ions and developmental processes.

6 Investigating the interplay between Astrocytes and Microglia in Huntington's disease

6.1 Introduction

Astrocytes are the most abundant glia cell type of the central nervous system. They are essential for brain homeostasis and regulate several different tasks to maintain and control healthy brain functions (Sofroniew, 2009). Astrocytes provide physical support to neurons, microglia and endothelial cells by forming a matrix-like organisation, as well as providing these cells with factors necessary for their proper function (Chen and Swanson, 2003). Astrocytes are also innate immune-competent cells that undergo a process called reactive astrogliosis in response to an insult to the brain (Zamanian *et al.*, 2012). Cytokines, growth factors and purines can activate astrocytes and lead to their transition into reactive states (Buffo, Rolando and Ceruti, 2010).

In HD patient brains, reactive astrogliosis, the response of activated astrocytes to changes in brain homeostasis, is observed. Increased number of GFAP positive reactive astrocytes in patients' striatum correlate with the gradient of striatal degeneration (Vonsattel et al., 1985). Transgenic mice expressing mutant *HTT* exclusively in astrocytes were shown to exhibit body weight loss, motor function deficits, and shorter lifespan compared with non-transgenic littermates. In these mice, reactive astrocytes were found to accumulate in proximity to degenerated neurons and they exhibited increased proliferation and cell hypertrophy (Bradford et al., 2009). HD astrocytes derived from patient iPSCs display electrophysiological impairments, reduced support for the maturation of iPSC-derived neurons (Garcia *et al.*, 2019) and they show pronounced cytoplasmic, electron clear vacuoles, a phenomenon previously documented in primary lymphocytes from HD patients (Juopperi *et al.*, 2012). A recent single-nuclei RNA-sequencing analysis of patient iPSC-derived astrocytes highlighted an effect of mHTT on expression of genes associated with glutamate uptake, dysregulation of astrocyte identity and maturation, and dysregulation of actin-mediated signalling (Reyes-Ortiz *et al.*, 2022).

There is emerging evidence that microglia and astrocytes influence and coordinate each other and their effects on the brain microenvironment. Different mechanisms of microglial interaction with other cell types are recently emerging, for example microglia express the CD200 receptor (CD200R), whereas other brain cells express CD200. This direct cell-cell contact signalling to microglia that the brain is in a homeostatic state (Szepesi *et al.*, 2018). iPSC-derived astrocytes and microglia in a co-culture model were shown to be in constant contact with each other via tunnelling nanotubes and other membrane structures (Rostami *et al.*, 2021). That same study

also found that intracellular deposits of alpha-synuclein (α-SYN) and amyloid-beta (Aβ) were significantly reduced in co-cultures of astrocytes and microglia, compared to monocultures of either cell type, indicating that the crosstalk between the two cell types increased the degradation of these aggregates (Rostami *et al.*, 2021). Another study found that the glucagon-like peptide-1 receptor (GLP-1R) pathway plays a critical role in microglia signalling to reactive astrocyte-associated neuroinflammation in Alzheimer's disease and highlights that the mediation of microglia can contribute to the inhibition of astrocyte reactivity (Park *et al.*, 2021). Microglia and astrocytes are innate immune-competent cells, that also crosstalk via the secretion of cytokines. In response to pathogens, it is assumed that microglia are directly activated via Toll-like receptors (TLR) and respond to pathogens via cytokine signalling. The cytokine secretion of microglia then activates astrocytes to induce the full inflammatory response in the brain (Garland, Hartnell and Boche, 2022). Both, microglia and astrocytes are known to secrete cytokines including interleukin IL-1β and TNF, and thereby regulate chemotaxis and phagocytosis functions of both cell types (Hanisch, 2002; Choi *et al.*, 2014). In primary mouse cultures it was shown that activated microglia induce the activation of astrocytes by secreting IL-1α, TNF and C1q. These astrocytes then lose the ability to promote neuronal survival, outgrowth, synaptogenesis and phagocytosis, and induce the death of neurons and oligodendrocytes (Liddelow and Barres, 2017).

Mass spectrometry is a central analytical technique for protein research. In tandem mass spectrometry, detailed structural features of peptides can be inferred from the analysis of the masses of the resulting fragments (Domon and Aebersold, 2006). The HD proteome, referring to the group of proteins expressed in the presence of mHTT, has previously been analysed using human post-mortem brains, patient CSF, and HD models. Pathways that were found to be enriched in HD proteome analyses were axonal guidance, oxidative phosphorylation, and protein ubiquitination pathways (Seeley and Kegel-Gleason, 2021). Tshilenge et al. differentiated HD iPSC with a *HTT* CAG repeat length of 72, as well as isogenic controls into medium spiny neurons and performed quantitative proteomic analysis. The authors identified amongst others dysregulated pathways related to the extracellular matrix, including TGF regulation of extracellular matrix, epithelial-mesenchymal transition, DNA replication, senescence, growth factor stimulus and fatty acid processes (Tshilenge et al., 2022). Even though proteome analysis has been conducted in HD models, we are the first to investigate the secretome of microglia and microglia-astrocyte co-cultures in HD.

6.2 Chapter aims

This chapter aimed to investigate effects of HD astrocytes on microglia phenotypes. First, microglia-like cells were investigated for their morphology and phagocytosis function in co-

culture with astrocytes. Then, the supernatant of Q109 and Q22 microglia-like cell monocultures and microglia-astrocyte co-cultures were collected, and a proteomic analysis performed to study the microglial secretome as well as secretory crosstalk of microglia and astrocytes in HD.

6.3 Results

6.3.1 The role of direct contact to astrocytes for microglia morphology and phagocytosis function

In order to selectively investigate microglia-like cells in co-culture with astrocytes, mCherry expressing reporter iPSC were used. mCherry-expressing Q109 and Q22 reporter iPSC lines were differentiated to microglia precursor cells. In parallel non-reporter Q109 and Q22 iPSC were differentiated to astrocytes and replated in experimental plates at a defined density. mCherry expressing MPC were plated onto astrocytes and were differentiated for 14 days. On day 14, microglia-like cells were imaged live at the Opera Phenix (Figure 6.1A, left). No differences were detected in cell area between Q109 and Q22 microglia-like cells in co-culture with Q109 or Q22 astrocytes, respectively. The two-way ANOVA revealed a significant effect of the astrocyte genotype on microglia roundness in co-culture ($F_{1,8} = 11.87$, $p = 0.0088$). The Tukey's honest significance test showed that Q22 microglia-like cells were significantly more round in co-culture with Q109 astrocytes than with Q22 astrocytes (Figure 6.1A, right). This effect was not significant for Q109 microglia roundness. Next, mCherry expressing microglia-like cells were investigated for their phagocytic uptake of pHrodo labelled *E. coli* particles and total *E. coli* area was measured specifically within mCherry expressing microglia-like cells. Uptake of *E. coli* was investigated live over a period of 4 hours (Figure 6.1B, left). The two-way ANOVA revealed a significant effect of the astrocyte genotype on microglia phagocytosis in co-culture ($F_{1,32} = 15.6$, $p = 0.0004$). The Tukey's honest significance test showed a significant increase in total spot area covered by *E. coli* particles for Q109 microglia-like cells co-cultured with Q109 astrocytes compared to Q22 astrocytes. This effect was not significant for Q22 microglia-like cells (Figure 6.1B, right).

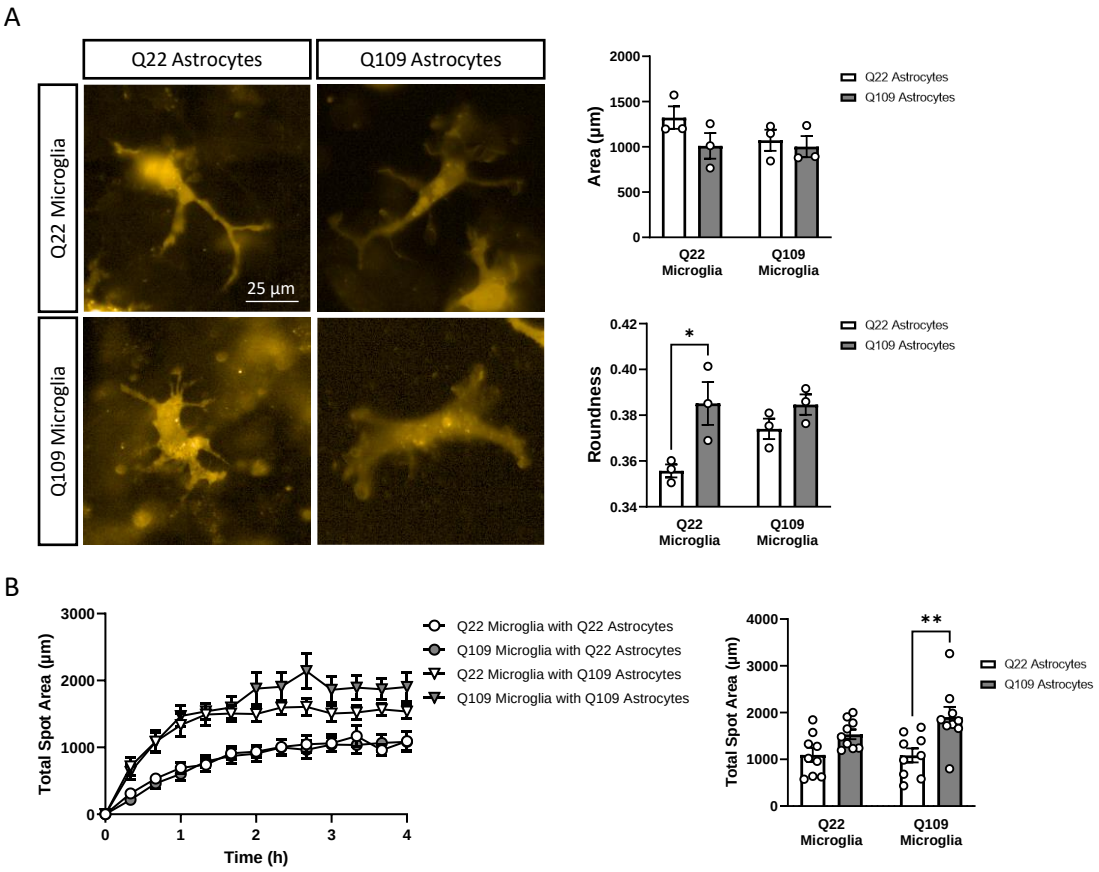

Figure 6.1: Co-culture with Q109 astrocytes induced changes in microglia morphology and phagocytosis. mCherry reporter Q109 and Q22 microglia-like cells were investigated for their morphology and phagocytosis of pHrodo labelled *E. coli* particles in co-culture with Q109 and Q22 astrocytes. (A) Representative images of Q109 and Q22 microglia-like cells differentiated in co-culture with either Q109 or Q22 astrocytes. No differences in cell area were detected. Q22 microglia-like cell roundness was significantly increased in co-culture with Q109 versus Q22 astrocytes. No difference was detected for Q109 microglia-like cells. (B) Microglia phagocytosis was investigated in co-culture with astrocytes. Q109 microglia-like cells showed a significant increase in their uptake of pHrodo labelled *E. coli* in co-culture with Q109 versus Q22 astrocytes. No difference was detected for Q22 microglia-like cells. Data are expressed as mean ± SEM. n = 3 biological replicates conducted in one or three technical replicates. Statistical analysis was performed using two-way ANOVA and Tukey's honest significance test. *p < 0.05, **p < 0.01. All unannotated comparisons are not significant.

6.3.2 Proteome analysis of culture supernatant: introduction and layout

Crosstalk between microglia and astrocytes is mediated via a range of secreted factors, including growth factors, neurotransmitters and gliotransmitters, cytokines, chemokines, innate-immunity mediators and tissue damage molecules, mitogenic factors, NO, ROS, and metabolic mediators (Matejuk and Ransohoff, 2020). In order to investigate secreted proteins in microglia-like cell monocultures and co-cultures with astrocytes, comparative proteome analysis of the culture supernatants was performed. In parallel, Q109 and Q22 microglia-like cells were cultured in monoculture using Q22 ACM or in co-culture with either Q109 or Q22 astrocytes. Microglia-like cells were derived from three Q109 and Q22 lines and astrocytes were derived from one line each (Figure 6.2A). On day 14, fresh serum free medium was added to all cultures and

supernatant was collected after 24 hours. The supernatant was directly frozen. Samples were then concentrated and underwent Nano-LC Mass Spectrometry (MS) at the Proteomics Facility at Bristol University. Due to the number of samples analysed, they were distributed over two MS experiments using a pool of all samples as a reference for normalization. A total of 2130 proteins were detected. When comparing all samples using principal component analysis (PCA), principal component (PC)1 separated the microglia-like cell monoculture (Q22 in violet, Q109 in red) samples from the co-culture samples. PC2 however separated the two MS experiments even though a normalization using the common pool has been applied (Figure 6.2B). Raw data including the lists of significantly different secreted proteins from the comparisons below, as well as tables for the gene ontology analysis conducted in this chapter are added to the appendix (see Chapter 0).

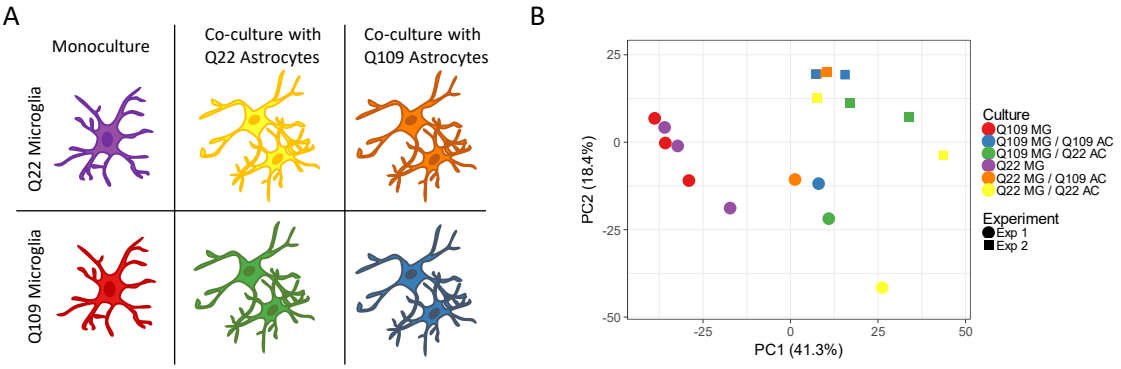

Figure 6.2: Proteome experiment layout and variance in the data. (A) Schemata of the microglia monocultures and microglia-astrocyte co-cultures. Supernatant was collected from Q109 and Q22 microglia-like cells, as well as from microglia-like cells in co-culture with Q109 or Q22 astrocytes. For each group, 3 lines of microglia-like cells were used, whereas the same astrocytes were used for all co-cultures. (B) Principal component analysis of all samples separated monoculture from co-culture samples in PC1, and Mass Spectrometry experimental runs in PC2. PC = principal component, MG = Microglia-like cells, AC = Astrocytes, Exp = Experiment.

6.3.3 Comparing the secretomes of microglia monocultures with microglia-astrocyte co-cultures

The secreted proteins from microglia-like cell monocultures were compared with microglia-astrocytes co-cultures of the same genotype (Q22 or Q109, respectively). The proteins detected to be significantly higher in the co-culture are likely to be secreted by astrocytes, however, astrocytes might also influence the microglia to increase their secretion of proteins. The proteins detected to be significantly lower in co-culture compared to monoculture supernatant might be microglial proteins that are secreted less with the occurrence of astrocytes in the culture. Q22 microglia-like cell monocultures were compared with Q22 microglia-astrocyte co-cultures (Figure 6.3A). 453 proteins were detected to be significantly (p-value of 0.05 and Log2 fold change of 1) higher, and 23 proteins were significantly lower in the Q22 co-culture (Figure 6.3C).

Both, significantly higher and lower secreted proteins underwent Gene Ontology enrichment analysis in order to identify the molecular functions of these proteins. The higher secreted proteins are involved in cell adhesion (including proteins ACTN1/4, ADAM10, CADM1, CALD1, CDH2, FLNA/B, GFAP, and others) and the extracellular matrix (including proteins AGRN, BGN, CCN1, COL1A1, ECM1, LAMA5/B1/C1 and others), as well protein binding (including proteins A2M, AEBP1, CADM1, CALD1 and others) (Figure 6.3E). The few significantly lower secreted proteins in the Q22 co-culture compared to the Q22 microglia monoculture are shown to be important for biological processes of hydrolase activity (proteins FUCA1, GLB1, GUSB, HEXB) (Figure 6.3G).

Next, Q109 microglia monocultures were compared with Q109 microglia-astrocyte co-cultures (Figure 6.3B). 401 proteins were detected to be higher and 53 proteins lower in the Q109 co-culture (Figure 6.3D). A GO enrichment analysis revealed that the molecular functions of the higher detected proteins in the Q109 co-culture overlapped with the molecular functions detected for the Q22 comparison. The top 10 molecular functions detected included cell adhesion (including proteins ACTN1/4, CALD1, CCN1, CDH2, FAP, FLNA/B, GFAP, ITGA3/B1 and others), extracellular matrix (including proteins AGRN, BGN, CCN1, COL1A1, ECM1, LAMA5/B1/C1 and others) and protein binding (including proteins AEBP1, CALD1, CCN1, CDH2 and others) (Figure 6.3F). Investigation of the molecular functions of the downregulated proteins in the Q109 comparison exhibited more terms and higher -Log10 values of the adjusted p-value than the Q22 comparison. The top 10 molecular functions included hydrolase activity (including proteins FUCA1, GLB1, GUSB, HEXB, CTSA/B/D/S/Z and others), catalytic and peptidase activity (including proteins ARSA/B, CTBS, DPP4/7, SOD2 and others) (Figure 6.3H).

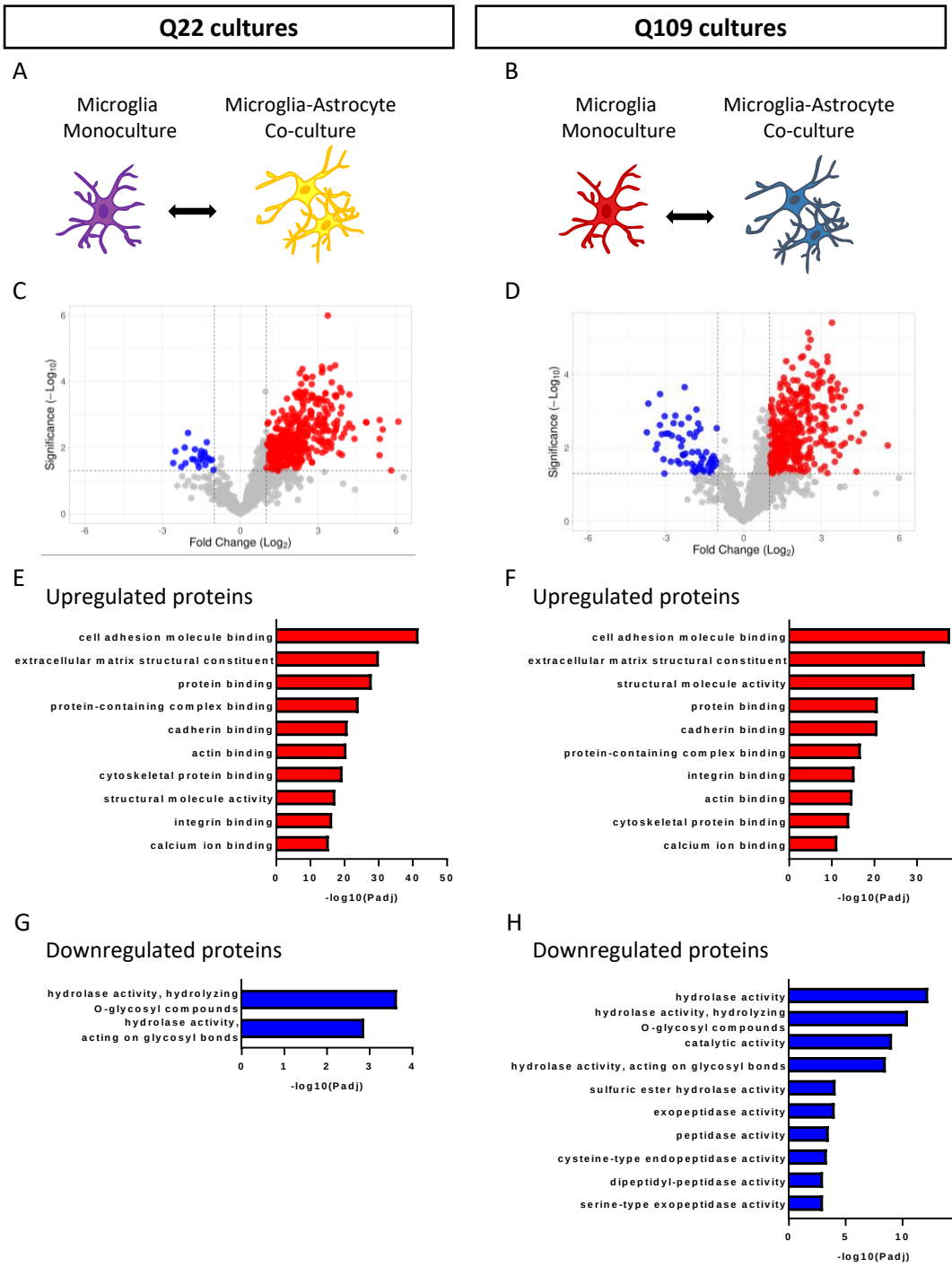

Figure 6.3: Comparing microglia-like cell monocultures with microglia-astrocyte co-cultures. (A) Q22 microglia-like cell monocultures were compared with Q22 microglia-astrocyte co-cultures. (B) Q109 microglia-like cell monocultures were compared with Q109 microglia-astrocyte co-cultures. (C) Volcano blot of the Q22 comparison showed 453 proteins that were significantly higher secreted in the co-culture compared to the monoculture in red, and 23 proteins that were lower secreted in blue. A p-value of 0.05 and Log2 fold change of 1 was chosen. (D) Volcano blot of the Q109 comparison showed 401 proteins that were significantly higher secreted in the co-culture compared to the monoculture in red, and 53 proteins that were lower secreted in blue. (E) Gene ontology (GO) enrichment analysis was performed on the proteins significantly higher in Q22 co-cultures versus Q22 microglia-like cell monocultures. The top 10 molecular functions enriched in that list of proteins were plotted with the -Log10 of the adjusted p-value. (F) Molecular functions enriched in the proteins significantly higher in Q109 co-cultures compared to Q109 microglia monocultures. (G) GO enrichment analysis of the significantly lower proteins of the Q22 comparison exhibited only two molecular functions enriched in the protein list. (H) Top 10 molecular functions of the significantly lower proteins of the Q109 comparison.

In order to investigate differences between the Q22 and Q109 monoculture vs. co-culture comparisons, a Venn diagram for the significantly different secreted proteins was generated. More than half (56%) of proteins were overlapping between the two comparisons. Around the same percentage of proteins was only significantly different in either the Q22 comparison (23%) or the Q109 comparison (21%) (Figure 6.4A). These protein lists were taken forward for GO enrichment analysis. Biological processes were identified for each of the three groups and the top 10 most significant terms were plotted. The overlapping secreted proteins were enriched for morphology (including different collagen types), cell adhesion (including proteins ACTG1/N1/N4, CCN1, CDH2 and others), development processes (including proteins BASP1, BMP1, CCN1 and others) and migration (including proteins CD44, CTNNA1, ECM1, MAP1B and others) (Figure 6.4B). The proteins only changed in the Q22 comparison were enriched for immune regulation (including complement C1QA/C and factor I, CD14, CST3, TIMP1 and others) (Figure 6.4C). Lastly, the proteins that only changed in the Q109 comparison were enriched for translation (including proteins CNBP, EIF3B, ribosomal proteins and others) and cellular biosynthetic, metabolic and catabolic processes (including proteins CTSZ, EEF1G, PKM, ribosomal proteins and others) (Figure 6.4D).

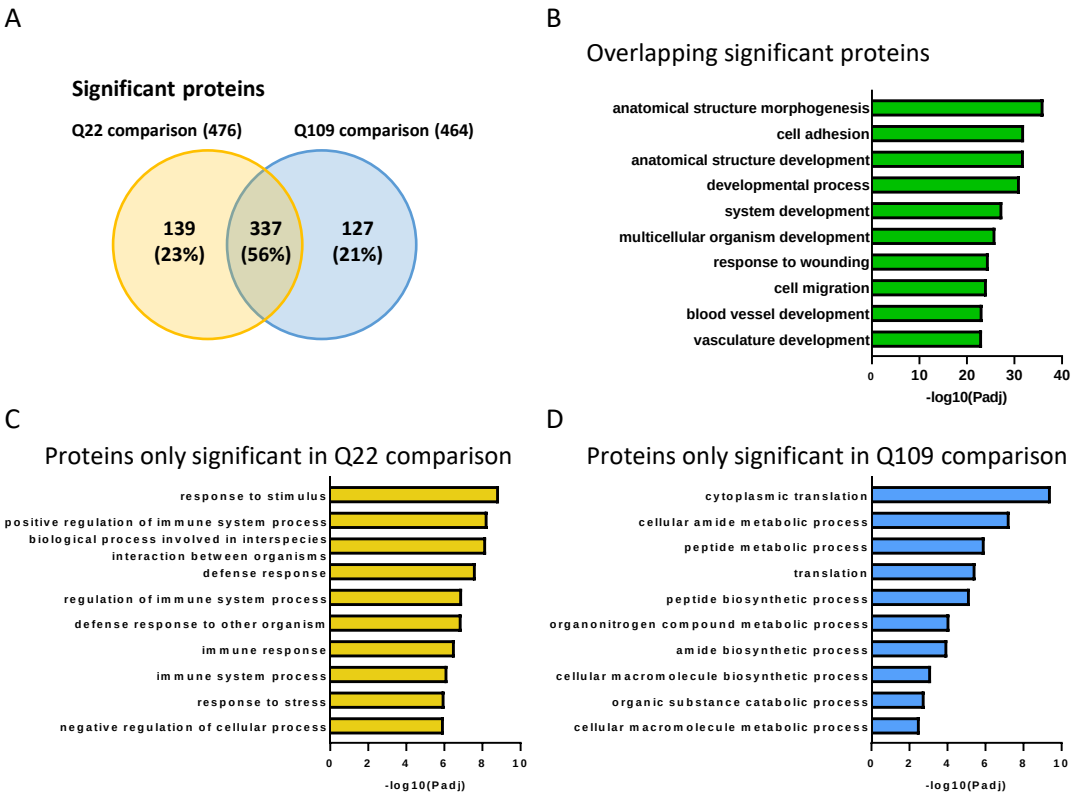

Figure 6.4: Differences between Q22 and Q109 microglia monoculture vs. co-culture comparisons. (A) Venn diagram showing the overlap between proteins that are significantly different in Q22 and Q109 co-cultures. (B) GO enrichment analysis of proteins that overlapped between the Q22 and Q109 comparison was performed, and the top 10 biological functions were plotted using the -Log10 of the adjusted p-value of the comparison. (D) Top 10 biological processes of proteins that were significant only in the Q22 comparison. (E) Top 10 biological processes of proteins that were significant only in the Q109 comparison.

6.3.4 Investigation of microglia monoculture secretomes

Supernatant was collected from Q22 and Q109 microglia-like cell monocultures after differentiation for 14 days (Figure 6.5A). Q22 and Q109 microglia-like cells showed distinct secretion of proteins, indicated by principal component analysis, where PC2 separated the two groups. PC1 however showed the variability between the different iPSC lines that were used to differentiate microglia-like cells (Figure 6.5B). 23 proteins were found to be significantly different between Q22 and Q109 microglia-like supernatants using a p-value of 0.05 and Log2 fold change cut-off of 1 and all these proteins were plotted in a heatmap (Figure 6.5C). A volcano plot showed 18 proteins in red that were secreted significantly higher in the Q109 microglia-like cells and 5 proteins in blue that were secreted significantly lower in Q109 microglia-like cells (Figure 6.5D).

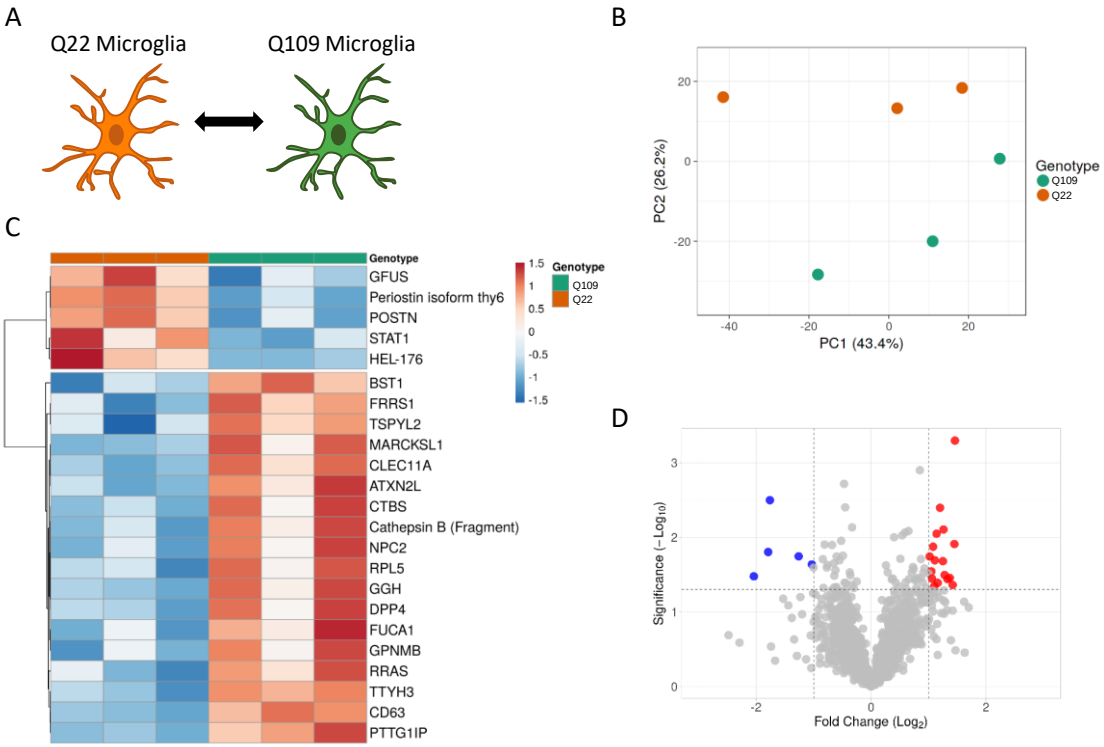

Figure 6.5: Q22 and Q109 microglia-like cells showed differences in their secreted proteins. (A) Schemata of comparison conducted. Three iPSC lines were used to differentiate Q22 and Q109 microglia-like cells, respectively. (B) Principal component analysis was applied to the dataset. Q22 and Q109 microglia-like cells separated by PC2. (C) Heatmap presenting all significantly changed proteins. (D) Volcano plot showed all detected proteins between Q109 and Q22 microglia-like secreted. 18 proteins were significantly upregulated (marked in red) and 5 proteins were significantly downregulated (marked in blue) in Q109 microglia-like cells versus Q22 microglia-like cells using a Log2 fold change of 1 and p-value of 0.05.

All p-value significant proteins (without fold change cut-off) between Q109 and Q22 microglia-like cell monocultures were taken forward for gene ontology analysis. Enriched biological processes for the significant upregulated and downregulated secreted proteins were generated. Upregulated proteins were enriched for two biological processes, the regulation of integrin-mediated signalling pathway (including proteins CD63, BST1 and TIMP1) and biological processes involved in interaction with host (including proteins CTSB, DPP4, FBLN1, HSPA1A, SCARB2) (Figure 6.6A). Downregulated proteins were enriched in ten biological processes, including translation (including proteins EIF2S2, EIF3B, PKM, RPS19, RPS25, SHFL, THBS1, VIM) and biosynthetic processes (including proteins EIF2S2, EIF3B, PKM, RPS19, RPS25, SHFL, THBS1, VIM), response to interferon-gamma (including proteins HSP90AB1, SHFL, SIRPA, STAT1, VIM) and viral processes (including proteins BANF1, EIF3B, HSP90AB1, LDLR, SHFL, STAT1) and regulation of protein metabolic processes (including proteins CORO1C, EIF3B, HSP90AB1, LDLR, NCF1, PKM, PSMD1, SHFL, SIRPA, THBS1, VBP1, VIM) (Figure 6.6B).

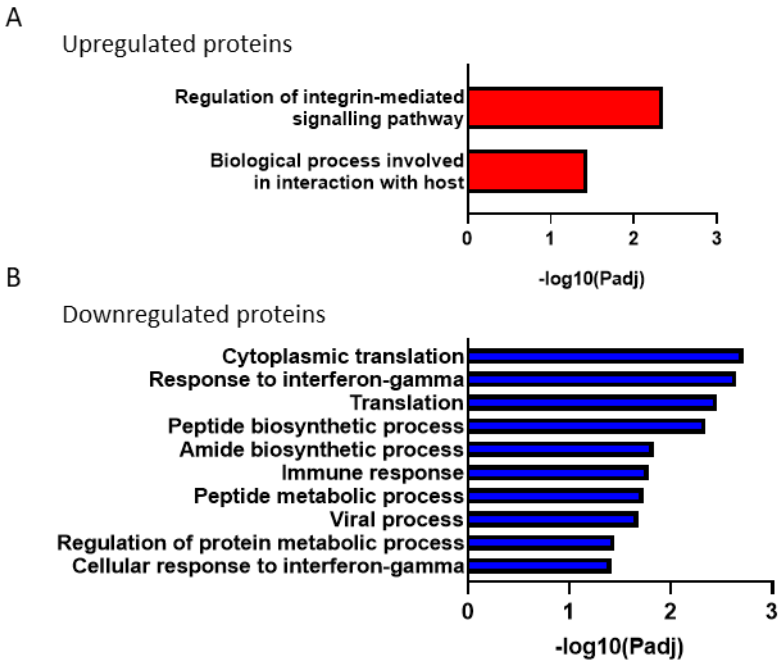

Figure 6.6: Enriched biological processes in Q109 versus Q22 microglia-like cells. P-value significant proteins were used for gene ontology analysis. Significantly enriched biological processes for (A) upregulated and (B) downregulated secreted proteins are presented with GO Term ID and ordered by the negative Log10 of adjusted p-value (-Log10(p_{adj})).

To investigate the p-value significant up- and downregulated proteins together, a protein-protein interaction enrichment analysis was conducted using the Metascape web tool (Zhou *et al.*, 2019). All significantly changed proteins were inputted and a network that contains the subsets of proteins that form physical interactions with at least one other member in the list was created (Figure 6.7A). If a network contained more than 3 proteins, the Molecular Complex Detection (MCODE) algorithm was applied to identify densely connected network components (Bader and Hogue, 2003), indicated in distinct colours. The three identified networks were further highlighted in Figure 6.7B. Pathway and process enrichment analysis was applied to the densely connected networks, and if significant, three functional descriptions for each network were outputted. No significant terms were found for the blue cluster. The red cluster was functionally described by terms of translation and the green cluster included proteins known to be important for platelet signalling including degranulation, a process taking part during phagocytosis, as well as response to elevated cytosolic Ca^{2+} (Figure 6.7C).

A

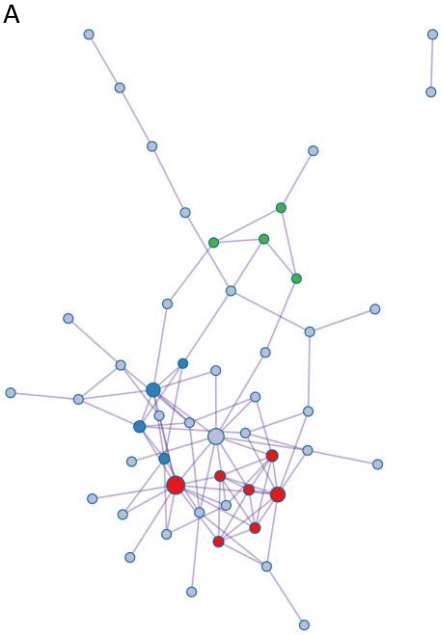

B

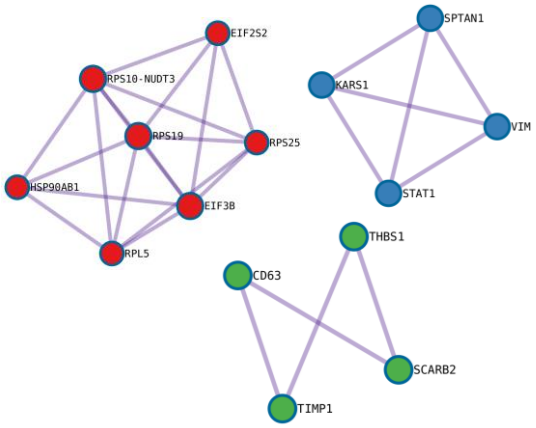

C

Colour	Functional Description	Log10(P)
	L13a-mediated translational silencing of Ceruloplasmin expression	-10.9
	GTP hydrolysis and joining of the 60S ribosomal subunit	-10.9
	Cap-dependent Translation Initiation	-10.7
	Platelet degranulation	-6.5
	Response to elevated platelet cytosolic Ca2+	-6.5
	Platelet activation, signalling and aggregation	-5.6

Figure 6.7: Protein-protein interaction enrichment analysis of significantly changed protein in microglia-like cell monocultures. (A) The list of all p-value significantly proteins was used to investigate protein-protein interactions. All proteins that formed physical interactions with at least one other protein of the list are shown as dots. Densely connected network components were highlighted in colour. (B) Zoom into the dense networks with protein name annotations. (C) Pathway and process enrichment analysis was successful for two of the dense networks and produced three significant function descriptions for each cluster.

6.3.5 Investigating the secretome of microglia-astrocyte co-cultures

In addition to microglia-like cell monoculture supernatant, the secreted proteins of microglia-astrocyte co-cultures were investigated. All possible combinations of Q109 and Q22 microglia-like cells with Q109 and Q22 astrocytes were cultured together (Figure 6.8A). The PCA showed how the four co-cultures clustered apart. PC1 separated co-cultures with Q22 astrocytes from co-cultures with Q109 astrocytes. PC2 separated the samples from the different MS experiments (Figure 6.8B). Volcano plots were generated to compare Q109 and Q22 microglia in co-culture with either Q22 astrocytes (Figure 6.8C) or Q109 astrocytes (Figure 6.8D). In both comparisons, no secreted proteins were found to be significantly changed. This stands in contrast to the microglia-like cell monoculture comparison, which showed a number of significantly different proteins. Volcano plots were further generated for the comparison of Q109 and Q22 astrocytes in co-culture. In co-culture with Q22 microglia-like cells 2 proteins were secreted significantly higher, and 77 proteins significantly lower in the Q109 astrocytes (Figure 6.8E). In co-culture with Q109 microglia-like cells 4 proteins were secreted significantly higher, and 34 proteins significantly lower in the Q109 astrocytes (Figure 6.8F).

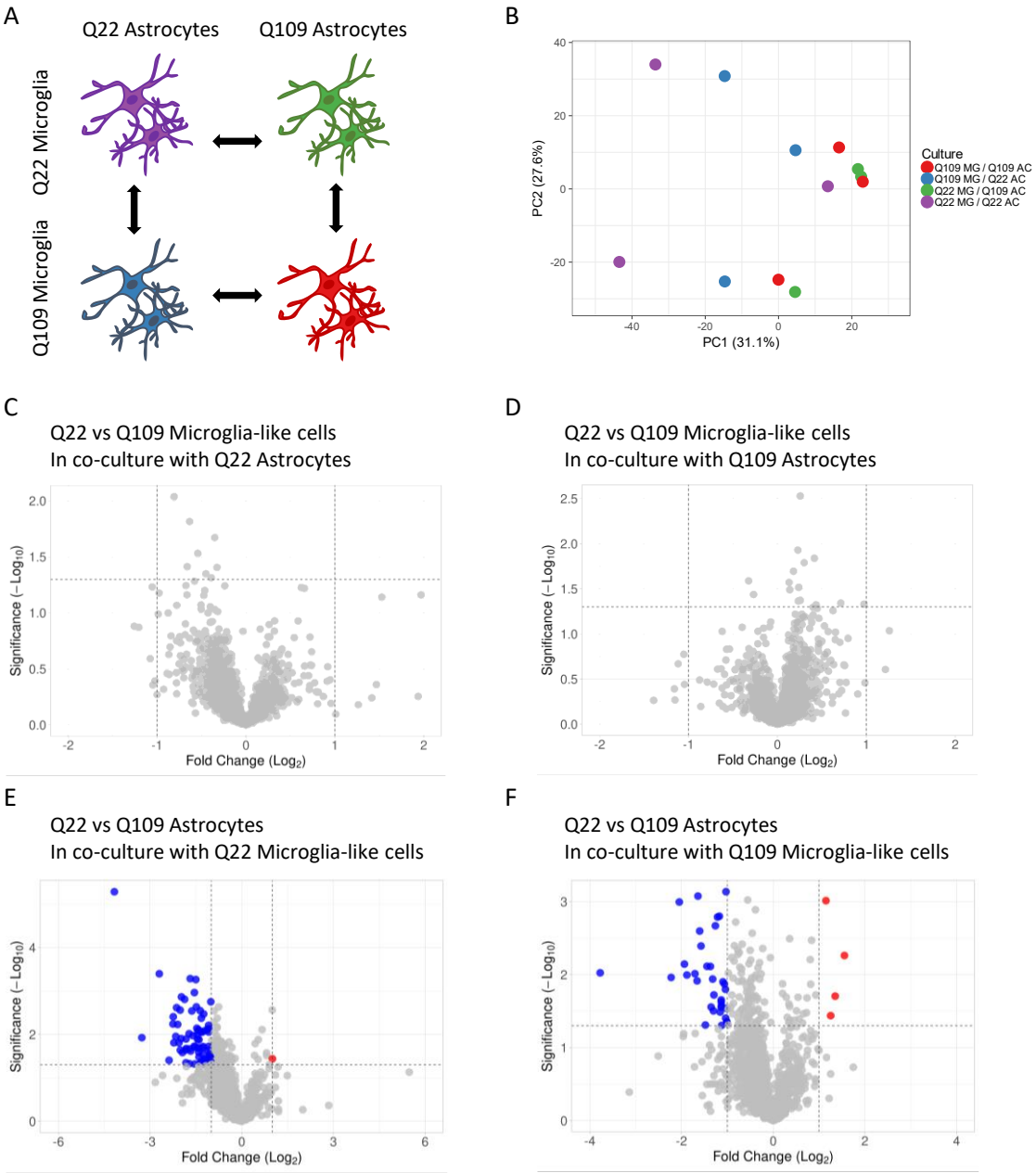

Figure 6.8: Analysis of changes in microglia-astrocyte co-cultures. (A) Schemata indicating the co-cultures that were compared. (B) PCA of all four co-culture conditions. PC1 separated co-cultures with either Q22 or Q109 astrocytes. PC2 separated samples run in different MS experiments. (C) Volcano plot comparing Q22 and Q109 microglia-like cells in co-culture with Q22 astrocytes indicated no significantly changed proteins using a Log2 fold change of 1 and significance of 0.05. (D) No differences in secreted proteins were detected when comparing Q22 and Q109 microglia-like cells in co-culture with Q109 astrocytes. (E) When comparing Q22 and Q109 astrocytes in co-culture with Q22 microglia-like cells 2 proteins were secreted significantly higher, and 77 proteins significantly lower in the Q109 astrocytes. (F) When comparing astrocytes in Q109 microglia-like cells 4 proteins were secreted significantly higher, and 34 proteins significantly lower in the Q109 astrocytes.

The previous comparisons indicated that when astrocyte genotypes were compared in co-culture with either Q22 or Q109 microglia-like cells, a number of significantly changed proteins were detected. The differences between Q109 and Q22 astrocytes were further investigated using all p-value significant proteins (without fold change cut-off). First, Q109 and Q22 astrocytes were compared when cultured with Q22 microglia-like cells (Figure 6.9A). Gene ontology analysis of significantly changed proteins highlighted biological processes enriched in inflammatory responses, the most significant called "defence response" (including complement proteins C1Q, C1S, C3, C4A, C5A, factor H, factor I, as well as CD14, CD44, CLU and others) and cell adhesion (including ACTG1, ARHGDIB, ARPC2, CADM1 CDH6 and others) (Figure 6.9B). The top 10 most p-value significantly changed proteins were plotted in a heatmap. All of them were detected at significantly lower levels in Q109 astrocytes versus Q22 astrocytes in co-culture with Q22 microglia-like cells (Figure 6.9C).

In addition, Q109 and Q22 astrocytes were compared when in co-culture with Q109 microglia-like cells (Figure 6.9D). Gene ontology analysis highlighted biological processes enriched for inflammatory responses, the most significant called "immune response" (including complement proteins C1C, C1S, C3, C4A, C5A, factor I, as well as CD14, CLU and others). In contrast to the comparison in Q22 microglia-like cell co-cultures, cell adhesion was not one of the top 10 enriched biological processes (Figure 6.9E). The top 10 most p-value significantly changed proteins were plotted in a heatmap. Two proteins were significantly higher in Q109 astrocytes versus Q22 astrocytes, and eight proteins were significantly lower (Figure 6.9F). Of these top 10 most significantly changed proteins, four are overlapping between the comparisons of astrocytes in co-culture with either Q22 or Q109 microglia-like cells. These included the complement factors C1S and C1R, as well as the cell-surface glycoprotein CD44 and the heavy chain of factor I.

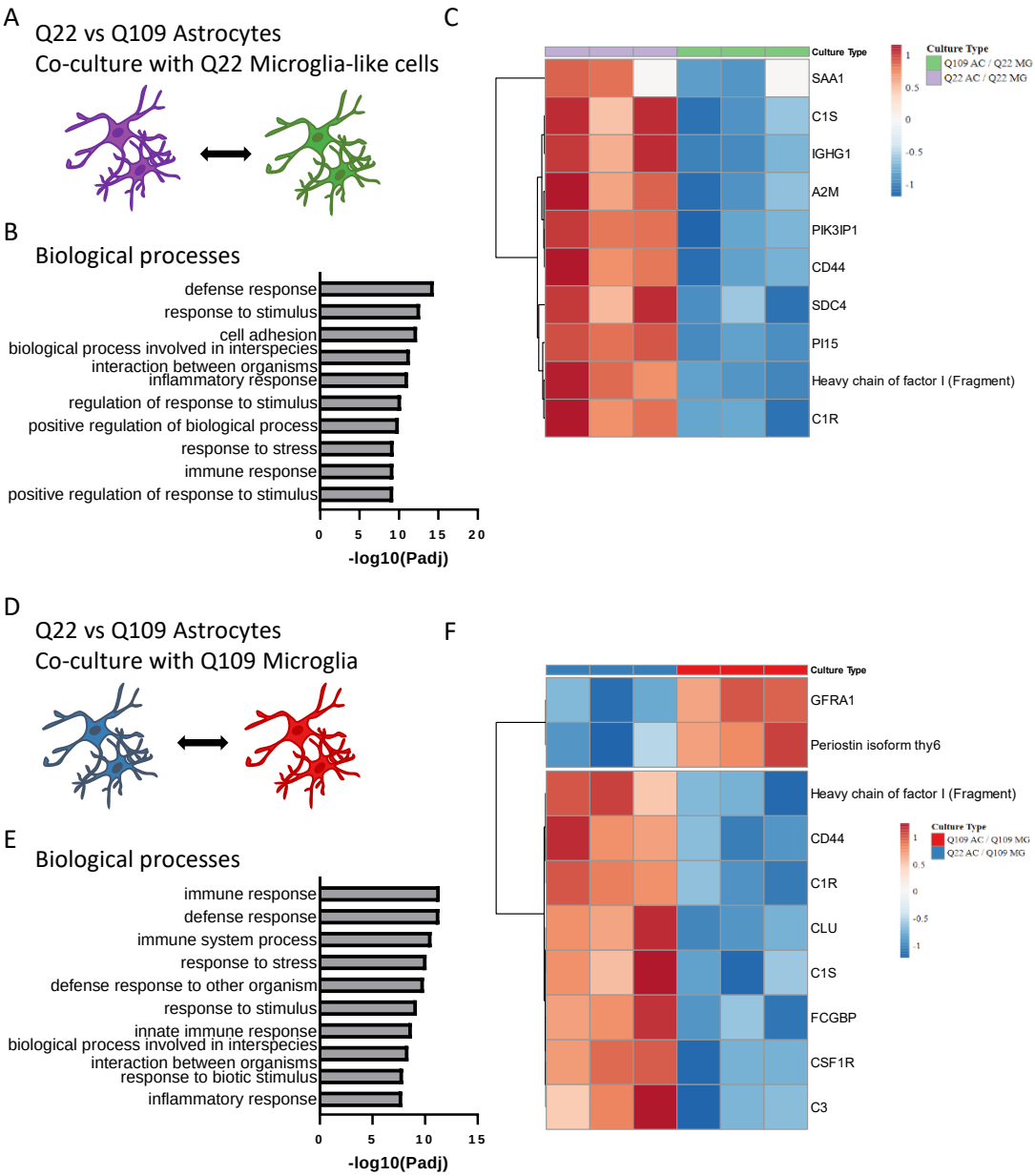

Figure 6.9: Comparison of Q109 and Q22 astrocytes in co-cultures with microglia-like cells. (A) Comparison of Q22 and Q109 astrocytes in co-culture with Q22 microglia-like cells. (B) Gene ontology was conducted to highlight enriched biological processes. (C) The top 10 most p-value significant proteins were plotted in a heatmap. (D) Comparison of Q22 and Q109 astrocytes in co-culture with Q109 microglia-like cells. (E) Biological processes enriched in the proteins significantly different between Q22 and Q109 astrocytes in Q109 microglia-like cell co-culture. (F) Top 10 most significantly different proteins were plotted in a heatmap.

6.3.6 Comparing Q109 with Q22 microglia-astrocyte co-cultures

Q22 microglia-Q22 astrocyte co-cultures were compared with Q109 microglia-Q109 astrocyte co-cultures to investigate potential disease specific secreted proteins in HD co-cultures (Figure 6.10A). Principle component analysis of the data showed that there is a lot of variances between the Q22 co-culture samples themselves, whereas the Q109 co-culture samples clustered closer

together. PC1 explained the biological variance in the samples, whereas PC2 separated samples that were run in the two separate MS experiments (Figure 6.10B). A heatmap highlighted the top 10 most significantly changed proteins (Figure 6.10C). Using a p-value of 0.05 and a Log2 fold change of 1, 58 proteins were found to be secreted significantly lower and 3 proteins secreted significantly higher in the Q109 co-cultures (Figure 6.10D).

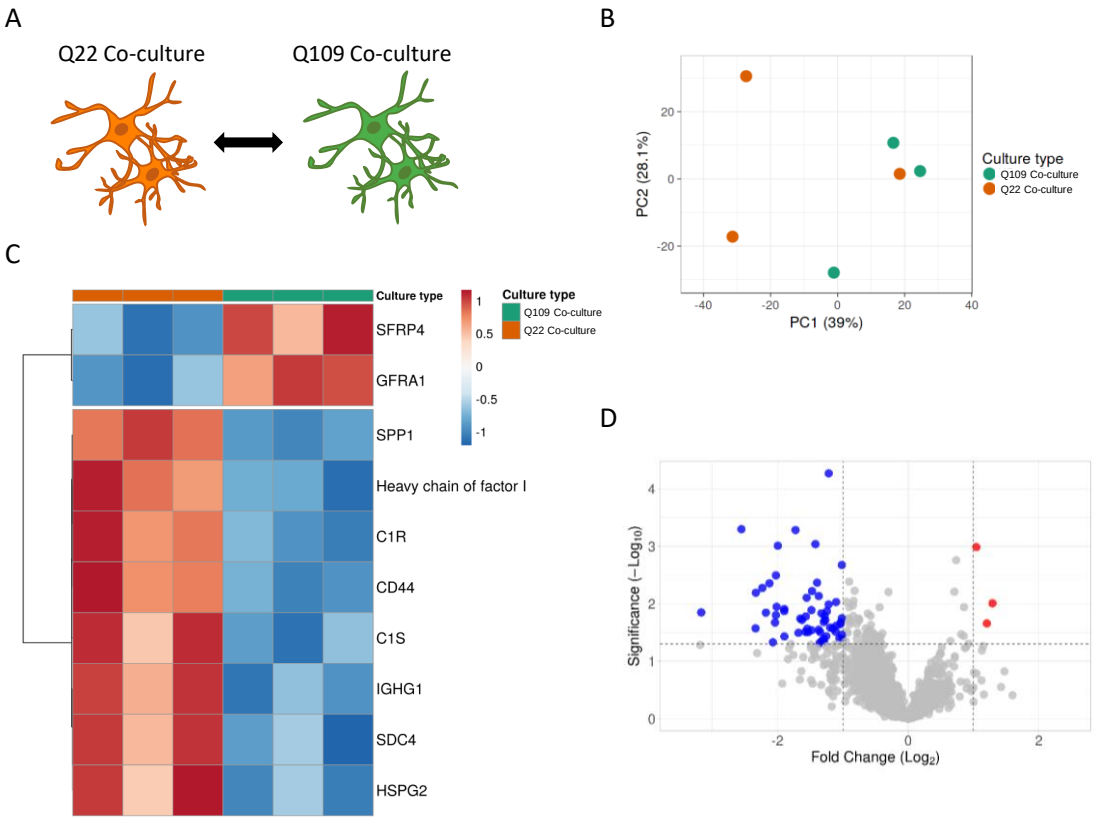

Figure 6.10: Q22 and Q109 co-cultures showed differences in their secretome. (A) Co-cultures of matching Q22 or Q109 microglia and astrocytes were plated, and supernatant collected. (A) Principal component analysis (PCA) was applied to the dataset. Groups separated in PC1, however there was great variability in the Q22 co-cultures. PC2 showed the difference between MS experiments. (C) Heatmap presenting the top 10 most significantly changed proteins. (D) The volcano plot showed 58 proteins to be secreted significantly lower in the Q109 co-cultures and 3 proteins to be secreted significantly higher in the Q109 co-cultures.

All p-value significant proteins (without fold change cut-off) were taken forward for gene ontology enrichment analysis. Enriched biological processes and molecular functions were generated. The top 10 enriched biological processes included a number of immune response related terms (including complement proteins, CD14, CD164, CD44 and others). as well as processes related to cell adhesion (including ACTG1, CADM1, DAG1, ITGB2, LAMA5/C1 and others) (Figure 6.11A). Top 10 molecular functions enriched in the significantly changed genes in the Q109 co-culture highlighted cell adhesion (including CADM1, GFAP, ICAM1, ITGB2, LAMA5, NRCAM and others), peptidase activity (including PI15, UBE2O, SERPINA1/B8/F1 and

others), and receptor binding (including C3, CLU, DBI, ITGB2, S100A4/8/9 and others) (Figure 6.11B).

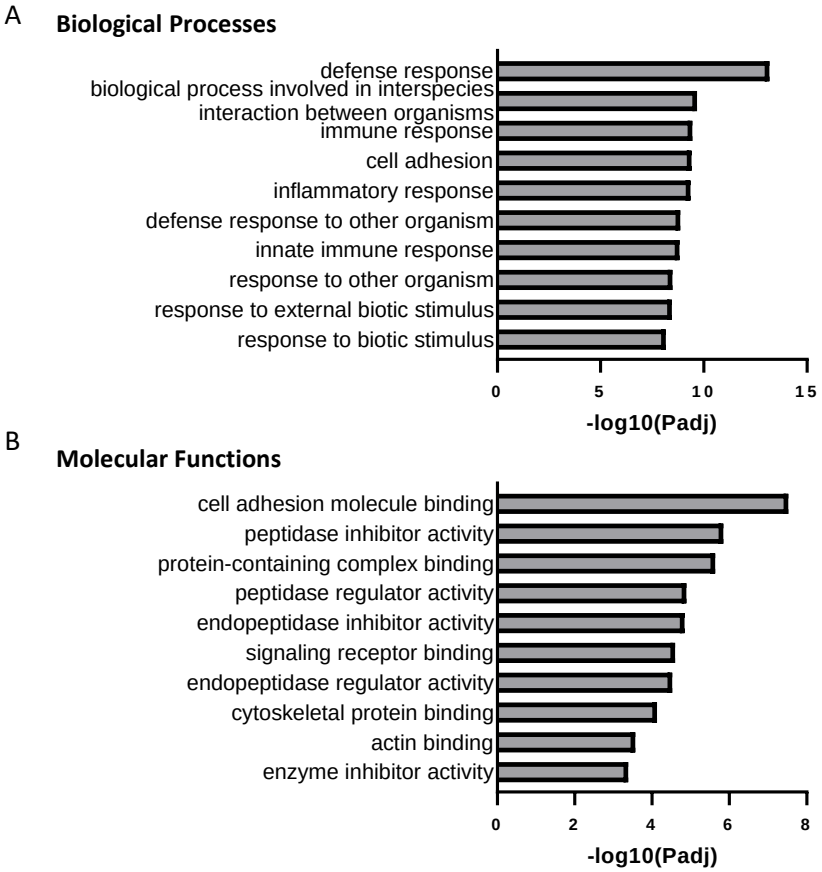

Figure 6.11: Enriched gene ontology for proteins significantly changed between Q22 and Q109 co-cultures. P-value significant changed proteins were used for GO enrichment analysis. Significantly enriched (A) biological processes and (B) molecular functions are presented with GO Term ID and ranked by the negative Log10 of adjusted p-value.

All p-value significant proteins were further investigated for protein-protein interactions using Metascape. All proteins that form physical interactions with at least one other protein in the list are shown in the network (Figure 6.12A). Two densely connected networks were detected and are highlighted in red and blue (Figure 6.12B). Pathway and process enrichment analysis provided functional descriptions for both network clusters (Figure 6.12C). The red cluster combined the functions of degranulation, a part of neurophil phagocytosis, RHO GTPase effectors which are implicated in cytoskeletal dynamics and cell migration (Heasman and Ridley, 2008), as well as cell-cell adhesion. The blue cluster consisted of a number of complement factors.

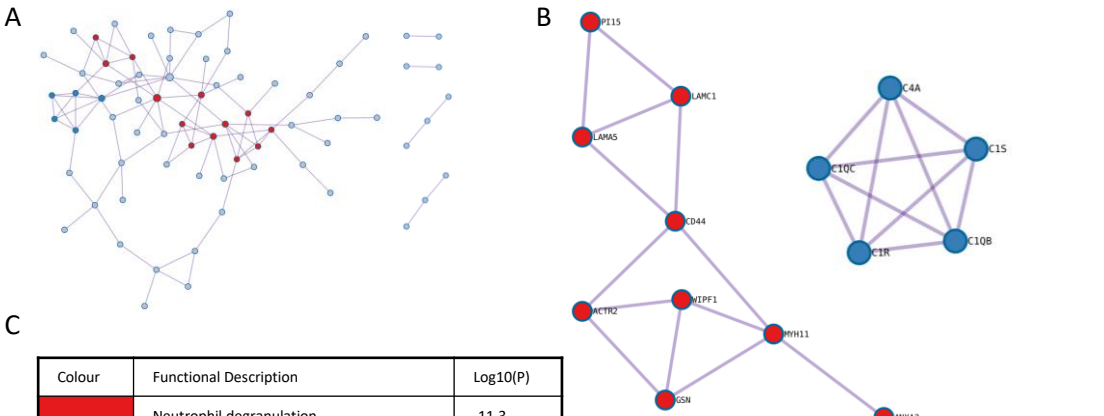

C

Colour	Functional Description	Log10(P)
	Neutrophil degranulation	-11.3
	RHO GTPase Effectors	-8.6
	Leukocyte cell-cell adhesion	-8.1
	Complement activation	-15.9
	Initial triggering of complement	-15.8
	Classical antibody-mediated complement activation	-14.7

Figure 6.12: Investigating protein-protein interactions of proteins different in Q109 co-cultures compared to Q22 co-cultures. All p-value significant proteins from the comparison of Q22 microglia - Q22 astrocyte vs. Q109 microglia - Q109 astrocyte co-cultures were inputted into Metascape. (A) All proteins that form physical interactions with at least one other protein in the list are shown. (B) Two densely connected protein networks were identified. (C) Pathway and process enrichment analysis provided functional descriptions for the identified network clusters.

6.4 Discussion

6.4.1 Summary

In this chapter, the influence of astrocyte secreted factors as well as direct contact with astrocytes on microglia-like cell morphology and phagocytosis was investigated. Furthermore, secreted factors of monocultures and co-cultures were compared using Mass Spectrometry. First, Q109 and Q22 microglia-like cell monocultures were compared. Then, co-cultures with combinations of genotypes of microglia-like cells and astrocytes were compared. Lastly, the Q22 co-culture was compared to the Q109 co-culture to potentially identify a disease phenotype.

6.4.2 Effect of direct contact with astrocytes on microglia-like cells

Q109 and Q22 microglia-like cells were investigated in co-culture with either Q109 or Q22 astrocytes. In order to identify and investigate the microglia-like cells, these were differentiated from mCherry expressing reporter Q109 and Q22 iPSCs. Astrocytes were first differentiated and then plated at a defined density in the experimental plates. MPC were then plated onto the astrocyte cultures and were differentiated for 14 days. Co-culture of microglia-like cells with Q109 versus Q22 astrocytes influenced both, microglia morphology and phagocytic function. Co-culture with Q109 versus Q22 astrocytes increased the roundness of Q22 microglia-like cells. It

is well established that microglia retract their processes towards an amoeboid cell morphology when activated (Leyh *et al.*, 2021b), indicating that Q109 astrocytes might induce microglia-like cell activation in co-culture. However, in order to confirm that hypothesis, further investigation beyond morphological analysis would be needed. Q109 astrocytes also increased the phagocytosis of Q109 microglia-like cells in co-culture compared to co-cultures with Q22 astrocytes. This result is in line with a study that found that microglia from the HD R6/2 mouse model demonstrated increased phagocytosis (Savage *et al.*, 2020), indicating that the HD brain environment might induce microglia to increase their capacity to phagocytose. However, this contrasts with the findings from chapter 4, which indicate that mutant *HTT* expression leads to a cell autonomous decrease in phagocytosis. How much cell autonomous mechanism and the influence by the brain environment contradict each other would need further investigation. In the brain, microglia phagocytosis is induced by "find-me" and "eat-me" signals and inhibited by "don't-eat-me" signals. The "find-me" signals include ADP that binds P2Y12 receptors and CX3CL1 that binds to the microglial CX3CR1, whereas "eat-me" signals include UDP that binds the P2Y6 receptor, complement factors, phosphatidylserines and desialylated proteins and lipids (Butler *et al.*, 2021).

6.4.3 Proteomic analysis of microglia monoculture and microglia-astrocyte co-culture supernatant

In order to investigate the secreted proteins of microglia-like cell monocultures and microglia-astrocyte co-cultures, supernatant samples underwent Nano-LC Mass Spectrometry (MS). Due to the high number of samples, they were distributed over two independent MS experiments, with a pool of all samples run with both experiments, which was then used for normalization of the data. Even though this practice has been applied before at the proteome facility at Bristol University, the variance between the experiments was still detectable via principal component analysis. For all the co-culture conditions, two replicates per group were run on one MS experiment, whereas the third replicate was run on the second MS experiment. All microglia monoculture samples were run on the same MS experiment. The biggest variance in the data comparing the complete dataset was the difference between microglia monoculture supernatants compared to microglia-astrocyte co-culture supernatants. In order to reduce variance from the cell culture procedures, all samples were setup the same day and all supernatants were collected at the same time. Cell numbers were counted when cultures were setup, however no further normalisation step for cell numbers was performed. After the collection of supernatants, RNA was isolated from all samples as we planned to validate some interesting proteins by qPCR. However, due to small culture volume, RNA yield was too small for cDNA synthesis and proteome findings were therefore not further validated.

6.4.4 Comparing the secretomes of microglia monocultures with microglia-astrocyte co-cultures

In the comparison of microglia monocultures with microglia-astrocyte co-cultures, the majority of significantly changed proteins were increased in the co-cultures, indicating that the astrocytes secreted a variety of proteins which were distinct from the microglia secretome. A few proteins were detected to be significantly lower in the co-culture, which could indicate that the interaction of microglia and astrocytes can regulate microglial protein secretion. The significantly higher proteins in the co-cultures underwent GO enrichment analysis and the molecular functions detected included the functions of cell adhesion and extracellular matrix, as well as protein binding. Astrocytes have been reported to be the source for extracellular matrix molecules in the brain (Wiese, Karus and Faissner, 2012) and their secretion of cell adhesion molecules is thought to be important for the tripartite synapse (Hillen, Burbach and Hol, 2018). No differences in the molecular functions of the upregulated proteins were detected between the Q109 and Q22 culture comparisons, indicating that these functions are key astrocyte functions which are not detrimentally affected by the mutant *HTT* expression. HD iPSC-derived astrocytes were shown to express common astrocyte markers and become functionally mature (Garcia *et al.*, 2019). The authors however stated that HD astrocytes provided reduced support for the maturation of iPSC-derived neurons in a co-culture model. In order to further investigate potential differences between Q22 and Q109 culture comparisons, the significantly secreted proteins were plotted in a Venn diagram showing the overlap between the Q22 and Q109 comparisons. 56% of higher secreted proteins overlapped between the Q109 and Q22 culture comparisons. These proteins further underwent GO enrichment analysis and were found to be enriched for development, cell adhesion and response to wound healing, all functions attributed to astrocytes (Hillen, Burbach and Hol, 2018; Siracusa, Fusco and Cuzzocrea, 2019; Zhou *et al.*, 2020). The proteins only significantly different in the comparison of Q22 cultures were enriched for terms around immune responses. These included CD14 and TIMP1. While CD14 was reported to fine-tune microglial damage-sensing capacity (Janova *et al.*, 2016), TIMP1 was shown to be secreted from primary rat astrocytes to protect primary rat neurons from Aβ mediated toxicity in a co-culture model (Saha *et al.*, 2020). Therefore, these immune response proteins might highlight a fine-tuning of cell-cell interaction between microglia and astrocytes in Q22 co-cultures.

6.4.5 Investigation of microglia monoculture secretomes

Supernatant was collected from Q109 and Q22 microglia-like cell monocultures. Only a low number of proteins were detected significantly different between the two groups. These

proteins were further investigated using GO enrichment analysis. The significant higher secreted proteins were detected to be important for integrin signalling and host interaction. Integrins are receptors that transduce biochemical signals into the cell. They regulate a variety of cellular functions, including actin cytoskeleton regulation for cell spreading and migration as well as proliferation and apoptosis (Cary, Han and Guan, 1999). The second GO term "biological process involved in interaction with host" indicated an upregulation of immune functions. Therefore, the detected upregulated secreted proteins in Q109 microglia-like cells would be in line with data indicating microglial activation in HD (Yang *et al.*, 2017). The downregulated proteins in Q109 microglia-like cells were found to be enriched for the biological processes of translation, biosynthetic and metabolic processes, immune response and response to interferon gamma.

The significantly changed proteins in the comparison between Q109 and Q22 microglia-like cells were further investigated using a protein-protein interaction enrichment analysis tool in order to determine direct interactions between these proteins. Three protein networks were found, and the software was able to determine functional descriptions for two of them. One network was best described with terms around translation, as already indicated in the GO term analysis of the downregulated proteins. The other network was described by terms of platelet activation, signalling and aggregation as well as degranulation and elevated cytosolic Ca^{2+}.

The last cluster of proteins that interact but were not described functionally included the protein STAT1. STAT1 has been described to contribute to microglial inflammation and can be activated by the interferon-gamma (IFN-γ) receptor complex (Krause *et al.*, 2006; Butturini, Boriero and Prati, 2019; Zhao *et al.*, 2022). STAT1 was amongst the top 10 most significant proteins in the monoculture comparison and was therefore plotted in the heatmap, which indicated that STAT1 is secreted at significant lower levels in the Q109 than Q22 microglia-like cells. This finding does not fit with the pro-inflammatory phenotype detected in chapter 4 of this thesis and will need further investigation.

6.4.6 Investigating the secretome of microglia-astrocyte co-cultures

In order to determine how a co-culture environment is affected by changing the genotype of one cell type, all possible combinations of microglia-astrocyte co-cultures of Q22 and Q109 were plated, and supernatants compared. Principal component analysis showed that astrocyte genotype had a stronger effect on culture variance than microglia-like cell genotype. This was also apparent when volcano plots for the individual comparisons were plotted. When Q22 and Q109 microglia-like cells were compared in either Q22 or Q109 astrocyte co-cultures, no significant changes to the secretome were detected. However, when the Q22 and Q109 astrocytes were compared in co-culture with either Q22 or Q109 microglia-like cells, a number of significantly affected proteins were detected. These proteins were further investigated.

Significantly changed proteins between Q109 and Q22 astrocytes in co-culture with Q22 microglia were enriched for the molecular functions around immune response and cell adhesion. This meant that the proteins important for the immune response were secreted by astrocytes rather than microglia-like cells. The comparison of Q22 and Q109 astrocytes in co-culture with Q109 microglia also showed enrichment for molecular functions around immune response. This indicates that the genotype of the microglia-like cells did not drastically affect the astrocytes. Hsiao et al. provided evidence of astrocyte induced inflammation in HD by studying primary astrocytes from the HD R6/2 mouse model. They found that the primary R6/2 astrocytes exhibited higher kB kinase (IKK) activity, resulting in prolonged NF-κB activation and the expression of pro-inflammatory factors, such as TNFα and IL-1β. In a co-culture of astrocytes with R6/2 neurons did the R6/2 astrocytes produce more damage to neurons than control astrocytes did (H. Hsiao *et al.*, 2014).

6.4.7 Comparing Q109 with Q22 microglia-astrocyte co-cultures

Lastly, Q22 co-cultures were compared to Q109 co-cultures. The Q22 co-cultures showed the highest variance and one sample overlapped with the Q109 co-culture samples. Nevertheless, a number of significantly different secreted proteins were detected, most of them found to be secreted lower in the Q109 co-cultures. Among the top 10 most significantly different proteins between Q109 versus Q22 co-cultures were C1R and C1S, proteases responsible for the activation and proteolytic activity of the C1 complex of the classical complement pathway (Rossi *et al.*, 2014). However, it is striking that these were found to be secreted at lower levels in the Q109 co-cultures, which is in direct contrast with the literature. Complement activation and increased staining for complement factors have been reported in post-mortem brains of HD patients compared to controls (Singhrao *et al.*, 1999). Single nucleus RNA-Seq was performed in cingulate cortex of patients with HD. In this study, gene expression profiles of detected HD astrocytes were enriched for multiple immune response genes including complement, toll-like receptor signalling, and interleukin pathways (Al-Dalahmah *et al.*, 2020). Among the top 10 most significantly affected proteins were two proteins detected to be higher in the Q109 co-cultures. These were secreted frizzled-related protein 4 (SFRP4) and GDNF family receptor alpha 1 (GFRA1). SFRP4 was found to be expressed at lower levels in neurogenesis-promoting astrocytes (Barkho *et al.*, 2006). GFRA1 is required for proper integration of adult-born hippocampal neurons into pre-existing circuits (Bonafina *et al.*, 2019). However, none of these two proteins were found to be associated with HD.

6.5 Chapter Summary

- Astrocyte secreted factors from Q22 or Q109 astrocytes had no effect on microglia-like cell morphology or phagocytic function
- Co-culture with astrocytes did effect microglia morphology and phagocytic function: Co-culture with Q109 versus Q22 astrocytes increased Q22 microglia-like cell roundness significantly as well as increased Q109 microglia-like cell phagocytosis of *E. coli* particles significantly
- Co-culture with astrocytes provided proteins to microglia-like cells which are important for cell adhesion and extracellular matrix
- Differences between Q109 and Q22 microglia-like cell monoculture secretomes were related to inflammation, translation and biosynthetic processes
- Differences between Q109 and Q22 microglia-astrocyte co-cultures were related to defence response, receptor binding, cell adhesion and cytoskeletal protein binding

7 Concluding remarks

7.1 Summary of findings

The overall aim of this thesis was to understand the effect of mutant *HTT* expression on microglia by investigation of cellular functions, gene expression changes and protein secretion. Although microglia activation is reported to take part in the pathology of Huntington's disease (Palpagama *et al.*, 2019), whether this activation is a cell-autonomous effect or solely a response to the detrimental HD brain environment is relatively unexplored. Furthermore, microglia dysfunctions in HD beyond the activated phenotype have barely been investigated.

In chapter 3, HD patient induced pluripotent stem cells with 109 CAG repeats in the *HTT* gene, as well as isogenic control iPSC were differentiated to microglia-like cells, as well as astrocytes and cortical neurons. All three cell types were validated using immunohistochemistry and microglia precursor cells were further characterised using flow cytometry in order to confirm cell identity. mCherry reporter iPSC were generated as a tool to investigate microglia-like cells in a co-culture with astrocytes as described in chapter 6. Co-cultures of microglia-like cells with astrocytes, as well as neurons with astrocytes were established in order to investigate cell types in long-term culture. It was shown previously that the *HTT* CAG repeats of the iPSC used in this thesis expands in culture (McAllister *et al.*, 2022). Here, it was shown that the expansion of the *HTT* CAG repeats is taking place at a similar rate in iPSC-derived Q109 neurons, astrocytes, and microglia-like cells.

In chapter 4, microglia morphology and function were investigated. Q109 microglia precursor cells exhibited impaired attachment to the extracellular matrix protein fibronectin. When differentiated to microglia-like cells, no differences in cell morphology were found between Q109 and Q22 control cells. HD microglia-like cells exhibited a significant increased secretion of the cytokines IL-8 and IL-6. Cargo-specific impairments in phagocytosis and endocytosis were detected in the Q109 microglia-like cells. Therefore, the endosomal-lysosomal pathway, which leads to the degradation of cargo taken up into microglia-like cells was investigated in more detail. Differences between Q109 and Q22 control microglia-like cells were found in late endosome numbers, but not in early endosomes, lysosomes, protease activity or autophagic vesicles. Furthermore, mitochondrial respiration was investigated, but no differences were detected between Q109 and Q22 microglia-like cells. Q109 microglia-like cells showed impaired calcium handling when challenged with ionomycin and ATP, but not ADP.

In chapter 5, the transcriptome profiles of Q109 and Q22 microglia-like cells were investigated. Many of the functional pathways investigated in chapter 4 were transcriptionally dysregulated

by mutant *HTT* expression. Amongst these were phagocytosis, endocytosis, inflammation, and lysosomes. Genes upregulated in Q109 microglia-like cells were enriched for cell cycle and mismatch repair genes. Q109 and Q22 microglia-like cells were further investigated after exposure to a pro-inflammatory stimulus. Genes downregulated in stimulated Q109 vs Q22 microglia-like cells showed enrichment for biological processes of response to ion and genes upregulated for development functions.

In chapter 6, Q109 and Q22 control microglia-like cells were co-cultured with astrocytes, to study the effect of astrocytes on microglia morphology and phagocytosis. The co-culture with Q109 astrocytes induced a significantly rounder morphology in Q22 microglia-like cells and significantly increased phagocytosis in Q109 microglia-like cells. Furthermore, the secretome of microglia monocultures and microglia-astrocyte co-cultures were investigated. In monoculture, Q109 and Q22 microglia-like cells showed differences in proteins related to integrin-mediated signalling, translation, and immune response. When compared in co-cultures, the astrocytes contributed more to the differences detected than microglia-like cells did. Differences between Q109 and Q22 microglia-astrocyte co-cultures were related to defence response, receptor binding, cell adhesion and cytoskeletal protein binding.

Collectively, these findings indicate that mutant *HTT* expression does effect microglia cellular function, gene transcription and protein secretion. Gene transcription changes were confirmed with functional assays and indicated that the transcriptional dysregulation, e.g. for endocytosis and phagocytosis, is translated into a dysfunctional phenotype. This study highlighted a microglial dysfunction of cell adhesion, phagocytosis, endocytosis and increased cytokine secretion. The only comparable study of HD microglia has been conducted by O'Regan *et al.*, 2021. The authors investigated the effect of mutant *HTT* expression on an isogenic series of ESC using controls containing 30 *HTT* CAG repeats and mutant lines containing 45 and 81 *HTT* CAG repeats. Thereby, the mutant *HTT* CAG repeat lengths were more physiological than the Q109 iPSC lines and by using different repeat lengths a HTT dose-dependent effect could be studied. The authors found a hyper-reactive response to stimulation with 1 µg/ml LPS and 10 ng/ml IFN-γ by showing an increased production of pro-inflammatory cytokines such as IL-6 and TNFα. However, cytokine secretion was not investigated in unstimulated microglia. The authors furthermore found an elevated release of reactive oxygen species and increased levels of apoptosis in the HD microglia. We are the first to show further cellular dysfunction of HD microglia-like cells including phagocytosis, which is one of microglia's main functions. We are also the first to conduct bulk RNA sequencing of HD microglia-like cells and we could show that some of the pathways detected to be dysregulated on a transcriptional level are translated to a cellular dysfunction. Investigation of the communication between Q109 astrocytes and

microglia in co-cultures by proteomic analysis of secreted factors showed an enrichment for biological processes of inflammatory responses and cell adhesion. Further analysis is needed to decipher the complex interaction of different cell types in HD.

7.2 The effect of mHTT expression on microglia function

HTT is a large protein with numerous functions, which interacts with effector proteins to mediate physiological processes. The subcellular localization of HTT is complex and dynamic. HTT colocalizes with many organelles, including the nucleus, endoplasmic reticulum, Golgi complex, and endosomes (Schulte and Littleton, 2011). In HD, mHTT is cleaved by proteases, generating N-terminal fragments containing the abnormal polyglutamine stretch. These fragments can interfere with the transcriptional and autophagic machineries and cause endoplasmic reticulum stress (Sari, 2011). mHTT impairs gene transcription through either intranuclear aggregates or sequestration to transcription factors that play a key role in HD. This mechanism is likely to play a role in HD microglia, as the RNA sequencing performed in this thesis showed dysregulation of a great number of genes in Q109 microglia-like cells. Also, the findings of increased cytokine secretion of Q109 microglia-like cells are likely to be explained by a transcriptional dysregulation, more specifically the interaction of mHTT with signalling pathways that are known to drive inflammatory responses, potentially NF-κB. Hsiao and colleagues showed that primary R6/2 astrocytes exhibited higher IκB kinase (IKK) activity that then caused prolongation of NF-κB activation, and thereby upregulating proinflammatory factors during inflammation (Hsiao *et al.*, 2013). The same cellular mechanisms are likely to occur in HD microglia. One of the main findings of this thesis is a dysfunction of microglial phagocytosis and endocytosis function. In HD, dysregulation of endocytosis is known to be mediated through interactions of the mutant huntingtin protein with its associated proteins, HIP1, HIP12, HIP14, PACSIN1 and SH3GL3, which are known as accessory factors in clathrin-dependent endocytosis (Sari 2011). Therefore, mHTT is known to cause cellular changes through the interaction with other proteins as well as binding to DNA, and some of these events are likely to induce the cell-autonomous HD microglia phenotype that has been studied in this thesis.

7.3 Wider implications

The most prominent neuropathology in HD occurs in the striatum, which is marked by extensive neuronal loss (Reiner, Dragatsis and Dietrich, 2011). Microglia are the brain's main phagocytes, and they remove dead or dying neurons to prevent the release of damaging and pro-inflammatory intracellular components into the extracellular space (Neher, Neniskyte and

Brown, 2012). Phagocytosis of apoptotic neurons however alters the microglial transcriptional profile, which can resemble the profile of disease-associated microglia (Krasemann *et al.*, 2017) and neuronal damage is known to cause microglia activation (Block and Hong, 2005). The problem is that activated microglia on the other hand can kill neurons by releasing TNF-α, glutamate, cathepsin B, superoxide or nitric oxide (Brown and Vilalta, 2015). This vicious cycle might explain the interplay between neurons and microglia in the pathology of HD. With a better understanding of how microglia might harm neurons in HD pathology, it could also be studies how treatment of microglia could potentially improve their homeostatic functions and thereby contribute to neuronal survival, opening a new avenue for future therapeutic interventions in HD.

On a cellular level, it is well studied what changes mutant *HTT* expression can cause. It leads to transcriptional dysregulation, alterations in proteasomes and autophagy, altered cellular trafficking and mitochondrial abnormalities (Ross and Tabrizi, 2011; Gatto *et al.*, 2020). These cellular phenotypes have been found in HD iPSC derived neurons. HD iPSC neurons were more susceptible to death than WT neurons, formed HTT aggregates under oxidative stress and showed reduced proteasome activity (Liu *et al.*, 2017). Furthermore, HD iPSC NPC displayed lower mitochondrial respiration and enhanced mitochondrial reactive oxygen species (Lopes *et al.*, 2020). In this thesis, these common HD cellular phenotypes have been studied in HD iPSC derived microglia-like cells. Even though transcriptional dysregulation as well as decreased numbers of late endosomes and affected endocytosis and phagocytosis were detected, the effect of mutant *HTT* on proteasomes and autophagy as well as mitochondria remains to be studied in more detail and might be important to address in future studies. Emerging findings in HD neurons will help guiding the analysis of an HD microglia phenotype for future investigations.

7.4 Future directions

Findings from O'Regan *et al.*, 2021 and this PhD thesis indicate that microglia activation is not just a response to the detrimental HD brain environment, but that mutant *HTT* expression does affect microglia function in a cell-autonomous way. Therefore, future studies can follow up on both, the effect of mHTT on microglia function in isolation, as well as how the interplay with other cell types that express mHTT affect microglia functionality. iPSC-models as well as primary rodent microglia offer great advances to study cell-autonomous phenotypes and emerging single cell methods allow the investigation of microglia in a brain environment (Masuda *et al.*, 2020). Single cell sequencing of HD post-mortem brain tissue, HD rodent brains, or in complex iPSC-derived co-cultures or organoid models could contribute to a better understanding of the role of microglia in HD pathology and could decipher cell-cell interactions of different CNS cell

types. A wide range of HD iPSC models are available (Kaye, Reisine and Finkbeiner, 2022), and a number of protocols exist to differentiate iPSC to a microglia-like phenotype (Speicher *et al.*, 2019). Protocols for the study of microglia in co-culture with neurons (Haenseler and Rajendran, 2019) or 3D brain organoids (Ormel *et al.*, 2018; Fagerlund *et al.*, 2021; Sabate-Soler *et al.*, 2022) have been established. These available methods can allow a deeper understanding of the cellular events induced by mHTT in HD microglia.

Furthermore, it has been shown that the addition of exogenous, primary wild-type microglia to mutant *HTT* expressing neurons increased neuronal survival, and this effect was proportional to the amount of microglia added, suggesting that wild-type microglia can rescue HD neuronal phenotypes (Kraft et al., 2012). This study conducted with primary rat and mouse cultures could be repeated using human iPSC-derived neuron-microglia co-cultures or 3D organoids. Furthermore, to choose an even more complex brain environment, the addition of wild-type microglia to the brain of HD mouse models could be studies. However, in order for human iPSC-derived microglia to survive in the mouse brain, mice that are Rag2/IL2rγ-deficient and also express the human forms of colony-stimulating factor 1 (CSF1) need to be used (Xu *et al.*, 2020). Using a mouse model, not only the cellular pathology but also behavioural phenotypes could be studied. Taken together, these experiments could widen the understanding of the role of microglia in HD pathology. Furthermore, future studies could investigate if improving microglia function might be a therapeutic target for the intervention of HD.

8 References

Abd-El-Basset, E. and Fedoroff, S. (1995) 'Effect of bacterial wall lipopolysaccharide (LPS) on morphology, motility, and cytoskeletal organization of microglia in cultures', *Journal of Neuroscience Research*, 41(2), pp. 222–237. doi: 10.1002/jnr.490410210.

Abud, E. M. *et al.* (2017) 'iPSC-Derived Human Microglia-like Cells to Study Neurological Diseases', *Neuron*. Elsevier Inc., 94(2), pp. 278-293.e9. doi: 10.1016/j.neuron.2017.03.042.

Akhter, R. *et al.* (2021) 'TREM2 alters the phagocytic, apoptotic and inflammatory response to Aβ(42) in HMC3 cells.', *Molecular immunology*. England, 131, pp. 171–179. doi: 10.1016/j.molimm.2020.12.035.

Al-Dalahmah, O. *et al.* (2020) 'Single-nucleus RNA-seq identifies Huntington disease astrocyte states.', *Acta neuropathologica communications*, 8(1), p. 19. doi: 10.1186/s40478-020-0880-6.

Alvarez-Periel, E. *et al.* (2018) 'Cdk5 Contributes to Huntington's Disease Learning and Memory Deficits via Modulation of Brain Region-Specific Substrates.', *Molecular neurobiology*. United States, 55(8), pp. 6250–6268. doi: 10.1007/s12035-017-0828-4.

Alvestegui, A. *et al.* (2019) 'TLR4 participates in the inflammatory response induced by the AAF/II fimbriae from enteroaggregative escherichia colion intestinal epithelial cells', *Frontiers in Cellular and Infection Microbiology*, 9(MAY), pp. 1–9. doi: 10.3389/fcimb.2019.00143.

Amos, P. J. *et al.* (2017) 'Modulation of hematopoietic lineage specification impacts TREM2 expression in microglia-like cells derived from human stem cells', *ASN Neuro*, 9(4). doi: 10.1177/1759091417716610.

An, M. C. *et al.* (2012) 'Genetic Correction of Huntington's Disease Phenotypes in Induced Pluripotent Stem Cells', *Cell Stem Cell*, 11(2), pp. 253–263. doi: 10.1016/j.stem.2012.04.026.

Andrade-Navarro, M. A. *et al.* (2020) 'RNA Sequencing of Human Peripheral Blood Cells Indicates Upregulation of Immune-Related Genes in Huntington's Disease.', *Frontiers in neurology*. Switzerland, 11, p. 573560. doi: 10.3389/fneur.2020.573560.

Andrew, S. E. *et al.* (1993) 'The relationship between trinucleotide (CAG) repeat length and clinical features of Huntington's disease.', *Nature genetics*. United States, 4(4), pp. 398–403. doi: 10.1038/ng0893-398.

Ao, Z. *et al.* (2021) 'Tubular human brain organoids to model microglia-mediated neuroinflammation', *Lab on a Chip*, 21(14), pp. 2751–2762. doi: 10.1039/d1lc00030f.

Arber, C. *et al.* (2015) 'Activin a directs striatal projection neuron differentiation of human pluripotent stem cells', *Development (Cambridge)*, 142(7), pp. 1375–1386. doi: 10.1242/dev.117093.

Arcuri, C. *et al.* (2017) 'The Pathophysiological Role of Microglia in Dynamic Surveillance, Phagocytosis and Structural Remodeling of the Developing CNS.', *Frontiers in molecular neuroscience*, 10, p. 191. doi: 10.3389/fnmol.2017.00191.

Augusto-Oliveira, M. *et al.* (2019) 'What Do Microglia Really Do in Healthy Adult Brain?', *Cells*. Switzerland, 8(10). doi: 10.3390/cells8101293.

Badanjak, K. *et al.* (2021) 'iPSC-Derived Microglia as a Model to Study Inflammation in Idiopathic Parkinson's Disease', *Frontiers in Cell and Developmental Biology*, 9(November), pp. 1–11. doi: 10.3389/fcell.2021.740758.

Bader, G. D. and Hogue, C. W. V (2003) 'An automated method for finding molecular complexes in large protein interaction networks.', *BMC bioinformatics*, 4(1), p. 2. doi: 10.1186/1471-2105-4-2.

Bakels, H. S. *et al.* (2022) 'Juvenile-Onset Huntington Disease Pathophysiology and Neurodevelopment: A Review.', *Movement disorders : official journal of the Movement Disorder Society*. United States, 37(1), pp. 16–24. doi: 10.1002/mds.28823.

Barbar, L. *et al.* (2020) 'CD49f Is a Novel Marker of Functional and Reactive Human iPSC-Derived

Astrocytes', *Neuron*, 107(3), pp. 436-453.e12. doi: 10.1016/j.neuron.2020.05.014.

Bardehle, S. *et al.* (2013) 'Live imaging of astrocyte responses to acute injury reveals selective juxtavascular proliferation.', *Nature neuroscience*. United States, 16(5), pp. 580–586. doi: 10.1038/nn.3371.

Barkho, B. Z. *et al.* (2006) 'Identification of astrocyte-expressed factors that modulate neural stem/progenitor cell differentiation.', *Stem cells and development*. United States, 15(3), pp. 407–421. doi: 10.1089/scd.2006.15.407.

Barral, D. C. *et al.* (2022) 'Current methods to analyze lysosome morphology, positioning, motility and function.', *Traffic (Copenhagen, Denmark)*. England, 23(5), pp. 238–269. doi: 10.1111/tra.12839.

Bassett, A. R. (2017) 'Editing the genome of hiPSC with CRISPR/Cas9: disease models', *Mammalian Genome*. Springer US, 28(7–8), pp. 348–364. doi: 10.1007/s00335-017-9684-9.

Bates, G. P. *et al.* (2015) 'Huntington disease', *Nature reviews. Disease primers*, (April), pp. 1–21. doi: 10.1038/nrdp.2015.5.

Bélanger, M. and Magistretti, P. J. (2009) 'The role of astroglia in neuroprotection', *Dialogues in Clinical Neuroscience*, 11(3), pp. 281–296.

Benarroch, E. E. (2005) 'Neuron-astrocyte interactions: Partnership for normal function and disease in the central nervous system', *Mayo Clinic Proceedings*. Mayo Foundation for Medical Education and Research, 80(10), pp. 1326–1338. doi: 10.4065/80.10.1326.

Benraiss, A. *et al.* (2016) 'Human glia can both induce and rescue aspects of disease phenotype in Huntington disease', *Nature Communications*. Nature Publishing Group, 7, pp. 1–13. doi: 10.1038/ncomms11758.

Benusa, S. D., George, N. M. and Dupree, J. L. (2020) 'Microglial heterogeneity: distinct cell types or differential functional adaptation?', *Neuroimmunology and Neuroinflammation*, 7(3), pp. 248–263. doi: 10.20517/2347-8659.2020.03.

Björkqvist, M. *et al.* (2008) 'A novel pathogenic pathway of immune activation detectable before clinical onset in Huntington's disease', *Journal of Experimental Medicine*, 205(8), pp. 1869–1877. doi: 10.1084/jem.20080178.

Block, M. L. and Hong, J.-S. (2005) 'Microglia and inflammation-mediated neurodegeneration: multiple triggers with a common mechanism.', *Progress in neurobiology*. England, 76(2), pp. 77–98. doi: 10.1016/j.pneurobio.2005.06.004.

Bodnar, B. *et al.* (2021) 'Novel Scalable and Simplified System to Generate Microglia-Containing Cerebral Organoids From Human Induced Pluripotent Stem Cells', *Frontiers in Cellular Neuroscience*, 15(July), pp. 1–12. doi: 10.3389/fncel.2021.682272.

Bonafina, A. *et al.* (2019) 'Article GDNF and GFR a 1 Are Required for Proper Integration of Adult-Born Hippocampal Neurons Article GDNF and GFR a 1 Are Required for Proper Integration of Adult-Born Hippocampal Neurons', pp. 4308–4319. doi: 10.1016/j.celrep.2019.11.100.

Bradford, J. *et al.* (2009) 'Expression of mutant huntingtin in mouse brain astrocytes causes age-dependent neurological symptoms', *Proceedings of the National Academy of Sciences*, 106(52), pp. 22480 LP – 22485. doi: 10.1073/pnas.0911503106.

Brand, M. D. *et al.* (2013) 'The role of mitochondrial function and cellular bioenergetics in ageing and disease.', *The British journal of dermatology*, 169 Suppl(0 2), pp. 1–8. doi: 10.1111/bjd.12208.

Brown, G. C. and Vilalta, A. (2015) 'How microglia kill neurons.', *Brain research*. Netherlands, 1628(Pt B), pp. 288–297. doi: 10.1016/j.brainres.2015.08.031.

Browne, S. E. *et al.* (1997) 'Oxidative damage and metabolic dysfunction in huntington's disease: Selective vulnerability of the basal ganglia', *Annals of Neurology*, 41(5), pp. 646–653. doi: 10.1002/ana.410410514.

Buffo, A., Rolando, C. and Ceruti, S. (2010) 'Astrocytes in the damaged brain: Molecular and cellular

insights into their reactive response and healing potential', *Biochemical Pharmacology*, 79(2), pp. 77–89. doi: https://doi.org/10.1016/j.bcp.2009.09.014.

Butler, C. A. *et al.* (2021) 'Microglial phagocytosis of neurons in neurodegeneration , and its regulation', (February), pp. 621–639. doi: 10.1111/jnc.15327.

Butovsky, O. *et al.* (2006) 'Glatiramer acetate fights against Alzheimer's disease by inducing dendritic-like microglia expressing insulin-like growth factor 1.', *Proceedings of the National Academy of Sciences of the United States of America*. United States, 103(31), pp. 11784–11789. doi: 10.1073/pnas.0604681103.

Butovsky, O. *et al.* (2014) 'Identification of a unique TGF-β-dependent molecular and functional signature in microglia', *Nature Neuroscience*, 17(1), pp. 131–143. doi: 10.1038/nn.3599.

Butturini, E., Boriero, D. and Prati, A. C. De (2019) 'STAT1 drives M1 microglia activation and neuroin fl ammation under hypoxia', 669(May), pp. 22–30. doi: 10.1016/j.abb.2019.05.011.

Camnasio, S. *et al.* (2012a) 'The first reported generation of several induced pluripotent stem cell lines from homozygous and heterozygous Huntington's disease patients demonstrates mutation related enhanced lysosomal activity', *Neurobiology of Disease*. Elsevier Inc., 46(1), pp. 41–51. doi: 10.1016/j.nbd.2011.12.042.

Camnasio, S. *et al.* (2012b) 'The first reported generation of several induced pluripotent stem cell lines from homozygous and heterozygous Huntington's disease patients demonstrates mutation related enhanced lysosomal activity', *Neurobiology of Disease*. Elsevier Inc., 46(1), pp. 41–51. doi: 10.1016/j.nbd.2011.12.042.

Carmo, C. *et al.* (2018) 'Mitochondrial Dysfunction in Huntington's Disease.', *Advances in experimental medicine and biology*. United States, 1049, pp. 59–83. doi: 10.1007/978-3-319-71779-1_3.

Cary, L. A., Han, D. C. and Guan, J. L. (1999) 'Integrin-mediated signal transduction pathways.', *Histology and histopathology*. Spain, 14(3), pp. 1001–1009. doi: 10.14670/HH-14.1001.

Castiglioni, V. *et al.* (2012) 'Induced pluripotent stem cell lines from Huntington's disease mice undergo neuronal differentiation while showing alterations in the lysosomal pathway', *Neurobiology of Disease*. Elsevier Inc., 46(1), pp. 30–40. doi: 10.1016/j.nbd.2011.12.032.

Cekanaviciute, E. *et al.* (2014) 'Astrocytic TGF-β Signaling Limits Inflammation and Reduces Neuronal Damage during Central Nervous System Toxoplasma Infection', *The Journal of Immunology*, 193(1), pp. 139 LP – 149. doi: 10.4049/jimmunol.1303284.

Cekanaviciute, E. and Buckwalter, M. S. (2016) 'Astrocytes: Integrative Regulators of Neuroinflammation in Stroke and Other Neurological Diseases', *Neurotherapeutics*, 13(4), pp. 685–701. doi: 10.1007/s13311-016-0477-8.

Chae, J. Il *et al.* (2012) 'Quantitative proteomic analysis of induced pluripotent stem cells derived from a human Huntington's disease patient', *Biochemical Journal*, 446(3), pp. 359–371. doi: 10.1042/BJ20111495.

Chakfe, Y. *et al.* (2002) 'ADP and AMP induce interleukin-1beta release from microglial cells through activation of ATP-primed P2X7 receptor channels', *The Journal of neuroscience : the official journal of the Society for Neuroscience*. Cell Biology of Excitable Tissue Group and Neuroimmunology Unit, Montreal Neurological Institute, Montreal, Quebec, Canada., 22(8), pp. 3061–3069. doi: 20026250.

Chamak, B. and Mallat, M. (1991) 'Fibronectin and laminin regulate the in vitro differentiation of microglial cells', *Neuroscience*, 45(3), pp. 513–527. doi: 10.1016/0306-4522(91)90267-R.

Chang, K. H. *et al.* (2015) 'Plasma inflammatory biomarkers for Huntington's disease patients and mouse model', *Brain, Behavior, and Immunity*. Elsevier Inc., 44, pp. 121–127. doi: 10.1016/j.bbi.2014.09.011.

Chaturvedi, R. K. *et al.* (2010) 'Impairment of PGC-1alpha expression, neuropathology and hepatic steatosis in a transgenic mouse model of Huntington's disease following chronic energy deprivation.', *Human molecular genetics*. England, 19(16), pp. 3190–3205. doi: 10.1093/hmg/ddq229.

Chazotte, B. (2009) 'Labeling pinocytotic vesicles and cytoplasm with fluorescent dextrans or ficolls for

imaging.', *Cold Spring Harbor protocols*. United States, 2009(11), p. pdb.prot4951. doi: 10.1101/pdb.prot4951.

Chen, Y. and Swanson, R. A. (2003) 'Astrocytes and brain injury', *Journal of Cerebral Blood Flow and Metabolism*, 23(2), pp. 137–149. doi: 10.1097/01.WCB.0000044631.80210.3C.

Chilakala, R. R. *et al.* (2020) 'Sulforaphane Attenuates Aβ Oligomers Mediated Decrease in Phagocytic Activity of Microglial Cells', *Neuroscience*. IBRO, 429(January), pp. 225–234. doi: 10.1016/j.neuroscience.2020.01.002.

Cho, I. K. *et al.* (2019) 'Amelioration of Huntington's disease phenotype in astrocytes derived from iPSC-derived neural progenitor cells of Huntington's disease monkeys', *PLoS ONE*, 14(3), pp. 1–22. doi: 10.1371/journal.pone.0214156.

Choi, S. S. *et al.* (2014) 'Human astrocytes: Secretome profiles of cytokines and chemokines', *PLoS ONE*, 9(4). doi: 10.1371/journal.pone.0092325.

Cisbani, G. and Cicchetti, F. (2012) 'An in vitro perspective on the molecular mechanisms underlying mutant huntingtin protein toxicity.', *Cell death & disease*. England, 3(8), p. e382. doi: 10.1038/cddis.2012.121.

Colombo, E. and Farina, C. (2016) 'Astrocytes: Key Regulators of Neuroinflammation', *Trends in Immunology*, 37(9), pp. 608–620. doi: 10.1016/j.it.2016.06.006.

Colonna, M. and Butovsky, O. (2017) 'Microglia Function in the Central Nervous System During Health and Neurodegeneration', *Annual Review of Immunology*, 35(1), pp. 441–468. doi: 10.1146/annurev-immunol-051116-052358.

Connor, B. (2018) 'Concise Review: The Use of Stem Cells for Understanding and Treating Huntington's Disease', *Stem Cells*, 36(2), pp. 146–160. doi: 10.1002/stem.2747.

Cortes, C. J. and La Spada, A. R. (2014) 'The many faces of autophagy dysfunction in Huntington's disease: From mechanism to therapy', *Drug Discovery Today*, 19(7), pp. 963–971. doi: 10.1016/j.drudis.2014.02.014.

Covarrubias-pazaran, G. *et al.* (2016) 'Fragman : an R package for fragment analysis', *BMC Genetics*. BMC Genetics, pp. 1–8. doi: 10.1186/s12863-016-0365-6.

Crotti, A. *et al.* (2014) 'Mutant Huntingtin promotes autonomous microglia activation via myeloid lineage-determining factors', *Nature Neuroscience*, 17(4), pp. 513–521. doi: 10.1038/nn.3668.

Crotti, A. and Glass, C. K. (2015) 'The choreography of neuroinflammation in Huntington's disease', *Trends in Immunology*, 36(6), pp. 364–373. doi: 10.1016/j.it.2015.04.007.

Damiano, M. *et al.* (2010) 'Mitochondria in Huntington's disease.', *Biochimica et biophysica acta*. Netherlands, 1802(1), pp. 52–61. doi: 10.1016/j.bbadis.2009.07.012.

Danen, E. H. J. *et al.* (2002) 'The fibronectin-binding integrins alpha5beta1 and alphavbeta3 differentially modulate RhoA-GTP loading, organization of cell matrix adhesions, and fibronectin fibrillogenesis.', *The Journal of cell biology*, 159(6), pp. 1071–1086. doi: 10.1083/jcb.200205014.

Davalos, D. *et al.* (2005) 'ATP mediates rapid microglial response to local brain injury in vivo', *Nature Neuroscience*, 8(6), pp. 752–758. doi: 10.1038/nn1472.

Davies, S. W. *et al.* (1997) 'Formation of Neuronal Intranuclear Inclusions Underlies the Neurological Dysfunction in Mice Transgenic for the HD Mutation', *Cell*, 90(3), pp. 537–548. doi: https://doi.org/10.1016/S0092-8674(00)80513-9.

Dobin, A. *et al.* (2013) 'STAR: Ultrafast universal RNA-seq aligner', *Bioinformatics*, 29(1), pp. 15–21. doi: 10.1093/bioinformatics/bts635.

Domon, B. and Aebersold, R. (2006) 'Mass spectrometry and protein analysis.', *Science (New York, N.Y.)*. United States, 312(5771), pp. 212–217. doi: 10.1126/science.1124619.

Donley, D. W. *et al.* (2019) 'Mutant huntingtin protein alters the response of microglial cells to inflammatory stimuli', *bioRxiv*, p. 550913. doi: 10.1101/550913.

Dragatsis, I., Levine, M. S. and Zeitlin, S. (2000) 'Inactivation of Hdh in the brain and testis results in progressive neurodegeneration and sterility in mice.', *Nature genetics*. United States, 26(3), pp. 300–306. doi: 10.1038/81593.

Du, F. *et al.* (2018) 'Astrocytes Attenuate Mitochondrial Dysfunctions in Human Dopaminergic Neurons Derived from iPSC', *Stem Cell Reports*. ElsevierCompany., 10(2), pp. 366–374. doi: 10.1016/j.stemcr.2017.12.021.

van Duijn, E., Kingma, E. M. and van der Mast, R. C. (2007) 'Psychopathology in Verified Huntington's Disease Gene Carriers', *The Journal of Neuropsychiatry and Clinical Neurosciences*. American Psychiatric Publishing, 19(4), pp. 441–448. doi: 10.1176/jnp.2007.19.4.441.

Duyao, M. P. *et al.* (1995) 'Inactivation of the mouse Huntington's disease gene homolog Hdh.', *Science (New York, N.Y.)*. United States, 269(5222), pp. 407–410. doi: 10.1126/science.7618107.

El-Daher, M.-T. *et al.* (2015) 'Huntingtin proteolysis releases non-polyQ fragments that cause toxicity through dynamin 1 dysregulation', *The EMBO Journal*. John Wiley & Sons, Ltd, 34(17), pp. 2255–2271. doi: 10.15252/embj.201490808.

Eng, L. F., Ghirnikar, R. S. and Lee, Y. L. (2000) 'Glial fibrillary acidic protein: GFAP-thirty-one years (1969-2000).', *Neurochemical research*. United States, 25(9–10), pp. 1439–1451. doi: 10.1023/a:1007677003387.

Erie, C. *et al.* (2015) 'Altered lysosomal positioning affects lysosomal functions in a cellular model of Huntington's disease', *European Journal of Neuroscience*, 42(3), pp. 1941–1951. doi: 10.1111/ejn.12957.

Estrada-Sánchez, A. M. and Rebec, G. V (2012) 'Corticostriatal dysfunction and glutamate transporter 1 (GLT1) in Huntington's disease: interactions between neurons and astrocytes', *Basal ganglia*, 2(2), pp. 57–66. doi: 10.1016/j.baga.2012.04.029.

Fagerlund, I. *et al.* (2021) 'Microglia-like Cells Promote Neuronal Functions in Cerebral Organoids.', *Cells*. Switzerland, 11(1). doi: 10.3390/cells11010124.

Feyeux, M. *et al.* (2012) 'Early transcriptional changes linked to naturally occurring Huntington's disease mutations in neural derivatives of human embryonic stem cells', *Human Molecular Genetics*, 21(17), pp. 3883–3895. doi: 10.1093/hmg/dds216.

Frasnelli, M. E. *et al.* (2005) 'TLR2 modulates inflammation in zymosan-induced arthritis in mice.', *Arthritis research & therapy*. England, 7(2), pp. R370-9. doi: 10.1186/ar1494.

Fu, R. *et al.* (2014) 'Phagocytosis of Microglia in the Central Nervous System Diseases', *Molecular Neurobiology*, 49(3), pp. 1422–1434. doi: 10.1007/s12035-013-8620-6.

Garcia, V. J. *et al.* (2019) 'Huntington's disease patient-derived astrocytes display electrophysiological impairments and reduced neuronal support', *Frontiers in Neuroscience*, 13(JUN), pp. 1–14. doi: 10.3389/fnins.2019.00669.

Garland, E. F., Hartnell, I. J. and Boche, D. (2022) 'Microglia and Astrocyte Function and Communication: What Do We Know in Humans?', *Frontiers in Neuroscience*, 16(February), pp. 1–21. doi: 10.3389/fnins.2022.824888.

Gatto, E. M. *et al.* (2020) 'Huntington disease: Advances in the understanding of its mechanisms.', *Clinical parkinsonism & related disorders*. England, 3, p. 100056. doi: 10.1016/j.prdoa.2020.100056.

Gil, J. M. and Rego, A. C. (2008) 'Mechanisms of neurodegeneration in Huntington ' s disease', 27(May 2007), pp. 2803–2820. doi: 10.1111/j.1460-9568.2008.06310.x.

Ginhoux, F. *et al.* (2010) 'Fate Mapping Analysis Reveals That Adult Microglia Derive from Primitive Macrophages', *Science*, 330(6005), pp. 841 LP – 845. doi: 10.1126/science.1194637.

Ginhoux, F. *et al.* (2013) 'Origin and differentiation of microglia', 7(April), pp. 1–14. doi: 10.3389/fncel.2013.00045.

Glick, D., Barth, S. and Macleod, K. F. (2010) 'Autophagy: Cellular and molecular mechanisms', *Journal of Pathology*, 221(1), pp. 3–12. doi: 10.1002/path.2697.

Goedhart, J. and Luijsterburg, M. S. (2020) 'VolcaNoseR is a web app for creating, exploring, labeling and sharing volcano plots', *Scientific Reports*. Nature Publishing Group UK, 10(1), pp. 1–5. doi: 10.1038/s41598-020-76603-3.

Gonitel, R. *et al.* (2008) 'DNA instability in postmitotic neurons', *Proceedings of the National Academy of Sciences of the United States of America*, 105(9), pp. 3467–3472. doi: 10.1073/pnas.0800048105.

Goodnight, A. V. *et al.* (2019) 'Chromatin accessibility and transcription dynamics during in vitro astrocyte differentiation of Huntington's Disease Monkey pluripotent stem cells', *Epigenetics and Chromatin*. BioMed Central, 12(1), pp. 1–25. doi: 10.1186/s13072-019-0313-6.

Goold, R. *et al.* (2019) 'FAN1 modifies Huntington's disease progression by stabilizing the expanded HTT CAG repeat', *Human Molecular Genetics*, 28(4), pp. 650–661. doi: 10.1093/hmg/ddy375.

Graveland, G. A., Williams, R. S. and DiFiglia, M. (1985) 'Evidence for degenerative and regenerative changes in neostriatal spiny neurons in Huntington's disease.', *Science (New York, N.Y.)*. United States, 227(4688), pp. 770–773. doi: 10.1126/science.3155875.

Graybiel, A. M. (1998) 'The Basal Ganglia and Chunking of Action Repertoires', *Neurobiology of Learning and Memory*, 70(1), pp. 119–136. doi: https://doi.org/10.1006/nlme.1998.3843.

Green, D. R., Oguin, T. H. and Martinez, J. (2016) 'The clearance of dying cells: table for two', *Cell Death & Differentiation*, 23(6), pp. 915–926. doi: 10.1038/cdd.2015.172.

Grigor'eva, E. V *et al.* (2020) 'Generation of GABAergic striatal neurons by a novel iPSC differentiation protocol enabling scalability and cryopreservation of progenitor cells', *Cytotechnology*, 72(5), pp. 649–663. doi: 10.1007/s10616-020-00406-7.

Gu, X. *et al.* (2021) 'Measurement of mitochondrial respiration in adherent cells by Seahorse XF96 Cell Mito Stress Test', *STAR Protocols*. Elsevier Inc., 2(1), p. 100245. doi: 10.1016/j.xpro.2020.100245.

Gutekunst, C. A. *et al.* (1999) 'Nuclear and neuropil aggregates in Huntington's disease: relationship to neuropathology.', *The Journal of neuroscience : the official journal of the Society for Neuroscience*. United States, 19(7), pp. 2522–2534. doi: 10.1523/JNEUROSCI.19-07-02522.1999.

Haenseler, W. *et al.* (2017) 'A Highly Efficient Human Pluripotent Stem Cell Microglia Model Displays a Neuronal-Co-culture-Specific Expression Profile and Inflammatory Response', *Stem Cell Reports*. ElsevierCompany., 8(6), pp. 1727–1742. doi: 10.1016/j.stemcr.2017.05.017.

Haenseler, W. and Rajendran, L. (2019) 'Concise Review: Modeling Neurodegenerative Diseases with Human Pluripotent Stem Cell-Derived Microglia', *Stem Cells*, 37(6), pp. 724–730. doi: 10.1002/stem.2995.

Hall-Roberts, H. *et al.* (2020) 'TREM2 Alzheimer's variant R47H causes similar transcriptional dysregulation to knockout, yet only subtle functional phenotypes in human iPSC-derived macrophages', *Alzheimer's Research and Therapy*. Alzheimer's Research & Therapy, 12(1), pp. 1–27. doi: 10.1186/s13195-020-00709-z.

Hands, S. L. *et al.* (2010) 'Metallothioneins and copper metabolism are candidate therapeutic targets in Huntington's disease.', *Biochemical Society transactions*. England, 38(2), pp. 552–558. doi: 10.1042/BST0380552.

Hanisch, U. K. (2002) 'Microglia as a source and target of cytokines', *Glia*, 40(2), pp. 140–155. doi: 10.1002/glia.10161.

Hanisch, U. K. and Kettenmann, H. (2007) 'Microglia: Active sensor and versatile effector cells in the normal and pathologic brain', *Nature Neuroscience*, 10(11), pp. 1387–1394. doi: 10.1038/nn1997.

Harjes, P. and Wanker, E. E. (2003) 'The hunt for huntingtin function: interaction partners tell many different stories', *Trends in Biochemical Sciences*, 28(8), pp. 425–433. doi: https://doi.org/10.1016/S0968-0004(03)00168-3.

Hatters, D. M. (2008) 'Protein misfolding inside cells: the case of huntingtin and Huntington's disease.', *IUBMB life*. England, 60(11), pp. 724–728. doi: 10.1002/iub.111.

HD iPSC Consortium (2020) 'Bioenergetic deficits in Huntington's disease iPSC-derived neural cells and rescue with glycolytic metabolites.', *Human molecular genetics*, 29(11), pp. 1757–1771. doi: 10.1093/hmg/ddy430.

Heasman, S. J. and Ridley, A. J. (2008) 'Mammalian Rho GTPases: New insights into their functions from in vivo studies', *Nature Reviews Molecular Cell Biology*, 9(9), pp. 690–701. doi: 10.1038/nrm2476.

Hedegaard, A. *et al.* (2020) 'Pro-maturational Effects of Human iPSC-Derived Cortical Astrocytes upon iPSC-Derived Cortical Neurons', *Stem Cell Reports*, 15(1), pp. 38–51. doi: 10.1016/j.stemcr.2020.05.003.

Hensley, K. (2010) 'Neuroinflammation in Alzheimer's disease: mechanisms, pathologic consequences, and potential for therapeutic manipulation.', *Journal of Alzheimer's disease : JAD*, 21(1), pp. 1–14. doi: 10.3233/JAD-2010-1414.

Hide, I. *et al.* (2000) 'Extracellular ATP triggers tumor necrosis factor-alpha release from rat microglia.', *Journal of neurochemistry*. England, 75(3), pp. 965–972. doi: 10.1046/j.1471-4159.2000.0750965.x.

Hillen, A. E. J., Burbach, J. P. H. and Hol, E. M. (2018) 'Progress in Neurobiology Cell adhesion and matricellular support by astrocytes of the tripartite synapse', *Progress in Neurobiology*. Elsevier, 165–167(May 2016), pp. 66–86. doi: 10.1016/j.pneurobio.2018.02.002.

Hoang, B. *et al.* (2012) 'The PP242 mammalian target of rapamycin (mTOR) inhibitor activates extracellular signal-regulated kinase (ERK) in multiple myeloma cells via a target of rapamycin complex 1 (TORC1)/ eukaryotic translation initiation factor 4E (eIF-4E)/ RAF pathway and act', *Journal of Biological Chemistry*, 287(26), pp. 21796–21805. doi: 10.1074/jbc.M111.304626.

Hoffmann, A. *et al.* (2003) 'Elevation of basal intracellular calcium as a central element in the activation of brain macrophages (microglia): Suppression of receptor-evoked calcium signaling and control of release function', *Journal of Neuroscience*, 23(11), pp. 4410–4419. doi: 10.1523/jneurosci.23-11-04410.2003.

Honda, S. *et al.* (2001) 'Extracellular ATP or ADP Induce Chemotaxis of Cultured Microglia through G_{i/o}-Coupled P2Y Receptors', *The Journal of Neuroscience*, 21(6), pp. 1975 LP – 1982. doi: 10.1523/JNEUROSCI.21-06-01975.2001.

Hrdlickova, R., Toloue, M. and Tian, B. (2017) 'RNA-Seq methods for transcriptome analysis', *Wiley Interdisciplinary Reviews: RNA*, 8(1). doi: 10.1002/wrna.1364.

Hsiao, H. *et al.* (2014) 'Inhibition of soluble tumor necrosis factor is therapeutic in Huntington ' s disease', 23(16), pp. 4328–4344. doi: 10.1093/hmg/ddu151.

Hsiao, H. Y. *et al.* (2013) 'A critical role of astrocyte-mediated nuclear factor-κB-dependent inflammation in huntington's disease', *Human Molecular Genetics*, 22(9), pp. 1826–1842. doi: 10.1093/hmg/ddt036.

Hsiao, H. Y. *et al.* (2014) 'Inhibition of soluble tumor necrosis factor is therapeutic in Huntington's disease', *Human Molecular Genetics*, 23(16), pp. 4328–4344. doi: 10.1093/hmg/ddu151.

Hu, Y.-B. *et al.* (2015) 'The endosomal-lysosomal system: from acidification and cargo sorting to neurodegeneration.', *Translational neurodegeneration*, 4, p. 18. doi: 10.1186/s40035-015-0041-1.

Hugh Perry, V. (1998) 'A revised view of the central nervous system microenvironment and major histocompatibility complex class II antigen presentation', *Journal of Neuroimmunology*, 90(2), pp. 113–121. doi: 10.1016/S0165-5728(98)00145-3.

Illes, P. *et al.* (2020) 'Regulation of Microglial Functions by Purinergic Mechanisms in the Healthy and Diseased CNS', *Cells*, 9(5), pp. 1–24. doi: 10.3390/cells9051108.

Inoue, K. (2002) 'Microglial activation by purines and pyrimidines', *Glia*, 40(2), pp. 156–163. doi: 10.1002/glia.10150.

Iyer, R. R. and Pluciennik, A. (2021) 'DNA Mismatch Repair and its Role in Huntington's Disease', *Journal of Huntington's Disease*, 10(1), pp. 75–94. doi: 10.3233/JHD-200438.

Janova, H. *et al.* (2016) 'CD14 is a key organizer of microglial responses to CNS infection and injury.', *Glia*. United States, 64(4), pp. 635–649. doi: 10.1002/glia.22955.

Jay, T. R., von Saucken, V. E. and Landreth, G. E. (2017) 'TREM2 in Neurodegenerative Diseases.', *Molecular neurodegeneration*. England, 12(1), p. 56. doi: 10.1186/s13024-017-0197-5.

Jeon, I. *et al.* (2012) 'Neuronal properties, in vivo effects, and pathology of a Huntington's disease patient-derived induced pluripotent stem cells', *Stem Cells*, 30(9), pp. 2054–2062. doi: 10.1002/stem.1135.

Juopperi, T. A. *et al.* (2012) 'Astrocytes generated from patient induced pluripotent stem cells recapitulate features of Huntingtons disease patient cells', *Molecular Brain*. Molecular Brain, 5(1), p. 1. doi: 10.1186/1756-6606-5-17.

Kaksonen, M. and Roux, A. (2018) 'Mechanisms of clathrin-mediated endocytosis', *Nature Reviews Molecular Cell Biology*. Nature Publishing Group, 19(5), pp. 313–326. doi: 10.1038/nrm.2017.132.

Kalsbeek, M. J. T., Mulder, L. and Yi, C. X. (2016) 'Microglia energy metabolism in metabolic disorder', *Molecular and Cellular Endocrinology*. Elsevier Ireland Ltd, 438, pp. 27–35. doi: 10.1016/j.mce.2016.09.028.

Kanehisa, M. and Goto, S. (2000) 'KEGG: Kyoto Encyclopedia of Genes and Genomes', *Nucleic Acids Research*, 28(1), pp. 27–30. doi: 10.1093/nar/28.1.27.

Kaye, J., Reisine, T. and Finkbeiner, S. (2022) 'Huntington's disease iPSC models-using human patient cells to understand the pathology caused by expanded CAG repeats.', *Faculty reviews*, 11, p. 16. doi: 10.12703/r/11-16.

Kennedy, L. *et al.* (2003) 'Dramatic tissue-specific mutation length increases are an early molecular event in Huntington disease pathogenesis.', *Human molecular genetics*. England, 12(24), pp. 3359–3367. doi: 10.1093/hmg/ddg352.

Kettenmann, H. *et al.* (2011) 'Physiology of Microglia', *Physiological Reviews*, 91(2), pp. 461–553. doi: 10.1152/physrev.00011.2010.

Khakh, B. S. and Alan North, R. (2006) 'P2X receptors as cell-surface ATP sensors in health and disease', *Nature*, 442(7102), pp. 527–532. doi: 10.1038/nature04886.

Klapper, S. D. *et al.* (2019) 'Astrocyte lineage cells are essential for functional neuronal differentiation and synapse maturation in human iPSC-derived neural networks', *Glia*, 67(10), pp. 1893–1909. doi: 10.1002/glia.23666.

Kolobkova, Y. A. *et al.* (2017a) 'an20758251-09-02-034', 9(33), pp. 34–46.

Kolobkova, Y. A. *et al.* (2017b) 'Huntington's Disease: Calcium Dyshomeostasis and Pathology Models.', *Acta naturae*, 9(2), pp. 34–46.

Korolchuk, V. I. *et al.* (2011) 'Lysosomal positioning coordinates cellular nutrient responses', *Nature Cell Biology*. Nature Publishing Group, 13(4), pp. 453–462. doi: 10.1038/ncb2204.

Kraft, A. D. *et al.* (2012) 'Activated microglia proliferate at neurites of mutant huntingtin-expressing neurons', *Neurobiology of Aging*, 33(3), pp. 621.e17-621.e33. doi: 10.1016/j.neurobiolaging.2011.02.015.

Krasemann, S. *et al.* (2017) 'The TREM2-APOE Pathway Drives the Transcriptional Phenotype of Dysfunctional Microglia in Neurodegenerative Diseases.', *Immunity*. United States, 47(3), pp. 566-581.e9. doi: 10.1016/j.immuni.2017.08.008.

Krause, C. D. *et al.* (2006) 'Modulation of the activation of Stat1 by the interferon-gamma receptor complex', pp. 113–123. doi: 10.1038/sj.cr.7310015.

Kremer, B. *et al.* (1993) 'Molecular analysis of late onset Huntington's disease.', *Journal of medical genetics*, 30(12), pp. 991–995. doi: 10.1136/jmg.30.12.991.

Krencik, R. *et al.* (2011) 'Specification of transplantable astroglial subtypes from human pluripotent stem cells', *Nature Biotechnology*. Nature Publishing Group, 29(6), pp. 528–534. doi: 10.1038/nbt.1877.

Kuemmerle, S. *et al.* (1999) 'Huntington aggregates may not predict neuronal death in Huntington's disease.', *Annals of neurology*. United States, 46(6), pp. 842–849.

Kumar, A., Vaish, M. and Ratan, R. R. (2014) 'Transcriptional dysregulation in Huntington's disease: a failure of adaptive transcriptional homeostasis.', *Drug discovery today*. England, 19(7), pp. 956–962. doi: 10.1016/j.drudis.2014.03.016.

Labadorf, A. *et al.* (2015) 'RNA Sequence Analysis of Human Huntington Disease Brain Reveals an Extensive Increase in Inflammatory and Developmental Gene Expression.', *PloS one*. United States, 10(12), p. e0143563. doi: 10.1371/journal.pone.0143563.

Labadorf, A. *et al.* (2016) 'Correction: RNA sequence analysis of human huntington disease brain reveals an extensive increase in inflammatory and developmental gene expression', *PLoS ONE*, 11(7), pp. 1–21. doi: 10.1371/journal.pone.0160295.

Lai, Y. *et al.* (2016) 'Crosstalk between MSH2-MSH3 and polβ promotes trinucleotide repeat expansion during base excision repair.', *Nature communications*. England, 7, p. 12465. doi: 10.1038/ncomms12465.

Lax, N. *et al.* (2020) 'Systemic microbial TLR2 agonists induce neurodegeneration in Alzheimer's disease mice', *Journal of Neuroinflammation*. Journal of Neuroinflammation, 17(1), pp. 1–12. doi: 10.1186/s12974-020-01738-z.

Lee, C.-T. *et al.* (2017) '3D brain Organoids derived from pluripotent stem cells: promising experimental models for brain development and neurodegenerative disorders.', *Journal of biomedical science*. England, 24(1), p. 59. doi: 10.1186/s12929-017-0362-8.

Lee, J.-M. *et al.* (2010) 'A novel approach to investigate tissue-specific trinucleotide repeat instability', *BMC Systems Biology*, 4(1), p. 29. doi: 10.1186/1752-0509-4-29.

Lee, J.-M. *et al.* (2015) 'Identification of Genetic Factors that Modify Clinical Onset of Huntington's Disease', *Cell*, 162(3), pp. 516–526. doi: 10.1016/j.cell.2015.07.003.

Lee, J.-M. *et al.* (2019) 'CAG Repeat Not Polyglutamine Length Determines Timing of Huntington's Disease Onset', *Cell*, 178(4), pp. 887-900.e14. doi: 10.1016/j.cell.2019.06.036.

Lee, J.-M. *et al.* (2022) 'Genetic modifiers of Huntington disease differentially influence motor and cognitive domains.', *American journal of human genetics*. United States, 109(5), pp. 885–899. doi: 10.1016/j.ajhg.2022.03.004.

Leyh, J. *et al.* (2021a) 'Classification of Microglial Morphological Phenotypes Using Machine Learning.', *Frontiers in cellular neuroscience*. Switzerland, 15, p. 701673. doi: 10.3389/fncel.2021.701673.

Leyh, J. *et al.* (2021b) 'Classification of Microglial Morphological Phenotypes Using Machine Learning', *Frontiers in Cellular Neuroscience*, 15(June), pp. 1–17. doi: 10.3389/fncel.2021.701673.

Li, J. *et al.* (2021) 'Microglial Phenotypic Transition: Signaling Pathways and Influencing Modulators Involved in Regulation in Central Nervous System Diseases', *Frontiers in Cellular Neuroscience*, 15(September), pp. 1–16. doi: 10.3389/fncel.2021.736310.

Li, S. H. *et al.* (1993) 'Huntington's disease gene (IT15) is widely expressed in human and rat tissues', *Neuron*, 11(5), pp. 985–993. doi: 10.1016/0896-6273(93)90127-D.

Liang, G. and Zhang, Y. (2013) 'Genetic and Epigenetic Variations in iPSCs: Potential Causes and Implications for Application', *Cell Stem Cell*, 13(2), pp. 149–159. doi: 10.1016/j.stem.2013.07.001.

Liang, Q. *et al.* (2011) 'Reduction of mutant huntingtin accumulation and toxicity by lysosomal cathepsins D and B in neurons.', *Molecular neurodegeneration*, 6, p. 37. doi: 10.1186/1750-1326-6-37.

Liao, Y., Smyth, G. K. and Shi, W. (2014) 'featureCounts: an efficient general purpose program for assigning sequence reads to genomic features.', *Bioinformatics (Oxford, England)*. England, 30(7), pp. 923–930. doi: 10.1093/bioinformatics/btt656.

Liddelow, S. A. *et al.* (2017) 'Neurotoxic reactive astrocytes are induced by activated microglia', *Nature*. Nature Publishing Group, 541(7638), pp. 481–487. doi: 10.1038/nature21029.

Liddelow, S. A. and Barres, B. A. (2017) 'Reactive Astrocytes: Production, Function, and Therapeutic Potential', *Immunity*. Elsevier Inc., 46(6), pp. 957–967. doi: 10.1016/j.immuni.2017.06.006.

Liesi, P., Kirkwood, T. and Vaheri, A. (1986) 'Fibronectin is expressed by astrocytes cultured from

embryonic and early postnatal rat brain', *Experimental Cell Research*, 163(1), pp. 175–185. doi: 10.1016/0014-4827(86)90570-7.

Liévens, J. C. *et al.* (2001) 'Impaired glutamate uptake in the R6 Huntington's disease transgenic mice.', *Neurobiology of disease*. United States, 8(5), pp. 807–821. doi: 10.1006/nbdi.2001.0430.

Lim, R. G. *et al.* (2017) 'Developmental alterations in Huntington's disease neural cells and pharmacological rescue in cells and mice', *Nature Neuroscience*, 20(5), pp. 648–660. doi: 10.1038/nn.4532.

Lin, L. *et al.* (2015) 'In Vitro Differentiation of Human Neural Progenitor Cells Into Striatal GABAergic Neurons', *STEM CELLS Translational Medicine*, 4(7), pp. 775–788. doi: 10.5966/sctm.2014-0083.

Liu, K.-Y. *et al.* (2015) 'Disruption of the nuclear membrane by perinuclear inclusions of mutant huntingtin causes cell-cycle re-entry and striatal cell death in mouse and cell models of Huntington's disease', *Human Molecular Genetics*, 24(6), pp. 1602–1616. doi: 10.1093/hmg/ddu574.

Liu, X. *et al.* (2018) 'LPS-induced proinflammatory cytokine expression in human airway epithelial cells and macrophages via NF-κB, STAT3 or AP-1 activation.', *Molecular medicine reports*. Greece, 17(4), pp. 5484–5491. doi: 10.3892/mmr.2018.8542.

Liu, X. *et al.* (2020) 'Chromosomal aberration arises during somatic reprogramming to pluripotent stem cells', *Cell Division*. BioMed Central, 15(1), pp. 1–13. doi: 10.1186/s13008-020-00068-z.

Liu, Y. *et al.* (2017) 'FOXOs modulate proteasome activity in human-induced pluripotent stem cells of Huntington's disease and their derived neural cells.', *Human molecular genetics*. England, 26(22), pp. 4416–4428. doi: 10.1093/hmg/ddx327.

Lively, S. and Schlichter, L. C. (2018) 'Microglia Responses to Pro-inflammatory Stimuli (LPS, IFNγ+TNFα) and Reprogramming by Resolving Cytokines (IL-4, IL-10)', *Frontiers in Cellular Neuroscience*, 12(July), pp. 1–19. doi: 10.3389/fncel.2018.00215.

Lo, B. and Parham, L. (2009) 'Ethical issues in stem cell research.', *Endocrine reviews*. 2009/04/14. The Endocrine Society, 30(3), pp. 204–13. doi: 10.1210/er.2008-0031.

Loane, C. and Politis, M. (2011) 'Positron emission tomography neuroimaging in Parkinson's disease', *American journal of translational research*. 2011/07/10. e-Century Publishing Corporation, 3(4), pp. 323–341. Available at: https://pubmed.ncbi.nlm.nih.gov/21904653.

Lopes, C. *et al.* (2020) 'Mitochondrial and Redox Modifications in Huntington Disease Induced Pluripotent Stem Cells Rescued by CRISPR/Cas9 CAGs Targeting.', *Frontiers in cell and developmental biology*. Switzerland, 8, p. 576592. doi: 10.3389/fcell.2020.576592.

López-Otín, C. and Bond, J. S. (2008) 'Proteases: multifunctional enzymes in life and disease.', *The Journal of biological chemistry*, 283(45), pp. 30433–30437. doi: 10.1074/jbc.R800035200.

Luchena, C. *et al.* (2022) 'A Neuron, Microglia, and Astrocyte Triple Co-culture Model to Study Alzheimer's Disease.', *Frontiers in aging neuroscience*, 14, p. 844534. doi: 10.3389/fnagi.2022.844534.

Lull, M. E. and Block, M. L. (2010) 'Microglial Activation and Chronic Neurodegeneration', *Neurotherapeutics*, 7(4), pp. 354–365. doi: 10.1016/j.nurt.2010.05.014.

Luthi-Carter, R. *et al.* (2002) 'Dysregulation of gene expression in the R6/2 model of polyglutamine disease: Parallel changes in muscle and brain', *Human Molecular Genetics*, 11(17), pp. 1911–1926. doi: 10.1093/hmg/11.17.1911.

Macdonald, M. E. *et al.* (1993) 'A novel gene containing a trinucleotide repeat that is expanded and unstable on Huntington's disease chromosomes. The Huntington's Disease Collaborative Research Group.', *Cell*, 72(6), pp. 971–983. doi: 10.1016/0092-8674(93)90585-E.

Maeda, T. *et al.* (2016) 'ATP increases the migration of microglia across the brain endothelial cell monolayer', *Bioscience Reports*, 36(2), pp. 1–8. doi: 10.1042/BSR20160054.

Maguire, E. *et al.* (2021) 'PIP2 depletion and altered endocytosis caused by expression of Alzheimer's disease-protective variant PLCγ2 R522', *The EMBO Journal*, 40(17), pp. 1–20. doi:

10.15252/embj.2020105603.

Maguire, E. *et al.* (2022) 'Assaying Microglia Functions In Vitro', *Cells*. doi: 10.3390/cells11213414.

Malaiya, S. *et al.* (2021) 'Single-Nucleus RNA-Seq Reveals Dysregulation of Striatal Cell Identity Due to Huntington's Disease Mutations.', *The Journal of neuroscience : the official journal of the Society for Neuroscience*. United States, 41(25), pp. 5534–5552. doi: 10.1523/JNEUROSCI.2074-20.2021.

Martin, D. D. O. *et al.* (2014) 'Identification of a post-translationally myristoylated autophagy-inducing domain released by caspase cleavage of Huntingtin', *Human Molecular Genetics*, 23(12), pp. 3166–3179. doi: 10.1093/hmg/ddu027.

Martinez-Vicente, M. *et al.* (2010) 'Cargo recognition failure is responsible for inefficient autophagy in Huntington's disease', *Nature Neuroscience*. Nature Publishing Group, 13(5), pp. 567–576. doi: 10.1038/nn.2528.

Marwaha, R. and Sharma, M. (2017) 'DQ-Red BSA Trafficking Assay in Cultured Cells to Assess Cargo Delivery to Lysosomes.', *Bio-protocol*, 7(19). doi: 10.21769/BioProtoc.2571.

Masgrau, R. *et al.* (2017) 'Should We Stop Saying "Glia" and "Neuroinflammation"?', *Trends in Molecular Medicine*, 23(6), pp. 486–500. doi: 10.1016/j.molmed.2017.04.005.

Masuda, T. *et al.* (2020) 'Microglia Heterogeneity in the Single-Cell Era.', *Cell reports*. United States, 30(5), pp. 1271–1281. doi: 10.1016/j.celrep.2020.01.010.

Matejuk, A. and Ransohoff, R. M. (2020) 'Crosstalk Between Astrocytes and Microglia: An Overview', *Frontiers in Immunology*, 11(July), pp. 1–11. doi: 10.3389/fimmu.2020.01416.

Mattis, V. B. *et al.* (2012) 'Induced pluripotent stem cells from patients with huntington's disease show CAG repeat expansion associated phenotypes', *Cell Stem Cell*, 11(2), pp. 264–278. doi: 10.1016/j.stem.2012.04.027.

Mattis, V. B. *et al.* (2015) 'HD iPSC-derived neural progenitors accumulate in culture and are susceptible to BDNF withdrawal due to glutamate toxicity', *Human Molecular Genetics*, 24(11), pp. 3257–3271. doi: 10.1093/hmg/ddv080.

Mauvezin, C. and Neufeld, T. P. (2015) 'Bafilomycin A1 disrupts autophagic flux by inhibiting both', *Autophagy*, 11(8), pp. 1437–1438.

Mayle, K. M., Le, A. M. and Kamei, D. T. (2012) 'The intracellular trafficking pathway of transferrin', *Biochimica et Biophysica Acta (BBA) - General Subjects*, 1820(3), pp. 264–281. doi: 10.1016/j.bbagen.2011.09.009.

Mayrhofer, F. *et al.* (2021) 'Reduction in CD11c(+) microglia correlates with clinical progression in chronic experimental autoimmune demyelination.', *Neurobiology of disease*. United States, 161, p. 105556. doi: 10.1016/j.nbd.2021.105556.

McAllister, B. *et al.* (2022) 'Exome sequencing of individuals with Huntington's disease implicates FAN1 nuclease activity in slowing CAG expansion and disease onset.', *Nature neuroscience*, 25(4), pp. 446–457. doi: 10.1038/s41593-022-01033-5.

McColgan, P. and Tabrizi, S. J. (2018) 'Huntington's disease: a clinical review', *European Journal of Neurology*, 25(1), pp. 24–34. doi: 10.1111/ene.13413.

Mehta, S. R. *et al.* (2018) 'Human Huntington's Disease iPSC-Derived Cortical Neurons Display Altered Transcriptomics, Morphology, and Maturation', *Cell Reports*. Elsevier, 25(4), pp. 1081-1096.e6. doi: 10.1016/j.celrep.2018.09.076.

Meriin, A. B. *et al.* (2003) 'Aggregation of expanded polyglutamine domain in yeast leads to defects in endocytosis.', *Molecular and cellular biology*. United States, 23(21), pp. 7554–7565. doi: 10.1128/MCB.23.21.7554-7565.2003.

Metsalu, T. and Vilo, J. (2015) 'ClustVis: A web tool for visualizing clustering of multivariate data using Principal Component Analysis and heatmap', *Nucleic Acids Research*, 43(W1), pp. W566–W570. doi: 10.1093/nar/gkv468.

Miller, J. *et al.* (2010) 'Quantitative Relationships between Huntingtin Levels, Polyglutamine Length, Inclusion Body Formation, and Neuronal Death Provide Novel Insight into Huntington's Disease Molecular Pathogenesis', *The Journal of Neuroscience*, 30(31), pp. 10541 LP – 10550. doi: 10.1523/JNEUROSCI.0146-10.2010.

Miller, J. R. C. *et al.* (2016) 'RNA-Seq of Huntington's disease patient myeloid cells reveals innate transcriptional dysregulation associated with proinflammatory pathway activation', *Human Molecular Genetics*, 25(14), p. ddw142. doi: 10.1093/hmg/ddw142.

Mollica, P. A. *et al.* (2018) 'Epigenetic alterations mediate iPSC-induced normalization of DNA repair gene expression and TNR stability in Huntington's disease cells.', *Journal of cell science*. England, 131(13). doi: 10.1242/jcs.215343.

Monzón-Sandoval, J. *et al.* (2022) 'Lipopolysaccharide distinctively alters human microglia transcriptomes to resemble microglia from Alzheimer's disease mouse models.', *Disease models & mechanisms*, 15(10). doi: 10.1242/dmm.049349.

Morgan, A. J. and Jacob, R. (1994) 'Ionomycin enhances Ca2+ influx by stimulating store-regulated cation entry and not by a direct action at the plasma membrane.', *The Biochemical journal*, 300 (Pt 3(Pt 3), pp. 665–672. doi: 10.1042/bj3000665.

Muffat, J. *et al.* (2016) 'Efficient derivation of microglia-like cells from human pluripotent stem cells', 22(11). doi: 10.1038/nm.4189.

Myers, R. H. *et al.* (1991) 'Decreased neuronal and increased oligodendroglial densities in Huntington's disease caudate nucleus.', *Journal of neuropathology and experimental neurology*. England, 50(6), pp. 729–742. doi: 10.1097/00005072-199111000-00005.

Nagata, E. *et al.* (2004) 'Autophagosome-like vacuole formation in Huntington's disease lymphoblasts.', *Neuroreport*. England, 15(8), pp. 1325–1328. doi: 10.1097/01.wnr.0000127073.66692.8f.

Nami, F. *et al.* (2021) 'Fast and Efficient Generation of Isogenic Induced Pluripotent Stem Cell Lines Using Adenine Base Editing.', *The CRISPR journal*. United States, 4(4), pp. 502–518. doi: 10.1089/crispr.2021.0006.

Nance, M. A. (2017) 'Genetics of Huntington disease', *Handbook of Clinical Neurology*. Elsevier, 144, pp. 3–14. doi: 10.1016/B978-0-12-801893-4.00001-8.

Nasir, J. *et al.* (1995) 'Targeted disruption of the Huntington's disease gene results in embryonic lethality and behavioral and morphological changes in heterozygotes', *Cell*, 81(5), pp. 811–823. doi: https://doi.org/10.1016/0092-8674(95)90542-1.

Nayak, D., Roth, T. L. and McGavern, D. B. (2014) 'Microglia Development and Function', *Annual Review of Immunology*, 32(1), pp. 367–402. doi: 10.1146/annurev-immunol-032713-120240.

Negro, S. *et al.* (2016) 'ATP Released by Injured Neurons Activates Schwann Cells ', *Frontiers in Cellular Neuroscience* , p. 134. Available at: https://www.frontiersin.org/article/10.3389/fncel.2016.00134.

Neher, J. J., Neniskyte, U. and Brown, G. C. (2012) 'Primary phagocytosis of neurons by inflamed microglia: potential roles in neurodegeneration.', *Frontiers in pharmacology*. Switzerland, 3, p. 27. doi: 10.3389/fphar.2012.00027.

Nekrasov, E. D. *et al.* (2016) 'Manifestation of Huntington's disease pathology in human induced pluripotent stem cell-derived neurons.', *Molecular neurodegeneration*, 11, p. 27. doi: 10.1186/s13024-016-0092-5.

Nihei, K. and Kowall, N. W. (1992) 'Neurofilament and neural cell adhesion molecule immunocytochemistry of Huntington's disease striatum.', *Annals of neurology*. United States, 31(1), pp. 59–63. doi: 10.1002/ana.410310111.

Novak, M. J. U. and Tabrizi, S. J. (2011) *HUNTINGTON ' S DISEASE : CLINICAL PRESENTATION*, *International Review of Neurobiology*. Elsevier Inc. doi: 10.1016/B978-0-12-381328-2.00013-4.

Nunnari, J. and Suomalainen, A. (2012) 'Mitochondria: In sickness and in health', *Cell*. Elsevier Inc., 148(6), pp. 1145–1159. doi: 10.1016/j.cell.2012.02.035.

O'Kusky, J. R. *et al.* (1999) 'Neuronal degeneration in the basal ganglia and loss of pallido-subthalamic synapses in mice with targeted disruption of the Huntington's disease gene', *Brain Research*, 818(2), pp. 468–479. doi: https://doi.org/10.1016/S0006-8993(98)01312-2.

O'Regan, G. C. *et al.* (2021) 'Human Huntington's disease pluripotent stem cell-derived microglia develop normally but are abnormally hyper-reactive and release elevated levels of reactive oxygen species', *Journal of Neuroinflammation*. Journal of Neuroinflammation, 18(1), pp. 1–17. doi: 10.1186/s12974-021-02147-6.

Oh, Y. M. *et al.* (2022) 'Age-related Huntington's disease progression modeled in directly reprogrammed patient-derived striatal neurons highlights impaired autophagy.', *Nature neuroscience*. United States, 25(11), pp. 1420–1433. doi: 10.1038/s41593-022-01185-4.

Ormel, P. R. *et al.* (2018) 'Microglia innately develop within cerebral organoids', *Nature Communications*. Springer US, 9(1). doi: 10.1038/s41467-018-06684-2.

Paine, H. (2015) 'Does loss of the normal protein function contribute to the pathogenesis of Huntington's disease?', *Bioscience Horizons*, 8, pp. 1–9. doi: 10.1093/biohorizons/hzv005.

Pal, A. *et al.* (2008) 'Regulation of endosome dynamics by Rab5 and Huntingtin-HAP40 effector complex in physiological versus pathological conditions.', *Methods in enzymology*. United States, 438, pp. 239–257. doi: 10.1016/S0076-6879(07)38017-8.

Palomba, N. P. *et al.* (2021) 'ATP-evoked intracellular Ca2+ transients shape the ionic permeability of human microglia from epileptic temporal cortex', *Journal of Neuroinflammation*. Journal of Neuroinflammation, 18(1), pp. 1–12. doi: 10.1186/s12974-021-02096-0.

Palpagama, T. H. *et al.* (2019) 'The Role of Microglia and Astrocytes in Huntington ' s Disease', 12(October), pp. 1–15. doi: 10.3389/fnmol.2019.00258.

Pandya, H. *et al.* (2017) 'Differentiation of human and murine induced pluripotent stem cells to microglia-like cells', *Nature Neuroscience*, 20(5), pp. 753–759. doi: 10.1038/nn.4534.

Paolicelli, R. C. *et al.* (2011) 'Synaptic Pruning by Microglia Is Necessary for Normal Brain Development', *Science*, 333(6048), pp. 1456 LP – 1458. doi: 10.1126/science.1202529.

Paolicelli, R. C. *et al.* (2022) 'Microglia states and nomenclature: A field at its crossroads.', *Neuron*. United States, 110(21), pp. 3458–3483. doi: 10.1016/j.neuron.2022.10.020.

Park, J. S. *et al.* (2021) 'Blocking microglial activation of reactive astrocytes is neuroprotective in models of Alzheimer's disease', *Acta Neuropathologica Communications*. BioMed Central, 9(1), pp. 1–15. doi: 10.1186/s40478-021-01180-z.

Pavese, N. *et al.* (2006) 'Microglial activation correlates with severity in Huntington disease', *Neurology*, 66(11), pp. 1638 LP – 1643. doi: 10.1212/01.wnl.0000222734.56412.17.

Petersén, Å. *et al.* (2001) 'Expanded CAG repeats in exon 1 of the Huntington's disease gene stimulate dopamine-mediated striatal neuron autophagy and degeneration', *Human Molecular Genetics*, 10(12), pp. 1243–1254. doi: 10.1093/hmg/10.12.1243.

Petkau, T. L. *et al.* (2019) 'Mutant huntingtin expression in microglia is neither required nor sufficient to cause the Huntington's disease-like phenotype in BACHD mice', *Human Molecular Genetics*, 28(10), pp. 1661–1670. doi: 10.1093/hmg/ddz009.

Pinto, R. M. *et al.* (2013) 'Mismatch repair genes Mlh1 and Mlh3 modify CAG instability in Huntington's disease mice: genome-wide and candidate approaches.', *PLoS genetics*. United States, 9(10), p. e1003930. doi: 10.1371/journal.pgen.1003930.

Pinto, R. M. *et al.* (2020) 'Patterns of CAG repeat instability in the central nervous system and periphery in Huntington ' s disease and in spinocerebellar ataxia type 1', 29(15), pp. 2551–2567. doi: 10.1093/hmg/ddaa139.

Plotkin, J. L. and Surmeier, D. J. (2015) 'Corticostriatal synaptic adaptations in Huntington's disease', *Current Opinion in Neurobiology*. Elsevier Ltd, pp. 53–62. doi: 10.1016/j.conb.2015.01.020.

Politis, M. *et al.* (2011) 'Microglial activation in regions related to cognitive function predicts disease onset in Huntington's disease: a multimodal imaging study.', *Human brain mapping*. United States, 32(2), pp. 258–270. doi: 10.1002/hbm.21008.

Preta, G., Cronin, J. G. and Sheldon, I. M. (2015) 'Dynasore - Not just a dynamin inhibitor', *Cell Communication and Signaling*, 13(1), pp. 1–7. doi: 10.1186/s12964-015-0102-1.

Pulido-Salgado, M. *et al.* (2018) 'RNA-Seq transcriptomic profiling of primary murine microglia treated with LPS or LPS + IFNγ.', *Scientific reports*. England, 8(1), p. 16096. doi: 10.1038/s41598-018-34412-9.

Qi, Y. *et al.* (2017) 'Combined small-molecule inhibition accelerates the derivation of functional cortical neurons from human pluripotent stem cells', *Nature Biotechnology*. Nature Publishing Group, 35(2), pp. 154–163. doi: 10.1038/nbt.3777.

Ransohoff, R. M. (2016) 'A polarizing question: Do M1 and M2 microglia exist', *Nature Neuroscience*, 19(8), pp. 987–991. doi: 10.1038/nn.4338.

Reiner, A., Dragatsis, I. and Dietrich, P. (2011) *GENETICS AND NEUROPATHOLOGY OF HUNTINGTON ' S DISEASE*, *International Review of Neurobiology*. Elsevier Inc. doi: 10.1016/B978-0-12-381328-2.00014-6.

Reinhardt, P. *et al.* (2013) 'Derivation and Expansion Using Only Small Molecules of Human Neural Progenitors for Neurodegenerative Disease Modeling', *PLoS ONE*. Edited by M. Daadi, 8(3), p. e59252. doi: 10.1371/journal.pone.0059252.

Reyes-ortiz, A. M. *et al.* (2022) 'Integrated transcriptome analysis of Huntington' s disease iPSC - derived and mouse astrocytes implicates dysregulated synaptogenesis , actin , and astrocyte maturation'.

Ribes, S. *et al.* (2009) 'Toll-like receptor prestimulation increases phagocytosis of Escherichia coli DH5α and Escherichia coli K1 strains by murine microglial cells', *Infection and Immunity*, 77(1), pp. 557–564. doi: 10.1128/IAI.00903-08.

Rink, J. *et al.* (2005) 'Rab conversion as a mechanism of progression from early to late endosomes.', *Cell*. United States, 122(5), pp. 735–749. doi: 10.1016/j.cell.2005.06.043.

Rodrigues, F. B. *et al.* (2016) 'Cerebrospinal fluid inflammatory biomarkers reflect clinical severity in huntington's disease', *PLoS ONE*, 11(9), pp. 1–10. doi: 10.1371/journal.pone.0163479.

Ross, C. A. *et al.* (2014) 'Huntington disease: natural history, biomarkers and prospects for therapeutics.', *Nature reviews. Neurology*. England, 10(4), pp. 204–216. doi: 10.1038/nrneurol.2014.24.

Ross, C. A. and Tabrizi, S. J. (2011) 'Huntington's disease: from molecular pathogenesis to clinical treatment', *The Lancet Neurology*. Elsevier Ltd, 10(1), pp. 83–98. doi: 10.1016/S1474-4422(10)70245-3.

Rossi, V. *et al.* (2014) 'Classical complement pathway components C1r and C1s: purification from human serum and in recombinant form and functional characterization.', *Methods in molecular biology (Clifton, N.J.)*. United States, 1100, pp. 43–60. doi: 10.1007/978-1-62703-724-2_4.

Rostami, J. *et al.* (2021) 'Crosstalk between astrocytes and microglia results in increased degradation of α-synuclein and amyloid-β aggregates', *Journal of Neuroinflammation*. Journal of Neuroinflammation, 18(1), pp. 1–20. doi: 10.1186/s12974-021-02158-3.

Roussakis, A. A. and Piccini, P. (2015) 'PET Imaging in Huntington's Disease', *Journal of Huntington's Disease*, 4(4), pp. 287–296. doi: 10.3233/JHD-150171.

Rüb, U. *et al.* (2016) 'Huntington's disease (HD): the neuropathology of a multisystem neurodegenerative disorder of the human brain.', *Brain pathology (Zurich, Switzerland)*, 26(6), pp. 726–740. doi: 10.1111/bpa.12426.

Rubinsztein, D. C. (2006) 'The roles of intracellular protein-degradation pathways in neurodegeneration', *Nature*, 443(7113), pp. 780–786. doi: 10.1038/nature05291.

Rushton, D. J. *et al.* (2013) 'Stimulation of GABA-induced Ca2+ influx enhances maturation of human induced pluripotent stem cell-derived neurons', *PLoS ONE*, 8(11), pp. 1–16. doi: 10.1371/journal.pone.0081031.

Sabate-Soler, S. *et al.* (2022) 'Microglia integration into human midbrain organoids leads to increased

neuronal maturation and functionality', *bioRxiv*, p. 2022.01.21.477192. doi: 10.1101/2022.01.21.477192.

Saha, P. *et al.* (2020) 'TIMP-1: A key cytokine released from activated astrocytes protects neurons and ameliorates cognitive behaviours in a rodent model of Alzheimer's disease.', *Brain, behavior, and immunity*. Netherlands, 87, pp. 804–819. doi: 10.1016/j.bbi.2020.03.014.

Samii, A., Nutt, J. G. and Ransom, B. R. (2004) 'Parkinson's disease.', *Lancet (London, England)*. England, 363(9423), pp. 1783–1793. doi: 10.1016/S0140-6736(04)16305-8.

Sapp, E *et al.* (2001) 'Early and progressive accumulation of reactive microglia in the Huntington disease brain.', *Journal of neuropathology and experimental neurology*. England, 60(2), pp. 161–172. doi: 10.1093/jnen/60.2.161.

Sapp, E. *et al.* (2001) 'Early and progressive accumulation of reactive microglia in the Huntington disease brain', *Journal of Neuropathology and Experimental Neurology*, 60(2), pp. 161–172. doi: 10.1093/jnen/60.2.161.

Sari, Y. (2011) 'Huntington's Disease: From Mutant Huntingtin Protein to Neurotrophic Factor Therapy.', *International journal of biomedical science : IJBS*. United States, 7(2), pp. 89–100.

Sato, M. *et al.* (2003) 'Direct binding of Toll-like receptor 2 to zymosan, and zymosan-induced NF-kappa B activation and TNF-alpha secretion are down-regulated by lung collectin surfactant protein A.', *Journal of immunology (Baltimore, Md. : 1950)*. United States, 171(1), pp. 417–425. doi: 10.4049/jimmunol.171.1.417.

Saudou, F. *et al.* (1998) 'Huntingtin Acts in the Nucleus to Induce Apoptosis but Death Does Not Correlate with the Formation of Intranuclear Inclusions', *Cell*, 95(1), pp. 55–66. doi: https://doi.org/10.1016/S0092-8674(00)81782-1.

Saudou, F. and Humbert, S. (2016) 'The Biology of Huntingtin', *Neuron*, 89(5), pp. 910–926. doi: 10.1016/j.neuron.2016.02.003.

Savage, J. C. *et al.* (2020) 'Microglial physiological properties and interactions with synapses are altered at presymptomatic stages in a mouse model of Huntington's disease pathology', *Journal of Neuroinflammation*. Journal of Neuroinflammation, 17(1), pp. 1–18. doi: 10.1186/s12974-020-01782-9.

Schafer, D. P. and Stevens, B. (2015) 'Microglia Function in Central Nervous System Development and Plasticity', *Cold Spring Harbor Perspectives in Biology*, 7(10), p. a020545. doi: 10.1101/cshperspect.a020545.

Schilling, L. P. *et al.* (2016) 'Imaging Alzheimer's disease pathophysiology with PET', *Dementia & neuropsychologia*. Associação de Neurologia Cognitiva e do Comportamento, 10(2), pp. 79–90. doi: 10.1590/S1980-5764-2016DN1002003.

Schilling, T. *et al.* (2001) 'Astrocyte-released cytokines induce ramification and outward K+ channel expression in microglia via distinct signalling pathways', *European Journal of Neuroscience*, 14(3), pp. 463–473. doi: 10.1046/j.0953-816X.2001.01661.x.

Schulte, J. and Littleton, J. T. (2011) 'The biological function of the Huntingtin protein and its relevance to Huntington's Disease pathology.', *Current trends in neurology*, 5, pp. 65–78. Available at: http://www.ncbi.nlm.nih.gov/pubmed/22180703%0Ahttp://www.pubmedcentral.nih.gov/articlerender.fcgi?artid=PMC3237673.

Scott, C. C., Vacca, F. and Gruenberg, J. (2014) 'Endosome maturation, transport and functions.', *Seminars in cell & developmental biology*. England, 31, pp. 2–10. doi: 10.1016/j.semcdb.2014.03.034.

Seeley, C. and Kegel-Gleason, K. B. (2021) 'Taming the Huntington's Disease Proteome: What Have We Learned?', *Journal of Huntington's disease*. Netherlands, 10(2), pp. 239–257. doi: 10.3233/JHD-200465.

Seifert, S. *et al.* (2011) 'Transmitter- and hormone-activated Ca(2+) responses in adult microglia/brain macrophages in situ recorded after viral transduction of a recombinant Ca(2+) sensor.', *Cell calcium*. Netherlands, 49(6), pp. 365–375. doi: 10.1016/j.ceca.2011.03.005.

Semple, B. D., Frugier, T. and Morganti-Kossmann, M. C. (2010) 'CCL2 modulates cytokine production in

cultured mouse astrocytes', *Journal of Neuroinflammation*, 7, pp. 1–11. doi: 10.1186/1742-2094-7-67.

Serio, A. *et al.* (2013) 'Astrocyte pathology and the absence of non-cell autonomy in an induced pluripotent stem cell model of TDP-43 proteinopathy', *Proceedings of the National Academy of Sciences of the United States of America*, 110(12), pp. 4697–4702. doi: 10.1073/pnas.1300398110.

Shaltouki, A. *et al.* (2013) 'Efficient Generation of Astrocytes from Human Pluripotent Stem Cells in Defined Conditions', *STEM CELLS*, 31(5), pp. 941–952. doi: 10.1002/stem.1334.

Shannon, K. M. (2011) 'Huntington's disease – clinical signs, symptoms, presymptomatic diagnosis, and diagnosis', *Handbook of Clinical Neurology*. Elsevier, 100, pp. 3–13. doi: 10.1016/B978-0-444-52014-2.00001-X.

Shearer, L. J. and Petersen, N. O. (2019) 'Distribution and Co-localization of endosome markers in cells.', *Heliyon*, 5(9), p. e02375. doi: 10.1016/j.heliyon.2019.e02375.

Shelbourne, P. F. *et al.* (2007) 'Triplet repeat mutation length gains correlate with cell-type specific vulnerability in Huntington disease brain', *Human Molecular Genetics*, 16(10), pp. 1133–1142. doi: 10.1093/hmg/ddm054.

Shemi, D., Azab, A. N. and Kaplanski, J. (2000) 'Time-dependent effect of LPS on PGE2 and TNF-alpha production by rat glial brain culture: influence of COX and cytokine inhibitors.', *Journal of endotoxin research*. United States, 6(5), pp. 377–381.

Shi, Y., Kirwan, P. and Livesey, F. J. (2012) 'Directed differentiation of human pluripotent stem cells to cerebral cortex neurons and neural networks.', *Nature protocols*, 7(10), pp. 1836–46. doi: 10.1038/nprot.2012.116.

Shigemoto-Mogami, Y. *et al.* (2001) 'Mechanisms underlying extracellular ATP-evoked interleukin-6 release in mouse microglial cell line, MG-5.', *Journal of neurochemistry*. England, 78(6), pp. 1339–1349. doi: 10.1046/j.1471-4159.2001.00514.x.

Silvestroni, A. *et al.* (2009) 'Distinct neuroinflammatory profile in post-mortem human Huntington's disease.', *Neuroreport*. England, 20(12), pp. 1098–1103. doi: 10.1097/WNR.0b013e32832e34ee.

Singhrao, S. K. *et al.* (1999) 'Increased complement biosynthesis by microglia and complement activation on neurons in Huntington's disease', *Experimental Neurology*, 159(2), pp. 362–376. doi: 10.1006/exnr.1999.7170.

Siracusa, R., Fusco, R. and Cuzzocrea, S. (2019) 'Astrocytes: Role and functions in brain pathologies', *Frontiers in Pharmacology*, 10(SEP), pp. 1–10. doi: 10.3389/fphar.2019.01114.

Sivagnanam, V., Zhu, X. and Schlichter, L. C. (2010) 'Dominance of E. coli phagocytosis over LPS in the inflammatory response of microglia', *Journal of Neuroimmunology*. Elsevier B.V., 227(1–2), pp. 111–119. doi: 10.1016/j.jneuroim.2010.06.021.

Smith-Dijak, A. I., Sepers, M. D. and Raymond, L. A. (2019) 'Alterations in synaptic function and plasticity in Huntington disease.', *Journal of neurochemistry*. England, 150(4), pp. 346–365. doi: 10.1111/jnc.14723.

Soares, T. R. *et al.* (2019a) 'Targeting the proteostasis network in Huntington's disease', *Ageing Research Reviews*. Elsevier, 49(November 2018), pp. 92–103. doi: 10.1016/j.arr.2018.11.006.

Soares, T. R. *et al.* (2019b) 'Targeting the proteostasis network in Huntington's disease', *Ageing Research Reviews*. Elsevier, 49(November 2018), pp. 92–103. doi: 10.1016/j.arr.2018.11.006.

Sofroniew, M. V. and Vinters, H. V. (2010) 'Astrocytes: Biology and pathology', *Acta Neuropathologica*, 119(1), pp. 7–35. doi: 10.1007/s00401-009-0619-8.

Sofroniew, M. V (2009) 'Molecular dissection of reactive astrogliosis and glial scar formation', *Trends in Neurosciences*, 32(12), pp. 638–647. doi: https://doi.org/10.1016/j.tins.2009.08.002.

Solé-Domènech, S. *et al.* (2016) 'The endocytic pathway in microglia during health, aging and Alzheimer's disease', *Ageing Research Reviews*. Elsevier B.V., 32, pp. 89–103. doi: 10.1016/j.arr.2016.07.002.

Speicher, A. M. *et al.* (2019) 'Generating microglia from human pluripotent stem cells: Novel in vitro models for the study of neurodegeneration', *Molecular Neurodegeneration*. Molecular Neurodegeneration, 14(1), pp. 1–16. doi: 10.1186/s13024-019-0347-z.

Steffan, J. S. (2010) 'Does Huntingtin play a role in selective macroautophagy?', *Cell cycle (Georgetown, Tex.)*. Landes Bioscience, 9(17), pp. 3401–3413. doi: 10.4161/cc.9.17.12718.

Strong, T. V *et al.* (1993) 'Widespread expression of the disease gene in brain and nonneural tissues', *Nature Genetics*, 5(november), pp. 259–265.

Sudwarts, A. *et al.* (2022) 'BIN1 is a key regulator of proinflammatory and neurodegeneration-related activation in microglia.', *Molecular neurodegeneration*. England, 17(1), p. 33. doi: 10.1186/s13024-022-00535-x.

Swami, M. *et al.* (2009) 'Somatic expansion of the Huntington ' s disease CAG repeat in the brain is associated with an earlier age of disease onset', 18(16), pp. 3039–3047. doi: 10.1093/hmg/ddp242.

Szepesi, Z. *et al.* (2018) 'Bidirectional Microglia–Neuron Communication in Health and Disease', *Frontiers in Cellular Neuroscience*, 12(September), pp. 1–26. doi: 10.3389/fncel.2018.00323.

Szlachcic, W. J. *et al.* (2015) 'Huntington disease iPSCs show early molecular changes in intracellular signaling, the expression of oxidative stress proteins and the p53 pathway.', *Disease models & mechanisms*, 8(9), pp. 1047–1057. doi: 10.1242/dmm.019406.

Ta, T. T. *et al.* (2019) 'Priming of microglia with IFN-γ slows neuronal gamma oscillations in situ', *Proceedings of the National Academy of Sciences of the United States of America*, 116(10), pp. 4637–4642. doi: 10.1073/pnas.1813562116.

Tabernero, A., Medina, J. M. and Giaume, C. (2006) 'Glucose metabolism and proliferation in glia: Role of astrocytic gap junctions', *Journal of Neurochemistry*, 99(4), pp. 1049–1061. doi: 10.1111/j.1471-4159.2006.04088.x.

Tai, Y. F. *et al.* (2007) 'Microglial activation in presymptomatic Huntington's disease gene carriers', *Brain*, 130(7), pp. 1759–1766. doi: 10.1093/brain/awm044.

Takahashi, K. and Yamanaka, S. (2006) 'Induction of Pluripotent Stem Cells from Mouse Embryonic and Adult Fibroblast Cultures by Defined Factors', 2, pp. 663–676. doi: 10.1016/j.cell.2006.07.024.

Takata, K. *et al.* (2017) 'Induced-Pluripotent-Stem-Cell-Derived Primitive Macrophages Provide a Platform for Modeling Tissue-Resident Macrophage Differentiation and Function', *Immunity*, 47(1), pp. 183-198.e6. doi: 10.1016/j.immuni.2017.06.017.

Telezhkin, V. *et al.* (2016) 'Forced cell cycle exit and modulation of GABAA, CREB, and GSK3β signaling promote functional maturation of induced pluripotent stem cell-derived neurons', *American Journal of Physiology - Cell Physiology*, 310(7), pp. C520–C541. doi: 10.1152/ajpcell.00166.2015.

Thomson, J. A. (1998) 'Embryonic stem cell lines derived from human blastocysts', *Science*, 282(5391), pp. 1145–1147. doi: 10.1126/science.282.5391.1145.

Thrupp, N. *et al.* (2020) 'Single-Nucleus RNA-Seq Is Not Suitable for Detection of Microglial Activation Genes in Humans.', *Cell reports*. United States, 32(13), p. 108189. doi: 10.1016/j.celrep.2020.108189.

Tidball, A. M. *et al.* (2016) 'Genomic Instability Associated with p53 Knockdown in the Generation of Huntington's Disease Human Induced Pluripotent Stem Cells.', *PloS one*, 11(3), p. e0150372. doi: 10.1371/journal.pone.0150372.

Trepte, P., Strempel, N. and Wanker, E. E. (2014) 'Spontaneous self-assembly of pathogenic huntingtin exon 1 protein into amyloid structures.', *Essays in biochemistry*. England, 56, pp. 167–180. doi: 10.1042/bse0560167.

Turnbull, I. R. *et al.* (2006) 'Cutting edge: TREM-2 attenuates macrophage activation.', *Journal of immunology (Baltimore, Md. : 1950)*. United States, 177(6), pp. 3520–3524. doi: 10.4049/jimmunol.177.6.3520.

Ulland, T. K. and Colonna, M. (2018) 'TREM2 - a key player in microglial biology and Alzheimer disease.',

Nature reviews. Neurology. England, 14(11), pp. 667–675. doi: 10.1038/s41582-018-0072-1.

Vahsen, B. F. *et al.* (2022) 'Human iPSC co - culture model to investigate the interaction between microglia and motor neurons', *Scientific Reports*. Nature Publishing Group UK, pp. 1–17. doi: 10.1038/s41598-022-16896-8.

Valekova, I. *et al.* (2016) 'Revelation of the IFNα, IL-10, IL-8 and IL-1β as promising biomarkers reflecting immuno-pathological mechanisms in porcine Huntington's disease model', *Journal of Neuroimmunology*. Elsevier B.V., 293, pp. 71–81. doi: 10.1016/j.jneuroim.2016.02.012.

Valor, L. M. (2015) 'Transcription, Epigenetics and Ameliorative Strategies in Huntington's Disease: a Genome-Wide Perspective', *Molecular Neurobiology*, 51(1), pp. 406–423. doi: 10.1007/s12035-014-8715-8.

Varet, H. *et al.* (2016) 'SARTools: A DESeq2- and EdgeR-Based R Pipeline for Comprehensive Differential Analysis of RNA-Seq Data.', *PloS one*, 11(6), p. e0157022. doi: 10.1371/journal.pone.0157022.

Vaz, I. M. *et al.* (2021) 'Chromosomal aberrations after induced pluripotent stem cells reprogramming', *Genetics and Molecular Biology*, 44(3). doi: 10.1590/1678-4685-GMB-2020-0147.

Verkhratsky, A. and Kettenmann, H. (1996) 'Calcium signalling in glial cells.', *Trends in neurosciences*. England, 19(8), pp. 346–352. doi: 10.1016/0166-2236(96)10048-5.

Vigont, V. A. *et al.* (2021) 'STIM2 Mediates Excessive Store-Operated Calcium Entry in Patient-Specific iPSC-Derived Neurons Modeling a Juvenile Form of Huntington's Disease.', *Frontiers in cell and developmental biology*, 9, p. 625231. doi: 10.3389/fcell.2021.625231.

Volpato, V. and Webber, C. (2020) 'Addressing variability in iPSC-derived models of human disease: guidelines to promote reproducibility.', *Disease models & mechanisms*. England, 13(1). doi: 10.1242/dmm.042317.

Vonsattel, J. P. *et al.* (1985) 'Neuropathological classification of Huntington's disease.', *Journal of neuropathology and experimental neurology*. England, 44(6), pp. 559–577. doi: 10.1097/00005072-198511000-00003.

Waelter, S. *et al.* (2001) 'The huntingtin interacting protein HIP1 is a clathrin and alpha-adaptin-binding protein involved in receptor-mediated endocytosis.', *Human molecular genetics*. England, 10(17), pp. 1807–1817. doi: 10.1093/hmg/10.17.1807.

Wanker, E. E. *et al.* (2019) 'The pathobiology of perturbed mutant huntingtin protein–protein interactions in Huntington's disease', *Journal of Neurochemistry*, 151(4), pp. 507–519. doi: 10.1111/jnc.14853.

Wexler, N. S. *et al.* (2004) 'Venezuelan kindreds reveal that genetic and environmental factors modulate Huntington's disease age of onset.', *Proceedings of the National Academy of Sciences of the United States of America*, 101(10), pp. 3498–3503. doi: 10.1073/pnas.0308679101.

White, J. K. *et al.* (1997) 'Huntingtin is required for neurogenesis and is not impaired by the Huntington's disease CAG expansion.', *Nature genetics*. United States, 17(4), pp. 404–410. doi: 10.1038/ng1297-404.

Wiese, S., Karus, M. and Faissner, A. (2012) 'Astrocytes as a source for extracellular matrix molecules and cytokines', *Frontiers in Pharmacology*, 3 JUN(June), pp. 1–13. doi: 10.3389/fphar.2012.00120.

van Wilgenburg, B. *et al.* (2013) 'Efficient, Long Term Production of Monocyte-Derived Macrophages from Human Pluripotent Stem Cells under Partly-Defined and Fully-Defined Conditions', *PLoS ONE*, 8(8). doi: 10.1371/journal.pone.0071098.

Xia, Y. *et al.* (2019) 'The macrophage-specific V-ATPase subunit ATP6V0D2 restricts inflammasome activation and bacterial infection by facilitating autophagosome-lysosome fusion.', *Autophagy*. United States, 15(6), pp. 960–975. doi: 10.1080/15548627.2019.1569916.

Xiang, S. (2018) 'Endocytosis and human innate immunity', *Journal of Immunological Sciences*, 2(1), pp. 65–70. doi: 10.29245/2578-3009/2018/1.1121.

Xiao, G. *et al.* (2013) 'Huntington disease arises from a combinatory toxicity of polyglutamine and

copper binding.', *Proceedings of the National Academy of Sciences of the United States of America*. United States, 110(37), pp. 14995–15000. doi: 10.1073/pnas.1308535110.

Xu, R. *et al.* (2020) 'Human iPSC-derived mature microglia retain their identity and functionally integrate in the chimeric mouse brain.', *Nature communications*. England, 11(1), p. 1577. doi: 10.1038/s41467-020-15411-9.

Yang, H. M. *et al.* (2017) 'Microglial activation in the pathogenesis of Huntington's Disease', *Frontiers in Aging Neuroscience*, 9(JUN), pp. 1–9. doi: 10.3389/fnagi.2017.00193.

Yang, I. *et al.* (2010) 'The role of microglia in central nervous system immunity and glioma immunology', *Journal of Clinical Neuroscience*, 17(1), pp. 6–10. doi: 10.1016/j.jocn.2009.05.006.

Yang, R. *et al.* (2019) 'Regulation of microglial process elongation, a featured characteristic of microglial plasticity', *Pharmacological Research*. Elsevier, 139(November 2018), pp. 286–297. doi: 10.1016/j.phrs.2018.11.028.

Ye, X. *et al.* (2020) 'Lipopolysaccharide induces neuroinflammation in microglia by activating the MTOR pathway and downregulating Vps34 to inhibit autophagosome formation', *Journal of Neuroinflammation*. Journal of Neuroinflammation, 17(1), pp. 1–17. doi: 10.1186/s12974-019-1644-8.

Yoshihara, M., Hayashizaki, Y. and Murakawa, Y. (2017) 'Genomic Instability of iPSCs: Challenges Towards Their Clinical Applications', *Stem Cell Reviews and Reports*. Stem Cell Reviews and Reports, 13(1), pp. 7–16. doi: 10.1007/s12015-016-9680-6.

Yu, A. *et al.* (2014) 'Protein aggregation can inhibit clathrin-mediated endocytosis by chaperone competition.', *Proceedings of the National Academy of Sciences of the United States of America*. United States, 111(15), pp. E1481-90. doi: 10.1073/pnas.1321811111.

von Zahn, J. *et al.* (1997) 'Microglial phagocytosis is modulated by pro-and anti-inflammatory cytokines', *NeuroReport*, 8(18). Available at: https://journals.lww.com/neuroreport/Fulltext/1997/12220/Microglial_phagocytosis_is_modulated_by_pro_and.3.aspx.

Zakrzewski, W. *et al.* (2019) 'Stem cells: past, present, and future', *Stem Cell Research & Therapy*, 10(1), p. 68. doi: 10.1186/s13287-019-1165-5.

Zamanian, J. L. *et al.* (2012) 'Genomic analysis of reactive astrogliosis', *Journal of Neuroscience*, 32(18), pp. 6391–6410. doi: 10.1523/JNEUROSCI.6221-11.2012.

Zhang, N. *et al.* (2010) 'Characterization of Human Huntington's Disease Cell Model from Induced Pluripotent Stem Cells.', *PLoS currents*, 2, p. RRN1193. doi: 10.1371/currents.RRN1193.

Zhao, Y. *et al.* (2022) 'STAT1 contributes to microglial/macrophage inflammation and neurological dysfunction in a mouse model of traumatic brain injury', *The Journal of Neuroscience*, p. JN-RM-0682-22. doi: 10.1523/JNEUROSCI.0682-22.2022.

Zhou, Y. *et al.* (2019) 'Metascape provides a biologist-oriented resource for the analysis of systems-level datasets', *Nature Communications*. Springer US, 10(1). doi: 10.1038/s41467-019-09234-6.

Zhou, Y. *et al.* (2020) 'Dual roles of astrocytes in plasticity and reconstruction after traumatic brain injury.', *Cell communication and signaling : CCS*. England, 18(1), p. 62. doi: 10.1186/s12964-020-00549-2.

9 Appendix

9.1 Additional data for Chapter 5: Investigating transcriptional changes in Huntington's disease microglia-like cells

A

Samples	Genotype	Sample names
1	Q22	2H1 unstimulated
2	Q22	2H1 3-hour LPS
3	Q22	2H1 12-hour LPS
4	Q22	3H2 unstimulated
5	Q22	3H2 3-hour LPS
6	Q22	3H2 12-hour LPS
7	Q22	5H9 unstimulated
8	Q22	5H9 3-hour LPS
9	Q22	5H9 12-hour LPS
10	Q109	109n1 unstimulated
11	Q109	109n1 3-hour LPS
12	Q109	109n1 12h-hour LPS
13	Q109	109n4 unstimulated
14	Q109	109n4 3-hour LPS
15	Q109	109n4 12-hour LPS
16	Q109	109n5 unstimulated
17	Q109	109n5 3-hour LPS
18	Q109	109n5 12-hour LPS

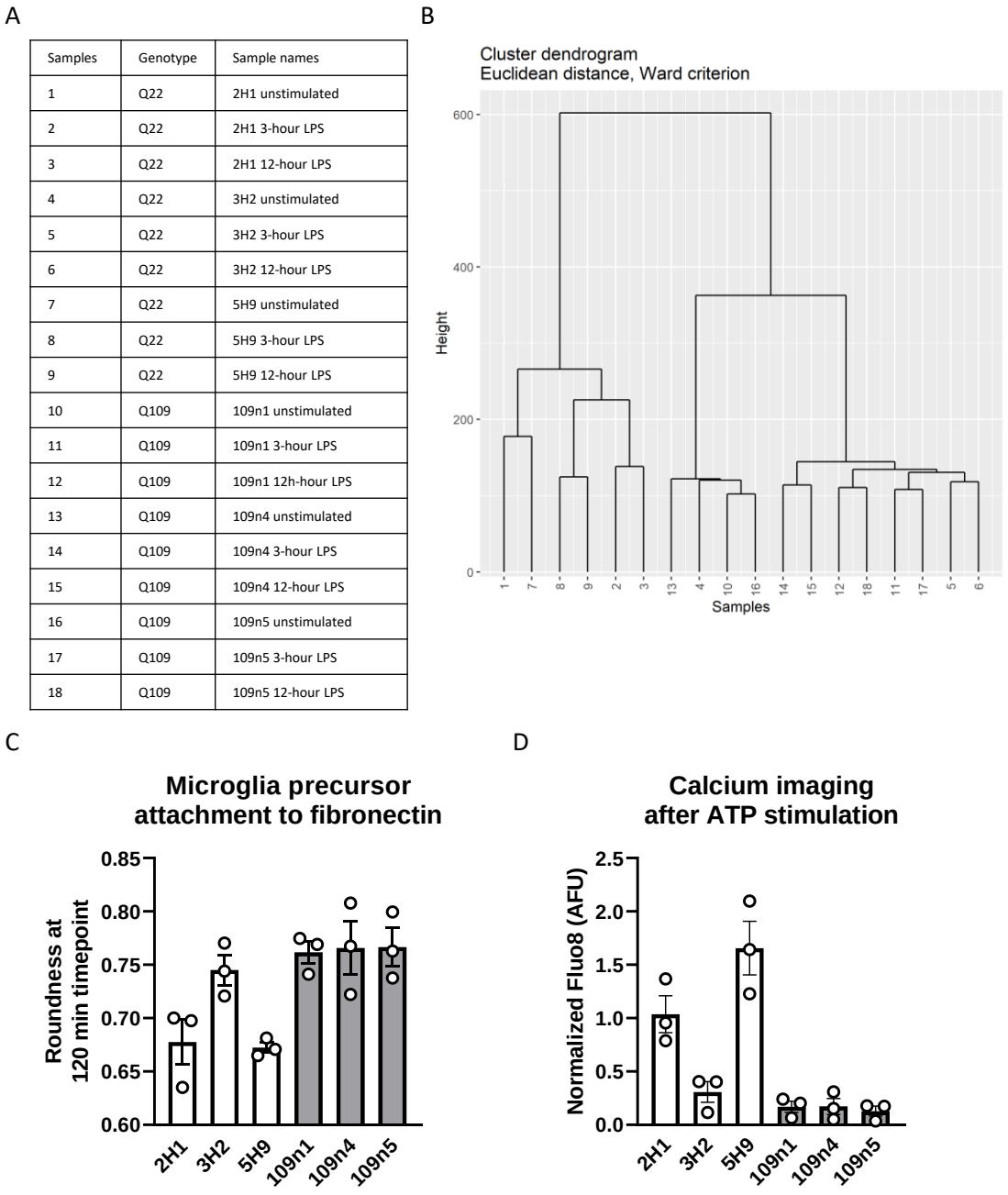

Figure 9.1: Hierarchical clustering of samples. (A) Table comprising all sample of the bulk RNA sequencing experiment, indicating their genotype and type of stimulation. (B) Hierarchical clustering of samples using Euclidean distance indicates that the Q22 samples 2H1 (sample 1-3) and 5H9 (sample 7-9) cluster together, and the Q22 sample 3H2 (sample 3-6) clustered with the Q109 samples (sample 10-18). Both of these clusters further cluster the unstimulated samples apart from the stimulated samples. (C) Microglia precursor cell attachment to fibronectin has been investigated using phalloidin staining and a measure for cellular roundness. 3H2 microglia precursors behaved like the Q109 samples. (D) Calcium signalling after stimulation with ATP has been conducted on microglia-like cells using the calcium indicator Fluo8. 3H2 microglia-like cells show a calcium response similar to the Q109 samples.

Raw data related to Figure 5.2:

Table 9-1: Unstimulated Q109 versus Q22: Top 50 DEG

Gene name	LogFC	Adjusted p-value
MMP12	-2.1	3.91E-91
PPP1R1A	-2.2	2.68E-62
TRIM47	-2.0	9.28E-43
SUCNR1	1.7	9.76E-43
CD9	-1.7	5.85E-41
VLDLR	1.7	2.17E-35
LINC02246	4.3	8.70E-33
ADD2	4.9	2.88E-31
PAICS	1.6	1.80E-28
MYO1D	-2.6	7.28E-25
ATP6V0D2	-2.2	1.07E-24
KCNC4	-1.7	8.94E-24
ARHGAP22	-1.5	2.99E-22
KCNJ5	-2.4	3.34E-22
HS3ST2	-2.3	4.64E-21
MIR3142HG	-2.4	8.73E-21
AGK	1.5	1.50E-20
CD80	-1.5	7.11E-20
AR	2.3	2.73E-19
VNN1	-1.7	5.99E-19
TMTC4	1.5	7.33E-19
CD28	-2.2	1.11E-18
UTP15	1.9	2.19E-18
ESCO2	1.8	2.17E-17
LEPR	1.7	4.24E-17
RETREG1	2.3	4.25E-17
SCIN	3.8	1.92E-16
HVCN1	-1.5	2.88E-16
ZNF717	5.4	3.13E-16
CLDN1	-2.4	3.90E-16
PFN2	1.5	7.67E-16
MCM4	1.5	9.28E-16
RMI2	2.3	1.27E-15
SNHG4	1.6	2.34E-15
A2M	-1.6	2.97E-15
HTR2B	-3.7	4.38E-15
LINC01857	-1.8	5.74E-15
GDAP1	1.8	5.96E-15
KCNAB3	3.0	6.01E-15
DHFR	1.6	6.70E-15
CASC15	3.6	1.84E-14
GAS6	-1.5	3.59E-14
AHNAK	-1.7	4.81E-14

CCNB2	1.9	7.02E-14
IGF1	-2.4	9.72E-14
CCDC34	2.3	1.13E-13
ZNF229	4.9	1.46E-13
TAF9B	1.5	1.47E-13
CHAF1B	2.0	3.17E-13
COL7A1	1.8	4.03E-13

Raw data related to Figure 5.3:

Table 9-2: Unstimulated Q109 versus Q22: Top 50 significant biological processes of downregulated DEG

Term name	Term ID	-Log10(p_{adj})	Term size	Query size	Inter-section
localization	GO:0051179	53.5	6436	2025	943
transport	GO:0006810	39.8	4742	2025	715
vesicle-mediated transport	GO:0016192	39.3	1604	2025	329
response to stimulus	GO:0050896	38.1	8885	2025	1142
establishment of localization	GO:0051234	38.0	4903	2025	727
intracellular signal transduction	GO:0035556	37.9	2629	2025	460
catabolic process	GO:0009056	36.3	2559	2025	447
regulation of response to stimulus	GO:0048583	35.3	3895	2025	604
cellular catabolic process	GO:0044248	34.4	2199	2025	396
immune system process	GO:0002376	33.7	2781	2025	467
cellular response to chemical stimulus	GO:0070887	33.1	3019	2025	494
cellular response to stimulus	GO:0051716	32.1	7399	2025	971
phosphorus metabolic process	GO:0006793	31.5	2803	2025	463
response to stress	GO:0006950	31.0	3851	2025	585
phosphate-containing compound metabolic process	GO:0006796	30.8	2781	2025	458
cell communication	GO:0007154	30.0	6508	2025	871
regulation of intracellular signal transduction	GO:1902531	29.2	1691	2025	316
regulation of localization	GO:0032879	28.8	2725	2025	445
signaling	GO:0023052	28.7	6451	2025	860
organonitrogen compound metabolic process	GO:1901564	27.9	6446	2025	856
response to organic substance	GO:0010033	27.8	3010	2025	476
regulation of catalytic activity	GO:0050790	27.0	2345	2025	393
regulation of signal transduction	GO:0009966	26.7	2947	2025	465
regulation of signaling	GO:0023051	26.6	3351	2025	512
response to external stimulus	GO:0009605	26.4	2788	2025	445
process utilizing autophagic mechanism	GO:0061919	26.2	541	2025	143
autophagy	GO:0006914	26.2	541	2025	143

regulation of molecular function	GO:0065009	26.1	3050	2025	475
regulation of cell communication	GO:0010646	25.9	3336	2025	508
regulation of immune system process	GO:0002682	25.8	1442	2025	274
cellular response to organic substance	GO:0071310	25.8	2391	2025	395
regulation of biological quality	GO:0065008	25.8	3768	2025	557
signal transduction	GO:0007165	25.2	5957	2025	794
biological process involved in interspecies interaction between organisms	GO:0044419	24.9	1659	2025	300
positive regulation of biological process	GO:0048518	24.8	6224	2025	820
positive regulation of cellular process	GO:0048522	24.4	5687	2025	762
positive regulation of response to stimulus	GO:0048584	24.0	2169	2025	362
immune response	GO:0006955	22.9	1906	2025	326
cell activation	GO:0001775	22.5	1094	2025	218
homeostatic process	GO:0042592	22.1	1658	2025	292
leukocyte activation	GO:0045321	22.0	953	2025	197
cellular localization	GO:0051641	21.3	3031	2025	456
response to other organism	GO:0051707	21.3	1507	2025	270
response to external biotic stimulus	GO:0043207	21.2	1509	2025	270
response to biotic stimulus	GO:0009607	20.4	1549	2025	273
response to chemical	GO:0042221	20.3	4336	2025	599
defense response	GO:0006952	20.1	1736	2025	296
cation homeostasis	GO:0055080	18.8	587	2025	136
positive regulation of signaling	GO:0023056	18.7	1715	2025	289
inflammatory response	GO:0006954	18.6	778	2025	164

Table 9-3: Unstimulated Q109 versus Q22: Top 50 significant KEGG pathways of downregulated DEG

Term name	**Term ID**	**-Log10(p_{adj})**	**Term size**	**Query size**	**Inter-section**
Lysosome	KEGG:04142	25.6	126	1019	69
Endocytosis	KEGG:04144	13.3	237	1019	80
Phagosome	KEGG:04145	10.9	137	1019	53
Osteoclast differentiation	KEGG:04380	9.1	124	1019	47
Rheumatoid arthritis	KEGG:05323	8.8	86	1019	37
Fc gamma R-mediated phagocytosis	KEGG:04666	8.7	94	1019	39
Yersinia infection	KEGG:05135	8.0	132	1019	47
B cell receptor signaling pathway	KEGG:04662	7.1	76	1019	32
Tuberculosis	KEGG:05152	6.5	173	1019	53
Chemokine signaling pathway	KEGG:04062	5.9	179	1019	53
Autophagy - animal	KEGG:04140	5.5	135	1019	43

Salmonella infection	KEGG:05132	5.4	236	1019	63
Human T-cell leukemia virus 1 infection	KEGG:05166	5.3	211	1019	58
Epithelial cell signaling in Helicobacter pylori infection	KEGG:05120	4.9	69	1019	27
Epstein-Barr virus infection	KEGG:05169	4.9	191	1019	53
Sphingolipid signaling pathway	KEGG:04071	4.8	114	1019	37
Leishmaniasis	KEGG:05140	4.6	71	1019	27
Th1 and Th2 cell differentiation	KEGG:04658	4.4	86	1019	30
Toll-like receptor signaling pathway	KEGG:04620	4.3	100	1019	33
Platelet activation	KEGG:04611	4.1	120	1019	37
Lipid and atherosclerosis	KEGG:05417	3.5	209	1019	53
Pathogenic Escherichia coli infection	KEGG:05130	3.5	183	1019	48
Th17 cell differentiation	KEGG:04659	3.4	104	1019	32
NOD-like receptor signaling pathway	KEGG:04621	3.3	175	1019	46
Leukocyte transendothelial migration	KEGG:04670	3.2	110	1019	33
Human cytomegalovirus infection	KEGG:05163	3.1	215	1019	53
Intestinal immune network for IgA production	KEGG:04672	3.1	44	1019	18
C-type lectin receptor signaling pathway	KEGG:04625	3.1	102	1019	31
NF-kappa B signaling pathway	KEGG:04064	3.1	102	1019	31
PD-L1 expression and PD-1 checkpoint pathway in cancer	KEGG:05235	3.1	88	1019	28
Shigellosis	KEGG:05131	3.0	239	1019	57
Allograft rejection	KEGG:05330	2.8	34	1019	15
Metabolic pathways	KEGG:01100	2.7	1457	1019	247
Viral myocarditis	KEGG:05416	2.7	55	1019	20
Fc epsilon RI signaling pathway	KEGG:04664	2.7	64	1019	22
Kaposi sarcoma-associated herpesvirus infection	KEGG:05167	2.6	191	1019	47
Pancreatic cancer	KEGG:05212	2.6	74	1019	24
Chagas disease	KEGG:05142	2.5	98	1019	29
Ras signaling pathway	KEGG:04014	2.5	225	1019	53
Other glycan degradation	KEGG:00511	2.4	18	1019	10
Neurotrophin signaling pathway	KEGG:04722	2.4	115	1019	32
Pertussis	KEGG:05133	2.3	76	1019	24
Influenza A	KEGG:05164	2.3	163	1019	41
Toxoplasmosis	KEGG:05145	2.2	107	1019	30
Phospholipase D signaling pathway	KEGG:04072	2.1	139	1019	36

SNARE interactions in vesicular transport	KEGG:04130	1.9	31	1019	13
Vibrio cholerae infection	KEGG:05110	1.9	48	1019	17
Antigen processing and presentation	KEGG:04612	1.8	67	1019	21
Natural killer cell mediated cytotoxicity	KEGG:04650	1.8	117	1019	31
T cell receptor signaling pathway	KEGG:04660	1.8	102	1019	28

Table 9-4: Unstimulated Q109 versus Q22: Top 50 significant biological processes of upregulated DEG

Term name	**Term ID**	**-Log10(p_{adj})**	**Term size**	**Query size**	**Inter-section**
cell cycle	GO:0007049	50.2	1774	1935	366
organelle organization	GO:0006996	44.3	3874	1935	608
chromosome organization	GO:0051276	44.0	1059	1935	252
cell cycle process	GO:0022402	41.1	1206	1935	268
mitotic cell cycle	GO:0000278	40.8	906	1935	223
DNA metabolic process	GO:0006259	39.4	1023	1935	238
mitotic cell cycle process	GO:1903047	35.0	755	1935	189
regulation of cell cycle	GO:0051726	33.2	1089	1935	235
biosynthetic process	GO:0009058	32.4	5861	1935	782
regulation of nitrogen compound metabolic process	GO:0051171	32.2	5654	1935	760
cellular nitrogen compound biosynthetic process	GO:0044271	32.1	4765	1935	667
cellular macromolecule metabolic process	GO:0044260	32.0	5766	1935	771
organic substance biosynthetic process	GO:1901576	31.8	5774	1935	771
cellular biosynthetic process	GO:0044249	31.4	5700	1935	762
regulation of primary metabolic process	GO:0080090	31.0	5812	1935	772
cell division	GO:0051301	30.1	646	1935	163
DNA replication	GO:0006260	29.3	309	1935	104
macromolecule biosynthetic process	GO:0009059	28.9	4770	1935	656
regulation of cell cycle process	GO:0010564	27.1	695	1935	165
chromosome segregation	GO:0007059	26.8	344	1935	107
regulation of nucleobase-containing compound metabolic process	GO:0019219	26.7	4048	1935	571
regulation of cellular metabolic process	GO:0031323	25.5	6004	1935	770
organic cyclic compound biosynthetic process	GO:1901362	24.9	4213	1935	582
nucleobase-containing compound biosynthetic process	GO:0034654	23.9	3984	1935	554

positive regulation of cellular process	GO:0048522	23.8	5687	1935	731
heterocycle biosynthetic process	GO:0018130	23.7	4057	1935	561
nuclear chromosome segregation	GO:0098813	23.4	284	1935	91
aromatic compound biosynthetic process	GO:0019438	23.4	4068	1935	561
positive regulation of biological process	GO:0048518	22.8	6224	1935	781
negative regulation of cellular process	GO:0048523	22.6	4856	1935	641
nuclear division	GO:0000280	22.6	454	1935	119
regulation of cellular component organization	GO:0051128	22.5	2276	1935	358
cell cycle phase transition	GO:0044770	21.9	538	1935	131
regulation of macromolecule biosynthetic process	GO:0010556	20.9	3926	1935	536
cellular response to DNA damage stimulus	GO:0006974	20.9	826	1935	171
sister chromatid segregation	GO:0000819	20.3	202	1935	71
organelle fission	GO:0048285	20.3	500	1935	122
nervous system development	GO:0007399	20.1	2430	1935	368
cellular component organization or biogenesis	GO:0071840	20.0	8070	1935	948
regulation of cellular biosynthetic process	GO:0031326	19.9	4085	1935	549
developmental process	GO:0032502	19.6	6317	1935	776
mitotic nuclear division	GO:0140014	19.4	301	1935	88
regulation of biosynthetic process	GO:0009889	19.3	4145	1935	553
multicellular organism development	GO:0007275	19.3	4768	1935	618
ribosome biogenesis	GO:0042254	19.1	304	1935	88
anatomical structure development	GO:0048856	19.0	5754	1935	717
DNA-templated DNA replication	GO:0006261	19.0	186	1935	66
DNA conformation change	GO:0071103	18.6	105	1935	48
regulation of RNA metabolic process	GO:0051252	18.0	3753	1935	506
regulation of DNA metabolic process	GO:0051052	18.0	470	1935	113

Table 9-5: Unstimulated Q109 versus Q22: All significant KEGG pathways of upregulated DEG

Term name	**Term ID**	**-Log10(p_{adj})**	**Term size**	**Query size**	**Inter-section**
Cell cycle	KEGG:04110	13.9	120	798	47
DNA replication	KEGG:03030	7.7	35	798	19
Base excision repair	KEGG:03410	3.7	32	798	14

Oocyte meiosis	KEGG:04114	3.0	123	798	30
Spliceosome	KEGG:03040	3.0	123	798	30
Mismatch repair	KEGG:03430	2.4	22	798	10
Fanconi anemia pathway	KEGG:03460	2.3	51	798	16
Adherens junction	KEGG:04520	1.6	69	798	18
p53 signaling pathway	KEGG:04115	1.3	72	798	18
Nucleocytoplasmic transport	KEGG:03013	1.3	91	798	21

Raw data related to Figure 5.6:

Table 9-6: 12h LPS vs 3h LPS: Top 50 DEG

Gene name	LogFC	Adjusted p-value
NOL4L	1.9	1.35E-46
NKX3-1	-2.5	3.93E-46
ZFX	-1.5	1.96E-43
MEGF9	1.5	2.95E-43
KCNQ3	3.3	8.67E-40
CCL20	-2.3	1.63E-39
PTX3	-2.6	1.08E-37
EGR2	-2.0	2.04E-35
ARRDC3	-1.7	3.06E-34
GPR157	2.3	1.55E-26
PTGES	3.0	1.52E-25
MBP	1.7	1.52E-25
KLF7	-1.7	2.37E-25
ARHGAP20	-2.0	6.59E-25
PLCB2	-1.6	1.08E-23
IL10	-2.3	1.45E-19
SLC11A1	2.0	3.89E-18
C20orf27	-1.6	1.55E-16
CPED1	-1.6	3.10E-16
AVPI1	2.6	1.81E-15
JAG1	-1.8	7.30E-15
SOS1	1.6	7.30E-15
BTG2	-1.8	1.87E-14
PYCARD	-1.4	3.24E-14
PRR16	2.0	5.14E-14
GALM	-1.6	4.29E-13
GPR34	-2.7	1.84E-12
CD70	1.7	1.04E-11
MS4A6A	-2.0	1.23E-11
KAT2A	-1.5	2.80E-11
CCR7	2.3	3.07E-11
SDS	2.3	4.04E-11
IL18	-1.8	4.30E-11
NECTIN4	2.5	4.78E-11
NLRP3	-1.6	4.98E-11

TLR7	-2.2	5.40E-11
P2RY13	-2.6	1.11E-10
STAB1	-1.5	2.35E-10
TMEM63C	-1.8	6.49E-10
RNASE1	-2.1	9.10E-10
ITGB3	2.0	1.12E-09
CSF3	1.6	3.31E-09
EGR3	-2.2	3.31E-09
GPR183	-2.0	9.82E-09
CLEC10A	-1.6	2.00E-08
HIVEP3	-1.5	3.17E-08
CTLA4	2.5	8.23E-08
ARAP3	1.6	8.57E-08
IFNLR1	2.4	1.82E-07
SIGLEC8	-2.2	1.90E-07

Table 9-7: 3h LPS vs no LPS: Top 50 DEG

Gene name	**LogFC**	**Adjusted p-value**
WARS	5.4	4.80E-288
ANKRD22	6.4	2.05E-263
GBP2	5.8	9.00E-246
CD274	6.5	1.93E-242
CALHM6	8.3	3.07E-237
CCL20	6.1	6.81E-230
CXCL11	14.1	2.70E-223
GBP5	9.0	2.00E-218
APOL3	7.5	7.86E-215
STAT1	3.1	3.62E-213
EGR2	5.6	3.64E-202
IL18BP	5.5	1.06E-191
KCNJ2	3.9	9.12E-190
ATF3	5.2	3.48E-184
IL6	9.3	2.29E-180
TNFAIP6	2.8	1.52E-179
HAPLN3	6.4	4.43E-179
NKX3-1	5.4	7.39E-177
IRF1	6.0	2.84E-171
HRH2	-3.9	5.16E-169
SLC11A1	-5.8	1.38E-166
GPR132	3.1	2.34E-165
HS3ST3B1	2.6	5.47E-164
CXCL1	3.8	1.11E-162
CSRNP1	2.7	8.47E-158
ELOVL7	3.8	1.06E-156
CCL7	4.2	3.56E-155
CXCL3	4.2	2.71E-154

TRAF1	6.0	2.79E-152
PTGS2	6.4	3.36E-152
MEFV	3.2	4.20E-139
MERTK	-2.5	2.47E-138
SERPINB9	2.9	6.34E-138
DUSP5	3.8	8.87E-132
GBP1	8.2	8.33E-126
STX11	2.3	4.00E-125
TIFA	4.0	1.49E-123
IL15RA	4.0	2.34E-121
IDO1	9.8	3.30E-121
PTX3	5.3	4.48E-120
HGF	6.4	1.10E-119
PSMB9	5.1	2.07E-119
GBP1P1	9.1	1.48E-118
FGL2	5.8	6.98E-118
ZFP36	2.4	7.28E-117
TNF	7.4	3.63E-116
GBP3	3.9	1.85E-115
ZC3H12A	2.8	7.71E-114
RSAD2	4.7	4.47E-110
SERPING1	3.2	7.59E-110

Table 9-8: 12h LPS vs no LPS: Top 50 DEG

Gene name	**LogFC**	**Adjusted p-value**
ANKRD22	6.6	3.65E-280
CCL7	5.4	6.59E-263
TNFAIP6	3.3	3.88E-256
CD274	6.3	3.30E-230
CALHM6	8.1	1.26E-224
APOL3	7.6	1.07E-218
GBP2	5.4	5.71E-218
GBP5	9.0	2.11E-215
CXCL11	13.4	2.35E-202
ELOVL7	4.2	1.24E-189
FUCA1	-2.1	6.83E-183
HAPLN3	6.2	8.89E-167
IL6	8.9	6.80E-165
RSAD2	5.8	1.63E-163
STAT1	2.7	4.85E-163
HS3ST3B1	2.6	8.16E-163
IRF1	5.8	3.69E-162
IL18BP	5.0	2.04E-156
OLFML2B	-3.4	1.29E-153
MEFV	3.3	6.70E-152
CXCL1	3.7	2.08E-150

NEURL3	5.2	9.12E-145
DUSP5	3.9	1.39E-142
STX11	2.5	6.23E-140
MERTK	-2.5	1.91E-138
HRH2	-3.4	8.48E-138
ATF3	4.4	4.82E-135
PTGS2	5.9	4.02E-129
IDO1	10.0	4.32E-126
TRAF1	5.4	1.07E-123
GBP1	8.1	4.35E-123
HGF	6.5	5.63E-123
GBP1P1	9.2	7.29E-122
KCNJ2	3.1	9.40E-120
ETV7	5.9	9.46E-110
GBP3	3.8	1.21E-109
ISG20	6.4	2.22E-109
IL15RA	3.7	3.07E-108
PSMB9	4.9	3.49E-108
XRN1	2.3	3.51E-108
CSRNP1	2.2	6.94E-106
CXCL3	3.4	1.54E-103
STAB1	-4.6	1.33E-102
SIRPB2	-2.9	1.04E-101
TPCN1	-2.5	3.45E-101
COLEC12	-4.7	9.66E-101
MAF	-3.5	2.37E-99
SERPINB9	2.5	4.32E-99
CR1	-4.5	1.56E-93
TIFA	3.4	4.68E-93

Raw data related to Figure 5.7:

Table 9-9: Interception between 3h LPS vs no LPS and 12h LPS vs no LPS: Top 50 significant biological processes of downregulated DEG

Term name	**Term ID**	**-Log10(p_{adj})**	**Term size**	**Query size**	**Inter-section**
regulation of multicellular organismal process	GO:0051239	7.5	2666	365	93
localization	GO:0051179	5.9	6436	365	167
multicellular organismal process	GO:0032501	5.9	7354	365	184
transmembrane transport	GO:0055085	5.8	1528	365	61
metal ion transport	GO:0030001	5.6	886	365	43
ion transport	GO:0006811	5.5	1551	365	61
cation transport	GO:0006812	5.5	1173	365	51
cell surface receptor signaling pathway	GO:0007166	4.8	2811	365	89
cell communication	GO:0007154	4.7	6508	365	164

response to stimulus	GO:0050896	4.6	8885	365	207
signaling	GO:0023052	4.5	6451	365	162
ion transmembrane transport	GO:0034220	4.5	1113	365	47
regulation of localization	GO:0032879	4.5	2725	365	86
cation transmembrane transport	GO:0098655	4.4	903	365	41
signal transduction	GO:0007165	4.0	5957	365	151
cell migration	GO:0016477	4.0	1461	365	55
regulation of response to stimulus	GO:0048583	3.8	3895	365	109
regulation of molecular function	GO:0065009	3.8	3050	365	91
inorganic ion transmembrane transport	GO:0098660	3.5	858	365	38
circulatory system process	GO:0003013	3.5	587	365	30
vascular process in circulatory system	GO:0003018	3.4	260	365	19
regulation of developmental process	GO:0050793	3.4	2425	365	76
system development	GO:0048731	3.4	4313	365	116
biological regulation	GO:0065007	3.1	13001	365	270
multicellular organism development	GO:0007275	3.1	4768	365	124
inorganic cation transmembrane transport	GO:0098662	3.0	792	365	35
regulation of catalytic activity	GO:0050790	3.0	2345	365	73
import into cell	GO:0098657	3.0	225	365	17
locomotion	GO:0040011	2.9	1833	365	61
cellular response to stimulus	GO:0051716	2.8	7399	365	173
negative regulation of multicellular organismal process	GO:0051241	2.7	1000	365	40
cell motility	GO:0048870	2.6	1655	365	56
localization of cell	GO:0051674	2.6	1655	365	56
anatomical structure formation involved in morphogenesis	GO:0048646	2.5	1134	365	43
immune system process	GO:0002376	2.5	2781	365	81
regulation of phosphate metabolic process	GO:0019220	2.4	1386	365	49
regulation of phosphorus metabolic process	GO:0051174	2.4	1388	365	49
transport	GO:0006810	2.4	4742	365	121
positive regulation of developmental process	GO:0051094	2.4	1268	365	46
bone resorption	GO:0045453	2.3	66	365	9
regulation of biological quality	GO:0065008	2.3	3768	365	101
import across plasma membrane	GO:0098739	2.3	174	365	14

anatomical structure development	GO:0048856	2.3	5754	365	140
regulation of cellular process	GO:0050794	2.3	11193	365	237
response to chemical	GO:0042221	2.2	4336	365	112
response to external stimulus	GO:0009605	2.2	2788	365	80
establishment of localization	GO:0051234	2.1	4903	365	123
regulation of multicellular organismal development	GO:2000026	2.1	1345	365	47
regulation of biological process	GO:0050789	2.0	12276	365	254
regulation of cell population proliferation	GO:0042127	1.9	1658	365	54

Table 9-10: 3h LPS vs no LPS only: Top 50 significant biological processes of downregulated DEG

Term name	**Term ID**	**-Log10(p_{adj})**	**Term size**	**Query size**	**Inter-section**
positive regulation of multicellular organismal process	GO:0051240	5.9	1434	139	32
intracellular signal transduction	GO:0035556	4.9	2629	139	43
response to stimulus	GO:0050896	4.4	8885	139	91
positive regulation of biological process	GO:0048518	4.3	6224	139	72
regulation of multicellular organismal process	GO:0051239	4.2	2666	139	42
positive regulation of metabolic process	GO:0009893	4.2	3776	139	52
osteoblast differentiation	GO:0001649	4.2	229	139	12
response to external stimulus	GO:0009605	4.1	2788	139	43
regulation of cytokine production	GO:0001817	4.0	726	139	20
cytokine production	GO:0001816	3.9	732	139	20
ossification	GO:0001503	3.8	413	139	15
regulation of response to stimulus	GO:0048583	3.7	3895	139	52
positive regulation of macromolecule metabolic process	GO:0010604	3.6	3465	139	48
biological regulation	GO:0065007	3.6	13001	139	114
cell communication	GO:0007154	3.5	6508	139	72
cellular response to stimulus	GO:0051716	3.3	7399	139	78
positive regulation of cytokine production	GO:0001819	3.1	470	139	15
response to stress	GO:0006950	3.0	3851	139	50

regulation of cellular process	GO:0050794	2.9	11193	139	102
positive regulation of nitrogen compound metabolic process	GO:0051173	2.9	3083	139	43
signaling	GO:0023052	2.9	6451	139	70
immune system process	GO:0002376	2.8	2781	139	40
signal transduction	GO:0007165	2.7	5957	139	66
positive regulation of response to stimulus	GO:0048584	2.7	2169	139	34
regulation of response to stress	GO:0080134	2.6	1312	139	25
positive regulation of signal transduction	GO:0009967	2.5	1513	139	27
positive regulation of cellular process	GO:0048522	2.4	5687	139	63
positive regulation of cell population proliferation	GO:0008284	2.3	929	139	20
regulation of cell population proliferation	GO:0042127	2.3	1658	139	28
positive regulation of cellular metabolic process	GO:0031325	2.2	3271	139	43
MAPK cascade	GO:0000165	2.1	788	139	18
regulation of type I interferon production	GO:0032479	2.1	102	139	7
type I interferon production	GO:0032606	2.1	102	139	7
response to other organism	GO:0051707	2.0	1507	139	26
response to external biotic stimulus	GO:0043207	2.0	1509	139	26
cell differentiation	GO:0030154	2.0	4160	139	50
regulation of biological process	GO:0050789	2.0	12276	139	106
cellular developmental process	GO:0048869	2.0	4184	139	50
cellular response to chemical stimulus	GO:0070887	1.9	3019	139	40
positive regulation of cell adhesion	GO:0045785	1.9	442	139	13
regulation of immune system process	GO:0002682	1.9	1442	139	25
regulation of cell adhesion	GO:0030155	1.9	740	139	17
tissue development	GO:0009888	1.9	1940	139	30
response to biotic stimulus	GO:0009607	1.8	1549	139	26
cell population proliferation	GO:0008283	1.8	1958	139	30
positive regulation of response to external stimulus	GO:0032103	1.8	453	139	13
regulation of signal transduction	GO:0009966	1.7	2947	139	39
positive regulation of RNA metabolic process	GO:0051254	1.7	1769	139	28

positive regulation of nucleobase-containing compound metabolic process	GO:0045935	1.7	1976	139	30
regulation of intracellular signal transduction	GO:1902531	1.6	1691	139	27

Table 9-11: 12h LPS vs no LPS only: All significant biological processes of downregulated DEG

Term name	**Term ID**	**-Log10(p_{adj})**	**Term size**	**Query size**	**Inter-section**
response to stimulus	GO:0050896	4.6	8885	168	107
response to external stimulus	GO:0009605	4.1	2788	168	49
antigen processing and presentation of exogenous peptide antigen	GO:0002478	3.1	59	168	7
response to other organism	GO:0051707	2.8	1507	168	31
response to external biotic stimulus	GO:0043207	2.8	1509	168	31
antigen processing and presentation of exogenous antigen	GO:0019884	2.6	70	168	7
response to biotic stimulus	GO:0009607	2.5	1549	168	31
immune response	GO:0006955	2.4	1906	168	35
antigen processing and presentation of peptide antigen via MHC class I	GO:0002474	2.3	49	168	6
Fc receptor signaling pathway	GO:0038093	2.2	79	168	7
antigen processing and presentation of peptide antigen	GO:0048002	2.1	82	168	7
antigen processing and presentation of exogenous peptide antigen via MHC class I	GO:0042590	2.0	32	168	5
biological process involved in interspecies interaction between organisms	GO:0044419	1.9	1659	168	31
antigen processing and presentation	GO:0019882	1.8	128	168	8
T cell differentiation	GO:0030217	1.7	267	168	11
innate immune response	GO:0045087	1.7	907	168	21
mononuclear cell differentiation	GO:1903131	1.6	440	168	14
lymphocyte differentiation	GO:0030098	1.5	391	168	13
signal transduction	GO:0007165	1.5	5957	168	73
cell activation	GO:0001775	1.4	1094	168	23
cellular response to stimulus	GO:0051716	1.3	7399	168	85

Table 9-12: Interception between 3h LPS vs no LPS and 12h LPS vs no LPS: Top 50 significant biological processes of upregulated DEG

Term name	Term ID	-Log10(p_{adj})	Term size	Query size	Inter-section
regulation of multicellular organismal process	GO:0051239	7.5	2666	365	93
localization	GO:0051179	5.9	6436	365	167
multicellular organismal process	GO:0032501	5.9	7354	365	184
transmembrane transport	GO:0055085	5.8	1528	365	61
metal ion transport	GO:0030001	5.6	886	365	43
ion transport	GO:0006811	5.5	1551	365	61
cation transport	GO:0006812	5.5	1173	365	51
cell surface receptor signaling pathway	GO:0007166	4.8	2811	365	89
cell communication	GO:0007154	4.7	6508	365	164
response to stimulus	GO:0050896	4.6	8885	365	207
signaling	GO:0023052	4.5	6451	365	162
ion transmembrane transport	GO:0034220	4.5	1113	365	47
regulation of localization	GO:0032879	4.5	2725	365	86
cation transmembrane transport	GO:0098655	4.4	903	365	41
signal transduction	GO:0007165	4.0	5957	365	151
cell migration	GO:0016477	4.0	1461	365	55
regulation of response to stimulus	GO:0048583	3.8	3895	365	109
regulation of molecular function	GO:0065009	3.8	3050	365	91
inorganic ion transmembrane transport	GO:0098660	3.5	858	365	38
circulatory system process	GO:0003013	3.5	587	365	30
vascular process in circulatory system	GO:0003018	3.4	260	365	19
regulation of developmental process	GO:0050793	3.4	2425	365	76
system development	GO:0048731	3.4	4313	365	116
biological regulation	GO:0065007	3.1	13001	365	270
multicellular organism development	GO:0007275	3.1	4768	365	124
inorganic cation transmembrane transport	GO:0098662	3.0	792	365	35
regulation of catalytic activity	GO:0050790	3.0	2345	365	73
import into cell	GO:0098657	3.0	225	365	17
locomotion	GO:0040011	2.9	1833	365	61
cellular response to stimulus	GO:0051716	2.8	7399	365	173
negative regulation of multicellular organismal process	GO:0051241	2.7	1000	365	40
cell motility	GO:0048870	2.6	1655	365	56
localization of cell	GO:0051674	2.6	1655	365	56
anatomical structure formation involved in morphogenesis	GO:0048646	2.5	1134	365	43

immune system process	GO:0002376	2.5	2781	365	81
regulation of phosphate metabolic process	GO:0019220	2.4	1386	365	49
regulation of phosphorus metabolic process	GO:0051174	2.4	1388	365	49
transport	GO:0006810	2.4	4742	365	121
positive regulation of developmental process	GO:0051094	2.4	1268	365	46
bone resorption	GO:0045453	2.3	66	365	9
regulation of biological quality	GO:0065008	2.3	3768	365	101
import across plasma membrane	GO:0098739	2.3	174	365	14
anatomical structure development	GO:0048856	2.3	5754	365	140
regulation of cellular process	GO:0050794	2.3	11193	365	237
response to chemical	GO:0042221	2.2	4336	365	112
response to external stimulus	GO:0009605	2.2	2788	365	80
establishment of localization	GO:0051234	2.1	4903	365	123
regulation of multicellular organismal development	GO:2000026	2.1	1345	365	47
regulation of biological process	GO:0050789	2.0	12276	365	254
regulation of cell population proliferation	GO:0042127	1.9	1658	365	54

Table 9-13: 3h LPS vs no LPS only: All significant biological processes of upregulated DEG

Term name	**Term ID**	**-Log10(p_{adj})**	**Term size**	**Query size**	**Inter-section**
regulation of cellular process	GO:0050794	3.3	11193	185	132
biological regulation	GO:0065007	2.8	13001	185	145
regulation of biological process	GO:0050789	2.4	12276	185	138
leukocyte migration involved in inflammatory response	GO:0002523	1.3	20	185	4

Table 9-14: 12h LPS vs no LPS only: All significant biological processes of upregulated DEG

Term name	**Term ID**	**-Log10(p_{adj})**	**Term size**	**Query size**	**Inter-section**
oxoacid metabolic process	GO:0043436	3.830738	966	206	29
small molecule metabolic process	GO:0044281	3.782489	1796	206	42
organic acid metabolic process	GO:0006082	3.623429	988	206	29
carboxylic acid metabolic process	GO:0019752	2.984095	940	206	27
regulation of localization	GO:0032879	2.27256	2725	206	51
monocarboxylic acid metabolic process	GO:0032787	1.868954	597	206	19
regulation of cell motility	GO:2000145	1.860984	952	206	25

regulation of multicellular organismal process	GO:0051239	1.830554	2666	206	49
lipid metabolic process	GO:0006629	1.547415	1392	206	31
regulation of locomotion	GO:0040012	1.519703	997	206	25
ameboidal-type cell migration	GO:0001667	1.483419	418	206	15
response to peptide	GO:1901652	1.406708	477	206	16
regulation of cell migration	GO:0030334	1.349011	893	206	23

Raw data related to Figure 5.8:

Table 9-15: Q109 12h LPS vs Q22 12h LPS: Top 50 DEG

Gene name	LogFC	Adjusted p-value
MMP12	-2.5	5.33E-93
MYO1D	-2.4	6.09E-21
PPP1R1A	-2.7	9.20E-21
GPR157	-1.6	3.85E-20
AR	3.5	1.52E-19
DDIT4L	-2.6	9.10E-19
TRIM47	-1.5	6.16E-15
CAPG	-1.6	3.16E-14
ARMCX4	2.0	3.96E-14
ATP6V0D2	-2.6	9.63E-14
KLF8	-2.4	1.47E-13
RARRES1	-1.5	3.20E-13
MIR3142HG	-2.4	4.26E-13
PLA1A	-2.3	1.53E-12
CNIH3	-2.6	1.01E-11
CD28	-1.9	2.60E-11
ADD2	2.3	9.51E-11
ATP6AP1L	2.0	1.57E-10
CD9	-1.9	1.96E-10
ZNF717	3.4	3.90E-10
ZNF229	4.7	1.45E-09
AF127577.4	1.6	1.63E-09
CACNA2D4	-2.1	1.79E-09
SIX1	4.0	2.77E-09
DNAAF1	-1.5	3.58E-09
RYR1	1.9	3.60E-09
COL7A1	2.3	7.42E-09
MT1H	-2.2	9.15E-09
PLS1	3.1	9.34E-09
TM4SF19-AS1	-3.0	1.17E-08
PLLP	2.1	1.21E-08
OLIG2	-1.8	1.55E-08
LHX2	-1.5	2.30E-08
SMS	-1.8	2.45E-08
MAP3K13	2.7	2.87E-08

NLE1	1.6	3.12E-08
MID2	2.3	3.41E-08
MT1M	-2.1	3.42E-08
KLHL3	3.6	3.96E-08
MT1G	-2.3	4.65E-08
CSTB	-1.5	6.11E-08
FAM117A	1.8	6.26E-08
TP63	3.8	6.65E-08
SLC16A7	1.7	1.00E-07
RPGRIP1L	2.8	1.32E-07
KIF21A	-1.6	1.50E-07
GPR137B	-1.6	1.67E-07
TSLP	3.6	1.85E-07
CLEC2B	-1.7	1.85E-07
ADTRP	-2.0	1.85E-07

Raw data related to Figure 5.9:

Table 9-16: Q109 12h vs Q22 12h: Top 50 significant biological processes of downregulated DEG

Term name	Term ID	-Log10(p_{adj})	Term size	Query size	Inter-section
cellular response to cadmium ion	GO:0071276	5.8	36	115	7
cellular response to copper ion	GO:0071280	5.1	26	115	6
detoxification of copper ion	GO:0010273	4.8	14	115	5
stress response to copper ion	GO:1990169	4.8	14	115	5
cellular response to chemical stimulus	GO:0070887	4.8	3019	115	41
detoxification of inorganic compound	GO:0061687	4.4	17	115	5
response to cadmium ion	GO:0046686	4.3	58	115	7
stress response to metal ion	GO:0097501	4.2	18	115	5
movement of cell or subcellular component	GO:0006928	4.2	2085	115	32
cellular zinc ion homeostasis	GO:0006882	4.0	38	115	6
cell migration	GO:0016477	4.0	1461	115	26
regulation of localization	GO:0032879	4.0	2725	115	37
developmental process	GO:0032502	4.0	6317	115	62
zinc ion homeostasis	GO:0055069	3.9	40	115	6
response to copper ion	GO:0046688	3.9	40	115	6
cellular response to zinc ion	GO:0071294	3.6	23	115	5
multicellular organismal process	GO:0032501	3.4	7354	115	67
anatomical structure development	GO:0048856	3.3	5754	115	57
positive regulation of cell communication	GO:0010647	3.2	1711	115	27
response to zinc ion	GO:0010043	3.2	52	115	6

positive regulation of signaling	GO:0023056	3.2	1715	115	27
response to chemical	GO:0042221	3.1	4336	115	47
cell motility	GO:0048870	2.9	1655	115	26
localization of cell	GO:0051674	2.9	1655	115	26
positive regulation of biological process	GO:0048518	2.9	6224	115	59
response to organic substance	GO:0010033	2.9	3010	115	37
regulation of multicellular organismal process	GO:0051239	2.7	2666	115	34
system development	GO:0048731	2.7	4313	115	46
locomotion	GO:0040011	2.6	1833	115	27
regulation of biological quality	GO:0065008	2.6	3768	115	42
positive regulation of signal transduction	GO:0009967	2.5	1513	115	24
animal organ development	GO:0048513	2.5	3513	115	40
cellular transition metal ion homeostasis	GO:0046916	2.4	111	115	7
cellular response to organic substance	GO:0071310	2.3	2391	115	31
cellular response to stimulus	GO:0051716	2.1	7399	115	64
positive regulation of intracellular signal transduction	GO:1902533	2.0	975	115	18
localization	GO:0051179	2.0	6436	115	58
response to stimulus	GO:0050896	1.9	8885	115	72
cellular response to tumor necrosis factor	GO:0071356	1.9	242	115	9
cell differentiation	GO:0030154	1.9	4160	115	43
negative regulation of growth	GO:0045926	1.9	245	115	9
leukocyte migration	GO:0050900	1.9	384	115	11
multicellular organism development	GO:0007275	1.8	4768	115	47
cellular developmental process	GO:0048869	1.8	4184	115	43
transition metal ion homeostasis	GO:0055076	1.8	136	115	7
cellular response to metal ion	GO:0071248	1.8	191	115	8
positive regulation of response to stimulus	GO:0048584	1.7	2169	115	28
anatomical structure morphogenesis	GO:0009653	1.7	2702	115	32
response to tumor necrosis factor	GO:0034612	1.6	262	115	9
signaling	GO:0023052	1.6	6451	115	57

Table 9-17: Q109 12h vs Q22 12h: Top 50 significant biological processes of upregulated DEG

Term name	**Term ID**	**-Log10(p_{adj})**	**Term size**	**Query size**	**Inter-section**
nervous system development	GO:0007399	21.0	2430	704	178
anatomical structure development	GO:0048856	20.7	5754	704	317
system development	GO:0048731	19.3	4313	704	256

multicellular organismal process	GO:0032501	19.3	7354	704	372
multicellular organism development	GO:0007275	19.1	4768	704	274
developmental process	GO:0032502	18.6	6317	704	332
cell development	GO:0048468	17.6	2094	704	154
neuron differentiation	GO:0030182	16.4	1366	704	115
neurogenesis	GO:0022008	16.3	1642	704	129
anatomical structure morphogenesis	GO:0009653	16.3	2702	704	179
generation of neurons	GO:0048699	15.6	1436	704	117
animal organ development	GO:0048513	15.1	3513	704	211
cellular developmental process	GO:0048869	14.9	4184	704	238
cell differentiation	GO:0030154	14.9	4160	704	237
cell projection organization	GO:0030030	14.5	1525	704	119
neuron development	GO:0048666	14.4	1108	704	97
plasma membrane bounded cell projection organization	GO:0120036	14.0	1485	704	116
synapse organization	GO:0050808	13.2	424	704	54
cell communication	GO:0007154	13.2	6508	704	322
signaling	GO:0023052	12.7	6451	704	318
cell junction organization	GO:0034330	12.6	691	704	70
neuron projection development	GO:0031175	11.5	957	704	83
regulation of cellular component organization	GO:0051128	10.8	2276	704	145
regulation of biological quality	GO:0065008	10.7	3768	704	208
cell morphogenesis	GO:0000902	10.6	1012	704	84
regulation of signaling	GO:0023051	10.4	3351	704	190
cell-cell signaling	GO:0007267	10.1	1661	704	115
cell morphogenesis involved in differentiation	GO:0000904	10.1	722	704	67
central nervous system development	GO:0007417	10.0	1037	704	84
regulation of cell communication	GO:0010646	10.0	3336	704	188
signal transduction	GO:0007165	9.5	5957	704	288
cellular response to stimulus	GO:0051716	9.4	7399	704	340
cell projection morphogenesis	GO:0048858	9.3	642	704	61
regulation of localization	GO:0032879	9.3	2725	704	160
cell morphogenesis involved in neuron differentiation	GO:0048667	9.1	564	704	56
cellular component morphogenesis	GO:0032989	9.1	757	704	67
neuron projection morphogenesis	GO:0048812	8.9	623	704	59
cell part morphogenesis	GO:0032990	8.8	661	704	61
plasma membrane bounded cell projection morphogenesis	GO:0120039	8.4	638	704	59
brain development	GO:0007420	8.0	762	704	65

anterograde trans-synaptic signaling	GO:0098916	8.0	709	704	62
chemical synaptic transmission	GO:0007268	8.0	709	704	62
axon development	GO:0061564	7.9	484	704	49
localization	GO:0051179	7.9	6436	704	299
cytoskeleton organization	GO:0007010	7.8	1453	704	99
head development	GO:0060322	7.8	809	704	67
trans-synaptic signaling	GO:0099537	7.8	717	704	62
regulation of signal transduction	GO:0009966	7.7	2947	704	164
response to stimulus	GO:0050896	7.4	8885	704	383
regulation of transport	GO:0051049	7.3	1724	704	110

Raw data related to Figure 5.10:

Table 9-18: Interception between unstimulated comparison and 12h LPS comparison: All significant biological processes of downregulated DEG

Term name	**Term ID**	**-Log10(p_{adj})**	**Term size**	**Query size**	**Inter-section**
stress response to copper ion	GO:1990169	6.5	14	52	5
detoxification of copper ion	GO:0010273	6.5	14	52	5
cellular response to cadmium ion	GO:0071276	6.2	36	52	6
cellular zinc ion homeostasis	GO:0006882	6.1	38	52	6
detoxification of inorganic compound	GO:0061687	6.1	17	52	5
zinc ion homeostasis	GO:0055069	5.9	40	52	6
stress response to metal ion	GO:0097501	5.9	18	52	5
cellular response to zinc ion	GO:0071294	5.3	23	52	5
response to zinc ion	GO:0010043	5.2	52	52	6
cellular response to copper ion	GO:0071280	5.0	26	52	5
response to cadmium ion	GO:0046686	4.9	59	52	6
response to copper ion	GO:0046688	4.1	40	52	5
cellular transition metal ion homeostasis	GO:0046916	3.2	112	52	6
transition metal ion homeostasis	GO:0055076	2.6	140	52	6
cellular divalent inorganic cation homeostasis	GO:0072503	2.6	327	52	8
cation homeostasis	GO:0055080	2.5	601	52	10
inorganic ion homeostasis	GO:0098771	2.4	616	52	10
negative regulation of growth	GO:0045926	2.3	247	52	7

divalent inorganic cation homeostasis	GO:0072507	2.3	358	52	8
ion homeostasis	GO:0050801	2.3	626	52	10
cellular cation homeostasis	GO:0030003	2.2	499	52	9
cellular ion homeostasis	GO:0006873	2.1	516	52	9
metal ion homeostasis	GO:0055065	2.1	520	52	9
cellular chemical homeostasis	GO:0055082	2.0	673	52	10
cellular metal ion homeostasis	GO:0006875	1.8	422	52	8
cellular response to metal ion	GO:0071248	1.7	199	52	6
extracellular matrix disassembly	GO:0022617	1.5	61	52	4
regulation of response to external stimulus	GO:0032101	1.5	948	52	11
cellular homeostasis	GO:0019725	1.5	772	52	10
detoxification	GO:0098754	1.4	135	52	5
cellular response to inorganic substance	GO:0071241	1.4	229	52	6

Table 9-19: Unstimulated comparison only: Top 50 significant biological processes of downregulated DEG

Term name	**Term ID**	**-Log10(p_{adj})**	**Term size**	**Query size**	**Inter-section**
inflammatory response	GO:0006954	9.0	786	114	25
defense response	GO:0006952	8.9	1742	114	36
immune response	GO:0006955	7.7	1913	114	36
response to stimulus	GO:0050896	7.5	9000	114	84
defense response to other organism	GO:0098542	6.1	1163	114	26
eosinophil chemotaxis	GO:0048245	6.0	19	114	6
immune system process	GO:0002376	5.7	2842	114	41
response to other organism	GO:0051707	5.6	1513	114	29
response to external biotic stimulus	GO:0043207	5.6	1516	114	29
eosinophil migration	GO:0072677	5.5	23	114	6
response to biotic stimulus	GO:0009607	5.4	1554	114	29
response to cytokine	GO:0034097	5.3	906	114	22
biological process involved in interspecies interaction between organisms	GO:0044419	5.3	1675	114	30
regulation of biological process	GO:0050789	5.2	12361	114	96
biological regulation	GO:0065007	5.2	13096	114	99
response to stress	GO:0006950	5.0	3938	114	48
positive regulation of immune system process	GO:0002684	4.9	954	114	22
cellular response to chemical stimulus	GO:0070887	4.8	3049	114	41
cellular response to interferon-gamma	GO:0071346	4.5	121	114	9
response to organic substance	GO:0010033	4.4	3034	114	40

chemokine-mediated signaling pathway	GO:0070098	4.3	89	114	8
cellular response to tumor necrosis factor	GO:0071356	4.2	222	114	11
cell activation	GO:0001775	4.2	1138	114	23
granulocyte chemotaxis	GO:0071621	4.2	131	114	9
cellular response to stimulus	GO:0051716	4.1	7494	114	69
positive regulation of MAPK cascade	GO:0043410	4.0	483	114	15
lymphocyte chemotaxis	GO:0048247	4.0	64	114	7
response to chemokine	GO:1990868	4.0	98	114	8
cellular response to chemokine	GO:1990869	4.0	98	114	8
regulation of multicellular organismal process	GO:0051239	3.9	2753	114	37
leukocyte chemotaxis	GO:0030595	3.9	239	114	11
regulation of immune system process	GO:0002682	3.9	1488	114	26
leukocyte activation	GO:0045321	3.9	995	114	21
cellular response to cytokine stimulus	GO:0071345	3.9	817	114	19
response to interferon-gamma	GO:0034341	3.9	142	114	9
response to tumor necrosis factor	GO:0034612	3.8	242	114	11
cellular response to organic substance	GO:0071310	3.8	2405	114	34
innate immune response	GO:0045087	3.8	916	114	20
positive regulation of T cell activation	GO:0050870	3.8	246	114	11
neutrophil chemotaxis	GO:0030593	3.7	106	114	8
response to external stimulus	GO:0009605	3.7	2814	114	37
positive regulation of response to stimulus	GO:0048584	3.6	2214	114	32
positive regulation of cell-cell adhesion	GO:0022409	3.6	316	114	12
cell communication	GO:0007154	3.5	6551	114	62
T cell activation	GO:0042110	3.4	538	114	15
granulocyte migration	GO:0097530	3.4	160	114	9
regulation of cell population proliferation	GO:0042127	3.4	1683	114	27
homeostatic process	GO:0042592	3.4	1684	114	27
positive regulation of leukocyte cell-cell adhesion	GO:1903039	3.4	269	114	11
T cell proliferation	GO:0042098	3.4	213	114	10

Table 9-20: 12h LPS comparison only: All significant biological processes of downregulated DEG

Term name	**Term ID**	**-Log10(p_{adj})**	**Term size**	**Query size**	**Inter-section**
epithelial cell apoptotic process	GO:1904019	2.3	134	35	5
response to hypoxia	GO:0001666	1.9	289	35	6

response to decreased oxygen levels	GO:0036293	1.8	302	35	6
response to oxygen levels	GO:0070482	1.5	331	35	6

Table 9-21: Interception between unstimulated comparison and 12h LPS comparison: Top 50 significant biological processes of upregulated DEG

Term name	**Term ID**	**-Log10(p_{adj})**	**Term size**	**Query size**	**Inter-section**
nervous system development	GO:0007399	11.5	2504	242	75
anatomical structure development	GO:0048856	9.6	5836	242	121
cell development	GO:0048468	9.6	2142	242	65
generation of neurons	GO:0048699	9.5	1465	242	52
multicellular organism development	GO:0007275	9.2	4823	242	106
neuron differentiation	GO:0030182	9.1	1393	242	50
system development	GO:0048731	8.9	4369	242	99
multicellular organismal process	GO:0032501	8.9	7463	242	140
neurogenesis	GO:0022008	8.8	1680	242	55
regulation of cellular component organization	GO:0051128	8.7	2355	242	67
regulation of cellular process	GO:0050794	8.2	11130	242	180
cellular developmental process	GO:0048869	8.2	4280	242	96
regulation of biological process	GO:0050789	8.0	12361	242	192
cell differentiation	GO:0030154	7.9	4256	242	95
biological regulation	GO:0065007	7.9	13096	242	199
developmental process	GO:0032502	7.3	6424	242	123
neuron development	GO:0048666	6.5	1122	242	40
anatomical structure morphogenesis	GO:0009653	6.4	2722	242	68
animal organ development	GO:0048513	6.2	3591	242	81
central nervous system development	GO:0007417	6.0	1065	242	38
signaling	GO:0023052	5.5	6492	242	119
cell communication	GO:0007154	5.3	6551	242	119
cell junction organization	GO:0034330	5.3	703	242	29
regulation of cell communication	GO:0010646	5.2	3363	242	75
regulation of signaling	GO:0023051	5.1	3374	242	75
regulation of biological quality	GO:0065008	5.0	3726	242	80
positive regulation of cellular process	GO:0048522	4.9	5641	242	106
regulation of signal transduction	GO:0009966	4.8	2968	242	68
cell-cell signaling	GO:0007267	4.4	1663	242	46
cellular response to stimulus	GO:0051716	4.4	7494	242	128

signal transduction	GO:0007165	4.3	5993	242	109
positive regulation of biological process	GO:0048518	4.3	6309	242	113
brain development	GO:0007420	4.3	780	242	29
head development	GO:0060322	4.3	828	242	30
cell morphogenesis	GO:0000902	4.2	1030	242	34
regulation of localization	GO:0032879	3.9	2089	242	52
tissue development	GO:0009888	3.9	1973	242	50
neuron projection development	GO:0031175	3.8	970	242	32
regulation of developmental process	GO:0050793	3.7	2499	242	58
cell projection organization	GO:0030030	3.5	1550	242	42
positive regulation of developmental process	GO:0051094	3.4	1337	242	38
response to stimulus	GO:0050896	3.2	9000	242	142
system process	GO:0003008	3.1	2275	242	53
cell surface receptor signaling pathway	GO:0007166	3.0	2816	242	61
plasma membrane bounded cell projection organization	GO:0120036	2.9	1509	242	40
regulation of ion transport	GO:0043269	2.9	702	242	25
regulation of transport	GO:0051049	2.9	1750	242	44
cell junction assembly	GO:0034329	2.9	431	242	19
synapse organization	GO:0050808	2.9	433	242	19
cellular component morphogenesis	GO:0032989	2.7	770	242	26

Table 9-22: Unstimulated comparison only: All significant biological processes of upregulated DEG

Term name	**Term ID**	**-Log10(p_{adj})**	**Term size**	**Query size**	**Inter-section**
regulation of cellular process	GO:0050794	20.5	11130	579	424
chromosome organization	GO:0051276	18.2	612	579	67
mitotic cell cycle process	GO:1903047	16.5	769	579	73
mitotic cell cycle	GO:0000278	16.4	927	579	81
cell cycle	GO:0007049	16.3	1794	579	120
cell cycle process	GO:0022402	16.3	1226	579	95
cell division	GO:0051301	15.8	658	579	66
nuclear division	GO:0000280	15.2	481	579	55
chromosome segregation	GO:0007059	14.2	373	579	47
organelle fission	GO:0048285	14.1	527	579	56
regulation of biological process	GO:0050789	13.6	12361	579	436
mitotic nuclear division	GO:0140014	13.5	326	579	43
sister chromatid segregation	GO:0000819	12.4	231	579	35
biological regulation	GO:0065007	12.2	13096	579	450
nuclear chromosome segregation	GO:0098813	11.8	314	579	40
mitotic sister chromatid segregation	GO:0000070	11.6	202	579	32

regulation of chromosome segregation	GO:0051983	11.6	128	579	26
regulation of cellular component organization	GO:0051128	11.6	2355	579	131
regulation of cell cycle process	GO:0010564	10.6	712	579	60
negative regulation of cellular process	GO:0048523	10.3	4749	579	210
developmental process	GO:0032502	10.3	6424	579	262
regulation of cell cycle	GO:0051726	9.9	1111	579	77
anatomical structure development	GO:0048856	9.7	5836	579	242
multicellular organism development	GO:0007275	9.6	4823	579	210
system development	GO:0048731	9.5	4369	579	195
multicellular organismal process	GO:0032501	9.5	7463	579	290
cytoskeleton organization	GO:0007010	9.4	1491	579	92
chromosome separation	GO:0051304	9.4	132	579	24
regulation of chromosome separation	GO:1905818	9.3	109	579	22
negative regulation of mitotic sister chromatid separation	GO:2000816	9.2	51	579	16
negative regulation of sister chromatid segregation	GO:0033046	9.2	51	579	16
negative regulation of mitotic sister chromatid segregation	GO:0033048	9.2	51	579	16
nervous system development	GO:0007399	9.2	2504	579	130
microtubule cytoskeleton organization	GO:0000226	9.1	644	579	54
attachment of spindle microtubules to kinetochore	GO:0008608	9.1	44	579	15
negative regulation of chromosome separation	GO:1905819	8.9	53	579	16
negative regulation of chromosome segregation	GO:0051985	8.9	53	579	16
neurogenesis	GO:0022008	8.8	1680	579	98
regulation of sister chromatid segregation	GO:0033045	8.7	105	579	21
mitotic spindle assembly checkpoint signaling	GO:0007094	8.6	47	579	15
spindle assembly checkpoint signaling	GO:0071173	8.6	47	579	15
mitotic spindle checkpoint signaling	GO:0071174	8.6	47	579	15
regulation of mitotic sister chromatid segregation	GO:0033047	8.5	56	579	16
regulation of mitotic sister chromatid separation	GO:0010965	8.5	96	579	20
spindle checkpoint signaling	GO:0031577	8.4	48	579	15
axon development	GO:0061564	8.4	490	579	45
regulation of mitotic nuclear division	GO:0007088	8.4	120	579	22

negative regulation of chromosome organization	GO:2001251	8.3	98	579	20
negative regulation of mitotic metaphase/anaphase transition	GO:0045841	8.3	49	579	15
mitotic sister chromatid separation	GO:0051306	8.2	99	579	20

Table 9-23: 12h LPS comparison only: All significant biological processes of upregulated DEG

Term name	**Term ID**	**-Log10(p_{adj})**	**Term size**	**Query size**	**Inter-section**
anatomical structure morphogenesis	GO:0009653	4.8	2722	117	39
anatomical structure development	GO:0048856	3.2	5836	117	58
plasma membrane bounded cell projection organization	GO:0120036	3.0	1509	117	25
cell projection organization	GO:0030030	2.7	1550	117	25
developmental process	GO:0032502	2.5	6424	117	60
macrophage colony-stimulating factor production	GO:0036301	2.2	6	117	3
regulation of macrophage colony-stimulating factor production	GO:1901256	2.2	6	117	3
system development	GO:0048731	1.9	4369	117	45
multicellular organism development	GO:0007275	1.8	4823	117	48
cell morphogenesis	GO:0000902	1.6	1030	117	18
animal organ morphogenesis	GO:0009887	1.4	1066	117	18

9.2 Additional data for Chapter 6: Investigating the interplay between Astrocytes and Microglia in Huntington's disease

Raw data related to Figure 6.3:

Table 9-24: Q22 monoculture vs co-culture: Top 50 differentially secreted proteins

Gene name / Protein name	**LogFC**	**T-test**
SPP1	3.37	1.02E-06
Heavy chain of factor I (Fragment)	3.65	3.29E-05
COL5A2	3.15	3.61E-05
COL1A1	3.46	3.99E-05
COL3A1	2.39	4.22E-05
HSPG2	3.17	4.49E-05
MFAP5	3.15	5.37E-05
BMP1	2.29	5.73E-05
TNC	2.78	7.28E-05

CCDC80	2.51	7.45E-05
SPOCK1	2.54	8.03E-05
FSTL1	3.52	1.07E-04
IGFBP3	2.35	1.19E-04
MMP2	2.75	1.22E-04
MFAP2	3.85	1.57E-04
GOLM1	2.51	2.00E-04
COL4A2	2.26	2.02E-04
LUM	3.91	2.03E-04
A2M	2.33	2.09E-04
LAMB1	3.28	2.10E-04
IPO9	2.11	2.26E-04
CLSTN1	2.51	2.33E-04
TGFB2	3.28	2.34E-04
CLU	4.21	2.34E-04
FBN1	2.17	2.49E-04
LAMC1	2.74	2.52E-04
LTBP2	2.43	2.55E-04
MXRA5	3.70	2.56E-04
CDH2	3.64	2.61E-04
COL1A1	2.80	2.67E-04
FN1	2.39	2.70E-04
FBLN1	3.69	2.78E-04
IGHG1	2.74	2.95E-04
SYT13	2.19	3.05E-04
RARRES2	2.43	3.07E-04
LOXL2	2.32	3.15E-04
DKK3	2.82	3.19E-04
CXCL14	3.02	3.23E-04
LAMA5	1.80	3.30E-04
MRC2	3.16	3.32E-04
LAMA4	3.00	3.45E-04
COL5A1	2.61	3.46E-04
SPARC	3.21	3.72E-04
SERPINE1	3.34	3.86E-04
APP	2.40	3.97E-04
LGALS3BP	2.91	4.36E-04
MCAM	3.01	4.72E-04
CNN1	3.49	4.96E-04
LOXL1	2.43	5.25E-04
C1S	3.91	5.28E-04

Table 9-25: Q109 monoculture vs co-culture: Top 50 differentially secreted proteins

Gene name / Protein name	**LogFC**	**T-test**
APP	2.49	3.87E-06
NIT2	3.40	7.24E-06

FN1	2.57	1.13E-05
HLA-B	2.49	1.84E-05
GOLM1	2.21	3.18E-05
CDH2	3.23	3.24E-05
FLNA	2.65	3.47E-05
MYL6	1.64	4.33E-05
UCHL1	3.23	4.52E-05
HLA-C	2.29	4.61E-05
IGFBP5	2.81	5.51E-05
FLNC	1.88	6.49E-05
COL1A1	3.59	8.19E-05
HSPG2	2.08	8.46E-05
IGFBP3	3.35	9.81E-05
COL4A2	2.88	1.04E-04
MXRA5	2.73	1.08E-04
COL1A1	3.41	1.17E-04
LOXL2	2.42	1.23E-04
LAMA5	1.56	1.43E-04
TPM3	2.25	1.46E-04
GPC1	2.67	1.47E-04
TAGLN	3.33	1.47E-04
SFRP4	2.44	1.59E-04
FLNB	2.30	1.67E-04
HEL-S-265	2.89	1.78E-04
CSRP2	3.03	1.78E-04
PDLIM7	2.84	1.88E-04
PTK7	1.75	1.92E-04
CALD1	3.90	1.95E-04
TIMP2	1.77	2.13E-04
VCL	2.24	2.20E-04
NRCAM	2.48	2.28E-04
EFNB2	3.37	2.33E-04
SPTBN1	1.91	2.34E-04
HSPB1	2.92	2.43E-04
QSOX1	1.55	2.45E-04
SEMA7A	1.69	2.55E-04
EEA1	1.41	2.59E-04
Testicular secretory protein Li 7	2.24	2.60E-04
SCRG1	2.93	2.65E-04
NES	3.04	2.66E-04
PHPT1	2.23	2.66E-04
COMP	3.62	2.69E-04
BTF3	1.42	2.70E-04
IGKV2D-29	-2.28	2.74E-04
TPM1	3.36	3.03E-04
TNC	1.99	3.11E-04

THBS3	2.05	3.41E-04
ACTN1	2.31	3.44E-04

Table 9-26: Q22 monoculture vs co-culture: Top 50 significant molecular functions of upregulated proteins

Term name	**Term ID**	**-Log10(p_{adj})**	**Term size**	**Query size**	**Inter-section**
cell adhesion molecule binding	GO:0050839	41.6	560	405	80
extracellular matrix structural constituent	GO:0005201	30.0	173	405	42
protein binding	GO:0005515	28.0	14833	405	386
protein-containing complex binding	GO:0044877	24.1	1283	405	92
cadherin binding	GO:0045296	20.9	333	405	45
actin binding	GO:0003779	20.5	448	405	51
cytoskeletal protein binding	GO:0008092	19.4	999	405	74
structural molecule activity	GO:0005198	17.3	979	405	70
integrin binding	GO:0005178	16.4	158	405	29
calcium ion binding	GO:0005509	15.4	725	405	57
growth factor binding	GO:0019838	14.1	132	405	25
extracellular matrix binding	GO:0050840	14.0	56	405	18
signaling receptor binding	GO:0005102	11.7	1556	405	80
glycosaminoglycan binding	GO:0005539	10.3	244	405	28
collagen binding	GO:0005518	9.7	69	405	16
actin filament binding	GO:0051015	8.9	218	405	25
laminin binding	GO:0043236	7.5	27	405	10
identical protein binding	GO:0042802	7.3	2105	405	86
amyloid-beta binding	GO:0001540	7.2	84	405	15
protease binding	GO:0002020	6.9	136	405	18
heparin binding	GO:0008201	6.8	172	405	20
endopeptidase inhibitor activity	GO:0004866	5.8	177	405	19
peptidase inhibitor activity	GO:0030414	5.5	183	405	19
sulfur compound binding	GO:1901681	5.5	268	405	23
extracellular matrix structural constituent conferring tensile strength	GO:0030020	5.5	41	405	10
binding	GO:0005488	5.5	18309	405	396
fibronectin binding	GO:0001968	5.5	31	405	9
endopeptidase regulator activity	GO:0061135	5.2	191	405	19
enzyme binding	GO:0019899	5.0	2048	405	78
peptidase regulator activity	GO:0061134	4.8	226	405	20
enzyme inhibitor activity	GO:0004857	4.3	389	405	26
structural constituent of muscle	GO:0008307	4.1	43	405	9
insulin-like growth factor II binding	GO:0031995	4.1	8	405	5
proteoglycan binding	GO:0043394	3.6	36	405	8

calmodulin binding	GO:0005516	3.4	202	405	17
platelet-derived growth factor binding	GO:0048407	3.2	11	405	5
dystroglycan binding	GO:0002162	3.2	11	405	5
peptide binding	GO:0042277	3.1	314	405	21
insulin-like growth factor binding	GO:0005520	3.0	20	405	6
protein domain specific binding	GO:0019904	2.7	689	405	33
amide binding	GO:0033218	2.6	391	405	23
threonine-type endopeptidase activity	GO:0004298	2.5	14	405	5
cell adhesion mediator activity	GO:0098631	2.5	65	405	9
cytokine binding	GO:0019955	2.5	143	405	13
actinin binding	GO:0042805	2.4	37	405	7
X11-like protein binding	GO:0042988	2.4	3	405	3
cell-cell adhesion mediator activity	GO:0098632	2.2	54	405	8
insulin-like growth factor receptor binding	GO:0005159	2.2	16	405	5
metal ion binding	GO:0046872	2.2	4273	405	122
cation binding	GO:0043169	2.2	4362	405	124

Table 9-27: Q22 monoculture vs co-culture: All significant molecular functions of downregulated proteins

Term name	**Term ID**	**-Log10(p_{adj})**	**Term size**	**Query size**	**Inter-section**
hydrolase activity, hydrolyzing O-glycosyl compounds	GO:0004553	3.6	97	16	4
hydrolase activity, acting on glycosyl bonds	GO:0016798	2.8	151	16	4

Table 9-28: Q109 monoculture vs co-culture: All significant molecular functions of upregulated proteins

Term name	**Term ID**	**-Log10(p_{adj})**	**Term size**	**Query size**	**Inter-section**
cell adhesion molecule binding	GO:0050839	37.8	560	369	73
extracellular matrix structural constituent	GO:0005201	31.8	173	369	42
structural molecule activity	GO:0005198	29.4	979	369	83
protein binding	GO:0005515	20.8	14833	369	346
cadherin binding	GO:0045296	20.7	333	369	43
protein-containing complex binding	GO:0044877	16.8	1283	369	76
integrin binding	GO:0005178	15.3	158	369	27
actin binding	GO:0003779	14.9	448	369	42
cytoskeletal protein binding	GO:0008092	14.1	999	369	62
calcium ion binding	GO:0005509	11.3	725	369	48
extracellular matrix binding	GO:0050840	10.6	56	369	15

glycosaminoglycan binding	GO:0005539	10.5	244	369	27
collagen binding	GO:0005518	9.2	69	369	15
actin filament binding	GO:0051015	8.2	218	369	23
signaling receptor binding	GO:0005102	7.8	1556	369	67
growth factor binding	GO:0019838	7.8	132	369	18
extracellular matrix structural constituent conferring tensile strength	GO:0030020	7.2	41	369	11
heparin binding	GO:0008201	5.9	172	369	18
fibronectin binding	GO:0001968	5.9	31	369	9
protease binding	GO:0002020	5.7	136	369	16
sulfur compound binding	GO:1901681	5.6	268	369	22
identical protein binding	GO:0042802	5.3	2105	369	75
laminin binding	GO:0043236	5.1	27	369	8
structural constituent of muscle	GO:0008307	4.5	43	369	9
dystroglycan binding	GO:0002162	3.4	11	369	5
platelet-derived growth factor binding	GO:0048407	3.4	11	369	5
binding	GO:0005488	3.2	18309	369	358
translation factor activity, RNA binding	GO:0008135	3.1	98	369	11
structural constituent of cytoskeleton	GO:0005200	2.8	104	369	11
actinin binding	GO:0042805	2.7	37	369	7
endopeptidase inhibitor activity	GO:0004866	2.6	177	369	14
calmodulin binding	GO:0005516	2.6	202	369	15
X11-like protein binding	GO:0042988	2.6	3	369	3
insulin-like growth factor II binding	GO:0031995	2.5	8	369	4
peptidase inhibitor activity	GO:0030414	2.5	183	369	14
endopeptidase regulator activity	GO:0061135	2.3	191	369	14
translation regulator activity, nucleic acid binding	GO:0090079	2.2	121	369	11
peptidase regulator activity	GO:0061134	2.1	226	369	15
chondroitin sulfate binding	GO:0035374	2.0	10	369	4
amyloid-beta binding	GO:0001540	2.0	84	369	9
heparan sulfate binding	GO:1904399	2.0	4	369	3
insulin-like growth factor binding	GO:0005520	1.9	20	369	5
translation regulator activity	GO:0045182	1.8	156	369	12
proteoglycan binding	GO:0043394	1.7	36	369	6
enzyme binding	GO:0019899	1.6	2048	369	62
RNA binding	GO:0003723	1.5	3107	369	85
isomerase activity	GO:0016853	1.5	169	369	12
insulin-like growth factor I binding	GO:0031994	1.5	13	369	4

translation initiation factor activity	GO:0003743	1.4	58	369	7

Table 9-29: Q109 monoculture vs co-culture: All significant molecular functions of downregulated proteins

Term name	Term ID	-Log10(p_{adj})	Term size	Query size	Inter-section
hydrolase activity	GO:0016787	12.2	2457	53	31
hydrolase activity, hydrolyzing O-glycosyl compounds	GO:0004553	10.5	97	53	10
catalytic activity	GO:0003824	9.1	5746	53	40
hydrolase activity, acting on glycosyl bonds	GO:0016798	8.5	151	53	10
sulfuric ester hydrolase activity	GO:0008484	4.1	19	53	4
exopeptidase activity	GO:0008238	4.0	96	53	6
peptidase activity	GO:0008233	3.5	635	53	11
cysteine-type endopeptidase activity	GO:0004197	3.3	125	53	6
dipeptidyl-peptidase activity	GO:0008239	3.0	10	53	3
serine-type exopeptidase activity	GO:0070008	3.0	10	53	3
arylsulfatase activity	GO:0004065	2.6	13	53	3
fucosidase activity	GO:0015928	2.5	2	53	2
N-acetylgalactosamine-4-sulfatase activity	GO:0003943	2.5	2	53	2
alpha-L-fucosidase activity	GO:0004560	2.5	2	53	2
hexosaminidase activity	GO:0015929	2.3	16	53	3
serine-type peptidase activity	GO:0008236	2.2	198	53	6
cysteine-type peptidase activity	GO:0008234	2.2	198	53	6
serine hydrolase activity	GO:0017171	2.1	202	53	6
endopeptidase activity	GO:0004175	2.0	446	53	8
serine-type carboxypeptidase activity	GO:0004185	1.5	5	53	2
galactosidase activity	GO:0015925	1.3	6	53	2
beta-N-acetylhexosaminidase activity	GO:0004563	1.3	6	53	2

Raw data related to Figure 6.4:

Table 9-30: Top 50 biological processes of overlapping proteins between Q22 and Q109 monoculture vs co-culture comparisons

Term name	Term ID	-Log10(p_{adj})	Term size	Query size	Inter-section
anatomical structure morphogenesis	GO:0009653	36.1	2702	298	130
cell adhesion	GO:0007155	32.0	1489	298	93

anatomical structure development	GO:0048856	32.0	5754	298	184
developmental process	GO:0032502	31.1	6317	298	192
system development	GO:0048731	27.5	4313	298	151
multicellular organism development	GO:0007275	26.0	4768	298	157
response to wounding	GO:0009611	24.6	558	298	53
cell migration	GO:0016477	24.2	1461	298	82
blood vessel development	GO:0001568	23.3	700	298	57
vasculature development	GO:0001944	23.2	731	298	58
circulatory system development	GO:0072359	23.1	1099	298	70
anatomical structure formation involved in morphogenesis	GO:0048646	23.1	1134	298	71
blood vessel morphogenesis	GO:0048514	22.6	613	298	53
multicellular organismal process	GO:0032501	22.2	7354	298	193
movement of cell or subcellular component	GO:0006928	22.1	2085	298	95
cell motility	GO:0048870	21.9	1655	298	84
localization of cell	GO:0051674	21.9	1655	298	84
supramolecular fiber organization	GO:0097435	21.8	778	298	58
cellular developmental process	GO:0048869	21.3	4184	298	138
cell differentiation	GO:0030154	21.0	4160	298	137
tissue development	GO:0009888	20.5	1940	298	89
tube development	GO:0035295	20.3	1054	298	65
locomotion	GO:0040011	20.2	1833	298	86
wound healing	GO:0042060	20.2	429	298	43
angiogenesis	GO:0001525	19.5	521	298	46
tube morphogenesis	GO:0035239	19.0	854	298	57
regulation of developmental process	GO:0050793	17.8	2425	298	96
extracellular matrix organization	GO:0030198	17.6	330	298	36
extracellular structure organization	GO:0043062	17.5	331	298	36
external encapsulating structure organization	GO:0045229	17.5	333	298	36
cell development	GO:0048468	17.0	2094	298	87
regulation of cellular component movement	GO:0051270	15.1	1028	298	57
response to organic substance	GO:0010033	14.9	3010	298	103
regulation of cell motility	GO:2000145	14.5	952	298	54
regulation of cell migration	GO:0030334	14.4	893	298	52
regulation of locomotion	GO:0040012	14.3	997	298	55

animal organ development	GO:0048513	13.9	3513	298	111
positive regulation of biological process	GO:0048518	13.7	6224	298	158
regulation of cellular component organization	GO:0051128	13.5	2276	298	85
muscle structure development	GO:0061061	13.2	621	298	42
response to chemical	GO:0042221	12.8	4336	298	124
cell-substrate adhesion	GO:0031589	12.6	362	298	32
actin cytoskeleton organization	GO:0030036	12.5	715	298	44
positive regulation of cellular component movement	GO:0051272	12.4	561	298	39
collagen fibril organization	GO:0030199	12.4	73	298	17
regulation of multicellular organismal process	GO:0051239	12.4	2666	298	91
regulation of anatomical structure morphogenesis	GO:0022603	12.3	930	298	50
positive regulation of cellular process	GO:0048522	11.8	5687	298	145
cellular response to chemical stimulus	GO:0070887	11.8	3019	298	97
localization	GO:0051179	11.8	6436	298	157

Table 9-31: Top 50 biological processes of proteins only significant in Q22 comparison

Term name	**Term ID**	**-Log10(p_{adj})**	**Term size**	**Query size**	**Inter-section**
response to stimulus	GO:0050896	8.9	8885	113	85
positive regulation of immune system process	GO:0002684	8.3	936	113	26
biological process involved in interspecies interaction between organisms	GO:0044419	8.2	1659	113	34
defense response	GO:0006952	7.6	1736	113	34
regulation of immune system process	GO:0002682	6.9	1442	113	30
defense response to other organism	GO:0098542	6.9	1167	113	27
immune response	GO:0006955	6.5	1906	113	34
immune system process	GO:0002376	6.2	2781	113	41
response to stress	GO:0006950	6.0	3851	113	49
negative regulation of cellular process	GO:0048523	6.0	4856	113	56
response to other organism	GO:0051707	5.8	1507	113	29
regulation of cellular process	GO:0050794	5.8	11193	113	91

response to external biotic stimulus	GO:0043207	5.8	1509	113	29
response to external stimulus	GO:0009605	5.5	2788	113	40
response to biotic stimulus	GO:0009607	5.5	1549	113	29
localization	GO:0051179	5.4	6436	113	65
innate immune response	GO:0045087	5.4	907	113	22
regulation of biological process	GO:0050789	5.3	12276	113	95
regulation of localization	GO:0032879	5.3	2725	113	39
cell adhesion	GO:0007155	5.2	1489	113	28
vesicle-mediated transport	GO:0016192	5.2	1604	113	29
positive regulation of biological process	GO:0048518	5.1	6224	113	63
developmental process	GO:0032502	4.8	6317	113	63
biological regulation	GO:0065007	4.7	13001	113	97
anatomical structure development	GO:0048856	4.5	5754	113	59
cell junction organization	GO:0034330	4.3	691	113	18
regulation of response to stimulus	GO:0048583	4.3	3895	113	46
regulation of cellular component organization	GO:0051128	4.0	2276	113	33
regulation of immune response	GO:0050776	4.0	903	113	20
synapse organization	GO:0050808	4.0	424	113	14
cellular response to chemical stimulus	GO:0070887	3.5	3019	113	38
cellular localization	GO:0051641	3.5	3031	113	38
positive regulation of response to stimulus	GO:0048584	3.4	2169	113	31
positive regulation of cellular process	GO:0048522	3.4	5687	113	56
postsynapse organization	GO:0099173	3.4	164	113	9
regulation of developmental process	GO:0050793	3.3	2425	113	33
negative regulation of biological process	GO:0048519	3.3	5876	113	57
endocytosis	GO:0006897	3.3	641	113	16
cellular response to stimulus	GO:0051716	3.2	7399	113	66
regulation of protein localization to membrane	GO:1905475	3.0	181	113	9
transport	GO:0006810	3.0	4742	113	49
establishment of localization	GO:0051234	3.0	4903	113	50
positive regulation of immune response	GO:0050778	2.9	600	113	15

response to chemical	GO:0042221	2.9	4336	113	46
positive regulation of response to external stimulus	GO:0032103	2.8	453	113	13
locomotion	GO:0040011	2.8	1833	113	27
movement of cell or subcellular component	GO:0006928	2.7	2085	113	29
humoral immune response	GO:0006959	2.7	318	113	11
signal transduction	GO:0007165	2.7	5957	113	56
signaling	GO:0023052	2.7	6451	113	59

Table 9-32: All biological processes of proteins only significant in Q109 comparison

Term name	**Term ID**	**-Log10(p_{adj})**	**Term size**	**Query size**	**Inter-section**
cytoplasmic translation	GO:0002181	9.4	157	117	14
cellular amide metabolic process	GO:0043603	7.3	1167	117	28
peptide metabolic process	GO:0006518	6	894	117	23
translation	GO:0006412	5.5	707	117	20
peptide biosynthetic process	GO:0043043	5.2	736	117	20
organonitrogen compound metabolic process	GO:1901564	4.1	6446	117	64
amide biosynthetic process	GO:0043604	4	867	117	20
cellular macromolecule biosynthetic process	GO:0034645	3.1	1171	117	22
organic substance catabolic process	GO:1901575	2.8	2103	117	30
cellular macromolecule metabolic process	GO:0044260	2.5	5766	117	56
protein metabolic process	GO:0019538	2.5	5487	117	54
catabolic process	GO:0009056	2.4	2559	117	33
cellular catabolic process	GO:0044248	1.5	2199	117	28
carbohydrate catabolic process	GO:0016052	1.4	154	117	7

Raw data related to Figure 6.5:

Table 9-33: Monoculture comparison: List of differentially secreted proteins

Gene name / Protein name	**LogFC**	**T-test**
CD63	1.46	5.07E-04
Periostin isoform thy6	-1.76	3.19E-03
TTYH3	1.20	4.03E-03
PTTG1IP	1.26	7.88E-03
BST1	1.14	8.98E-03
CLEC11A	1.45	1.23E-02
FRRS1	1.08	1.34E-02

POSTN	-1.79	1.58E-02
GFUS	-1.26	1.80E-02
RRAS	1.02	1.81E-02
ATXN2L	1.11	2.04E-02
Cathepsin B (Fragment)	1.25	2.09E-02
STAT1	-1.03	2.32E-02
NCF1	-1.00	2.56E-02
RPL5	1.05	2.87E-02
TSPYL2	1.00	3.07E-02
FUCA1	1.28	3.21E-02
HEL-176	-2.04	3.34E-02
GPNMB	1.37	3.51E-02
NPC2	1.06	3.58E-02
GGH	1.33	3.64E-02
DPP4	1.16	4.09E-02
MARCKSL1	1.42	4.37E-02
CTBS	1.10	4.53E-02

Raw data related to Figure 6.6:

Table 9-34: Monoculture comparison: All significant biological processes of upregulated proteins

Term name	**Term ID**	**-Log10(p_{adj})**	**Term size**	**Query size**	**Inter-section**
regulation of integrin-mediated signaling pathway	GO:2001044	2.3	15	39	3
biological process involved in interaction with host	GO:0051701	1.4	183	39	5

Table 9-35: Monoculture comparison: All significant biological processes of downregulated proteins

Term name	**Term ID**	**-Log10(p_{adj})**	**Term size**	**Query size**	**Inter-section**
cytoplasmic translation	GO:0002181	2.7	148	27	5
response to interferon-gamma	GO:0034341	2.6	153	27	5
translation	GO:0006412	2.5	713	27	8
peptide biosynthetic process	GO:0043043	2.3	738	27	8
amide biosynthetic process	GO:0043604	1.8	867	27	8
immune response	GO:0006955	1.8	1888	27	11
peptide metabolic process	GO:0006518	1.7	895	27	8
viral process	GO:0016032	1.7	419	27	6
regulation of protein metabolic process	GO:0051246	1.4	2472	27	12
cellular response to interferon-gamma	GO:0071346	1.4	132	27	4

Raw data related to Figure 6.8:

Table 9-36: Q22 vs Q109 astrocytes in co-culture with Q22 microglia-like cells: Top 50 differentially secreted proteins

Gene name / Protein name	LogFC	T-test
PI15	-4.17	5.21E-06
C1R	-2.70	4.02E-04
SAA1	-1.69	5.20E-04
CD44	-1.50	5.47E-04
A2M	-1.55	1.09E-03
IGHG1	-1.97	1.37E-03
Heavy chain of factor I (Fragment)	-1.87	1.56E-03
SDC4	-1.01	1.77E-03
PIK3IP1	-1.48	2.33E-03
C1S	-2.13	2.42E-03
IGFBP3	1.00	2.73E-03
SERPINA1	-2.01	2.76E-03
SRGN	-1.36	2.84E-03
LAMA4	-1.63	2.88E-03
ADGRE1	-1.25	3.38E-03
C3/C5 convertase	-2.24	3.93E-03
CD163	-1.32	4.22E-03
C3	-2.25	5.76E-03
MARCO	-2.10	5.90E-03
COL3A1	-1.09	6.20E-03
VSIG4	-1.47	7.21E-03
SIRPA	-1.08	7.37E-03
GNG2	-1.13	7.72E-03
GMFG	-1.41	7.85E-03
SPP1	-1.43	8.14E-03
SYT13	-1.22	8.29E-03
LUM	-1.34	8.72E-03
EMILIN2	-1.08	8.82E-03
SHISA5	-1.30	8.89E-03
VASN	-1.72	9.65E-03
CFH	-1.45	1.01E-02
CLU	-1.60	1.07E-02
CSF1R	-2.16	1.11E-02
SAA2	-3.27	1.19E-02
EFEMP1	-1.98	1.25E-02
CD14	-1.82	1.27E-02
C1QA	-1.44	1.30E-02
C1QC	-1.40	1.32E-02
GFAP	-2.22	1.55E-02
FCGBP	-2.06	1.56E-02
LILRB2	-1.55	1.87E-02
AIF1	-1.26	1.91E-02
ARHGDIB	-1.09	1.91E-02

C1QB	-1.54	1.94E-02
UBE2O	-1.45	2.02E-02
ADA2	-1.25	2.04E-02
FCGR3B	-1.39	2.04E-02
CHI3L1	-1.82	2.12E-02
LAIR1	-1.71	2.15E-02
FCGR3A	-1.84	2.29E-02

Table 9-37: Q22 vs Q109 astrocytes in co-culture with Q109 microglia-like cells: List of differentially secreted proteins

Gene name / Protein name	**LogFC**	**T-test**
CD44	-1.03	7.29E-04
FCGBP	-1.64	8.38E-04
GFRA1	1.15	9.68E-04
C1R	-2.05	1.01E-03
CLU	-1.17	1.58E-03
CSF1R	-1.21	1.62E-03
Heavy chain of factor I (Fragment)	-1.26	2.14E-03
C1S	-1.60	2.53E-03
C3	-1.57	4.05E-03
Periostin isoform thy6	1.55	5.47E-03
SERPINA3	-1.94	7.17E-03
MT1F	-1.44	7.68E-03
CCL2	-1.37	7.72E-03
PI15	-3.77	9.44E-03
GFAP	-1.71	9.71E-03
C4A	-1.88	1.01E-02
EFEMP1	-2.23	1.09E-02
IGHG1	-1.32	1.15E-02
FCGR3A	-1.66	1.22E-02
NDUFS6	-1.10	1.25E-02
LDHA	-1.07	1.34E-02
LAIR1	-1.04	1.59E-02
CFI	-1.29	1.90E-02
C6orf15	1.35	1.97E-02
A2M	-1.13	2.22E-02
Metallothionein	-1.13	2.36E-02
SERPINA1	-1.13	2.66E-02
SRGN	-1.13	2.77E-02
C3/C5 convertase	-1.35	2.78E-02
CD14	-1.02	2.90E-02
VASN	-1.30	3.14E-02
S100A4	-1.16	3.25E-02
SLC2A1	1.26	3.65E-02
ADAMDEC1	-1.04	3.94E-02
LAMA4	-1.01	4.42E-02

C1QC	-1.01	4.47E-02
CXCL8	-1.48	4.90E-02
MARCO	-1.12	4.96E-02

Raw data related to Figure 6.9:

Table 9-38: Q22 vs Q109 astrocytes in co-culture with Q22 microglia-like cells: Top 50 significant biological processes

Term name	Term ID	-Log10(p_{adj})	Term size	Query size	Inter-section
defense response	GO:0006952	14.4	1736	140	48
response to stimulus	GO:0050896	12.7	8885	140	107
cell adhesion	GO:0007155	12.3	1489	140	42
biological process involved in interspecies interaction between organisms	GO:0044419	11.4	1659	140	43
inflammatory response	GO:0006954	11.2	778	140	30
regulation of response to stimulus	GO:0048583	10.3	3895	140	65
positive regulation of biological process	GO:0048518	10.0	6224	140	84
response to stress	GO:0006950	9.3	3851	140	63
immune response	GO:0006955	9.3	1906	140	43
positive regulation of response to stimulus	GO:0048584	9.3	2169	140	46
regulation of cellular process	GO:0050794	9.1	11193	140	115
innate immune response	GO:0045087	8.6	907	140	29
regulation of peptidase activity	GO:0052547	8.6	440	140	21
response to other organism	GO:0051707	8.5	1507	140	37
response to external biotic stimulus	GO:0043207	8.5	1509	140	37
immune system process	GO:0002376	8.4	2781	140	51
positive regulation of immune system process	GO:0002684	8.3	936	140	29
cell migration	GO:0016477	8.2	1461	140	36
response to biotic stimulus	GO:0009607	8.1	1549	140	37
regulation of biological process	GO:0050789	8.0	12276	140	119
negative regulation of peptidase activity	GO:0010466	7.8	249	140	16
regulation of immune system process	GO:0002682	7.7	1442	140	35
anatomical structure development	GO:0048856	7.7	5754	140	76
defense response to other organism	GO:0098542	7.4	1167	140	31
regulation of cellular component organization	GO:0051128	7.3	2276	140	44
cell motility	GO:0048870	7.3	1655	140	37

localization of cell	GO:0051674	7.3	1655	140	37
cell-substrate adhesion	GO:0031589	7.2	362	140	18
response to external stimulus	GO:0009605	7.2	2788	140	49
cellular response to chemical stimulus	GO:0070887	7.0	3019	140	51
complement activation	GO:0006956	6.9	130	140	12
positive regulation of cellular process	GO:0048522	6.9	5687	140	74
movement of cell or subcellular component	GO:0006928	6.8	2085	140	41
regulation of cell adhesion	GO:0030155	6.7	740	140	24
negative regulation of hydrolase activity	GO:0051346	6.4	353	140	17
positive regulation of multicellular organismal process	GO:0051240	6.4	1434	140	33
regulation of localization	GO:0032879	6.4	2725	140	47
biological regulation	GO:0065007	6.3	13001	140	120
regulation of endopeptidase activity	GO:0052548	6.3	412	140	18
cell-cell adhesion	GO:0098609	6.3	913	140	26
negative regulation of cellular process	GO:0048523	6.3	4856	140	66
humoral immune response	GO:0006959	6.2	318	140	16
locomotion	GO:0040011	6.0	1833	140	37
response to organic substance	GO:0010033	6.0	3010	140	49
negative regulation of endopeptidase activity	GO:0010951	5.9	240	140	14
positive regulation of cell adhesion	GO:0045785	5.8	442	140	18
regulation of cell migration	GO:0030334	5.8	893	140	25
negative regulation of proteolysis	GO:0045861	5.8	339	140	16
regulation of catalytic activity	GO:0050790	5.8	2345	140	42
cell junction organization	GO:0034330	5.7	691	140	22

Table 9-39: Q22 vs Q109 astrocytes in co-culture with Q109 microglia-like cells: Top 50 significant biological processes

Term name	**Term ID**	**-Log10(p_{adj})**	**Term size**	**Query size**	**Inter-section**
immune response	GO:0006955	11.4	1906	129	44
defense response	GO:0006952	11.4	1736	129	42
immune system process	GO:0002376	10.6	2781	129	52
response to stress	GO:0006950	10.1	3851	129	61
defense response to other organism	GO:0098542	9.9	1167	129	33
response to stimulus	GO:0050896	9.2	8885	129	95
innate immune response	GO:0045087	8.8	907	129	28

biological process involved in interspecies interaction between organisms	GO:0044419	8.4	1659	129	37
response to biotic stimulus	GO:0009607	7.9	1549	129	35
inflammatory response	GO:0006954	7.8	778	129	25
positive regulation of immune system process	GO:0002684	7.6	936	129	27
response to other organism	GO:0051707	7.6	1507	129	34
response to external biotic stimulus	GO:0043207	7.5	1509	129	34
regulation of multicellular organismal process	GO:0051239	7.5	2666	129	46
regulation of immune system process	GO:0002682	7.4	1442	129	33
supramolecular fiber organization	GO:0097435	7.0	778	129	24
regulation of peptidase activity	GO:0052547	6.4	440	129	18
anatomical structure development	GO:0048856	6.3	5754	129	69
multicellular organismal process	GO:0032501	6.3	7354	129	80
regulation of endopeptidase activity	GO:0052548	6.0	412	129	17
locomotion	GO:0040011	5.9	1833	129	35
cell adhesion	GO:0007155	5.7	1489	129	31
proteolysis	GO:0006508	5.6	1787	129	34
movement of cell or subcellular component	GO:0006928	5.6	2085	129	37
regulation of response to stimulus	GO:0048583	5.5	3895	129	53
positive regulation of multicellular organismal process	GO:0051240	5.5	1434	129	30
developmental process	GO:0032502	5.4	6317	129	71
system development	GO:0048731	5.3	4313	129	56
cell migration	GO:0016477	5.3	1461	129	30
response to external stimulus	GO:0009605	5.2	2788	129	43
localization of cell	GO:0051674	5.2	1655	129	32
cell motility	GO:0048870	5.2	1655	129	32
cellular response to chemical stimulus	GO:0070887	5.2	3019	129	45
negative regulation of peptidase activity	GO:0010466	5.1	249	129	13
regulation of cellular component organization	GO:0051128	5.1	2276	129	38
localization	GO:0051179	5.0	6436	129	71
regulation of hydrolase activity	GO:0051336	4.9	992	129	24
complement activation	GO:0006956	4.9	130	129	10
humoral immune response	GO:0006959	4.8	318	129	14

positive regulation of biological process	GO:0048518	4.8	6224	129	69
multicellular organism development	GO:0007275	4.6	4768	129	58
extracellular matrix organization	GO:0030198	4.6	330	129	14
positive regulation of response to stimulus	GO:0048584	4.5	2169	129	36
extracellular structure organization	GO:0043062	4.5	331	129	14
external encapsulating structure organization	GO:0045229	4.5	333	129	14
regulation of localization	GO:0032879	4.5	2725	129	41
immune effector process	GO:0002252	4.4	661	129	19
cellular developmental process	GO:0048869	4.4	4184	129	53
vesicle-mediated transport	GO:0016192	4.3	1604	129	30
negative regulation of endopeptidase activity	GO:0010951	4.3	240	129	12

Raw data related to Figure 6.10:

Table 9-40: Q22 vs Q109 co-cultures: Top 50 differentially secreted proteins

Gene name / Protein name	LogFC	T-test
SPP1	-1.22	5.37E-05
C1R	-2.55	5.02E-04
Heavy chain of factor I (Fragment)	-1.72	5.20E-04
CD44	-1.42	9.14E-04
IGHG1	-2.00	9.77E-04
GFRA1	1.04	1.03E-03
SDC4	-1.01	2.11E-03
C1S	-2.02	3.19E-03
CD163	-1.39	4.28E-03
C3	-2.12	4.40E-03
FCGBP	-2.23	5.30E-03
PIK3IP1	-1.47	6.01E-03
FEX1	-2.33	6.42E-03
A2M	-1.37	7.32E-03
SERPINA1	-1.55	7.83E-03
CADM1	-1.10	9.30E-03
SERPINF1	1.29	9.77E-03
VSIG4	-1.22	1.03E-02
EFEMP1	-2.01	1.13E-02
CSF1R	-1.90	1.23E-02
CLU	-1.48	1.28E-02
CD14	-1.90	1.34E-02
AIF1	-1.24	1.34E-02
SAA2	-3.17	1.41E-02

MARCO	-2.18	1.42E-02
C1QC	-1.33	1.46E-02
FCGR3A	-2.02	1.57E-02
LUM	-1.28	1.63E-02
LAIR1	-1.57	1.66E-02
PI15	-4.17	1.78E-02
GNG2	-1.02	1.78E-02
IGKV2D-29	-1.65	1.80E-02
LILRB2	-1.62	1.90E-02
UBE2O	-1.27	1.91E-02
C1QB	-1.29	2.06E-02
CYBA	-1.03	2.10E-02
GFAP	-2.04	2.12E-02
C6orf15	1.20	2.19E-02
PNP	-1.04	2.26E-02
RARRES1	-1.10	2.41E-02
SRGN	-1.19	2.59E-02
LRRC25	-2.34	2.67E-02
LAMA4	-1.15	2.68E-02
VASN	-1.54	2.71E-02
GMFG	-1.37	2.83E-02
LDHA	-1.48	2.89E-02
S100A8	-1.11	3.06E-02
CHI3L1	-1.57	3.07E-02
ADAM DEC1	-1.35	3.09E-02
FCGR3B	-1.53	3.12E-02

Raw data related to Figure 6.11:

Table 9-41: Q22 vs Q109 co-cultures: Top 50 significant biological processes

Term name	**Term ID**	**-Log10(p_{adj})**	**Term size**	**Query size**	**Inter-section**
defense response	GO:0006952	13.2	1736	101	39
biological process involved in interspecies interaction between organisms	GO:0044419	9.7	1659	101	34
immune response	GO:0006955	9.4	1906	101	36
cell adhesion	GO:0007155	9.4	1489	101	32
inflammatory response	GO:0006954	9.4	778	101	24
defense response to other organism	GO:0098542	8.9	1167	101	28
innate immune response	GO:0045087	8.8	907	101	25
response to other organism	GO:0051707	8.5	1507	101	31
response to external biotic stimulus	GO:0043207	8.5	1509	101	31
response to biotic stimulus	GO:0009607	8.2	1549	101	31
immune system process	GO:0002376	7.9	2781	101	41

response to external stimulus	GO:0009605	7.2	2788	101	40
complement activation	GO:0006956	7.2	130	101	11
response to stimulus	GO:0050896	7.0	8885	101	75
positive regulation of immune system process	GO:0002684	6.8	936	101	23
regulation of immune system process	GO:0002682	6.7	1442	101	28
positive regulation of response to stimulus	GO:0048584	6.4	2169	101	34
negative regulation of peptidase activity	GO:0010466	6.4	249	101	13
response to stress	GO:0006950	6.2	3851	101	46
regulation of peptidase activity	GO:0052547	6.2	440	101	16
cell migration	GO:0016477	5.8	1461	101	27
regulation of endopeptidase activity	GO:0052548	5.6	412	101	15
positive regulation of biological process	GO:0048518	5.5	6224	101	59
regulation of response to stimulus	GO:0048583	5.5	3895	101	45
negative regulation of hydrolase activity	GO:0051346	5.5	353	101	14
negative regulation of endopeptidase activity	GO:0010951	5.4	240	101	12
cell-cell adhesion	GO:0098609	5.4	913	101	21
regulation of cell adhesion	GO:0030155	5.4	740	101	19
humoral immune response	GO:0006959	5.1	318	101	13
positive regulation of cytokine production	GO:0001819	4.8	470	101	15
regulation of cellular protein metabolic process	GO:0032268	4.8	2370	101	33
negative regulation of proteolysis	GO:0045861	4.7	339	101	13
regulation of cytokine production	GO:0001817	4.7	726	101	18
cell motility	GO:0048870	4.7	1655	101	27
localization of cell	GO:0051674	4.7	1655	101	27
regulation of protein metabolic process	GO:0051246	4.6	2536	101	34
cytokine production	GO:0001816	4.6	732	101	18
regulation of cellular process	GO:0050794	4.6	11193	101	81
movement of cell or subcellular component	GO:0006928	4.3	2085	101	30
regulation of catalytic activity	GO:0050790	4.3	2345	101	32
regulation of multicellular organismal process	GO:0051239	4.1	2666	101	34
regulation of cellular component organization	GO:0051128	4.0	2276	101	31
regulation of immune response	GO:0050776	4.0	903	101	19

endocytosis	GO:0006897	3.9	641	101	16
regulation of proteolysis	GO:0030162	3.8	731	101	17
regulation of biological process	GO:0050789	3.8	12276	101	84
acute inflammatory response	GO:0002526	3.8	115	101	8
locomotion	GO:0040011	3.7	1833	101	27
vesicle-mediated transport	GO:0016192	3.7	1604	101	25
myeloid leukocyte migration	GO:0097529	3.5	228	101	10

Table 9-42: Q22 vs Q109 co-cultures: All significant molecular functions

Term name	**Term ID**	**-Log10(p_{adj})**	**Term size**	**Query size**	**Inter-section**
cell adhesion molecule binding	GO:0050839	7.5	560	102	19
peptidase inhibitor activity	GO:0030414	5.8	183	102	11
protein-containing complex binding	GO:0044877	5.6	1283	102	25
peptidase regulator activity	GO:0061134	4.9	226	102	11
endopeptidase inhibitor activity	GO:0004866	4.8	177	102	10
signaling receptor binding	GO:0005102	4.6	1556	102	26
endopeptidase regulator activity	GO:0061135	4.5	191	102	10
cytoskeletal protein binding	GO:0008092	4.1	999	102	20
actin binding	GO:0003779	3.6	448	102	13
enzyme inhibitor activity	GO:0004857	3.4	389	102	12
calcium ion binding	GO:0005509	3.3	725	102	16
integrin binding	GO:0005178	3.0	158	102	8
protein binding	GO:0005515	2.9	14833	102	94
serine-type endopeptidase inhibitor activity	GO:0004867	2.1	99	102	6
RAGE receptor binding	GO:0050786	2.0	10	102	3
fibronectin binding	GO:0001968	1.9	31	102	4
protein tyrosine phosphatase activator activity	GO:0008160	1.8	2	102	2
extracellular matrix structural constituent	GO:0005201	1.7	173	102	7
opsonin binding	GO:0001846	1.4	15	102	3
cargo receptor activity	GO:0038024	1.4	82	102	5
calcium-dependent protein binding	GO:0048306	1.4	83	102	5
amyloid-beta binding	GO:0001540	1.4	84	102	5